STRUCTURAL ANALYSIS AND OPTIMIZED DESIGN OF GENERAL NONPRISMATIC I-SECTION MEMBERS

A Dissertation

Presented to

The Academic Faculty

By

Woo Yong Jeong

In Partial Fulfillment
Of the Requirements for the Degree
Doctor of Philosophy in the
School of Civil and Environmental Engineering

Georgia Institute of Technology
December 2014

Copyright ©2014 by Woo Yong Jeong

STRUCTURAL ANALYSIS AND OPTIMIZED DESIGN OF GENERAL NONPRISMATIC I-SECTION MEMBERS

Approved by:

Dr. Donald W. White, Advisor
School of Civil and Environmental Engineering
Georgia Institute of Technology

Dr. Barry Goodno
School of Civil and Environmental Engineering
Georgia Institute of Technology

Dr. Lawrence F. Kahn
School of Civil and Environmental Engineering
Georgia Institute of Technology

Dr. Arash Yavari
School of Civil and Environmental Engineering
Georgia Institute of Technology

Dr. George Kardomateas
School of Aerospace Engineering
Georgia Institute of Technology

Date Approved: 2014

To my parents, Tae Ki Jeong and Doo Rae Kim, my wife Ji Won Han, my sons Philip Minjoon Jeong and David Minwook Jeong for their enormous support and love.

ACKNOWLEDGEMENTS

I would like to express my gratitude to all who have helped me for the last three years to complete my doctorate at Georgia Tech.

First, I owe my deepest gratitude to my advisor, Dr. Donald W. White, for his academic advising, guidance, and encouragement during pursuing my doctoral research and study. It was my honor to do my doctoral research under him.

My gratitude also goes to my thesis committee members, Dr. Barry Goodno, Dr. Lawrence F. Kahn, Dr. Arash Yavari, and Dr. George Kardomateas for their encouragements and invaluable comments. Especially, Dr. Goodno gave me opportunities to work and teach at Deformable bodies and Statics classes as Teaching Assistant.

During my graduate study, it was my pleasure to meet my colleagues, Yoon Duk Kim, Cliff Bishop, Nauyen Van Thanh, and Lakshmi Palamadai for their input and friendship at Georgia Tech.

My greatest gratitude goes to my parents, Tae Ki Jeong and Doo Rae Kim. I very respect them for their endless love and dedications.

Last but not least, I owe my loving thanks to my wife (Ji Won Han) and my sons (Philip Minjoon Jeong, and David Minwook Jeong). During my doctorate, Ji Won Han is my great spiritual leader. She encouraged me and believed me under any circumstances. Philip Minjoon Jeong and David Minwook Jeong are everything for me. Their loves make it easier for me to concentrate doing my research and completing this dissertation.

TABLE OF CONTENTS

LIST OF TABLES

LIST OF FIGURES

LIST OF SYMBOLS

X : The position vector of a material point in the reference configuration.

x : The position vector of a given material point in the current configuration.

u: The displacement of a given material point.

$\mathbf{e}_i$: Orthonormal basis vector of a Cartesian coordinate system in the material coordinate system.

$\hat{\mathbf{e}}_i$: Orthonormal basis vector of a Cartesian coordinate system in the current coordinate system.

X_i: The components of the position vector **X**in the material coordinate system.

$\hat{x}_i$: The components of the position vector **x** in the current coordinate system.

x_i: The components of the position vector **x**in the material coordinate system.

u_i: The components of the displacement **u** in the material coordinate system.

V_o : Domain (Volume) of the body in the reference configuration.

V : Domain (Volume) of the body in the current configuration.

t: Time for deformation.

F : Deformation gradient tensor.

F_{ij}: The components of the deformation gradient tensor **F**.

J : Jacobian determinant.

R: The rotation tensor or rotation matrix.

R_{ij} : The components of the rotation tensor or rotation matrix **R**.

I: Identity matrix.

δ_{kl} : Kronecker delta or the components of the identity matrix **I**.

$\mathbf{x_T}$: Translation of a given material point.

x_{T_i}: The components of translation of a given material point $\mathbf{x_T}$.

d**x**: The length of an infinitesimal segment in current configuration.

dx_k: The components of the length of an infinitesimal segment d**x**.

d**X**: The length of an infinitesimal segment in reference configuration.

dX_k : The components of the length of an infinitesimal segment d**X**.

$\hat{\mathbf{e}}_i$: Orthonormal basis vector of a Cartesian coordinate system which are different to $\mathbf{e}_i$.

r : Random or arbitrary vector.

r_i: The components of random or arbitrary vector **r**corresponding to base vector $\mathbf{e}_i$.

$\hat{r}_i$: The components of random or arbitrary vector **r**corresponding to base vector $\hat{\mathbf{e}}_i$.

$\mathbf{r}'$: The rotated vector of random or arbitrary vector **r**.

$\delta\mathbf{x}$: Variation of the current position vector **x**.

$\delta\mathbf{R}$: Variation of the rotation tensor **R**.

$\delta\mathbf{x_T}$: Variation of the translation $\mathbf{x_T}$.

$\delta\boldsymbol{\Omega}_{\mathbf{R}}$: Spin tensor, skew-symmetric tensor or anti-symmetric tensor of **R**.

$\delta\Omega_{\mathbf{R}_{ik}}$: The components of $\delta\boldsymbol{\Omega}_{\mathbf{R}}$.

$\delta\boldsymbol{\omega}_{\mathbf{R}}$: Axial vector or pseudo-vector of **R**.

$\delta\omega_{\mathbf{R}_j}$: The components of $\delta\boldsymbol{\omega}_{\mathbf{R}}$.

ε_{ijk} : Permutation symbol.

E : Green-Lagrange strain tensor.

E_{ij}: The components of Green-Lagrange strain tensor **E**.

$\mathbf{R}^S$: The cross-section rotation tensor or rotation matrix having twist $\phi(X_1)$.

R_{ij}^S : The components of $\mathbf{R}^S$.

$\boldsymbol{\sigma}$: Current or Cauchy stress.

σ_{ii}: The axial stress components of current or Cauchy stress$\boldsymbol{\sigma}$.

τ_{ij}: The shear stress components of current or Cauchy stress$\boldsymbol{\sigma}$.

y : Current position of a material point in the direction of 2 within cross-section.

z : Current position of a material point in the direction of 3 within cross-section.

s : Cross-section parameter.

u : Total axial displacement in the direction of 1.

v : Total transverse displacement in the direction of 2

w : Total transverse displacement in the direction of 3

v_o: Translational displacement in the direction of 2

w_o:Translational displacement in the direction of 3

$\emptyset$: Twist of the cross section in the direction of 1

O^g : The origin of the global frame.

O^e : The origin of the element frame.

O^c : The origin of the co-rotational frame.

L : Deformed element length.

L_o : Un-deformed element length.

$\mathbf{e}_1{}^g$: Global frame basis vector in direction 1.

$\mathbf{e}_2{}^g$: Global frame basis vector in direction 2.

$\mathbf{e}_3{}^g$: Global frame basis vector in direction 3.

$\mathbf{e}_1{}^e$: Element frame basis vector in direction 1.

$\mathbf{e}_2{}^e$: Element frame basis vector in direction 2.

$\mathbf{e}_3{}^e$: Element frame basis vector in direction 3.

$\mathbf{e}_1{}^c$: Co-rotational frame basis vector in direction 1.

$\mathbf{e}_2{}^{c}$: Co-rotational frame basis vector in direction 2.

$\mathbf{e}_3{}^{c}$: Co-rotational frame basis vector in direction 3.

$\mathbf{E}_e^g$: Frame transformation matrix from element frame to global frame.

$\mathbf{E}_c^g$: Frame transformation matrix from co-rotational frame to global frame.

$\mathbf{E}_c^e$: Frame transformation matrix from co-rotational frame to element frame.

$\mathbf{d}^g$: Element displacement vector in global frame.

$\mathbf{d}^e$: Element displacement vector in element frame.

$\mathbf{d}^c$: Element displacement vector in co-rotational frame.

$\mathbf{F}^g$: Element internal force vector in global frame.

$\mathbf{F}^e$: Element internal force vector in element frame.

$\mathbf{F}^c$: Element internal force vector in co-rotational frame.

$\mathbf{K}^g$: Element stiffness matrix in global frame.

$\mathbf{K}^e$: Element stiffness matrix in element frame.

$\mathbf{K}^c$: Element stiffness matrix in co-rotational frame.

$\mathbf{U}^g$: Coordinate transformation of displacement and internal force from the element frame to the global frame.

$\mathbf{U}^e$: Coordinate transformation of displacement and internal force from the co-rotational frame to the element frame.

$\mathbf{P}$: Projection motion between element frame and co-rotational frame by removing translations. The projection matrix is described in element frame for the co-rotational frame.

M: Mapping of displacement and internal force between the original degrees of freedom (14) and the reduced degrees of freedom (9).

$\mathbf{x}^{e}{}_{p}$: Current position vector of nodal point p in the element frame.

$\mathbf{u}^{e}{}_{p}$: Displacement vector of nodal point p in the element frame.

$\mathbf{X}^{e}{}_{p}$: Material position vector of nodal point p in the element frame.

$\mathbf{x}^{e}{}_{o}$: Position vector of the co-rotational origin in the element frame.

$\mathbf{P}'$: Current point represents of current nodal point p.

$\mathbf{P}$: Material point represents of current nodal point p.

$\mathbf{x}^{c}{}_{p}$: Current position vector of nodal point p in the co-rotational frame.

$\mathbf{u}^{c}{}_{p}$: Displacement between the deformed element and the un-deformed element in the co-rotational frame.

$\mathbf{T}^{c}{}_{p}$: Transformation of nodal point from $\mathbf{P}$to $\mathbf{P}'$ in the co-rotational frame.

$\mathbf{T}^{e}{}_{p}$:Transformation of nodal point from $\mathbf{P}$to $\mathbf{P}'$ in the element frame.

$\boldsymbol{\omega}_{E}{}^{e}$: Axial vector between element frame and co-rotational frame.

$\delta\boldsymbol{\Omega}_{\mathbf{E}_c^e}$: Spin tensor, skew-symmetric tensor or anti-symmetric tensor of $\mathbf{E}_c^e$.

$\boldsymbol{\omega}_p{}^e$: Axial vector between element frame and nodal traid p .

$\boldsymbol{\omega}_p{}^c$: Axial vector between the co-rotational frame and nodal traid p .

$\delta\boldsymbol{\Omega}_{\mathbf{T}^e{}_p}$: Spin tensor, skew-symmetric tensor or anti-symmetric tensor of $\mathbf{T}^e{}_p$.

$\delta\boldsymbol{\Omega}_{\mathbf{T}^c{}_p}$: Spin tensor, skew-symmetric tensor or anti-symmetric tensor of $\mathbf{T}^c{}_p$.

$\mathbf{e}_1{}^p$: Local basis vector in direction 1 at nodal traid of p.

$\mathbf{e}_3{}^p$: Local basis vector in direction 2 at nodal traid of p.

$\mathbf{e}_3{}^p$: Local basis vector in direction 3 at nodal traid of p.

$\mathbf{e}_1{}^q$: Local basis vector in direction 1 at nodal traid of q.

$\mathbf{e}_3{}^q$: Local basis vector in direction 2 at nodal traid of q.

$\mathbf{e}_3{}^q$: Local basis vector in direction 3 at nodal traid of q.

$\mathbf{x}^e{}_p$: Deformed position vector of node p.

$\mathbf{x}^e{}_q$: Deformed position vector of node q.

$\mathbf{y}_{avg}$: The average of nodal traid basis vectors in direction 2

$\mathbf{N}_u$: Shape function vectors for u_o in the co-rotational frame.

$\mathbf{N}_v$: Shape function vectors for v_o in the co-rotational frame.

$\mathbf{N}_w$: Shape function vectors for w_o in the co-rotational frame.

$\mathbf{N}_\emptyset$: Shape function vectors for $\emptyset$ in the co-rotational frame.

N_e : Shape function for elongation in the co-rotational frame.

$N_{\theta^c_{1_p}}$: Shape function for rotation of p in the direction of 1 and in the co-rotational frame.

$N_{\theta^c_{2_p}}$: Shape function for rotation of p in the direction of 2 and in the co-rotational frame.

$N_{\theta^c_{3_p}}$: Shape function for rotation of p in the direction of 3 and in the co-rotational frame.

$N_{\theta^c_{1_q}}$: Shape function for rotation of q in the direction of 1 and in the co-rotational frame.

$N_{\theta^c_{2_q}}$: Shape function for rotation of q in the direction of 2 and in the co-rotational frame.

$N_{\theta^c_{3_q}}$: Shape function for rotation of q in the direction of 3 and in the co-rotational frame.

$N_{\phi'_p}$: Shape function for warping of p in the direction of 1.

$N_{\phi'_q}$: Shape function for warping of q in the direction of 1.

L : Current element length

U^e : Internal energy which is the function of current displacement.

$\mathbf{f}^e$: Internal force vector in the element frame.

$\mathbf{f}^c$: Internal force vector in the co-rotational frame.

$\mathbf{u}^e$: Translation vector in the element frame.

$\boldsymbol{\theta}^e$: Rotation vector in the element frame.

$\mathbf{u}^c$: Translation vector in the co-rotational frame.

$\boldsymbol{\theta}^{c}$: Rotation vector in the co-rotational frame.

$\mathbf{f}^{e}_{iu}$:Internal force vector in the element frame by translation.

$\mathbf{f}^{e}_{i\theta}$:Internal force vector in the element frame by rotation.

$\mathbf{f}^{c}_{iu}$:Internal force vector in the co-rotational frame by translation.

$\mathbf{f}^{e}_{i\theta}$:Internal force vector in the co-rotational frame by rotation.

SUMMARY

Tapered I-section members have been employed widely for the design of long-span structures such as large clear-span buildings, stadiums, and bridges because of their structural efficiency. For optimized member design providing maximum strength and stiffness at minimum cost, general nonprismatic (tapered and/or stepped cross-sections) as well as singly-symmetric cross-sections have been commonly employed. AISC/ MBMA Design Guide 25 (DG25) provides guidance for the application of the provisions of the ANSI/AISC 360 Specification to the design of frames composed of web-tapered members as well as any other types of nonprismatic members. To employ DG25 most effectively, designers need a robust and general capability for determining elastic buckling loads. Furthermore, the most effective use of nonprismatic member geometries can be achieved by advancing capabilities for automatic optimized design of these types of members, and frames composed of these types of members.

This research first addresses the calculation of the elastic buckling load for general nonprismatic member geometries, and frames composed of general nonprismatic members, subjected to general loadings and general boundary conditions (typically involving multiple brace points along a given member). A finite element elastic eigenvalue buckling calculation tool, named SABRE2, is developed that allows users to define the structure characteristics and obtain a rigorous elastic buckling load levels for general problems. The 3D finite element formulation utilizes a Total Lagrangian co-rotational approach based on open section thin-walled beam theory and the assumption of large displacements, large rotations, and small strains. Load height and support height effects are addressed. In addition, the handling of steps in the cross-section geometry,

which cause a discontinuity the warping function and potentially in the cross-section shear center, is considered. The research clearly demonstrates that the use of stepped prismatic beam finite elements to model tapered members generally produces significantly incorrect Lateral Torsional Buckling (LTB) solutions.

Secondly, this research addresses an algorithmic means for automatic optimized member or frame design of the above types of members using Genetic Algorithms (GA). An automatic member or frame design tool, named SABRE2Design, is developed for optimized member or frame strength design based on minimum cost. Updates to the Design Guide 25 procedures are presented that: (1) account for draft ANSI/AISC 360-16 (AISC 2014) improvements in the characterization of column resistances by using a unified effective area approach and (2) fully utilize the above 3D FEA capabilities to calculate the buckling load multipliers required for the member designs. The proper application of the above buckling analysis capabilities to members with multiple bracing locations is addressed.

CHAPTER 1

INTRODUCTION

1.1 Problem Statement

General nonprismatic as well as singly-symmetric cross-sections have been widely employed for optimized member design due to their structural efficiency. Fabricators and manufacturers equipped to produce web-tapered members can create a wide range of optimized members from a minimal stock of coil and/or plates. Linearly tapered web plates can be nested to minimize scrap. In many situations, the savings in material and the manufacturing efficiencies lead to significant cost savings relative to the use of comparable rolled shapes.

AISC published its Design Guide 25 (DG25) on "Design of Frames using Web-Tapered Members" in 2011. This guide is based on the 2005 and 2010 AISC 360 Specifications and provides guidance in the application of the Specification provisions to the design of frames composed of web-tapered members as well as general nonprismatic members. For member design using Design Guide 25 (DG25), the term

$$\gamma_e = \frac{F_e}{f_r} \qquad \text{(Eq. 1.1)}$$

is employed extensively for defining the strength limit states,

where:

- γ_e = The ratio of the member elastic buckling load to the required strength. This term is convenient for expressing the elastic buckling strength of the various

buckling limit states. When the required design load is used as the reference load for an elastic buckling analysis, this term is simply the lowest eigenvalue returned from the buckling analysis.

- F_e = Elastic buckling stress.
- f_r = Corresponding required stress caused by the design load.

The governing column strength limit state for doubly-symmetric I-section members is generally either:

- In-plane column flexural buckling,
- Out-of-plane column flexural buckling, or
- Torsional buckling (i.e., buckling by twisting about the section shear center)

unless the member has off-axis constraints along its length. The limit state with the smallest eigenvalue buckling load governs. For singly-symmetric I-section members, the critical column strength limit state is either:

- In-plane column flexural buckling or
- Flexural-torsional buckling (FTB)

unless the member has off-axis constraints. For doubly-symmetric members having off-axis constraints, the second two of the limit states listed above are replaced by the constrained-axis torsional buckling (CATB) limit state, and for singly-symmetric members with off-axis constraints, the general flexural-torsional buckling limit state is replaced by the CATB limit state. The CATB limit state involves twisting of the member about the constrained axis.

Regarding the flexural resistance, if sufficient lateral and/or torsional bracing is not provided, the limit states result in out-of-plane (lateral) bending displacement and twisting of a cross-section. This strength limit state is commonly referred to as Lateral Torsional Buckling (LTB), which in DG25 is quantified by the ratio

$$\gamma_{eLTB} = \frac{F_{eLTB}}{f_r} \qquad \text{(Eq. 1.2)}$$

where:

- γ_{eLTB} = Nominal buckling strength multiplier.
- F_{eLTB} = Elastic lateral-torsional buckling stress at the location with the largest compressive flexural stress.
- f_r = Corresponding maximum compressive flexural stress within the unbraced length.

To employ DG25, designers typically need to:

1) Calculate the elastic buckling load factors γ_e and γ_{eLTB}.
2) Calculate the ratio of the corresponding maximum stress to the yield stress at the factored design load.

(In general the calculations are slightly more complex than simply focusing on the most highly stressed cross-section locations.) Once these two values are determined for a given unbraced length, the calculations proceed with a specific mapping from the elastic buckling strength ratios γ_e and γ_{eLTB} to the design strength ratios $\frac{M_u}{\phi M_n}$ and $\frac{P_u}{\phi P_n}$.

DG25 provides simple equations for estimating γ_e or γ_{eLTB} addressing members with linearly-tapered web depths. However, these equations are approximate and are

based on the assumption of flexurally and torsionally simply-supported boundary conditions at the ends of the unbraced lengths. Although these assumptions are common design practice, Smith, et al. (2013) and others have shown that in certain cases, significant improvements in design economy can be gained by accounting for the continuity conditions between adjacent unbraced lengths. For these cases, as well as for the design of more general nonprismatic members, designers need a robust and general capability for determining the γ_e and γ_{eLTB} values.

One of the areas of complexity that this research addresses is the calculation of the elastic buckling load for general nonprismatic geometries subjected to general loadings and general bracing conditions (typically involving multiple brace points along a given member). The research develops a calculation tool, named SABRE2, that can be used to define the problem and obtain a rigorous elastic eigenvalue buckling load level. A number of tools are readily available that do this for basic cases (e.g., LTBeam (2013)). However, to the author's knowledge, no capabilities presently exist that can accommodate the calculation of the elastic buckling multipliers for completely general nonprismatic geometries, general loadings and general displacement boundary conditions. The current research aims to develop an efficient means for determining the buckling strength multiplier γ_e and γ_{eLTB} for singly- and/or doubly-symmetric cross-section and prismatic- and/or nonprismatic (tapered and/or stepped cross-section) members.

Furthermore, the member design for a general nonprismatic geometry requires the selection of an appropriate web-taper angle or angles, member section sizes, and the location of braces (influencing the number and magnitude of the unbraced lengths). Currently, such an optimized member typically is performed essentially through trial and

error methods. Although in industries such as metal building manufacturing, engineers typically have sophisticated algorithms for achieving their designs, the optimized design of frames composed of general nonprismatic members has been largely unexplored as an academic problem. The current research seeks to develop an automatic algorithmic means for the optimized design of nonprismatic steel I-section members based on minimum cost. The selection of optimized designs for these types of members is relatively complex because of the large number of variables. These include the web-taper angle or angles, the base (or starting) member section sizes (top and bottom flange width, top and bottom flange thickness, web depth, and web thickness), and the location of braces (influencing the number and magnitude of the unbraced lengths). For the optimization, the current research investigates how Genetic Algorithms can be best applied to this design optimization problem. Genetic Algorithms is selected for investigation in this work because it is:

- A proven stochastic (probabilistic) search method to find an optimized solution.
- Composed of a straightforward population of possible solutions.
- A robust automatic algorithm that does not require the calculation of gradient information pertaining to the optimal solution.

The design tool corresponding to the above capabilities is referred to as SABRE2Design.

1.2 Research Objectives and Scope

The objectives of the research are:

1. The development of 3D finite element capabilities to calculate the buckling strength multipliers γ_e and γ_{eLTB} for general singly-symmetric, tapered and/or stepped cross-section considering:
    a) General loadings within the plane of the structure, including load height in the direction through the depth of the member web,
    b) Multiple brace locations, and
    c) Support height.

    It is desired to be able to show pre-buckling nodal displacements and member force diagrams as well as to graphically depict the elastic buckling eigenvalues and buckling modes on a three-dimensional rendering of the member or frame.

2. The development of an algorithmic means for automatic optimized member design of the above types of members based on Genetic Algorithms (GA). The focus of this portion of the research includes:
    a) Development and recommendation of several updates to AISC/MBMA Design Guide 25 (Kaehler et al., 2011).
    b) Proper application of the above buckling analysis capabilities to members with multiple bracing locations.
    c) Automatic optimized member or frame design and graphical rendering of the corresponding 3D model using Genetic Algorithms.

1.3 Organization

Chapter 2 first reviews various methods for lateral torsional buckling analysis. Then, the fundamental continuum mechanics are presented for the derivation of the finite element equations using open section thin-walled beam theory for large displacement, large rotation, and small strain problems. The geometric nonlinear finite element equations are then derived and formulated using a Total Lagrangian co-rotational approach. Various benchmark problems are studied for demonstration and validation.

Chapter 3 addresses the automatic optimized design of general nonprismatic members and frames utilizing these types of members. Updated AISC/MBMA Design Guide 25 (DG25) provisions are discussed and recommended pertaining to: (1) the proper application of the eigenvalue buckling capabilities considering members with multiple brace locations, and (2) the application of a new unified effective area approach for determining axial compressive resistances, introduced in ANSI/AISC 360-16 (AISC 2014), to general nonprismatic members. Doubly-symmetric and singly-symmetric member design check examples from DG25 are then studied and compared to the current DG25 solutions. Next, pertaining to optimized design, the basic theory of Genetic Algorithms is reviewed. Then, the search ranges for the genes such as top flange width, top flange thickness, bottom flange width, bottom flange thickness, web thickness, web depth, web tapering angle, and web tapering location are defined. This is followed by a study of an algorithmic means for the design optimization of these types of structures using Genetic Algorithms. Lastly, using SABRE2Design, several benchmark problems are presented to validate the optimized member and frame design capabilities.

In Chapter 4, the above research is summarized, general conclusions are provided and potential future work is recommended.

CHAPTER 2

GENERAL NONPRISMATIC BEAM FINITE ELEMENT BASED ON OPEN SECTION THIN-WALLED THEORY

2.1 Background

This research aims to develop a general Lateral Torsional Buckling (LTB) calculation tool using open section thin-walled beam theory for large displacement, large rotation, and small strain problems. In structural stability problems, equilibrium is considered in the deflected geometry; in a finite element context, the solution is referred to as a geometric nonlinear problem. Despite numerous papers, theories, and commercial software that provide various buckling solutions for I-section members, the capabilities for determining the buckling strength multiplier γ_e and γ_{eLTB} for a comprehensive range of problems including nonprismatic geometries subjected to general loadings and general boundary conditions (e.g., multiple brace points along a given member), do not exist. Furthermore, there are various considerations involving the accuracy of the calculations for the different formulations and methods in the present literature. Prior to proceeding with a finite element formulation using open section thin-walled theory, the limitations of Lateral Torsional Buckling (LTB) calculations using the method of successive approximation, the Rayleigh Ritz method, the finite difference method, and finite element analysis using shell elements are reviewed.

The theoretical developments in this research build upon the work by Chang (2006). The nonlinear 3D finite element analysis capabilities developed in this work are

based on a Total Lagrangian (TL) co-rotational (CR) description. That is, the undeformed configuration is employed as the reference configuration for each iteration and the element displacements are separated into a set of degrees of freedom describing rigid-body motion, and a set describing the actual element deformations.

Chang (2006) employed Rankin and Nour-Omid's (1988) projector concept to separate the element displacements into rigid-body motion and the actual element deformation. However, the derivation of the projection matrix by Rankin and Nour-Omid does not explain the transformation between the global frame and element frame nor does it address elements with warping degrees of freedom. This research derives a new projection matrix employing Rankin and Nour-Omid's projector concept as a starting point of the formulation. Rankin and Nour-Omid use the rotations solely at the element starting nodal point to establish the orientation of the co-rotational reference frame in terms of a rotation about the chord between the element end nodes. Since the nodes at the element ends can potentially have a significant rotation difference, the projection matrix in this work is derived based on an orientation of the co-rotational reference frame using the average rotations of the two end nodal points. This is consistent with the recommendations by Crisfield (1990) and Chang (2006).

2.2 Review of Formulations for Lateral Torsional Buckling Analysis

To employ AISC/MBMA Design Guide 25 (DG25) (Kaehler et al., 2011), designers need to calculate the buckling strength multipliers γ_e and γ_{eLTB}. There are various ways that one may calculate these values including analytical solutions, the method of successive approximations, and 3D Finite Element Analysis. Timoshenko addressed analytical solutions for lateral torsional buckling of members subjected to pure bending and simply-supported end conditions. These solutions are limited to prismatic I-beam. Also, the method of successive approximation was studied by Stűssi (1935), Timoshenko (1936), Newmark (1942), and Timoshenko and Gere (1961). These solutions are limited to prismatic doubly symmetric I-beams. 3D Finite Element Analysis has been utilized extensively to calculate elastic buckling loads of I-section members and frames. 3D Finite Element Analysis (FEA) based on a 3D solid or shell description is very expensive in computing and is inefficient for analysis of frames. Furthermore, buckling analysis using 3D solid and shell descriptions generally produces a large number of local buckling modes for members composed of slender plate elements. Particularly for I-section webs, the postbuckling response is stable; hence, the overall member buckling modes are of greater importance to the overall member design. 3D FEA based on open thin-walled section theory has been used extensively to determine these buckling modes.

Kitipornchai (1985) investigated the elastic lateral buckling of simply supported singly-symmetric prismatic I-beams under moment gradient. He used a finite integral method and the Rayleigh-Ritz energy approach to obtain independent solutions. This

paper shows the elastic buckling moments depend on the degree of the beam single-symmetry as well as the nature of the moment gradient loadings.

Yang and Yau (1987) derived the differential equations of equilibrium for a tapered I-beam and formulated a finite element for the beam. They employed an updated Lagrangian approach for their geometric nonlinear formulation. Their paper focused only on doubly-symmetric tapered I-section beams.

Ronagh (2000a) derived equations for the nonlinear axial strain and Kirchhoff stress resultants for a thin-walled beam-column whose cross-section is tapered. In this paper, the first variation of the Total Potential Energy for nonlinear equilibrium analysis and the second variation of the Total Potential Energy for a stability analysis were derived. These variations were employed for finite element analysis in the companion paper Ronagh (2000b). However Ronagh (2000b) only provided finite element results for a doubly-symmetric tapered I-section beam.

Andrade and Camotim (2005) developed a beam model characterizing the elastic-torsional buckling behavior of singly-symmetric tapered thin-walled open-section members. Their paper employed a Rayleigh-Ritz approach and sinusoidal functions for lateral torsional buckling analysis of singly-symmetric tapered I-beams having simply supported and cantilever boundary conditions.

Chang (2006) presented a theory similar to Ronagh (2000a) for geometric nonlinear analysis of general members. Chang (2006) employed a co-rotational formulation to solve the geometric nonlinear problem. Chang (2006) showed results for lateral torsional bucking analysis of singly-symmetric tapered I-beams.

2.3 Review of Alternative Methods for Lateral Torsional Buckling Analysis

Prior to investigating general nonprismatic beam finite element based on open section thin-walled theory, the limitations of other formulations and their implementation in various numerical approximation methods are studied. To calculate the buckling strength multipliers γ_e and γ_{eLTB}, generally three steps are required:

- Step1: The definition of the problem involving the geometry, and the load and displacement boundary conditions.
- Step2: The determination of the governing differential equations for the problem.
- Step3: The solution of the problem using analytical methods, various approximation methods, and general numerical methods.

The governing differential equation (Step 2) can be established by the variation of the total potential energy, or from the principle of virtual displacements, considering the problem definition in Step 1. If the problem is well posed, analytical solutions can be obtained. However, the governing differential equations to calculate the buckling strength multipliers γ_e and γ_{eLTB} for the buckling load of general singly-symmetric, tapered and/or stepped cross-section (steps in the flange thickness, web thickness, or flange width) members are complex and ill posed, which means that the analytical solution cannot be calculated. In Step 3, approximation methods or numerical methods can be employed for the complex problems. Herein, the method of successive approximation and the Rayleigh Ritz methods are discussed as common approximation solutions. The finite difference method and finite element method using shell elements are discussed as common numerical solutions.

2.3.1 Method of successive approximation

The method of successive approximation can be employed to estimate the upper and lower bound critical buckling loads for structural members. In this method, first an initial approximation of the buckling displacements is assumed.

Stűssi (1935) employed the method of successive approximations to calculate the elastic critical buckling load for simply supported rectangular cross-section and doubly-symmetric I-section beams subjected to pure bending moment, uniformly distributed load, or a point load at the mid-span, as well as a rectangular cross-section cantilever subjected to a downward load applied at its free end. Timoshenko (1936) employed a graphical application of the method of successive approximation to solve for the elastic flexural buckling of a simply-supported column having a stepped cross-section subjected to a concentrically applied end axial loads. Newmark (1943) developed a specific numerical procedure for calculating column buckling loads via successive approximation, which is commonly referred to as Newmark's method. While Stűssi's method combined geometric sequences and their sums with the concept of a conjugate beam, Newmark combined a Picard iteration procedure with the concept of a conjugate beam to overcome difficulties with the numerical procedures and employed successive approximation to solve the governing differential equations. Timoshenko and Gere (1961) improved the previous solutions by Timoshenko (1936) using Newmark's method. Chen and Lui (1987) presented buckling solutions for both elastic doubly-symmetric simply supported and cantilever columns using Newmark's method.

Although the method of successive approximation provides upper- and lower-bounds for the buckling load in each of its iterations, the method is not suitable for the calculation of the buckling strength multiplier γ_{eLTB} for general nonprismatic beams subjected to general loadings and general boundary conditions (e.g., beams with multiple brace points along their length). This is because of the following problems:

- Difficulty in describing and satisfying boundary conditions at intermediate points along the length of a beam.
- Difficulty in determining the critical buckling multipliers due to the fact that the LTB problem involves multiple displacement fields.

2.3.2 Rayleigh Ritz method

The Rayleigh-Ritz method is one approximation method to find displacements based on the theorem of minimum total potential energy. This method has been widely employed due to its simplicity. Kitipornchai (1986) investigated the elastic lateral buckling of simply-supported singly-symmetric I-beams under moment gradient loading using the Rayleigh-Ritz approach. Andrade (2004) determined the critical moments for doubly-symmetric web-tapered I-section simply-supported beams and cantilevers acted on by concentrated loads using this method along with trigonometric functions to approximate the beam critical buckling modes.

The Rayleigh-Ritz method can be employed only to estimate upper bound solutions. Unlike the method of successive approximation, this method employs

continuous shape functions for the displacements throughout the problem domain (i.e., the member length). These displacements can be a linear combination of preselected displacement shape functions that are defined over the entire length of the problem. However, the displacements in general nonprismatic members cannot be estimated accurately by this type of approach. From a design perspective, the Rayleigh-Ritiz approach is undesirable because it gives an upper bound approximate solution and does not generally provide a simple means to evaluate its convergence for general geometries and loadings. It is difficult to satisfy general member boundary conditions, such as unequally spaced intermediate bracing conditions, using the Rayleigh-Ritz method.

2.3.3 Finite difference method

The finite difference method is one of the numerical methods based on the application of a local Taylor series expansion near a point of interest. In the finite difference method, a given member or frame can be discretized by several nodes which can be expressed by linear algebraic equations. In this method, warping, longitudinal displacement, translational displacements, and twist in structural analysis can only be obtained by a linear order approximation. However, in the physical structure, the displacements can vary in a highly nonlinear fashion along a member length.

2.3.4 Finite element analysis using shell elements

As explained above, the method of successive approximation, Rayleigh-Ritz method, and finite difference method are not well suited for the calculation of the buckling strength multipliers γ_e and γ_{eLTB} for general nonprismatic geometries subjected to general load and displacement boundary conditions. These issues are a prime motivation for the use of finite element method, which is widely employed for structural and mechanical analysis. The finite element method can overcome the disadvantages of the above methods. Finite element analysis for structural problems is generally based on Poisson's equation. Open section thin-walled beams such as I-beams, T-beams, and channel beams can be modelled using shell elements in finite element analysis. However, finite element structural analysis using shell elements can result in the capture of a large number of local buckling modes for members composed of slender plate elements. Particularly for I-section webs, the postbuckling response is stable; hence, the overall member buckling modes are of greater importance to the member design. To employ AISC/MBMA Design Guide 25 (DG25) (Kaehler et al., 2011), the overall member buckling modes are needed for the determination of γ_e and γ_{eLTB} for general nonprismatic geometries subjected to general loadings and general bracing conditions.

2.4 Fundamental Continuum Mechanics Equations

The theoretical developments in this research build on the research by Chang (2006). The geometric nonlinear 3D FEA formulation is based on a Total Lagrangian co-rotational description. The term Total Lagrangian connotes that the original undeformed geometry is used as the reference geometry. The term co-rotational indicates that the element displacements are separated into a set of degrees of freedom describing rigid-body motion and a set of degrees of freedom describing the actual element deformations. Prior to deriving the equations, the required fundamental continuum mechanics is reviewed.

2.4.1 Geometric Nonlinear Analysis

Linear elastic analysis is based on an infinitesimal deformation and the application of Hooke's law. In structural stability problems, equilibrium is considered on the deformed geometry. In a finite element context, the problem is referred to as geometrically nonlinear. Any point along the load-deflection equilibrium path for a structure at which the global tangent stiffness is singular is generally referred to as a critical point. Critical points can be characterized further as either limit points or bifurcation points. Limit points correspond to reaching a local maximum or minimum load in the load-deflection response and are determined from an overall load-deflection analysis. Bifurcation points are points at which multiple equilibrium paths cross each other. Bifurcation points are commonly determined by an eigenvalue buckling analysis.

2.4.2 Lagrangian Description

This research employs the Green-Lagrange strain tensor to describe the deformation of a body. The motion of a volume of the body in continuum mechanics is characterized by the transformation of the material points from a reference configuration to a current configuration. In Figure 2.1, V_o is the volume of the body in the reference configuration and V is the volume of the body in the current configuration.

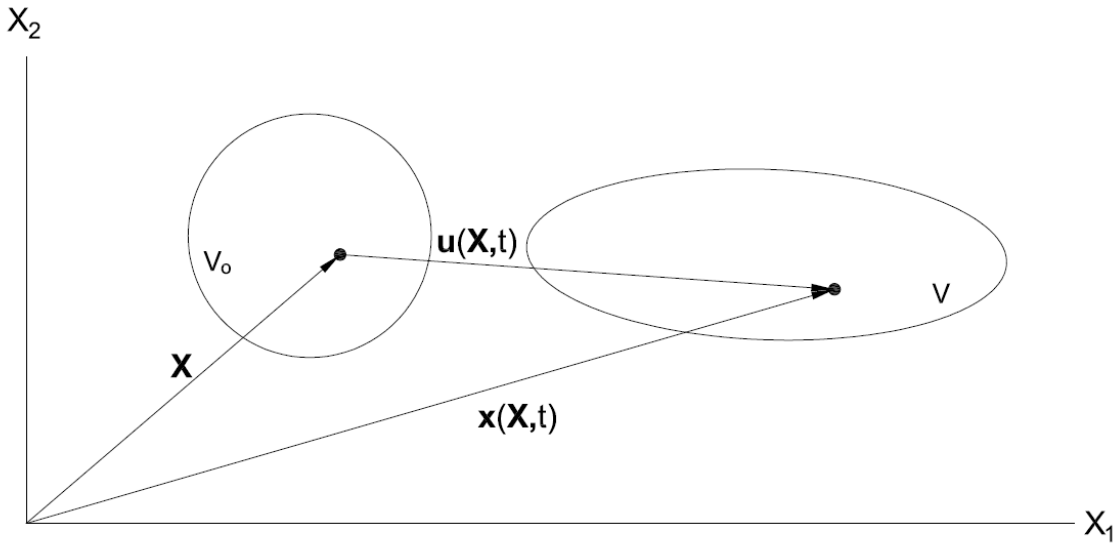

Figure 2.1 Mapping between reference and current configuration in material coordinate system.

In Figure 2.1, the position vector **X** of a material point in the reference configuration is defined by

$$\mathbf{X} = X_i \mathbf{e}_i \qquad i = 1,2,3 \qquad \text{(Eq. 2.1)}$$

where:

- X_i: The components of the position vector $\mathbf{X}$ in the material system (i.e., in the reference configuration).
- $\mathbf{e}_i$: Orthonormal basis vector of a Cartesian material coordinate system.

The components of $\mathbf{X}$ are called the material coordinates. These coordinates are used for the Lagrangian description.

The position vector $\mathbf{x}$ of a given material point in the current configuration is defined by

$$\mathbf{x} = \hat{x}_i \hat{\mathbf{e}}_i \qquad i = 1,2,3 \qquad (\text{Eq. } 2.2)$$

where:

- $\hat{x}_i$: The components of the position vector $\mathbf{x}$ in the current geometry.
- $\hat{\mathbf{e}}_i$: Orthonormal basis vector of a Cartesian current, or spatial, coordinate system.

The components of $\mathbf{x}$ are called the spatial coordinates. In the Lagrangian description, $\mathbf{x}$ is the current position of the material point $\mathbf{X}$ at time t, which is given by $\mathbf{x}(\mathbf{X}, t)$ and Eq. 2.2 is replaced by

$$\mathbf{x} = \mathbf{x}(\mathbf{X}, t) = x_i \mathbf{e}_i \qquad i = 1,2,3 \qquad (\text{Eq. } 2.3)$$

where:

- x_i: The components of the position vector $\mathbf{x}$ in the current geometry, but using the material basis vectors.

At time $t = 0$, $\mathbf{x}(\mathbf{X}, 0) = \mathbf{X}$.

In the Lagrangian description, the displacement **u** of a given material point is defined by

$$\mathbf{u} = u_i \mathbf{e}_i \qquad i = 1,2,3 \qquad \text{(Eq. 2.4)}$$

where:

- u_i: The components of the displacement **u** in the material coordinate system.

The displacement **u** is the transformation of a material point between the current position **x** and the original material position **X** and given by

$$\mathbf{u}(\mathbf{X}, t) = \mathbf{x}(\mathbf{X}, t) - \mathbf{X} \qquad \text{or} \qquad u_i = x_i - X_i \qquad \text{(Eq. 2.5)}$$

2.4.3 Deformation Gradient

An important deformation measure used in nonlinear continuum mechanics is the deformation gradient tensor, which is given by

$$\mathbf{F} \equiv \frac{\partial \mathbf{x}}{\partial \mathbf{X}} \quad \text{or} \quad F_{ij} \equiv \frac{\partial x_i}{\partial X_j} \qquad i, j = 1,2,3 \qquad \text{(Eq. 2.6)}$$

where:

- Index i : row values $i = 1,2,3$
- index j : column values $j = 1,2,3$

If we consider an infinitesimal line segment d**X** in the reference configuration and an infinitesimal line segment d**x** in the current configuration, Eq. 2.6 can be expressed as

$$\mathbf{F} = \frac{d\mathbf{x}}{d\mathbf{X}} \quad \text{or} \quad F_{ij} = \frac{dx_i}{dX_j} \qquad i, j = 1,2,3 \qquad \text{(Eq. 2.7)}$$

In matrix form,

$$\mathbf{F} = \begin{bmatrix} \frac{dx_1}{dX_1} & \frac{dx_1}{dX_2} & \frac{dx_1}{dX_3} \\ \frac{dx_2}{dX_1} & \frac{dx_2}{dX_2} & \frac{dx_2}{dX_3} \\ \frac{dx_3}{dX_1} & \frac{dx_3}{dX_2} & \frac{dx_3}{dX_3} \end{bmatrix} \qquad \text{(Eq. 2.8)}$$

The determinant of the deformation gradient tensor **F** is expressed by a scalar J which is called Jacobian determinant.

In matrix form,

$$J = \det(\mathbf{F}) = \begin{vmatrix} \frac{dx_1}{dX_1} & \frac{dx_1}{dX_2} & \frac{dx_1}{dX_3} \\ \frac{dx_2}{dX_1} & \frac{dx_2}{dX_2} & \frac{dx_2}{dX_3} \\ \frac{dx_3}{dX_1} & \frac{dx_3}{dX_2} & \frac{dx_3}{dX_3} \end{vmatrix} \qquad \text{(Eq. 2.9)}$$

The Jacobian determinant is the ratio between the volume in the reference configuration and in the current configuration. For rigid body motion, the Jacobian determinant is equal to 1 since there is no volume change.

2.4.4 Coordinate Transformation

In Figure 2.2, the transformation between two different coordinate frames, one in the original reference geometry and the other in the current geometry, is described by working with the orthonormal basis vectors for these frames, $\mathbf{e}_i$ and $\hat{\mathbf{e}}_j$, for which

$$\mathbf{e}_i \cdot \mathbf{e}_j = \delta_{ij} \quad \text{and} \quad \hat{\mathbf{e}}_i \cdot \hat{\mathbf{e}}_j = \delta_{ij} \qquad i,j = 1,2,3 \qquad (\text{Eq. } 2.10)$$

where:

- δ_{ij}: Kronecker delta, or the components of the identity matrix **I**.

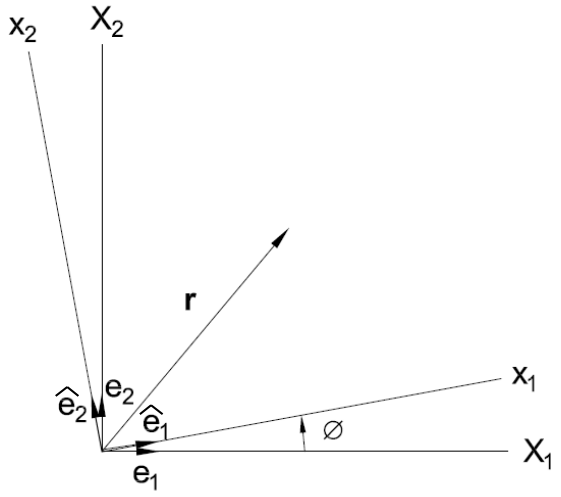

Figure 2.2 Coordinate transformation of a vector **r**.

A vector **r** can be expressed in each coordinate system as

$$\mathbf{r} = r_i \mathbf{e}_i = \hat{r}_i \hat{\mathbf{e}}_i \qquad i = 1,2,3 \qquad (\text{Eq. } 2.11)$$

Upon taking the scalar product with $\mathbf{e}_j$, Eq. 2.11 can be written as

$$\mathbf{r} \cdot \mathbf{e}_j = r_i \mathbf{e}_i \cdot \mathbf{e}_j = \hat{r}_i \hat{\mathbf{e}}_i \cdot \mathbf{e}_j \qquad i, j = 1,2,3 \qquad (\text{Eq. } 2.12)$$

$$r_i \delta_{ij} = \hat{r}_i \hat{\mathbf{e}}_i \cdot \mathbf{e}_j \qquad (\text{Eq. } 2.13)$$

$$r_j = \mathbf{e}_j \cdot \hat{\mathbf{e}}_i \hat{r}_i \qquad (\text{Eq. } 2.14)$$

If the coordinate transform from $\hat{\mathbf{e}}_i$ to $\mathbf{e}_i$ is expressed by

$$\mathbf{e}_j \cdot \hat{\mathbf{e}}_i = T_{ji} \qquad (\text{Eq. } 2.15)$$

then Eq. 2.14 may be written as

$$r_j = T_{ji} \hat{r}_i \quad \text{or} \quad \mathbf{r} = \mathbf{T}\hat{\mathbf{r}} \qquad i, j = 1,2,3 \qquad (\text{Eq. } 2.16)$$

In matrix form with respect to the rotation angle between the two different coordinate systems, $\emptyset$, Eq. 2.15 can be written as

$$\mathbf{T} = \begin{bmatrix} \mathbf{e}_1 \cdot \hat{\mathbf{e}}_1 & \mathbf{e}_1 \cdot \hat{\mathbf{e}}_2 \\ \mathbf{e}_2 \cdot \hat{\mathbf{e}}_1 & \mathbf{e}_2 \cdot \hat{\mathbf{e}}_2 \end{bmatrix} = \begin{bmatrix} \|\mathbf{e}_1\| \|\hat{\mathbf{e}}_1\| \cos\emptyset & \|\mathbf{e}_1\| \|\hat{\mathbf{e}}_2\| \cos(\frac{\pi}{2} + \emptyset) \\ \|\mathbf{e}_2\| \|\hat{\mathbf{e}}_1\| \cos(2\pi - \emptyset) & \|\mathbf{e}_2\| \|\hat{\mathbf{e}}_2\| \cos(\emptyset) \end{bmatrix}$$

$$= \begin{bmatrix} \cos\emptyset & -\sin\emptyset \\ \sin\emptyset & \cos\emptyset \end{bmatrix} \qquad (\text{Eq. } 2.17)$$

where:

- $\|\mathbf{e}_i\| = 1, \|\hat{\mathbf{e}}_i\| = 1$ since these are orthonomal vectors.

Therefore, the coordinate transformation from $\mathbf{e}_i$ to $\hat{\mathbf{e}}_i$ is given by

$$\hat{\mathbf{r}} = \mathbf{T}^T\mathbf{r} \qquad \text{(Eq. 2.18)}$$

As shown in Figure 2.3, a rotation of vector $\mathbf{r}$ to $\mathbf{r}'$with respect to rotation angle between $\mathbf{r}$ and $\mathbf{r}'$ $\emptyset$ is directly given by

$$\mathbf{r}' = \mathbf{T}\mathbf{r} \qquad \text{(Eq. 2.19)}$$

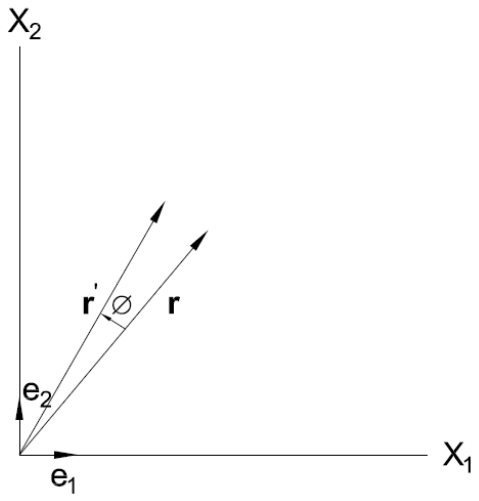

Figure 2.3 Transformation from a vector $\mathbf{r}$ to a vector $\mathbf{r}'$

2.4.5 Rigid Body Motion

For an object in rigid body motion, the distances between particles in the reference configuration remain the same in the current configuration. Rigid body motion consists of a rigid body rotation $\mathbf{R}(t)$ with respect to the origin and a translation $\mathbf{x_T}(t)$. For rigid body motion, the current position of a material point may be written as

$$\mathbf{x}(\mathbf{X},t) = \mathbf{R}(t)\cdot\mathbf{X} + \mathbf{x_T}(t) \quad \text{or} \quad x_i(\mathbf{X},t) = R_{ij}(t)X_j + x_{T_i}(t) \qquad (\text{Eq. } 2.20)$$

The rotation matrix **R** is an orthogonal matrix and has the characteristic

$$\mathbf{R}^T\cdot\mathbf{R} = \mathbf{R}\cdot\mathbf{R}^T = \mathbf{I} \qquad (\text{Eq. } 2.21)$$

This orthogonality results in no change in length since $d\mathbf{x_T}(t) = 0$ and

$$d\mathbf{x}\cdot d\mathbf{x} = (\mathbf{R}\cdot d\mathbf{X})\cdot(\mathbf{R}\cdot d\mathbf{X}) = d\mathbf{X}\cdot(\mathbf{R}^T\cdot\mathbf{R})\cdot d\mathbf{X} = d\mathbf{X}\cdot d\mathbf{X} \qquad \text{or}$$

$$dx_i dx_i = R_{ik}dX_k R_{il}dX_l = dX_k R_{ki}R_{il}dX_l = dX_k\delta_{kl}dX_l = dX_k dX_k \qquad (\text{Eq. } 2.22)$$

2.4.6 3D Finite Rotation Tensor

From Felippa and Haugen (2005), the 3D finite rotation tensor **R** is given by

$$\mathbf{R} = \mathbf{I} + \frac{\sin(\theta)}{\omega}\boldsymbol{\Omega} + \frac{1}{2}\left(\frac{\sin(\theta/2)}{\omega/2}\right)^2\boldsymbol{\Omega}^2 \qquad (\text{Eq. } 2.23)$$

where:

- The magnitude of the axial vector or pseudovector $\boldsymbol{\omega} = (\omega_1 \quad \omega_2 \quad \omega_3)^T$ associated with $\boldsymbol{\Omega}$ is

$$\omega = \sqrt{{\omega_1}^2 + {\omega_2}^2 + {\omega_3}^2} \qquad \text{(Eq. 2.24)}$$

- The magnitude of the rotation vector $\boldsymbol{\theta} = (\theta_1 \quad \theta_2 \quad \theta_3)^{\mathrm{T}}$ in Figure 2.4 is defined by

$$\theta = \sqrt{{\theta_1}^2 + {\theta_2}^2 + {\theta_3}^2} \qquad \text{(Eq. 2.25)}$$

- The spin tensor $\boldsymbol{\Omega}$ associated with $\boldsymbol{\omega}$ is given by

$$\boldsymbol{\Omega} = \mathbf{Spin}(\boldsymbol{\omega}) = \begin{bmatrix} 0 & \Omega_{12} & \Omega_{13} \\ -\Omega_{12} & 0 & \Omega_{23} \\ -\Omega_{13} & -\Omega_{23} & 0 \end{bmatrix} = \begin{bmatrix} 0 & -\omega_3 & \omega_2 \\ \omega_3 & 0 & -\omega_1 \\ -\omega_2 & \omega_1 & 0 \end{bmatrix} \qquad \text{(Eq. 2.26)}$$

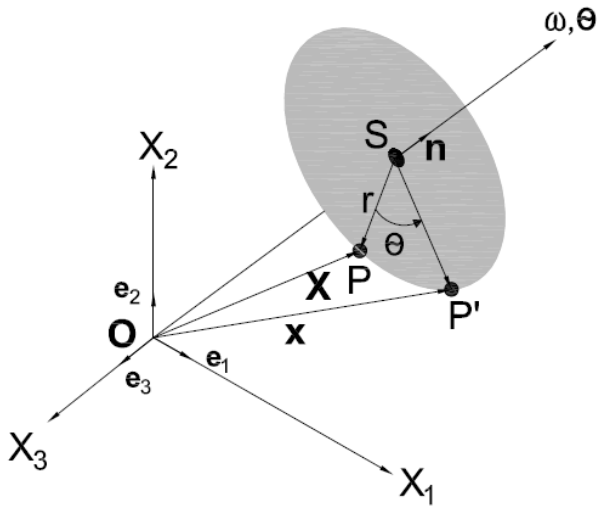

Figure 2.4 Description of 3D finite rotation

In Figure 2.4, the normalized axial vector $\boldsymbol{\omega}$ is defined by

$$\mathbf{n} = \frac{\boldsymbol{\omega}}{\omega} = \begin{bmatrix} n_1 \\ n_2 \\ n_3 \end{bmatrix} = \begin{bmatrix} \omega_1/\omega \\ \omega_2/\omega \\ \omega_3/\omega \end{bmatrix} \qquad \text{(Eq. 2.27)}$$

Then, the normalized spin tensor is defined by

$$\mathbf{N} = \frac{\boldsymbol{\Omega}}{\omega} = \mathbf{Spin}\left(\frac{\boldsymbol{\omega}}{\omega}\right) = \mathbf{Spin}(\mathbf{n}) = \begin{bmatrix} 0 & -n_3 & n_2 \\ n_3 & 0 & -n_1 \\ -n_2 & n_1 & 0 \end{bmatrix} \qquad \text{(Eq. 2.28)}$$

Given that the rotation tensor $\boldsymbol{\Theta}$ associated with $\boldsymbol{\theta}$ is

$$\boldsymbol{\Theta} = \mathbf{Spin}(\boldsymbol{\theta}) = \begin{bmatrix} 0 & \Theta_{12} & \Theta_{13} \\ -\Theta_{12} & 0 & \Theta_{23} \\ -\Theta_{13} & -\Theta_{23} & 0 \end{bmatrix} = \begin{bmatrix} 0 & -\theta_3 & \theta_2 \\ \theta_3 & 0 & -\theta_1 \\ -\theta_2 & \theta_1 & 0 \end{bmatrix} \qquad \text{(Eq. 2.29)}$$

then from Eq. 2.28, Eq. 2.29 can be expressed as

$$\boldsymbol{\Theta} = \mathbf{Spin}(\boldsymbol{\theta}) = \theta\mathbf{N} = \theta\frac{\boldsymbol{\Omega}}{\omega} \qquad \text{(Eq. 2.30)}$$

Therefore, the spin tensor $\boldsymbol{\Omega}$ can be replaced by the rotation tensor $\boldsymbol{\Theta}$ and given by

$$\boldsymbol{\Omega} = \frac{\omega}{\theta}\boldsymbol{\Theta} \qquad \text{(Eq. 2.31)}$$

By substituting Eq. 2.31 into Eq. 2.23, Eq. 2.23 can be expressed as

$$\mathbf{R} = \mathbf{I} + \frac{\sin(\theta)}{\omega}\left(\frac{\omega}{\theta}\boldsymbol{\Theta}\right) + \frac{1}{2}\left(\frac{\sin\left(\frac{\theta}{2}\right)}{\frac{\omega}{2}}\right)^2\left(\frac{\omega}{\theta}\boldsymbol{\Theta}\right)^2 \qquad \text{(Eq. 2.32)}$$

As such, the 3D finite rotation tensor $\mathbf{R}$ with respect to the rotation θ and the rotation tensor $\boldsymbol{\Theta}$ is given by

$$\mathbf{R} = \mathbf{I} + \frac{\sin(\theta)}{\theta}\boldsymbol{\Theta} + \frac{1}{2}\left(\frac{\sin(\theta/2)}{\theta/2}\right)^2 \boldsymbol{\Theta}^2 \qquad \text{(Eq. 2.33)}$$

2.4.7 Variation in the 3D Rotation Tensor

The variation for a rigid body motion is obtained by taking the variation of the current position vector $\mathbf{x}(X, t)$ and is given by

$$\delta\mathbf{x}(\mathbf{X}, t) = \delta\mathbf{R}(t) \cdot \mathbf{X} + \delta\mathbf{x_T}(t) \qquad \text{(Eq. 2.34)}$$

By inserting Eq. 2.20 into Eq. 2.34, the variation for the rigid body motion is described by

$$\delta\mathbf{x}(\mathbf{X}, t) = \delta\mathbf{R}(t) \cdot \mathbf{R}(t)^T(\mathbf{x}(\mathbf{X}, t) - \mathbf{x_T}(t)) + \delta\mathbf{x_T}(t) \qquad \text{(Eq. 2.35)}$$

Then, the spin tensor corresponding to the variation of the axial vector is defined by

$$\delta\boldsymbol{\Omega}_\mathbf{R} = \delta\mathbf{R}(t) \cdot \mathbf{R}(t)^T \qquad \text{(Eq. 2.36)}$$

The spin tensor has skew-symmetric (i.e., anti-symmetric) characteristics:

$$\delta(\mathbf{R}(t) \cdot \mathbf{R}(t)^T) = \delta\mathbf{R}(t) \cdot \mathbf{R}(t)^T + \mathbf{R}(t) \cdot \delta\mathbf{R}(t)^T = \delta(\mathbf{I}) = \mathbf{0} \qquad \text{(Eq. 2.37)}$$

$$\delta\boldsymbol{\Omega}_{\mathbf{R}} + \delta\boldsymbol{\Omega}_{\mathbf{R}}{}^{T} = 0 \qquad \text{(Eq. 2.38)}$$

Due to the above characteristics, $\delta\boldsymbol{\Omega}_{\mathbf{R}}$ is called the spin tensor, the skew-symmetric tensor, or the anti-symmetric tensor.

The skew-symmetric tensor $\delta\boldsymbol{\Omega}_{\mathbf{R}}$ can be expressed in terms of the axial vector or pseudovector $\delta\boldsymbol{\omega}_{\mathbf{R}}$. The matrix product $\delta\boldsymbol{\Omega}_{\mathbf{R}}\mathbf{r}$ can be expressed by the cross product $\delta\boldsymbol{\omega}_{\mathbf{R}} \times \mathbf{r}$ and is given by

$$\delta\boldsymbol{\Omega}_{\mathbf{R}}\mathbf{r} = \delta\boldsymbol{\omega}_{\mathbf{R}} \times \mathbf{r} \quad \text{or} \quad \delta\Omega_{\mathbf{R}_{ik}} r_k = \varepsilon_{ijk}\delta\omega_{\mathbf{R}_j} r_k \qquad i, j, k = 1,2,3 \quad \text{(Eq. 2.39)}$$

where:

- $\delta\boldsymbol{\omega}_{\mathbf{R}}$ = the variation of the axial vector $\boldsymbol{\omega}_{\mathbf{R}}$ is

$$\delta\boldsymbol{\omega}_{\mathbf{R}} = \left(\delta\omega_{\mathbf{R}_1}, \delta\omega_{\mathbf{R}_2}, \delta\omega_{\mathbf{R}_3}\right) \qquad \text{(Eq. 2.40)}$$

The relations between the skew-symmetric tensor $\delta\boldsymbol{\Omega}_{\mathbf{R}}$ and its axial vector $\delta\boldsymbol{\omega}_{\mathbf{R}}$ are

$$\delta\Omega_{\mathbf{R}_{ik}} = \varepsilon_{ijk}\delta\omega_{\mathbf{R}_j} \qquad \text{(Eq. 2.41)}$$

The spin tensor is defined as

$$\delta\boldsymbol{\Omega}_{\mathbf{R}} = \mathbf{Spin}(\delta\boldsymbol{\omega}_{\mathbf{R}}) \qquad \text{(Eq. 2.42)}$$

In matrix form,

$$\delta\boldsymbol{\Omega}_{\mathbf{R}} = \begin{bmatrix} 0 & \delta\Omega_{\mathbf{R}_{12}} & \delta\Omega_{\mathbf{R}_{13}} \\ -\delta\Omega_{\mathbf{R}_{12}} & 0 & \delta\Omega_{\mathbf{R}_{23}} \\ -\delta\Omega_{\mathbf{R}_{13}} & -\delta\Omega_{\mathbf{R}_{23}} & 0 \end{bmatrix} = \begin{bmatrix} 0 & -\delta\omega_{\mathbf{R}_3} & \delta\omega_{\mathbf{R}_2} \\ \delta\omega_{\mathbf{R}_3} & 0 & -\delta\omega_{\mathbf{R}_1} \\ -\delta\omega_{\mathbf{R}_2} & \delta\omega_{\mathbf{R}_1} & 0 \end{bmatrix} \quad \text{(Eq. 2.43)}$$

then,

$$\varepsilon_{ijk}\delta\Omega_{\mathbf{R}_{jk}} = -\varepsilon_{ijk}\varepsilon_{jik}\delta\omega_{\mathbf{R}_j} = -\left(\delta_{ji}\delta_{kk} - \delta_{jk}\delta_{ki}\right)\delta\omega_{\mathbf{R}_j} = -2\delta_{ji}\delta\omega_{\mathbf{R}_j} = -2\delta\omega_{\mathbf{R}_i}$$

$$\delta\omega_{\mathbf{R}_i} = -\frac{1}{2}\varepsilon_{ijk}\delta\Omega_{\mathbf{R}_{jk}} \quad \text{(Eq. 2.44)}$$

The axial vector is defined as

$$\delta\boldsymbol{\omega}_{\mathbf{R}} = \mathbf{axial}(\delta\boldsymbol{\Omega}_{\mathbf{R}}) \quad \text{(Eq. 2.45)}$$

2.4.8 Green-Lagrange Strain Tensor

The relative displacement using Eq. 2.5 is given by

$$\mathbf{du}(\mathbf{X}, t) = d\mathbf{x}(\mathbf{X}, t) - d\mathbf{X} \qquad \text{or} \qquad du_i = dx_i - dX_i \quad \text{(Eq. 2.46)}$$

The relationship between the relative displacement Eq. 2.46 and the Green-Lagrange strain tensor is given by

$$d\mathbf{x}^2 - d\mathbf{X}^2 = 2d\mathbf{X}\cdot\mathbf{E}\cdot d\mathbf{X} \quad \text{or} \quad dx_k dx_k - dX_k dX_k = 2dX_i E_{ij} dX_j \quad \text{(Eq. 2.47)}$$

By introducing Eq. 2.7, Eq. 2.47 can be expressed as

$$(F_{ki}dX_i)\left(F_{kj}dX_j\right) - dX_k\left(\frac{dX_i}{dX_i}\right)\left(\frac{dX_j}{dX_j}\right)dX_k = 2dX_i E_{ij} dX_j \quad \text{(Eq. 2.48)}$$

$$dX_i\left\{F_{ki}F_{kj} - \left(\frac{dX_k}{dX_i}\right)\left(\frac{dX_k}{dX_j}\right) - 2E_{ij}\right\}dX_j = 0 \qquad \text{(Eq. 2.49)}$$

For all d**X**, Eq. 2.49 can be given by

$$F_{ki}F_{kj} - \left(\frac{dX_k}{dX_i}\right)\left(\frac{dX_k}{dX_j}\right) - 2E_{ij} = 0 \qquad \text{(Eq. 2.50)}$$

Then, the Green-Lagrange strain tensor may be expressed as

$$E_{ij} = \frac{1}{2}\left(F_{ik}{}^{T}F_{kj} - \left(\frac{dX_i}{dX_k}\right)^{T}\left(\frac{dX_k}{dX_j}\right)\right) \quad \text{or} \quad \mathbf{E} = \frac{1}{2}\left(\mathbf{F}^{T}\cdot\mathbf{F} - \left(\frac{dX_i}{dX_k}\right)^{T}\cdot\left(\frac{dX_k}{dX_j}\right)\right) \qquad \text{(Eq. 2.51)}$$

The derivative of X_i with respect to X_j is expressed as

$$\frac{dX_i}{dX_j} = \delta_{ij} \mathrm{i,j} = 1,2,3 \qquad \text{(Eq. 2.52)}$$

Using this definition, Eq. 2.51 can be given by

$$E_{ij} = \frac{1}{2}\left(F_{ik}{}^{T}F_{kj} - (\delta_{ik})^{T}(\delta_{kj})\right) = \frac{1}{2}\left(F_{ik}{}^{T}F_{kj} - \delta_{ij}\right)$$

$$\mathbf{E} = \frac{1}{2}(\mathbf{F}^{T}\cdot\mathbf{F} - \mathbf{I}) \quad \text{or} \quad E_{ij} = \frac{1}{2}\left(F_{ik}{}^{T}\cdot F_{kj} - \delta_{ij}\right) \quad \mathrm{i,j,k} = 1,2,3 \qquad \text{(Eq. 2.53)}$$

From the above derivation, the Green-Lagrange strain tensor has the following important characteristic for rigid body rotation, which gives $\mathbf{F} = \mathbf{R}$, the Green-Lagrange strain tensor is

$$\mathbf{E} = \frac{1}{2}(\mathbf{F}^{T}\cdot\mathbf{F} - \mathbf{I}) = \frac{1}{2}(\mathbf{R}^{T}\cdot\mathbf{R} - \mathbf{I}) = \mathbf{0} \qquad \text{(Eq. 2.54)}$$

2.5 Open Section Thin-Walled Beam Theory for Large Displacement, Large Rotation, and Small Strain Problems

2.5.1 Open Section Thin-Walled Beam Concept

For the derivation of the Green-Lagrange strain tensor and for the broader finite element formulation, the 3D Cartesian coordinate system shown in Figure 2.5 is employed and the three directions are defined as

- Direction 1 : Longitudinal direction. The 1 axis is located at the cross-section shear center.
- Directions 2 and 3 : Transverse directions or cross-section directions.

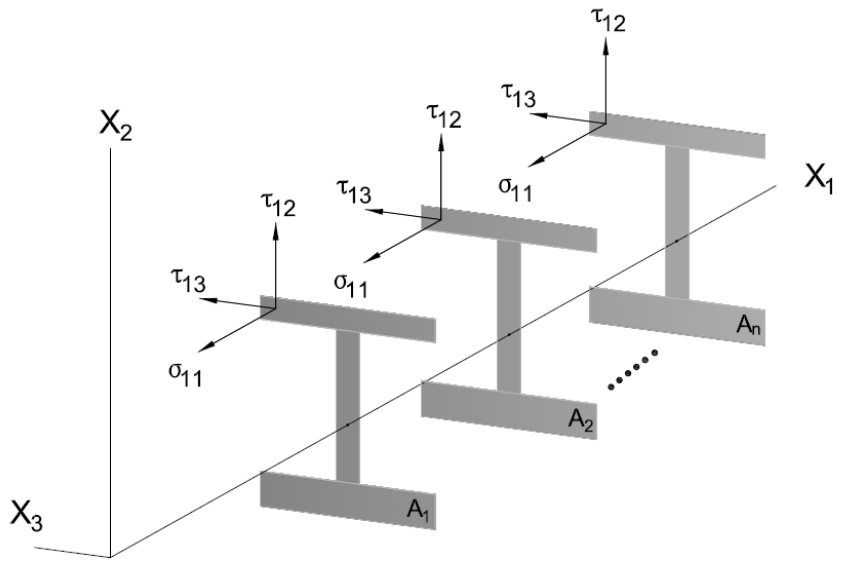

Figure 2.5 Open section thin-wall beam coordinate system and cross-section stresses.

The Green-Lagrange strain tensor based on open-section thin-walled beam theory for large displacement, large rotation, and small strain problems is derived by invoking the following assumptions:

- The normal stress σ_{11} is considered.
- The shear stresses τ_{12} and τ_{13} are considered, but solely due to St. Venant torsion.
- The other stresses $\sigma_{22} = \sigma_{33} = \tau_{23} = \tau_{32} = 0$.
- The solution parameters are a function of the longitudinal or uniaxial direction 1 and are given by
    - $y(\mathrm{X}_1, \mathrm{s}), z(\mathrm{X}_1, \mathrm{s}), u(\mathrm{X}_1, \mathrm{s}), v(\mathrm{X}_1, \mathrm{s}), w(\mathrm{X}_1, \mathrm{s}), \omega(\mathrm{X}_1, \mathrm{s}), \psi(\mathrm{X}_1, s)$
    - $u_o(\mathrm{X}_1), v_o(\mathrm{X}_1), w_o(\mathrm{X}_1), \phi(\mathrm{X}_1), \alpha_z(\mathrm{X}_1), \alpha_y(\mathrm{X}_1)$
    - Where, $\mathrm{s} = \mathrm{s}(\mathrm{y}, \mathrm{z})$ is a cross-section parameter.
- Plane cross-sections remain plane in the surface perpendicular to the longitudinal or uniaxial direction 1 and have the following characteristics:
    - Rigid body rotation $\mathbf{F} = \mathbf{R}^{\mathrm{S}}$within the cross-section.
    - The stretch values with respect to transverse directions 2 and 3 are zero. Therefore:

$$\mathrm{E}_{12} = \mathrm{E}_{21} = \mathrm{E}_{13} = \mathrm{E}_{31} = 0 \quad or \quad \mathrm{E}_{1\mathrm{s}} = \mathrm{E}_{\mathrm{s}1} = 0$$

    - A given material position vector in the current configuration is given by

$$\mathrm{x}_\mathrm{i}(\mathbf{X}, \mathrm{t}) = \mathrm{R}^{\mathrm{S}}_{\mathrm{ij}}(\mathrm{t})\mathrm{X}_\mathrm{j} + \mathrm{u}_{\mathrm{T}_\mathrm{i}}(\mathrm{t}) \qquad \mathrm{i}, \mathrm{j} = 2,3 \qquad \text{(Eq. 2.55)}$$

$$\begin{Bmatrix} \mathrm{x}_2 \\ \mathrm{x}_3 \end{Bmatrix} = \begin{bmatrix} \mathrm{R}^{\mathrm{S}}_{22} & \mathrm{R}^{\mathrm{S}}_{23} \\ \mathrm{R}^{\mathrm{S}}_{32} & \mathrm{R}^{\mathrm{S}}_{33} \end{bmatrix} \begin{Bmatrix} \mathrm{X}_2 \\ \mathrm{X}_3 \end{Bmatrix} + \begin{Bmatrix} \mathrm{u}_{\mathrm{T}_2} \\ \mathrm{u}_{\mathrm{T}_3} \end{Bmatrix} = \begin{Bmatrix} \mathrm{X}_2 + \mathrm{u}_2 \\ \mathrm{X}_3 + \mathrm{u}_3 \end{Bmatrix} \qquad \text{(Eq. 2.56)}$$

$$\begin{Bmatrix} u_2 \\ u_3 \end{Bmatrix} = \begin{bmatrix} R^S_{22} & R^S_{23} \\ R^S_{32} & R^S_{33} \end{bmatrix} \begin{Bmatrix} X_2 \\ X_3 \end{Bmatrix} + \begin{Bmatrix} u_{T_2} \\ u_{T_3} \end{Bmatrix} - \begin{Bmatrix} X_2 \\ X_3 \end{Bmatrix} \quad \text{(Eq. 2.57)}$$

- Displacements on each cross-section along uniaxial direction 1 corresponding to reference axis.
    - A given material position vector in the current configuration is given by

$$x_1(\mathbf{X}, t) = X_1 + u_1(\mathbf{X}, t) \quad \text{(Eq. 2.58)}$$

- The cross-section profile is unchanged by any element deformations.

Therefore, member local and/or distortional buckling are not addressed within the element formulation.

2.5.2 Motion of the Cross-section

The motion of cross-section in the Lagrangian description is shown in Figure 2.6 (a). Point O is the origin of the rotation of the cross-section. In the Lagrangian description, the position vector **X** of a material point in the reference configuration in Eq 2.1 can be given by

$$\mathbf{X} = X_1\mathbf{e_1} + X_2\mathbf{e}_2 + X_3\mathbf{e_3} \quad \text{(Eq. 2.59)}$$

In the Lagrangian description, the position vector **x** of a given material point in the current configuration in Eq. 2.3 can be given by

$$\mathbf{x} = x_1\mathbf{e_1} + x_2\mathbf{e}_2 + x_3\mathbf{e_3} \quad \text{(Eq. 2.60)}$$

Furthermore, in the Lagrangian description, the displacement **u** of a given material point in Eq. 2.4 can be given by

$$\mathbf{u} = u_1\mathbf{e_1} + u_2\mathbf{e}_2 + u_3\mathbf{e_3} \qquad \text{(Eq. 2.61)}$$

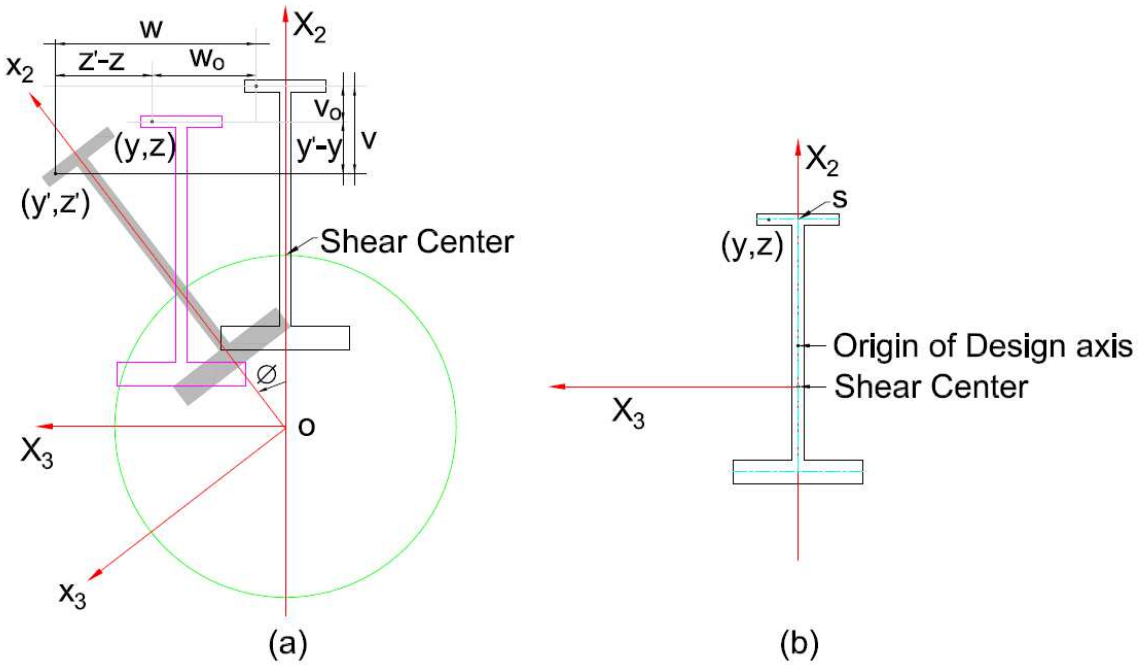

Figure2.6 (a) Motion of the cross-section in Lagrangian description and (b) reference axis (shear center), design axis and cross-section parameter s.

For the convenience of the derivation of the Green-Lagrange strain tensor, the vectors in Eqs. 2.59, 2.60, and 2.61 are replaced by

$$\mathbf{X} = x\mathbf{e_1} + y\mathbf{e_2} + z\mathbf{e_3} \qquad \text{(Eq. 2.62)}$$

$$\mathbf{x} = x'\mathbf{e_1} + y'\mathbf{e_2} + z'\mathbf{e_3} \qquad \text{(Eq. 2.63)}$$

$$\mathbf{u} = u\mathbf{e_1} + v\mathbf{e_2} + w\mathbf{e_3} \qquad \text{(Eq. 2.64)}$$

where:

- $\mathrm{X}_1 = x, \mathrm{X}_2 = y(x,s), \mathrm{X}_3 = z(x,s)$
- $\mathrm{x}_1 = x'(x), \mathrm{x}_2 = y'(x,s), \mathrm{x}_3 = z'(x,s)$
- $\mathrm{u}_1 = u(x,s), \mathrm{u}_2 = v(x,s), \mathrm{u}_3 = w(x,s)$

Figure 2.6 (b) shows the cross-section parameter s, the reference axis for the finite element calculations, and the design axis which is the axis the designer uses to define the model geometry. For the derivation of the Green-Lagrange strain tensor, the cross-section parameter $s = s(y,z)$is employed and the shear center is employed as the reference axis.

As shown in Figure 2.6(a), a given material position vector in the current configuration within the cross-section can be described by two translations and a rigid body rotation with respect to the origin O. The cross-section displacement in Eq. 2.56 can be given by:

- Translational displacement $v_o$and w_o

$$\mathrm{u}_{\mathrm{T}_2} = v_o(x) \qquad \text{(Eq. 2.65)}$$

$$\mathrm{u}_{\mathrm{T}_3} = w_o(x) \qquad \text{(Eq. 2.66)}$$

- Twist of the cross section $\emptyset$

$$\emptyset = \emptyset(x) \qquad \text{(Eq. 2.67)}$$

As such, the rigid body rotation of the cross-section in Eq. 2.56 can be given by

$$\mathbf{R}^{S} = \begin{bmatrix} \cos\emptyset & -\sin\emptyset \\ \sin\emptyset & \cos\emptyset \end{bmatrix} \quad \text{(Eq. 2.68)}$$

By substituting Eq. 2.65, Eq. 2.66, and Eq. 2.68, Eq. 2.57 may be written as

$$\begin{Bmatrix} u_2 \\ u_3 \end{Bmatrix} = \begin{Bmatrix} v \\ w \end{Bmatrix} = \begin{bmatrix} \cos\emptyset & -\sin\emptyset \\ \sin\emptyset & \cos\emptyset \end{bmatrix} \begin{Bmatrix} y \\ z \end{Bmatrix} + \begin{Bmatrix} v_o \\ w_o \end{Bmatrix} - \begin{Bmatrix} y \\ z \end{Bmatrix} \quad \text{(Eq. 2.69)}$$

$$v = v_o + y\cos\emptyset - z\sin\emptyset - y = v_o - z\sin\emptyset - y(1 - \cos\emptyset) \quad \text{(Eq. 2.70)}$$

$$w = w_o + y\sin\emptyset + z\cos\emptyset - z = w_o + y\sin\emptyset - z(1 - \cos\emptyset) \quad \text{(Eq. 2.71)}$$

The derivative of the two transverse displacements in Eq. 2.70 and Eq. 2.71 with respect to the cross-section parameter s is given by

$$v_{,s} = -z_{,s}\sin\emptyset - y_{,s}(1 - \cos\emptyset) \quad \text{(Eq. 2.72)}$$

$$w_{,s} = y_{,s}\sin\emptyset - z_{,s}(1 - \cos\emptyset) \quad \text{(Eq. 2.73)}$$

The derivative of the two transverse displacements in Eq. 2.70 and Eq. 2.71 with respect to x is given by

$$v_{,x} = v_{o\,,x} - z_{,x}\sin\emptyset - z\cos\emptyset \cdot \emptyset_{,x} - y_{,x}(1 - \cos\emptyset) - y\sin\emptyset \cdot \emptyset_{,x} \quad \text{(Eq. 2.74)}$$

$$w_{,x} = w_{o\,,x} + y_{,x}\sin\emptyset + y\cos\emptyset \cdot \emptyset_{,x} - z_{,x}(1 - \cos\emptyset) - z\sin\emptyset \cdot \emptyset_{,x} \quad \text{(Eq. 2.75)}$$

2.5.3 Green-Lagrange Strain Tensor

The Green-Lagrange strain tensor expression in Eq. 2.51 is employed since $y = y(x, s)$ and $z = z(x, s)$. As such, the Green-Lagrange strain may be written as

$$\mathrm{E_{ij}} = \frac{1}{2}\left(\mathrm{F_{ik}}^{\mathrm{T}}\mathrm{F_{kj}} - \left(\frac{\mathrm{dX_i}}{\mathrm{dX_k}}\right)^{\mathrm{T}}\left(\frac{\mathrm{dX_k}}{\mathrm{dX_j}}\right)\right) = \frac{1}{2}\left(\frac{\mathrm{dx_k}}{\mathrm{dX_i}}\frac{\mathrm{dx_k}}{\mathrm{dX_j}} - \frac{\mathrm{dX_k}}{\mathrm{dX_i}}\frac{\mathrm{dX_k}}{\mathrm{dX_j}}\right) \quad \mathrm{i,j,k} = 1,2,3 \quad \text{(Eq. 2.76)}$$

The Green-Lagrange strain tensor based on open section thin-walled beam theory for large displacement, large rotation, and small strain problems is constructed from the assumption that only the cross-section axial stress (σ_{11}) and shear stresses (τ_{12} and τ_{13}) are considered. Thus, two Green-Lagrange finite strains $\mathrm{E_{11}}$ or E_{xx} (axial strain) and $\mathrm{E_{1s}}$ or E_{xs} (shear strain) are employed and are given by

Green-Lagrange axial strain

$$\mathrm{E_{11}} = \frac{1}{2}\left(\frac{\mathrm{dx_k}}{\mathrm{dX_1}}\frac{\mathrm{dx_k}}{\mathrm{dX_1}} - \frac{\mathrm{dX_k}}{\mathrm{dX_1}}\frac{\mathrm{dX_k}}{\mathrm{dX_1}}\right) = \mathrm{E}_{xx} = \frac{1}{2}\left(\frac{\mathrm{dx_k}}{\mathrm{d}x}\frac{\mathrm{dx_k}}{\mathrm{d}x} - \frac{\mathrm{dX_k}}{\mathrm{d}x}\frac{\mathrm{dX_k}}{\mathrm{d}x}\right) \quad \mathrm{k} = 1,2,3 \text{ (Eq. 2.77)}$$

Green-Lagrange shear strain

$$\mathrm{E_{1}}_{s} = \frac{1}{2}\left(\frac{\mathrm{dx_k}}{\mathrm{dX_1}}\frac{\mathrm{dx_k}}{\mathrm{d}s} - \frac{\mathrm{dX_k}}{\mathrm{dX_1}}\frac{\mathrm{dX_k}}{\mathrm{d}s}\right) = \mathrm{E}_{xs} = \frac{1}{2}\left(\frac{\mathrm{dx_k}}{\mathrm{d}x}\frac{\mathrm{dx_k}}{\mathrm{d}s} - \frac{\mathrm{dX_k}}{\mathrm{d}x}\frac{\mathrm{dX_k}}{\mathrm{d}s}\right) \quad \mathrm{k} = 1,2,3 \text{ (Eq. 2.78)}$$

where:

$$\frac{\mathrm{d}\mathbf{X}}{\mathrm{d}s} = \mathbf{X}_{,s} = y_{,s}\mathbf{e_2} + z_{,s}\mathbf{e_3} \qquad \text{(Eq. 2.79)}$$

$$\frac{\mathrm{d}\mathbf{X}}{\mathrm{d}x} = \mathbf{X}_{,x} = \mathbf{e_1} + y_{,x}\mathbf{e_2} + z_{,x}\mathbf{e_3} \qquad \text{(Eq. 2.80)}$$

$$\frac{\mathrm{d}\mathbf{x}}{\mathrm{d}s} = \mathbf{X}_{,s} + u_{,s}\mathbf{e_1} + v_{,s}\mathbf{e_2} + w_{,s}\mathbf{e_3} = u_{,s}\mathbf{e_1} + \left(y_{,s} + v_{,s}\right)\mathbf{e_2} + \left(z_{,s} + w_{,s}\right)\mathbf{e_3} \qquad \text{(Eq. 2.81)}$$

$$\frac{\mathrm{d}\mathbf{x}}{\mathrm{d}x} = \mathbf{X}_{,x} + u_{,x}\mathbf{e_1} + v_{,x}\mathbf{e_2} + w_{,x}\mathbf{e_3}$$

$$= \left(1 + u_{,x}\right)\mathbf{e_1} + \left(y_{,x} + v_{,x}\right)\mathbf{e_2} + \left(z_{,x} + w_{,x}\right)\mathbf{e_3} \qquad \text{(Eq. 2.82)}$$

From Eqs. 2.77 through 2.82 , two Green-Lagrange finite strains E_{11}or E_{xx} (axial strain) and E_{1s} or E_{xs} (shear strain) are derived as follows.

Green-Lagrange shear strain

$$\mathrm{E}_{xs} = \frac{1}{2}\left\{\begin{bmatrix}(1 + u_{,x}) & \left(y_{,x} + v_{,x}\right) & (z_{,x} + w_{,x})\end{bmatrix}\begin{bmatrix}u_{,s} \\ \left(y_{,s} + v_{,s}\right) \\ (z_{,s} + w_{,s})\end{bmatrix} - \begin{bmatrix}1 & y_{,x} & z_{,x}\end{bmatrix}\begin{bmatrix}0 \\ y_{,s} \\ z_{,s}\end{bmatrix}\right\}$$

$$\mathrm{E}_{xs} = \frac{1}{2}\left\{\left(1 + u_{,x}\right)u_{,s} + \left(y_{,x} + v_{,x}\right)\left(y_{,s} + v_{,s}\right) + \left(z_{,x} + w_{,x}\right)\left(z_{,s} + w_{,s}\right) - y_{,x}y_{,s} - z_{,x}z_{,s}\right\}$$

$$\mathrm{E}_{xs} = \frac{1}{2}\{\left(1 + u_{,x}\right)u_{,s} + \left(\cancel{y_{,x}y_{,s}} + y_{,x}v_{,s} + v_{,x}y_{,s} + v_{,x}v_{,s}\right) + (\cancel{z_{,x}z_{,s}} + z_{,x}w_{,s} + w_{,x}z_{,s}$$

$$+ w_{,x}w_{,s}) - \cancel{y_{,x}y_{,s}} - \cancel{z_{,x}z_{,s}}\}$$

$$\mathrm{E}_{xs} = \frac{1}{2}\Big\{(1+u_{,x})u_{,s} + y_{,x}\left(\cancel{-z_{,s}sin\emptyset} - y_{,s}(1-\cancel{cos\,\emptyset})\right)$$

$$+\left(v_{o\,,x} - z_{,x}sin\emptyset - zcos\emptyset\cdot\emptyset_{,x} - y_{,x}(\cancel{1}-cos\,\emptyset) - ysin\emptyset\cdot\emptyset_{,x}\right)\Big(\cancel{y_{,s}}$$

$$- z_{,s}sin\emptyset - y_{,s}(\cancel{1}-cos\,\emptyset)\Big) + z_{,x}\left(\cancel{y_{,s}sin\emptyset} - z_{,s}(1-\cancel{cos\,\emptyset})\right)$$

$$+\left(w_{o\,,x} + y_{,x}sin\emptyset + ycos\emptyset\cdot\emptyset_{,x} - z_{,x}(\cancel{1}-cos\,\emptyset) - zsin\emptyset\cdot\emptyset_{,x}\right)\Big(\cancel{z_{,s}}$$

$$+ y_{,s}sin\emptyset - z_{,s}(\cancel{1}-cos\,\emptyset)\Big)\Big\}$$

$$\mathrm{E}_{xs} = \frac{1}{2}\Big\{(1+u_{,x})u_{,s} - y_{,x}y_{,s}$$

$$+\left(v_{o\,,x} - z_{,x}sin\emptyset - zcos\emptyset\cdot\emptyset_{,x} + y_{,x}\,cos\,\emptyset - ysin\emptyset\cdot\emptyset_{,x}\right)\left(-z_{,s}sin\emptyset\right.$$

$$\left.+ y_{,s}\,cos\,\emptyset\right) - z_{,x}z_{,s}$$

$$+\left(w_{o\,,x} + y_{,x}sin\emptyset + ycos\emptyset\cdot\emptyset_{,x} + z_{,x}\,cos\,\emptyset - zsin\emptyset\cdot\emptyset_{,x}\right)\left(y_{,s}sin\emptyset\right.$$

$$\left.+ z_{,s}\,cos\,\emptyset\right)\Big\}$$

$$\mathrm{E}_{xs} = \frac{1}{2}\Big\{(1+u_{,x})u_{,s} - \cancel{y_{,x}y_{,s}} - \cancel{z_{,x}z_{,s}} + v_{o\,,x}\left(-z_{,s}sin\emptyset + y_{,s}\,cos\,\emptyset\right)$$

$$+ w_{o\,,x}\left(y_{,s}sin\emptyset + z_{,s}\,cos\,\emptyset\right)$$

$$+\left(\cancel{z_{,x}z_{,s}sin\emptyset^{2}} - \cancel{z_{,x}y_{,s}sin\emptyset\,cos\,\emptyset} + \cancel{zz_{,s}sin\emptyset cos\emptyset\cdot\emptyset_{,x}} - zy_{,s}cos\emptyset^{2}\cdot\emptyset_{,x}\right.$$

$$\left.- \cancel{z_{,s}y_{,x}sin\emptyset\,cos\,\emptyset} + \cancel{y_{,x}y_{,s}cos\emptyset^{2}} + yz_{,s}sin\emptyset^{2}\cdot\emptyset_{,x} - \cancel{yy_{,s}sin\emptyset\,cos\,\emptyset}\right.$$

$$\left.\cdot\,\emptyset_{,x}\right) + \left(\cancel{y_{,x}y_{,s}sin\emptyset^{2}} + \cancel{y_{,x}z_{,s}sin\emptyset\,cos\,\emptyset} + \cancel{yy_{,s}sin\emptyset cos\emptyset\cdot\emptyset_{,x}}\right.$$

$$\left.+ yz_{,s}cos\emptyset^{2}\cdot\emptyset_{,x} + \cancel{z_{,x}y_{,s}sin\emptyset\,cos\,\emptyset} + \cancel{z_{,x}z_{,s}cos\emptyset^{2}} - zy_{,s}sin\emptyset^{2}\cdot\emptyset_{,x}\right.$$

$$\left.- \cancel{zz_{,s}sin\emptyset\,cos\,\emptyset\cdot\emptyset_{,x}}\right)\Big\}$$

$$\mathrm{E}_{xs} = \frac{1}{2}\Big\{(1+u_{,x})u_{,s} + v_{o,x}(-z_{,s}sin\emptyset + y_{,s}\,cos\,\emptyset) + w_{o,x}(y_{,s}sin\emptyset + z_{,s}\,cos\,\emptyset) + (yz_{,s} - zy_{,s})\cdot\emptyset_{,x}\Big\} \quad \text{(Eq. 2.83)}$$

Assumption1: Vlasov theory of zero shear strain is extended to geometric nonlinear singly-symmetric cross-section member analysis.

$$\mathrm{E}_{xs} = 0 \quad \text{(Eq. 2.84)}$$

Assumption 2:

$$u_{,x} \ll 1 \quad \text{(Eq. 2.85)}$$

Given Eqs. 2.84 and 2.85, E may be written as

$$0 = \Big\{u_{,s} + v_{o,x}(-z_{,s}sin\emptyset + y_{,s}\,cos\,\emptyset) + w_{o,x}(y_{,s}sin\emptyset + z_{,s}\,cos\,\emptyset) + (yz_{,s} - zy_{,s})\cdot\emptyset_{,x}\Big\}$$

$$u_{,s} = -\Big(v_{o,x}(-z_{,s}sin\emptyset + y_{,s}\,cos\,\emptyset) + w_{o,x}(y_{,s}sin\emptyset + z_{,s}\,cos\,\emptyset) + (yz_{,s} - zy_{,s})\cdot\emptyset_{,x}\Big) \quad \text{(Eq. 2.86)}$$

To calculate the axial displacement, the integration of Eq. 2.86 with respect to the cross-section parameter s is required and is given by

$$u = \int_s u_{,s}\; ds = v_{o,x}zsin\emptyset - v_{o,x}ycos\emptyset - w_{o,x}ysin\emptyset - w_{o,x}zcos\emptyset - \int_s (yz_{,s} - zy_{,s})\; ds\cdot\emptyset_{,x} + C \quad \text{(Eq. 2.87)}$$

From the boundary condition $u(0) = u_o(x) = C$, Eq. 2.87 is given by

$$u = u_o - y\left(v_{o,x}\cos\emptyset + w_{o,x}sin\emptyset\right) - z\left(w_{o,x}\cos\emptyset - v_{o,x}sin\emptyset\right)$$

$$-\int_s \left(yz_{,s} - zy_{,s}\right)\, ds \cdot \emptyset_{,x} \qquad \text{(Eq. 2.88)}$$

For the convenience of the following derivation, Eq. 2.88 may be written as

$$u = u_o - y\alpha_z - z\alpha_y - \omega \cdot \emptyset_{,x} \qquad \text{(Eq. 2.89)}$$

where:

$$\alpha_z = v_{o,x}\cos\emptyset + w_{o,x}sin\emptyset$$

$$\alpha_y = w_{o,x}\cos\emptyset - v_{o,x}sin\emptyset$$

$$\omega = \int_s \left(yz_{,s} - zy_{,s}\right) ds$$

$\alpha_z = \alpha_z(x), \alpha_y = \alpha_y(x), \text{and } \omega = \omega(x, \text{s})$

Green-Lagrange axial strain

$$\mathrm{E}_{xx} = \frac{1}{2}\left\{\begin{bmatrix}(1+u_{,x}) & (y_{,x}+v_{,x}) & (z_{,x}+w_{,x})\end{bmatrix}\begin{bmatrix}(1+u_{,x})\\(y_{,x}+v_{,x})\\(z_{,x}+w_{,x})\end{bmatrix} - \begin{bmatrix}1 & y_{,x} & z_{,x}\end{bmatrix}\begin{bmatrix}1\\y_{,x}\\z_{,x}\end{bmatrix}\right\}$$

$$\mathrm{E}_{xx} = \frac{1}{2}\left\{\left(1+u_{,x}\right)^2 + \left(y_{,x}+v_{,x}\right)^2 + \left(z_{,x}+w_{,x}\right)^2 - \left(1 + {y_{,x}}^2 + {z_{,x}}^2\right)\right\}$$

$$\mathrm{E} = \frac{1}{2}\left\{2\left(u_{,x} + y_{,x}v_{,x} + z_{,x}w_{,x}\right) + {u_{,x}}^2 + {v_{,x}}^2 + {w_{,x}}^2\right\}$$

$$\mathrm{E}_{xx} = \left(u_{,x} + y_{,x}v_{,x} + z_{,x}w_{,x}\right) + \frac{1}{2}\left\{{u_{,x}}^2 + {v_{,x}}^2 + {w_{,x}}^2\right\} \quad \text{(Eq. 2.90)}$$

Then, the derivative of the axial displacement in Eq. 2.88 with respect to longitudinal direction x is given by

$$\begin{aligned} u_{,x} = {} & u_{o,x} - y_{,x}\left(v_{o,x}\cos\emptyset + w_{o,x}\sin\emptyset\right) \\ & - y\left(v_{o,xx}\cos\emptyset - v_{o,x}\sin\emptyset\cdot\emptyset_{,x} + w_{o,xx}\sin\emptyset + w_{o,x}\cos\emptyset\cdot\emptyset_{,x}\right) \\ & - z_{,x}\left(w_{o,x}\cos\emptyset - v_{o,x}\sin\emptyset\right) \\ & - z\left(w_{o,xx}\cos\emptyset - w_{o,x}\sin\emptyset\cdot\emptyset_{,x} - v_{o,xx}\sin\emptyset - v_{o,x}\cos\emptyset\cdot\emptyset_{,x}\right) \\ & - \omega_{,x}\cdot\emptyset_{,x} - \omega\cdot\emptyset_{,xx} \end{aligned} \quad \text{(Eq. 2.91)}$$

The derivative of the axial displacement in Eq. 2.89 with respect to longitudinal direction x is given by

$$u_{,x} = u_{o,x} - y_{,x}\alpha_z - y\alpha_{z,x} - z_{,x}\alpha_y - z\alpha_{y,x} - \omega_{,x}\cdot\emptyset_{,x} - \omega\cdot\emptyset_{,xx} \quad \text{(Eq. 2.92)}$$

From Eq. 2.74, Eq. 2.75, and Eq. 2.91, the Green-Lagrange axial strain in Eq. 2.90 is given by

$$\begin{aligned} \mathrm{E}_{xx} = {} & \left(u_{,x} + y_{,x}v_{,x} + z_{,x}w_{,x}\right) \\ & + \frac{1}{2}\Big\{{u_{,x}}^2 + v_{,x}(v_{o,x} - z_{,x}\sin\emptyset - z\cos\emptyset\cdot\emptyset_{,x} - y_{,x}(1-\cos\emptyset) - y\sin\emptyset \\ & \cdot\emptyset_{,x}) + w_{,x}(w_{o,x} + y_{,x}\sin\emptyset + y\cos\emptyset\cdot\emptyset_{,x} - z_{,x}(1-\cos\emptyset) - z\sin\emptyset \\ & \cdot\emptyset_{,x})\Big\} \end{aligned}$$

$$\mathrm{E}_{xx} = u_{,x}\left(1+\frac{1}{2}u_{,x}\right) + \frac{1}{2}\Big\{v_{,x}(v_{o_{,x}} - z_{,x}sin\emptyset - zcos\emptyset\cdot\emptyset_{,x} + 2y_{,x} - (y_{,x} - y_{,x}\cos\emptyset) - ysin\emptyset \cdot \emptyset_{,x}) + w_{,x}(w_{o_{,x}} + y_{,x}sin\emptyset + ycos\emptyset\cdot\emptyset_{,x} + 2z_{,x} - (z_{,x} - z_{,x}\cos\emptyset) - zsin\emptyset\cdot\emptyset_{,x})\Big\}$$

$$\mathrm{E}_{xx} = u_{,x}\left(1+\frac{1}{2}u_{,x}\right) + \frac{1}{2}\Big\{\left(v_{o_{,x}}\right)^2 + \left(w_{o_{,x}}\right)^2\Big\} + (z_{,x}y - y_{,x}z)\emptyset_{,x} + \frac{1}{2}(z^2+y^2)\left(\emptyset_{,x}\right)^2 + \left(z_{,x} + y\emptyset_{,x}\right)\left(w_{o_{,x}}\cos\emptyset - v_{o_{,x}}sin\emptyset\right) - (\mathrm{z}\emptyset_{,x} - y_{,x})(v_{o_{,x}}\cos\emptyset + w_{o_{,x}}sin\emptyset)$$

$$\mathrm{E}_{xx} = u_{,x}\left(1+\frac{1}{2}u_{,x}\right) + \frac{1}{2}\Big\{\left(v_{o_{,x}}\right)^2 + \left(w_{o_{,x}}\right)^2\Big\} + (z_{,x}y - y_{,x}z)\emptyset_{,x} + \frac{1}{2}(z^2+y^2)\left(\emptyset_{,x}\right)^2 + \left(z_{,x} + y\emptyset_{,x}\right)\alpha_y - (\mathrm{z}\emptyset_{,x} - y_{,x})\alpha_z \qquad \text{(Eq. 2.93)}$$

From the assumption 2 (Eq. 2.85), the Green-Lagrange axial strain in Eq. 2.93 is given by

$$\mathrm{E}_{xx} = u_{,x} + \frac{1}{2}\Big\{\left(v_{o_{,x}}\right)^2 + \left(w_{o_{,x}}\right)^2\Big\} + (z_{,x}y - y_{,x}z)\emptyset_{,x} + \frac{1}{2}(z^2+y^2)\left(\emptyset_{,x}\right)^2 + \left(z_{,x} + y\emptyset_{,x}\right)\alpha_y - (\mathrm{z}\emptyset_{,x} - y_{,x})\alpha_z \qquad \text{(Eq. 2.94)}$$

By inserting Eq. 2.92 into Eq. 2.94, the Green-Lagrange axial strain is given by

$$E_{xx} = u_{o,x} - \cancel{y_{,x}\alpha_z} - y\alpha_{z,x} - \cancel{z_{,x}\alpha_y} - z\alpha_{y,x} - \omega_{,x}\cdot\emptyset_{,x} - \omega\cdot\emptyset_{,xx}$$
$$+\frac{1}{2}\left\{\left(v_{o,x}\right)^2 + \left(w_{o,x}\right)^2\right\} + \left(z_{,x}y - y_{,x}z\right)\emptyset_{,x} + \frac{1}{2}(z^2+y^2)\left(\emptyset_{,x}\right)^2$$
$$+\left(\cancel{z_{,x}} + y\emptyset_{,x}\right)\alpha_y - (z\emptyset_{,x} - \cancel{y_{,x}})\alpha_z$$

$$E_{xx} = u_{o,x} - y\alpha_{z,x} - z\alpha_{y,x} - \omega_{,x}\cdot\emptyset_{,x} - \omega\cdot\emptyset_{,xx} + \frac{1}{2}\left\{\left(v_{o,x}\right)^2 + \left(w_{o,x}\right)^2\right\}$$
$$+\left(z_{,x}y - y_{,x}z\right)\emptyset_{,x} + \frac{1}{2}(z^2+y^2)\left(\emptyset_{,x}\right)^2 + y\emptyset_{,x}\alpha_y - z\emptyset_{,x}\alpha_z$$

$$E_{xx} = u_{o,x} - y\alpha_{z,x} - z\alpha_{y,x} - \omega\cdot\emptyset_{,xx} + \frac{1}{2}\left\{\left(v_{o,x}\right)^2 + \left(w_{o,x}\right)^2\right\} + \left(z_{,x}y - y_{,x}z - \omega_{,x}\right)$$
$$\cdot\emptyset_{,x} + \frac{1}{2}(z^2+y^2)\left(\emptyset_{,x}\right)^2 + y\emptyset_{,x}\alpha_y - z\emptyset_{,x}\alpha_z \qquad \text{(Eq. 2.95)}$$

From Eq. 2.95, the following equation is derived:

$$-y\alpha_{z,x} - z\alpha_{y,x} + y\emptyset_{,x}\alpha_y - z\emptyset_{,x}\alpha_z$$
$$= -y\left(v_{o,xx}\cos\emptyset - \cancel{v_{o,x}\sin\emptyset\,\emptyset_{,x}} + w_{o,xx}\sin\emptyset + \cancel{w_{o,x}\cos\emptyset\emptyset_{,x}}\right)$$
$$- z\left(w_{o,xx}\cos\emptyset - \cancel{w_{o,x}\sin\emptyset\emptyset_{,x}} - v_{o,xx}\sin\emptyset - \cancel{v_{o,x}\cos\emptyset\emptyset_{,x}}\right)$$
$$+ y\emptyset_{,x}(\cancel{w_{o,x}\cos\emptyset} - \cancel{v_{o,x}\sin\emptyset}) - z\emptyset_{,x}(\cancel{v_{o,x}\cos\emptyset} + \cancel{w_{o,x}\sin\emptyset})$$

$$-y\alpha_{z,x} - z\alpha_{y,x} + y\emptyset_{,x}\alpha_y - z\emptyset_{,x}\alpha_z$$
$$= -y\left(v_{o,xx}\cos\emptyset + w_{o,xx}\sin\emptyset\right)$$
$$- z\left(w_{o,xx}\cos\emptyset - v_{o,xx}\sin\emptyset\right) \qquad \text{(Eq. 2.96)}$$

By inserting Eq. 2.96 into Eq. 2.95, the Green-Lagrange axial strain is expressed as

$$\mathrm{E}_{xx} = u_{o,x} - y\left(v_{o,xx}\cos\emptyset + w_{o,xx}\sin\emptyset\right) - z\left(w_{o,xx}\cos\emptyset - v_{o,xx}\sin\emptyset\right) - \omega\cdot\emptyset_{,xx}$$
$$+\frac{1}{2}\left\{\left(v_{o,x}\right)^2 + \left(w_{o,x}\right)^2\right\} - \left(-z_{,x}y + y_{,x}z + \omega_{,x}\right)\cdot\emptyset_{,x}$$
$$+\frac{1}{2}(z^2+y^2)\left(\emptyset_{,x}\right)^2 \qquad \text{(Eq. 2.97)}$$

Assumption 3: Small displacement,

$$\sin\emptyset \cong \emptyset; \cos\emptyset \cong 1$$

From this assumption, the nonlinear Green-Lagrange axial strain in Eq. 2.97 is simplified to

$$\mathrm{E}_{xx} = u_{o,x} - \left(yv_{o,xx} + zw_{o,xx}\right) + \bar{\omega}\emptyset_{,xx} + \left(\bar{\omega}_{,x} - y_{,x}z + z_{,x}y\right)\emptyset_{,x}$$
$$+\frac{1}{2}\left\{\left(v_{o,x}\right)^2 + \left(w_{o,x}\right)^2\right\} + \left(zv_{o,xx} - yw_{o,xx}\right)\emptyset$$
$$+\frac{1}{2}(z^2+y^2)\left(\emptyset_{,x}\right)^2 \qquad \text{(Eq. 2.98)}$$

where:

$\bar{\omega} = \int_s \left(y_{,s}\cdot z - z_{,s}\cdot y\right)\, ds,$

$\bar{\omega}_{,x} - y_{,x}z + z_{,x}y = \psi(x,s)$: Tapering parameter

The above derivation possesses a key assumption which is zero Green-Lagrange shear strain $\mathrm{E}_{xs} = 0$ from Vlasov assumption. From this assumption, the nonlinear Green-Lagrange axial strain is given by Eq. 2.98. This is the same strain expression presented by Ronagh (2000a) and by Chang (2006).

In Eq. 2.98, the causes of the axial strain can be explained as follows:

$u_{o,x}$ = Axial strain due to elongation

$-\left(yv_{o,xx} + zw_{o,xx}\right)$ = Axial strain due to bending with respect y and z axis.

$\bar{\omega}\emptyset_{,xx}$ = Axial strain due to cross-section warping.

$\left(\bar{\omega}_{,x} - y_{,x}z + z_{,x}y\right)\emptyset_{,x}$ = Nonprismatic member effects associated with warping.

$\frac{1}{2}\left\{\left(v_{o,x}\right)^2 + \left(w_{o,x}\right)^2\right\}$ = Coupling between axial strain and bending.

$\left(zv_{o,xx} - yw_{o,xx}\right)\emptyset$ = Coupling between axial strain and combined bending and torsion.

$\frac{1}{2}(z^2 + y^2)\left(\emptyset_{,x}\right)^2$ = Wagner effect, coupling between axial strain and torsion.

The shear strain due to uniform (St. Venant) torsion is considered to obtain the total strains and is taken as

$$\gamma = -2\hat{\gamma}\emptyset_{,x} \qquad \text{(Eq. 2.99)}$$

2.5.4 Variation in the Strain Tensor

The variation of the Green-Lagrange strain in Eq. 2.98 is given by

$$\delta \mathrm{E}_{xx} = \delta u_{o,x} - \left(y\delta v_{o,xx} + z\delta w_{o,xx}\right) + \bar{\omega}\delta\emptyset_{,xx} + \left(\bar{\omega}_{,x} - y_{,x}z + z_{,x}y\right)\delta\emptyset_{,x} + \left\{v_{o,x}\delta v_{o,x} + w_{o,x}\delta w_{o,x}\right\} + \left(z\delta v_{o,xx} - y\delta w_{o,xx}\right)\emptyset + \left(zv_{o,xx} - yw_{o,xx}\right)\delta\emptyset + (z^2 + y^2)\emptyset_{,x}\delta\emptyset_{,x} \quad \text{(Eq. 2.100)}$$

$$\delta \mathrm{E}_{xx} = \left(\delta u_{o,x} + v_{o,x}\delta v_{o,x} + w_{o,x}\delta w_{o,x}\right) - y\left(\delta v_{o,xx} + \emptyset\delta w_{o,xx} + w_{o,xx}\delta\emptyset\right) + z\left(\emptyset\delta v_{o,xx} - \delta w_{o,xx} + v_{o,xx}\delta\emptyset\right) + (y^2 + z^2)\emptyset_{,x}\delta\emptyset_{,x} + \bar{\omega}\delta\emptyset_{,xx} + \left(\bar{\omega}_{,x} - y_{,x}z + z_{,x}y\right)\delta\emptyset_{,x} \quad \text{(Eq. 2.101)}$$

The variation of the shear strain due to uniform torsion in Eq. 2.99 is given by

$$\delta\gamma = -2\hat{\gamma}\delta\emptyset_{,x} \quad \text{(Eq. 2.102)}$$

Thus, the total strain tensor is given by

$$\delta\mathbf{E} = \begin{bmatrix} \delta \mathrm{E}_{xx} \\ \delta\gamma \end{bmatrix} \quad \text{(Eq. 2.103)}$$

Based on Eqs. 2.100 and 2.101, Eq. 2.103 may be written as

$$\delta\mathbf{E} = \begin{bmatrix} 1 & -y & z(y^2 + z^2) & \bar{\omega} & \psi \\ 0 & 0 & 0 & 0 & -2\hat{\gamma} \end{bmatrix} \begin{bmatrix} \left(\delta u_{o,x} + v_{o,x}\delta v_{o,x} + w_{o,x}\delta w_{o,x}\right) \\ \left(\delta v_{o,xx} + \emptyset\delta w_{o,xx} + w_{o,xx}\delta\emptyset\right) \\ \left(\emptyset\delta v_{o,xx} - \delta w_{o,xx} + v_{o,xx}\delta\emptyset\right) \\ \emptyset_{,x}\delta\emptyset_{,x} \\ \delta\emptyset_{,xx} \\ \delta\emptyset_{,x} \end{bmatrix} \quad \text{(Eq. 2.104)}$$

where:

- $\psi = \left(\overline{\omega}_{,x} - y_{,x}z + z_{,x}y\right)$

Equation 2.104 may be written as

$$\delta\mathbf{E} = \mathbf{WV}\begin{bmatrix} \delta u_{o,x} \\ \delta v_{o,x} \\ \delta w_{o,x} \\ \delta v_{o,xx} \\ \delta w_{o,xx} \\ \delta\emptyset \\ \delta\emptyset_{,x} \\ \delta\emptyset_{,xx} \end{bmatrix} \qquad \text{(Eq. 2.105)}$$

where,

- $\mathbf{W} = \begin{bmatrix} 1 & -y & z(y^2 + z^2) & \overline{\omega} & \psi \\ 0 & 0 & 0 & 0 & -2\hat{\gamma} \end{bmatrix}$
- $\mathbf{V} = \begin{bmatrix} 1 & v_{o,x} & w_{o,x} & 0 & 0 & 0 & 0 & 0 \\ 0 & 0 & 0 & 1 & \emptyset & w_{o,xx} & 0 & 0 \\ 0 & 0 & 0 & \emptyset & -1 & v_{o,xx} & 0 & 0 \\ 0 & 0 & 0 & 0 & 0 & 0 & \emptyset_{,x} & 0 \\ 0 & 0 & 0 & 0 & 0 & 0 & 0 & 1 \\ 0 & 0 & 0 & 0 & 0 & 0 & 1 & 0 \end{bmatrix}$

2.6 Co-Rotational Finite Element Analysis Theory

2.6.1 Co-Rotational Concept

The current research employs a Total Lagrangian co-rotational (TLCR) formulation. This approach has to the following advantages:

- It reduces the number of operations involved in the element calculations substantially for elements with a small number of degrees of freedom.
- Kinematic simplifications can be applied over a larger range of cases within the co-rotational frame:
    - For elements with rotational degrees of freedom:
        - Standard linear axial displacement and cubic transverse displacement interpolation can be used within the co-rotational frame without any significant loss of accuracy, for small deformation problems.
        - Small curvature expressions are applicable for a wider range of deformations within the co-rotational frame.

The co-rotational formulation concept is illustrated in Figure 2.7. The element displacements are separated into a set of degrees of freedom (dofs) describing rigid-body motion of the element frame and a set of dofs describing the actual element deformations (the element co-rotational degrees of freedom in the co-rotational frame. Given the element nodal displacements in the fixed global coordinate system (which includes element rigid-body motion), one obtains the element nodal displacements in the element

co-rotational frame (which do not include any effect from element rigid-body motion) as well as the rigid-body motion of the co-rotational frame. The base element calculations (generation of the element tangent stiffness matrices and recovery of element nodal forces) are performed corresponding to the co-rotational dofs within the co-rotational frame.

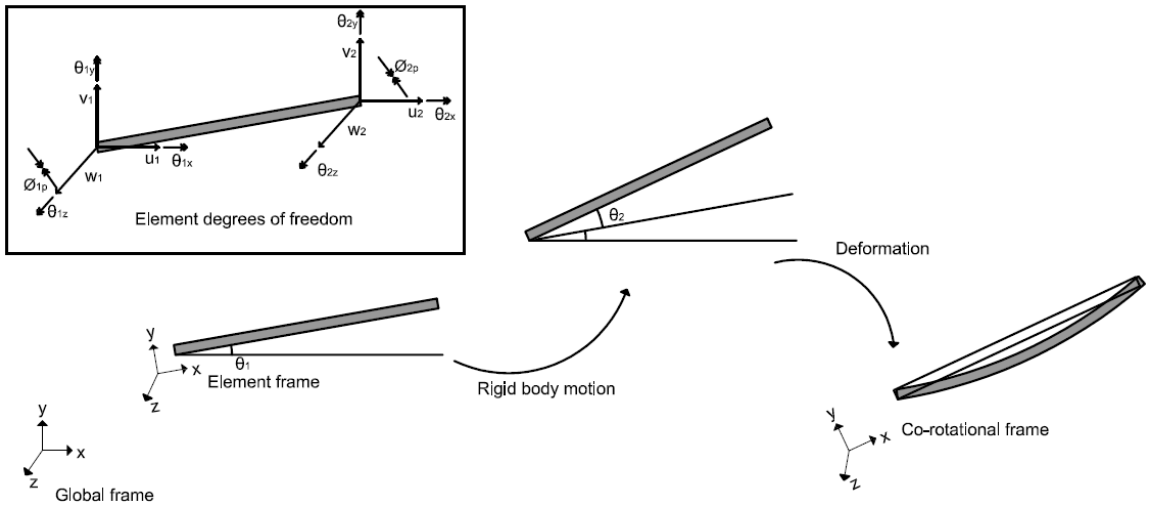

Figure 2.7 Concept of co-rotational FEA formulation

2.6.2 Co-Rotational Kinematics

2.6.2.1 Frame transformations

In a co-rotational formulation, three coordinate systems or three frames are employed as shown in Figure 2.8:

- The global coordinate system or global frame: One global frame is employed for all the elements. The global frame is fixed.

- Element coordinate system or element frame: Each element has its own element frame, which is based on the model geometry in the reference configuration. The number of element frames is equal to the number of elements. The element frame is fixed in this research, since a Total Lagrangian description is used.
- The co-rotational coordinate system or co-rotational frame: Each element has its own element co-rotational frame. The movement of the co-rotational frame defines the rigid body motion of each element.

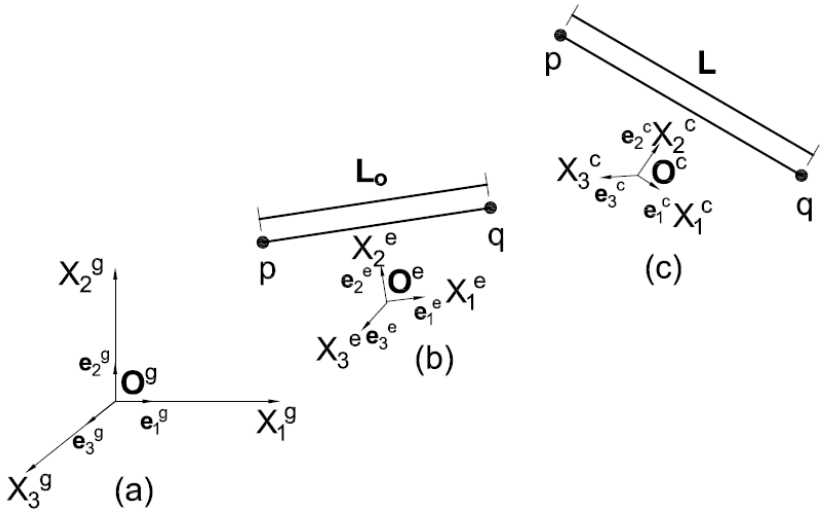

Figure 2.8 (a) Global coordinate system or global frame. (b) Element coordinate system or element frame. (c) Co-rotational coordinate system or co-rotational frame.

For implementation of the co-rotational formulation, transformations among three coordinate systems are needed. Figure 2.8 shows the three frames (i.e., coordinate

systems) with respect to each origin. The employed basis vectors are denoted by the following superscripts:

- Superscript c is representative of denotes the basis vectors of the co-rotational frame.
- Superscript e is representative of denotes the basis vectors of the element frame.
- Superscript g is representative of denotes the basis vectors of the global frame.

The three frames are each Cartesian which results in orthogonality of the basis vectors in each coordinate system. As shown in Figure 2.9, each frame can be expressed using the other coordinate systems as follows:

- In the global frame(frame (a) in Figure 2.8)
  - The global frame basis vectors are given by

$$\mathbf{e}_1{}^{g} = [1 \quad 0 \quad 0]^{T}$$

$$\mathbf{e}_2{}^{g} = [0 \quad 1 \quad 0]^{T}$$

$$\mathbf{e}_3{}^{g} = [0 \quad 0 \quad 1]^{T}$$

  - Element frame basis vectors is described by the transformation between the global frame and the element frame given by

$$\mathbf{r} = r_i{}^{g}\mathbf{e}_i{}^{g} = r_i{}^{e}\mathbf{e}_i{}^{e} \leftrightarrow r_i{}^{g}\mathbf{e}_i{}^{g} \cdot \mathbf{e}_j{}^{g} = r_i{}^{e}\mathbf{e}_i{}^{e} \cdot \mathbf{e}_j{}^{g} \leftrightarrow r_j{}^{g} = \mathbf{e}_j{}^{g} \cdot \mathbf{e}_i{}^{e} r_i{}^{e} = E_{ji}{}_{e}^{g} r_i{}^{e}$$

$$\mathbf{r}^{g} = \mathbf{E}_{e}^{g}\mathbf{r}^{e} \quad \text{so} \quad \mathbf{r}^{e} = \left(\mathbf{E}_{e}^{g}\right)^{T}\mathbf{r}^{g} \qquad \text{(Eq. 2.106)}$$

  - The co-rotational frame basis vectors is described by the transformation between the global frame and the co-rotational frame given by

$$\mathbf{r} = r_i{}^g \mathbf{e}_i{}^g = r_i{}^c \mathbf{e}_i{}^c \;\leftrightarrow\; r_i{}^g \mathbf{e}_i{}^g \cdot \mathbf{e}_j{}^g = r_i{}^c \mathbf{e}_i{}^c \cdot \mathbf{e}_j{}^g \;\leftrightarrow\; r_j{}^g = \mathbf{e}_j{}^g \cdot \mathbf{e}_i{}^c r_i{}^c = E_{ji}{}_c^g r_i{}^c$$

$$\mathbf{r}^g = \mathbf{E}_c^g \mathbf{r}^c \quad \text{so} \quad \mathbf{r}^c = \left(\mathbf{E}_c^g\right)^T \mathbf{r}^g \qquad \text{(Eq. 2.107)}$$

- In the element frame(frame (b) in Figure 2.8)
  - The element frame basis vectors are given by

$$\mathbf{e}_1{}^e = [1 \quad 0 \quad 0]^T$$

$$\mathbf{e}_2{}^e = [0 \quad 1 \quad 0]^T$$

$$\mathbf{e}_3{}^e = [0 \quad 0 \quad 1]^T$$

  - The co-rotational frame basis vectors is described by the transformation between the element frame and the co-rotational frame given by

$$\mathbf{r} = r_i{}^e \mathbf{e}_i{}^e = r_i{}^c \mathbf{e}_i{}^c \;\leftrightarrow\; r_i{}^e \mathbf{e}_i{}^e \cdot \mathbf{e}_j{}^e = r_i{}^c \mathbf{e}_i{}^c \cdot \mathbf{e}_j{}^e \;\leftrightarrow\; r_j{}^e = \mathbf{e}_j{}^e \cdot \mathbf{e}_i{}^c r_i{}^c = E_{ji}{}_c^e r_i{}^c$$

$$\mathbf{r}^e = \mathbf{E}_c^e \mathbf{r}^c \quad \text{so} \quad \mathbf{r}^c = (\mathbf{E}_c^e)^T \mathbf{r}^e \qquad \text{(Eq. 2.107)}$$

- In the co-rotational frame(frame (c) in Figure 2.8)
  - The co-rotational frame basis vectors are given by

$$\mathbf{e}_1{}^c = [1 \quad 0 \quad 0]^T$$

$$\mathbf{e}_2{}^c = [0 \quad 1 \quad 0]^T$$

$$\mathbf{e}_3{}^c = [0 \quad 0 \quad 1]^T$$

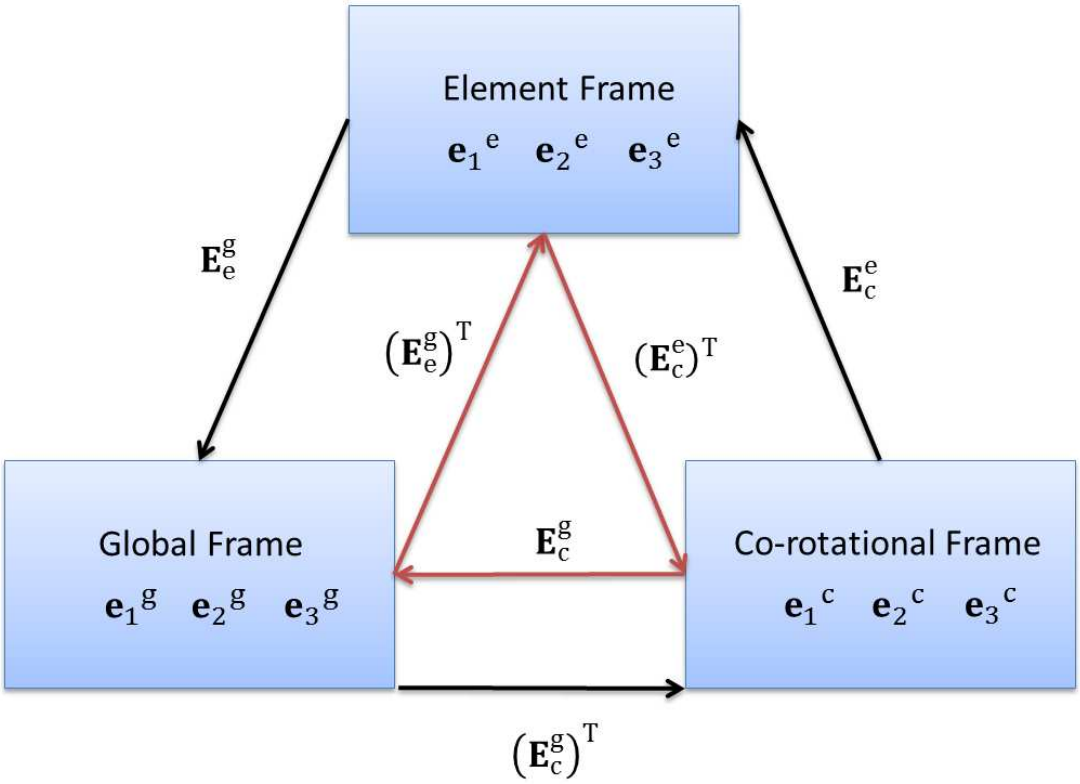

Figure 2.9 Transformation between different coordinate frames.

2.6.2.2 Element displacement vectors

The element displacement vectors with respect to the global frame, the element frame, and the co-rotational frame are shown in Figure 2.10 and expressed as

$$\mathbf{d}^g = \left\{u_{1p}^g \quad u_{2p}^g \quad u_{3p}^g \quad \theta_{1p}^g \quad \theta_{2p}^g \quad \theta_{3p}^g \quad \phi_p' \quad u_{1q}^g \quad u_{2q}^g \quad u_{3q}^g \quad \theta_{1q}^g \quad \theta_{2q}^g \quad \theta_{3q}^g \quad \phi_q'\right\}^T$$

$$\mathbf{d}^e = \left\{u_{1p}^e \quad u_{2p}^e \quad u_{3p}^e \quad \theta_{1p}^e \quad \theta_{2p}^e \quad \theta_{3p}^e \quad \phi_p' \quad u_{1q}^e \quad u_{2q}^e \quad u_{3q}^e \quad \theta_{1q}^e \quad \theta_{2q}^e \quad \theta_{3q}^e \quad \phi_q'\right\}^T$$

$$\mathbf{d}^c = \left\{e \quad \theta_{1p}^c \quad \theta_{3p}^c \quad \theta_{2p}^c \quad \phi_p' \quad \theta_{1q}^c \quad \theta_{3q}^c \quad \theta_{2q}^c \quad \phi_q'\right\}^T \qquad (\text{Eq. } 2.108)$$

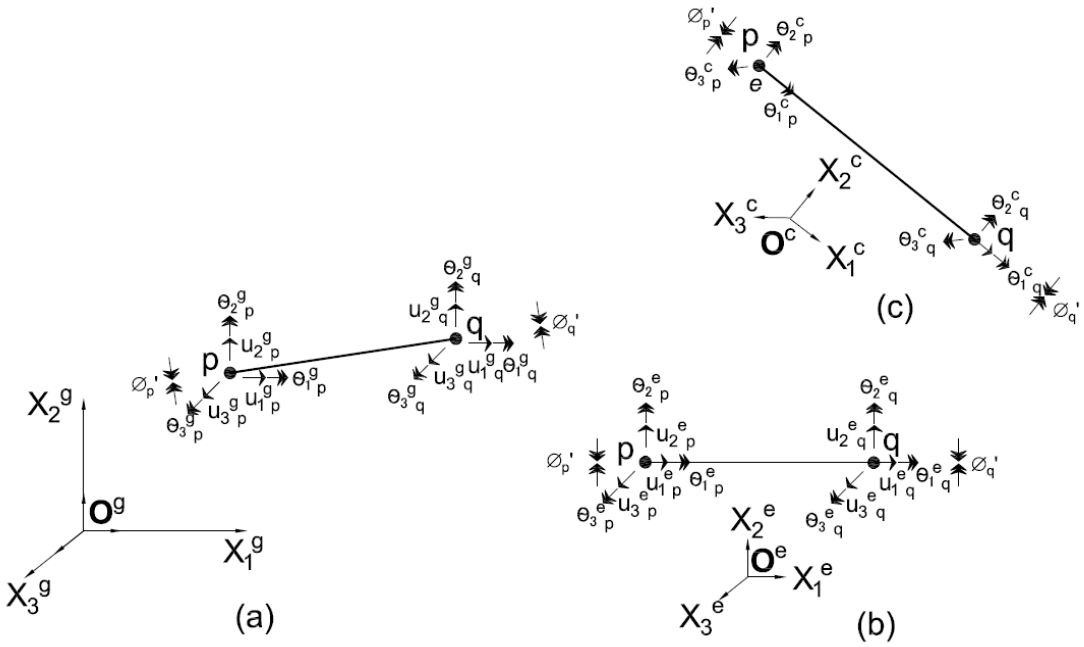

Figure 2.10 Employed element degrees of freedom with respect to different configurations

Each node in the global and element frames holds seven degrees of freedom which are three translations, three rotations, and one warping dof. Namely, each element holds 14 degrees of freedom. After removing the rigid body motions between the element frame and the co-rotational frame, each element holds nine degrees of freedom in its co-rotational frame which are composed of three rotations and one warping dof at node p, three rotations and one warping dof at node q, and one dof representing the elongation of the element.

The internal force vectors corresponding to the element displacement vectors are given by

$$\mathbf{F}^{g} = \left\{ F^{g}_{1_p} \;\; F^{g}_{2_p} \;\; F^{g}_{3_p} \;\; M^{g}_{1_p} \;\; M^{g}_{2_p} \;\; M^{g}_{3_p} \;\; B_p \;\; F^{g}_{1_q} \;\; F^{g}_{2_q} \;\; F^{g}_{3_q} \;\; M^{g}_{1_q} \;\; M^{g}_{2_q} \;\; M^{g}_{3_q} \;\; B_q \right\}^{T}$$

$$\mathbf{F}^{e} = \left\{ F^{e}_{1_p} \;\; F^{e}_{2_p} \;\; F^{e}_{3_p} \;\; M^{e}_{1_p} \;\; M^{e}_{2_p} \;\; M^{e}_{3_p} \;\; B_p \;\; F^{e}_{1_q} \;\; F^{e}_{2_q} \;\; F^{e}_{3_q} \;\; M^{e}_{1_q} \;\; M^{e}_{2_q} \;\; M^{e}_{3_q} \;\; B_q \right\}^{T}$$

$$\mathbf{F}^{c} = \left\{ P \;\; M^{c}_{1_p} \;\; M^{c}_{3_p} \;\; M^{c}_{2_p} \;\; B_p \;\; M^{c}_{1_q} \;\; M^{c}_{3_q} \;\; M^{c}_{2_q} \;\; B_q \right\}^{T} \qquad \text{(Eq. 2.109)}$$

The relationship between the element force and displacement vectors are given by the stiffness matrices and are defined as

$$\mathbf{F}^{g} = \mathbf{K}^{g}\mathbf{d}^{g} \qquad \text{(Eq. 2.110)}$$

$$\mathbf{F}^{e} = \mathbf{K}^{e}\mathbf{d}^{e} \qquad \text{(Eq. 2.111)}$$

$$\mathbf{F}^{c} = \mathbf{K}^{c}\mathbf{d}^{c} \qquad \text{(Eq. 2.112)}$$

2.6.2.3 Transformation of the element displacement and internal force vectors

As shown in Figure 2.11, the relationship between the displacement and internal force vectors within the element frames can be described by the coordinate **U**, projection **P**, and mapping **M** transformations, and is given by

$$\delta\mathbf{d}^{c} = \left(\frac{\delta\mathbf{d}^{c}}{\delta\mathbf{d}^{e}}\right)\delta\mathbf{d}^{e} = \mathbf{M}^{T}\mathbf{P}(\mathbf{U}^{e})^{T}\left(\frac{\delta\mathbf{d}^{e}}{\delta\mathbf{d}^{g}}\right)\delta\mathbf{d}^{g} = \mathbf{M}^{T}\mathbf{P}(\mathbf{U}^{e})^{T}(\mathbf{U}^{g})^{T}\delta\mathbf{d}^{g} \qquad \text{(Eq. 2.113)}$$

where:

$\mathbf{U}^{g}$: Coordinate transformation of the displacement and the internal force from the element frame to the global frame.

$\mathbf{U}^{e}$: Coordinate transformation of the displacement and the internal force from the co-rotational frame to the element frame.

P : Projection between the element frame and the co-rotational frame, which removes the element rigid body motions. The projection matrix may be described in the element frame for the co-rotational frame.

M : Mapping of the displacement and the internal force between the original degrees of freedom (14) and the reduced degrees of freedom (9).

From the transformation from the co-rotational frame to the global frame, the internal force vector in the global frame, based on work conjugacy, is obtained as

$$\mathbf{F}^{g} = (\mathbf{M}^{T}\mathbf{P}(\mathbf{U}^{e})^{T}(\mathbf{U}^{g})^{T})\mathbf{F}^{c} = \mathbf{U}^{g}\mathbf{U}^{e}\mathbf{P}^{T}\mathbf{M}\mathbf{F}^{c} \qquad \text{(Eq. 2.114)}$$

The variation of the internal force vector in global frame is then given by

$$\delta\mathbf{F}^{g} = \delta\mathbf{U}^{g}\mathbf{U}^{e}\mathbf{P}^{T}\mathbf{M}\mathbf{F}^{c} + \mathbf{U}^{g}\delta\mathbf{U}^{e}\mathbf{P}^{T}\mathbf{M}\mathbf{F}^{c} + \mathbf{U}^{g}\mathbf{U}^{e}\delta\mathbf{P}^{T}\mathbf{M}\mathbf{F}^{c} + \mathbf{U}^{g}\mathbf{U}^{e}\mathbf{P}^{T}\delta\mathbf{M}\mathbf{F}^{c}$$
$$+ \mathbf{U}^{g}\mathbf{U}^{e}\mathbf{P}^{T}\mathbf{M}\delta\mathbf{F}^{c} \qquad \text{(Eq. 2.115)}$$

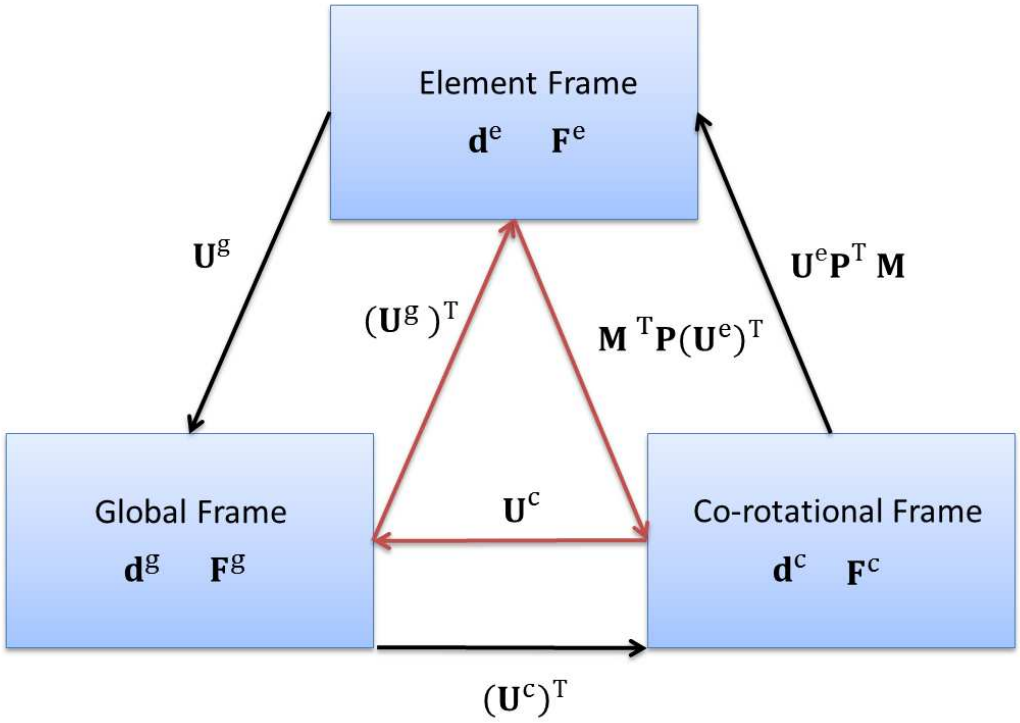

Figure 2.11 Conceptual representation of the transformation of the element displacement and internal force vectors

The variation of the internal force results in an additional geometric stiffness relative to the base element geometric stiffness in the co-rotational frame. The coordinate transformation between the displacement and the internal force from the element frame to the global frame is given by

$$\mathbf{U}^g = \begin{bmatrix} \mathbf{E}_e^g & \mathbf{0} & 0 & \mathbf{0} & \mathbf{0} & 0 \\ \mathbf{0} & \mathbf{E}_e^g & 0 & \mathbf{0} & \mathbf{0} & 0 \\ 0 & 0 & 1 & 0 & 0 & 0 \\ \mathbf{0} & \mathbf{0} & 0 & \mathbf{E}_e^g & \mathbf{0} & 0 \\ \mathbf{0} & \mathbf{0} & 0 & \mathbf{0} & \mathbf{E}_e^g & 0 \\ 0 & 0 & 0 & 0 & 0 & 1 \end{bmatrix} \qquad \text{(Eq. 2.116)}$$

Since both the global frame and the element frame are fixed in the Total Lagrangian description, the variation of the transformation matrix $\mathbf{U}^g$is vanishes, i.e.,

$$\delta \mathbf{U}^{g} = \mathbf{0} \qquad \text{(Eq. 2.117)}$$

Therefore, the first term of the variation of the internal force vector in Eq. 2.115 is vanished and is given by also vanishes, i.e.,

$$\delta \mathbf{U}^{g}\mathbf{U}^{e}\mathbf{P}^{T}\mathbf{M}\mathbf{F}^{c} = \mathbf{0} \qquad \text{(Eq. 2.118)}$$

The mapping matrix of the displacement and the internal force between the original degrees of freedom (14) and the reduced degrees of freedom (9) is

$$\mathbf{M} = \begin{bmatrix} 0 & 0 & 0 & 0 & 0 & 0 & 0 & 0 & 0 \\ 0 & 0 & 0 & 0 & 0 & 0 & 0 & 0 & 0 \\ 0 & 0 & 0 & 0 & 0 & 0 & 0 & 0 & 0 \\ 0 & 1 & 0 & 0 & 0 & 0 & 0 & 0 & 0 \\ 0 & 0 & 0 & 1 & 0 & 0 & 0 & 0 & 0 \\ 0 & 0 & 1 & 0 & 0 & 0 & 0 & 0 & 0 \\ 0 & 0 & 0 & 0 & 1 & 0 & 0 & 0 & 0 \\ 1 & 0 & 0 & 0 & 0 & 0 & 0 & 0 & 0 \\ 0 & 0 & 0 & 0 & 0 & 0 & 0 & 0 & 0 \\ 0 & 0 & 0 & 0 & 0 & 0 & 0 & 0 & 0 \\ 0 & 0 & 0 & 0 & 0 & 1 & 0 & 0 & 0 \\ 0 & 0 & 0 & 0 & 0 & 0 & 0 & 1 & 0 \\ 0 & 0 & 0 & 0 & 0 & 0 & 1 & 0 & 0 \\ 0 & 0 & 0 & 0 & 0 & 0 & 0 & 0 & 1 \end{bmatrix} \qquad \text{(Eq. 2.119)}$$

Therefore, the variation of the mapping matrix also vanishes and the fourth term of the variation of the internal force vector is zero:

$$\mathbf{U}^{g}\mathbf{U}^{e}\mathbf{P}^{T}\delta\mathbf{M}\mathbf{F}^{c} = \mathbf{0} \qquad \text{(Eq. 2.120)}$$

Given Eqs. 2.118 and 2.120, the variation of the internal force vector in Eq. 2.115is obtained as

$$\delta \mathbf{F}^{g} = \mathbf{U}^{g}\delta\mathbf{U}^{e}\mathbf{P}^{T}\mathbf{M}\mathbf{F}^{c} + \mathbf{U}^{g}\mathbf{U}^{e}\delta\mathbf{P}^{T}\mathbf{M}\mathbf{F}^{c} + \mathbf{U}^{g}\mathbf{U}^{e}\mathbf{P}^{T}\mathbf{M}\delta\mathbf{F}^{c} \qquad \text{(Eq. 2.121)}$$

2.6.2.4 Nodal triads

The element deformations in the co-rotational frame result in different coordinate systems between the two nodal points **p** and **q** in as illustrated in Figure 2.12. The element nodal triads in the co-rotational frame are given by

$$\mathbf{p}(\mathbf{e}^{p}{}_{1}, \mathbf{e}^{p}{}_{2}, \mathbf{e}^{p}{}_{3}) \qquad \text{(Eq. 2.122)}$$

and

$$\mathbf{q}(\mathbf{e}^{q}{}_{1}, \mathbf{e}^{q}{}_{2}, \mathbf{e}^{q}{}_{3}) \qquad \text{(Eq. 2.123)}$$

where:

p = The matrix composed of the components of the basis vectors of node p.

q = The matrix composed of the components of the basis vectors of node q.

The element co-rotational frame is taken as the average of the basis vectors of the nodal traids in this work, and is expressed as

$$\mathbf{E}_{c}^{e} = [\mathbf{e}_{1}{}^{c} \quad \mathbf{e}_{2}{}^{c} \quad \mathbf{e}_{3}{}^{c}] \qquad \text{(Eq. 2.124)}$$

The basis vectors in Eq. 2.122 are described precisely in Section 2.6.3.4.

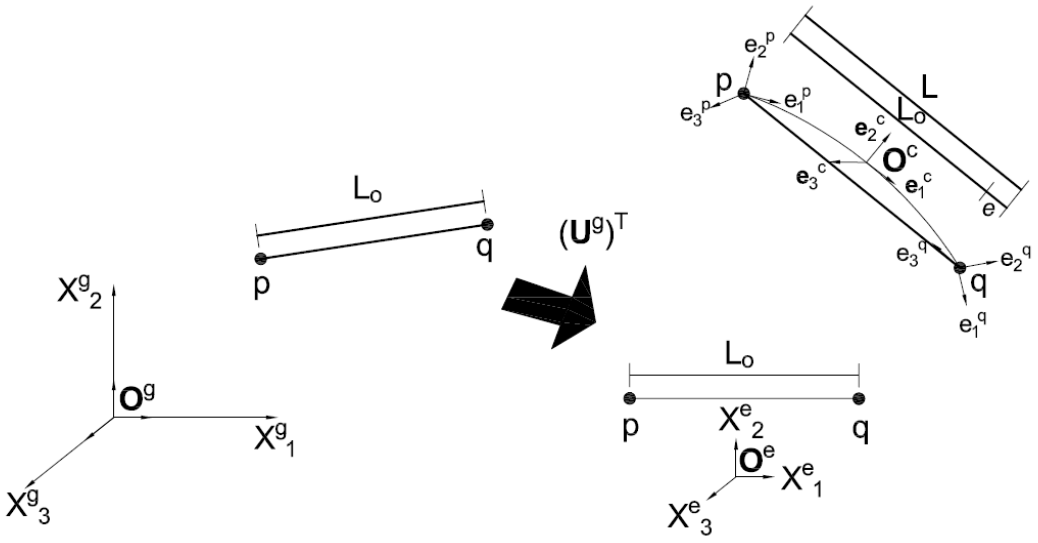

Figure 2.12 Concept of nodal traids

The element displacement vector in the co-rotational frame is given by Eq. 2.108. The specific terms in this vector are calculated as follows:

- The axial elongation in the element co-rotational frame is given by

$$e = L - L_o \qquad \text{(Eq. 2.125)}$$

where:

  - L : Element length in current configuration.
  - L_o : Element length in reference configuration.

- The rotational deformations (Crisfield 1990) at the two nodal points **p** and **q** in Figure 2.12 are given by

$$\theta^c_{1p} = \sin^{-1}\left(\frac{-(\mathbf{e}^p{}_3)^T\mathbf{e}_2{}^c + (\mathbf{e}^p{}_2)^T\mathbf{e}_3{}^c}{2}\right) \qquad \text{(Eq. 2.126)}$$

$$\theta^{c}_{3_p} = \sin^{-1}\left(\frac{-(\mathbf{e}^{p}{}_{2})^{T}\mathbf{e}_{1}{}^{c} + (\mathbf{e}_{2}{}^{c})^{T}\mathbf{e}^{p}{}_{1}}{2}\right) \quad \text{(Eq. 2.127)}$$

$$\theta^{c}_{2_p} = -\sin^{-1}\left(\frac{-(\mathbf{e}^{p}{}_{3})^{T}\mathbf{e}_{1}{}^{c} + (\mathbf{e}_{3}{}^{c})^{T}\mathbf{e}^{p}{}_{1}}{2}\right) \quad \text{(Eq. 2.128)}$$

$$\theta^{c}_{1_q} = \sin^{-1}\left(\frac{-(\mathbf{e}^{q}{}_{3})^{T}\mathbf{e}_{2}{}^{c} + (\mathbf{e}^{q}{}_{2})^{T}\mathbf{e}_{3}{}^{c}}{2}\right) \quad \text{(Eq. 2.129)}$$

$$\theta^{c}_{3_q} = \sin^{-1}\left(\frac{-(\mathbf{e}^{q}{}_{2})^{T}\mathbf{e}_{1}{}^{c} + (\mathbf{e}_{2}{}^{c})^{T}\mathbf{e}^{q}{}_{1}}{2}\right) \quad \text{(Eq. 2.130)}$$

$$\theta^{c}_{2_q} = -\sin^{-1}\left(\frac{-(\mathbf{e}^{q}{}_{3})^{T}\mathbf{e}_{1}{}^{c} + (\mathbf{e}_{3}{}^{c})^{T}\mathbf{e}^{q}{}_{1}}{2}\right) \quad \text{(Eq. 2.131)}$$

- The warping deformations ϕ'_p and ϕ'_q at two nodal points **p** and **q** are independent of the coordinate systems.

2.6.3 Key Equations Pertaining to the Element Displacements and Basis Vectors

2.6.3.1 Consideration of large displacements in the element configuration

Chang (2006) employs Rankin and Nour-Omid's (1988) projection operator to separate the element displacements into rigid-body motion and the actual element deformations. However, the derivation by Rankin and Nour-Omid does not explain the transformation between global frame and element frame. This research derives a new projection matrix employing Rankin and Nour-Omid's projector concept as an initial point of the derivation. Rankin and Nour-Omid employ one nodal traid as a current position vector. Since a co-rotational element is composed of two nodal points and each

nodal point can have a significant difference in its rotations, the projection matrix is derived based on two nodal points and the average rotations of the two nodal points are employed for the co-rotational element rotation.

The following derivations are based on nodal point P. As the concept are the same at each of the element end nodes, the following quantities derived for nodal point P are the same for nodal point Q in Figure 2.14.

As shown in Figure 2.13 for the element frame, the position vector $\mathbf{x}^{e}{}_{p}$ of a given material point in the current configuration is given by

$$\mathbf{x}^{e}{}_{p} = \mathbf{u}^{e}{}_{p} + \mathbf{X}^{e}{}_{p} \qquad \text{(Eq. 2.132)}$$

A vector $\overrightarrow{\mathbf{O}^{c}\mathbf{P}'}$ between the origin of the co-rotational frame and the current position $\mathbf{P}'$ is defined by $\mathbf{x}^{c}{}_{p}$ and is given by

- In co-rotational frame, using Eq. 2.107

$$\mathbf{x}^{c}{}_{p} = (\mathbf{E}_{c}^{e})^{T}\left(\mathbf{x}^{e}{}_{p} - \mathbf{x}^{e}{}_{o}\right) \qquad \text{(Eq. 2.133)}$$

  where:

  - $\mathbf{E}_{c}^{e}$: The coordinate transformation matrix from the co-rotational frame to the element frame.

- In the element frame

$$\mathbf{x}^{c}{}_{p} = \left(\mathbf{x}^{e}{}_{p} - \mathbf{x}^{e}{}_{o}\right) \qquad \text{(Eq. 2.134)}$$

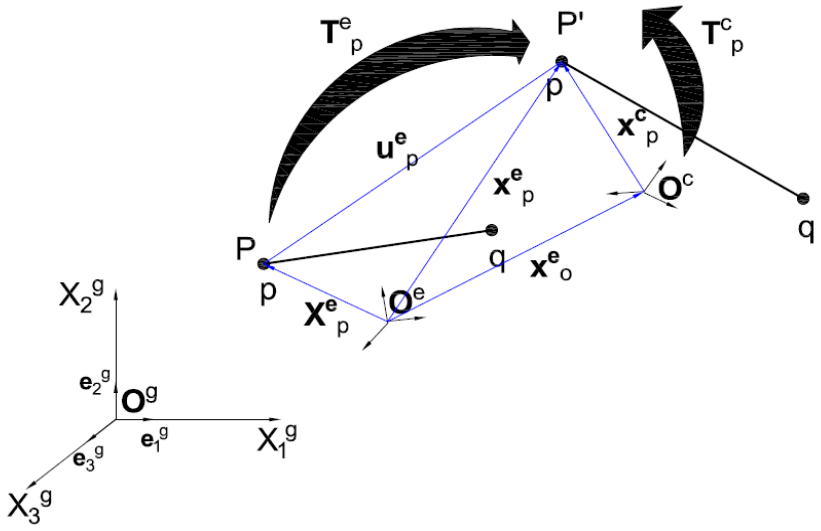

Figure 2.13 Transformation of node **p** with respect to element frame and co-rotational frame

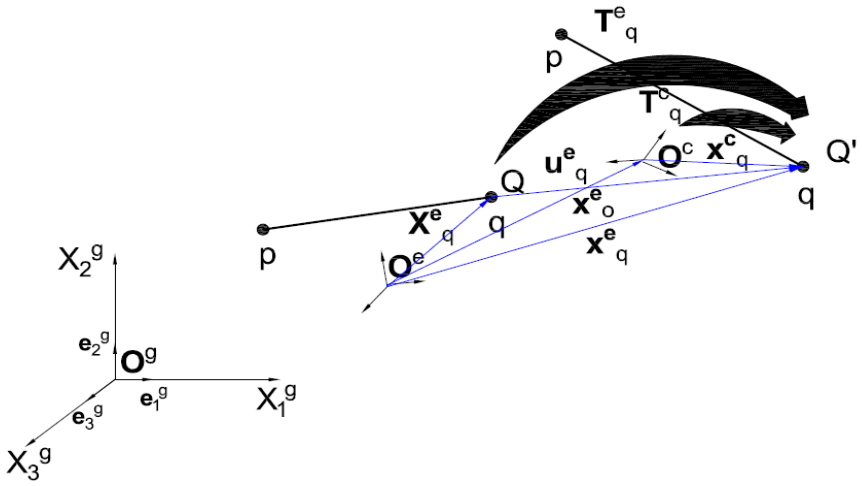

Figure 2.14 Transformation of node **q** with respect to element frame and co-rotational frame

The displacement between the deformed element and the un-deformed element in the co-rotational frame is given by

$$\mathbf{u}^{c}{}_{p} = (\mathbf{E}_{c}^{e})^{T}\left(\mathbf{x}^{e}{}_{p} - \mathbf{x}^{e}{}_{o}\right) - \mathbf{X}^{e}{}_{p} \qquad \text{(Eq. 2.135)}$$

From Eq. 2.107, the transformation of the position vector $\mathbf{x}^{e}{}_{p}$ of a given material point from the reference configuration **P** to the current configuration **P′**can beis given by

$$\mathbf{T}^{c}{}_{p} = (\mathbf{E}_{c}^{e})^{T}\mathbf{T}^{e}{}_{p} \qquad \text{(Eq. 2.136)}$$

2.6.3.2 Variation of the displacement vector and the transformation tensor

The variation of the displacement vector $\mathbf{u}^{c}{}_{p}$ in the co-rotational frame is given by

$$\delta\mathbf{u}^{c}{}_{p} = (\delta\mathbf{E}_{c}^{e})^{T}\left(\mathbf{x}^{e}{}_{p} - \mathbf{x}^{e}{}_{o}\right) + (\mathbf{E}_{c}^{e})^{T}\left(\delta\mathbf{x}^{e}{}_{p} - \delta\mathbf{x}^{e}{}_{o}\right) - \delta\mathbf{X}^{e}{}_{p} \qquad \text{(Eq. 2.137)}$$

Since $\mathbf{X}^{e}{}_{p}$ is fixed,

$$\delta\mathbf{X}^{e}{}_{p} = 0 \qquad \text{(Eq. 2.138)}$$

Using Eq. 2.138, Eq. 2.137 may be expressed as

$$\delta\mathbf{u}^{c}{}_{p} = (\delta\mathbf{E}_{c}^{e})^{T}\left(\mathbf{x}^{e}{}_{p} - \mathbf{x}^{e}{}_{o}\right) + (\mathbf{E}_{c}^{e})^{T}\left(\delta\mathbf{x}^{e}{}_{p} - \delta\mathbf{x}^{e}{}_{o}\right) \qquad \text{(Eq. 2.139)}$$

From Eq. 2.36 and Eq. 2.42, the spin tensor of the variation of the axial vector $\boldsymbol{\omega}_{E}{}^{e}$ is given by

$$\delta\boldsymbol{\Omega}_{\mathbf{E}_{c}^{e}} = \mathbf{Spin}(\delta\boldsymbol{\omega}_{E}{}^{e}) = \delta\mathbf{E}_{c}^{e}(\mathbf{E}_{c}^{e})^{T} \qquad \text{(Eq. 2.140)}$$

where:

- $\boldsymbol{\omega}_E{}^e$: Axial vector corresponding to the coordinate transformation between the element frame and the co-rotational frame, expressed in the element frame.

Using Eq. 2.140, Eq. 2.139 is given by

$$\delta\mathbf{u}^c{}_p = (\mathbf{Spin}(\delta\boldsymbol{\omega}_E{}^e)\mathbf{E}_c^e)^T\left(\mathbf{x}^e{}_p - \mathbf{x}^e{}_o\right) + (\mathbf{E}_c^e)^T\left(\delta\mathbf{x}^e{}_p - \delta\mathbf{x}^e{}_o\right)$$

$$\delta\mathbf{u}^c{}_p = -(\mathbf{E}_c^e)^T\mathbf{Spin}(\delta\boldsymbol{\omega}_E{}^e)\mathbf{E}_c^e(\mathbf{E}_c^e)^T\left(\mathbf{x}^e{}_p - \mathbf{x}^e{}_o\right) + (\mathbf{E}_c^e)^T\left(\delta\mathbf{x}^e{}_p - \delta\mathbf{x}^e{}_o\right) \quad (\text{Eq. } 2.141)$$

In the element frame, the variation of the displacement vector $\mathbf{u}^c{}_p$ can be given by

$$\delta\mathbf{u}^c{}_p = \left(-\mathbf{Spin}(\delta\boldsymbol{\omega}_E{}^e)\left(\mathbf{x}^e{}_p - \mathbf{x}^e{}_o\right) + \left(\delta\mathbf{x}^e{}_p - \delta\mathbf{x}^e{}_o\right)\right)$$

$$\delta\mathbf{u}^c{}_p = \mathbf{Spin}\left(\mathbf{x}^e{}_p - \mathbf{x}^e{}_o\right)\delta\boldsymbol{\omega}_E{}^e + \left(\delta\mathbf{x}^e{}_p - \delta\mathbf{x}^e{}_o\right) \quad (\text{Eq. } 2.142)$$

The spin tensor of the variation of the axial vector, the current position vector, and the variation of the current position in the co-rotational frame and in the element frame are shown in Table 2.1.

Table 2.1 The spin tensor of the variation of the axial vector, the current position vector, and the variation of the current position in the co-rotational frame and in the element frame.

In the co-rotational frame	In the element frame
$(\mathbf{E}_c^e)^T\mathbf{Spin}(\delta\boldsymbol{\omega}_E{}^e)\mathbf{E}_c^e$	$\mathbf{Spin}(\delta\boldsymbol{\omega}_E{}^e)$
$(\mathbf{E}_c^e)^T\left(\mathbf{x}^e{}_p - \mathbf{x}^e{}_o\right)$	$\left(\mathbf{x}^e{}_p - \mathbf{x}^e{}_o\right)$
$(\mathbf{E}_c^e)^T\left(\delta\mathbf{x}^e{}_p - \delta\mathbf{x}^e{}_o\right)$	$\left(\delta\mathbf{x}^e{}_p - \delta\mathbf{x}^e{}_o\right)$

Using the coordinate transformation matrix from the co-rotational frame to the element frame $\mathbf{E}_c^e$, the components of the various element tensors can be expressed in the different coordinate systems.

The variation of the transformation $\mathbf{T}^c{}_p$ in the co-rotational frame is given by

$$\delta\mathbf{T}^c{}_p = \delta(\mathbf{E}_c^e)^T\mathbf{T}^e{}_p + (\mathbf{E}_c^e)^T\delta\mathbf{T}^e{}_p \qquad (\text{Eq. } 2.143)$$

From Eq. 2.36 and Eq. 2.42, the spin tensor of the variation of the axial vector $\boldsymbol{\omega}_p{}^e$ is given by

$$\delta\boldsymbol{\Omega}_{\mathbf{T}^e{}_p} = \mathbf{Spin}\left(\delta\boldsymbol{\omega}_p{}^e\right) = \delta\mathbf{T}^e{}_p\left(\mathbf{T}^e{}_p\right)^T \qquad (\text{Eq. } 2.144)$$

where:

- $\boldsymbol{\omega}_p{}^e$: Axial vector with respect to the transformation of the position vector $\mathbf{x}^e{}_p$ of a given material point from the element frame to the current configuration $\mathbf{P}'$, expressed in the element frame.

Using Eq. 2.144, Eq. 2.143 may be expressed as

$$\delta\mathbf{T}^c{}_p = (\mathbf{Spin}(\delta\boldsymbol{\omega}_E{}^e)(\mathbf{E}_c^e))^T\mathbf{T}^e{}_p + (\mathbf{E}_c^e)^T\left(\mathbf{Spin}\left(\delta\boldsymbol{\omega}^e{}_p\right)\mathbf{T}^e{}_p\right)$$

$$\delta\mathbf{T}^c{}_p = -(\mathbf{E}_c^e)^T\mathbf{Spin}(\delta\boldsymbol{\omega}_E{}^e)\mathbf{T}^e{}_p + (\mathbf{E}_c^e)^T\left(\mathbf{Spin}\left(\delta\boldsymbol{\omega}^e{}_p\right)\mathbf{T}^e{}_p\right)$$

$$\delta\mathbf{T}^c{}_p = (\mathbf{E}_c^e)^T\left(-\mathbf{Spin}(\delta\boldsymbol{\omega}_E{}^e) + \mathbf{Spin}\left(\delta\boldsymbol{\omega}^e{}_p\right)\right)\mathbf{T}^e{}_p$$

$$\delta\mathbf{T}^c{}_p = (\mathbf{E}_c^e)^T\left(-\mathbf{Spin}(\delta\boldsymbol{\omega}_E{}^e) + \mathbf{Spin}\left(\delta\boldsymbol{\omega}^e{}_p\right)\right)\mathbf{E}_c^e(\mathbf{E}_c^e)^T\mathbf{T}^e{}_p \qquad (\text{Eq. } 2.145)$$

Next, upon introducing Eq. 2.136, Eq. 2.145 may be expressed as

$$\delta \mathbf{T}^{c}{}_{p} = (\mathbf{E}_{c}^{e})^{T} \left(-\mathbf{Spin}(\delta \boldsymbol{\omega}_{E}{}^{e}) + \mathbf{Spin}\left(\delta \boldsymbol{\omega}^{e}{}_{p}\right) \right) \mathbf{E}_{c}^{e} \mathbf{T}^{c}{}_{p} \qquad (\text{Eq. } 2.146)$$

By multiplying by $(\mathbf{T}^{c}{}_{p})^{T}$ on both sides in Eq. 2.146 and recognizing that $\mathbf{T}^{c}{}_{p}(\mathbf{T}^{c}{}_{p})^{T} = \mathbf{I}$, Eq. 2.146 can be expressed as

$$\delta \mathbf{T}^{c}{}_{p}(\mathbf{T}^{c}{}_{p})^{T} = (\mathbf{E}_{c}^{e})^{T} \left(\mathbf{Spin}\left(\delta \boldsymbol{\omega}^{e}{}_{p} - \delta \boldsymbol{\omega}_{E}{}^{e}\right) \right) \mathbf{E}_{c}^{e} \qquad (\text{Eq. } 2.147)$$

In the element frame, the variation of the transformation $\mathbf{T}^{c}{}_{p}$ is given by

$$\delta \mathbf{T}^{c}{}_{p}(\mathbf{T}^{c}{}_{p})^{T} = \mathbf{Spin}\left(\delta \boldsymbol{\omega}^{e}{}_{p} - \delta \boldsymbol{\omega}_{E}{}^{e}\right) \qquad (\text{Eq. } 2.148)$$

In Table 2.2, the spin tensor of the variation of the axial vector is explained in the co-rotational frame and in the element frame.

Table 2.2 The spin tensor of the variation of the axial vector in the co-rotational frame and in the element frame.

In the co-rotational frame	In the element frame
$(\mathbf{E}_{c}^{e})^{T} \left(-\mathbf{Spin}(\delta \boldsymbol{\omega}_{E}{}^{e}) + \mathbf{Spin}\left(\delta \boldsymbol{\omega}^{e}{}_{p}\right) \right) \mathbf{E}_{c}^{e}$	$-\mathbf{Spin}(\delta \boldsymbol{\omega}_{E}{}^{e}) + \mathbf{Spin}\left(\delta \boldsymbol{\omega}^{e}{}_{p}\right)$

From Eq. 2.36 and Eq. 2.42, the spin tensor of the variation of the axial vector $\boldsymbol{\omega}_{p}{}^{c}$ is given by

$$\delta \boldsymbol{\Omega}_{\mathbf{T}^{c}{}_{p}} = \mathbf{Spin}\left(\delta \boldsymbol{\omega}_{p}{}^{c}\right) = \delta \mathbf{T}^{c}{}_{p}(\mathbf{T}^{c}{}_{p})^{T} \qquad (\text{Eq. } 2.149)$$

where:

- $\boldsymbol{\omega}_{\mathrm{p}}{}^{\mathrm{c}}$: Axial vector with respect to transformation of the position vector $\mathbf{x}^{\mathrm{c}}{}_{\mathrm{p}}$ of a given material point from the co-rotational frame to the current configuration $\mathbf{P}'$, expressed in the element frame.

From Eq. 2.148 and Eq. 2.149, the variation of the transformation $\mathbf{T}^{\mathrm{c}}{}_{\mathrm{p}}$ is given by

$$\delta\mathbf{T}^{\mathrm{c}}{}_{\mathrm{p}}(\mathbf{T}^{\mathrm{c}}{}_{\mathrm{p}})^{\mathrm{T}} = \mathbf{Spin}\left(\delta\boldsymbol{\omega}_{\mathrm{p}}{}^{\mathrm{c}}\right) = \mathbf{Spin}\left(\delta\boldsymbol{\omega}^{\mathrm{e}}{}_{\mathrm{p}} - \delta\boldsymbol{\omega}_{\mathrm{E}}{}^{\mathrm{e}}\right) \qquad (\text{Eq. } 2.150)$$

Lastly, the axial vector within the co-rotational frame is described by removing the axial vector of the coordinate transformation from the axial vector within element frame and is given by

$$\delta\boldsymbol{\omega}^{\mathrm{c}}{}_{\mathrm{p}} = \delta\boldsymbol{\omega}^{\mathrm{e}}{}_{\mathrm{p}} - \delta\boldsymbol{\omega}_{\mathrm{E}}{}^{\mathrm{e}} \qquad (\text{Eq. } 2.151)$$

2.6.3.3 Co-rotational basis vectors

In this work, the element co-rotational frame is calculated from the average of the basis vector of the two nodal traids **p** and **q** in Eq. 2.122 and Eq. 2.123.

The co-rotational basis vector along direction 1 in the element frame is given by

$$\mathbf{e}_1{}^{\mathbf{c}} = \frac{\mathbf{x}^{\mathrm{e}}{}_{\mathrm{q}} - \mathbf{x}^{\mathrm{e}}{}_{\mathrm{p}}}{\left|\mathbf{x}^{\mathrm{e}}{}_{\mathrm{q}} - \mathbf{x}^{\mathrm{e}}{}_{\mathrm{p}}\right|} = \frac{\mathbf{x}^{\mathrm{e}}{}_{\mathrm{q}} - \mathbf{x}^{\mathrm{e}}{}_{\mathrm{p}}}{\mathrm{L}} \qquad (\text{Eq. } 2.150)$$

where:

- L := Deformed or current element length, given by

$$\mathrm{L} = \sqrt{\left(\mathbf{x}^{\mathrm{e}}{}_{\mathrm{q}} - \mathbf{x}^{\mathrm{e}}{}_{\mathrm{p}}\right)^{T}\left(\mathbf{x}^{\mathrm{e}}{}_{\mathrm{q}} - \mathbf{x}^{\mathrm{e}}{}_{\mathrm{p}}\right)} \qquad (\text{Eq. } 2.151)$$

The average of the nodal traid basis vectors along direction 2 in the element frame is given by

$$\boldsymbol{y}_{avg} = \frac{\mathbf{e}_2{}^{\mathrm{p}} + \mathbf{e}_2{}^{\mathrm{q}}}{2} \qquad (\text{Eq. } 2.152)$$

GivenEqs. 2.150 and 2.152, the co-rotational basis vector along direction 3 in the element frame may be calculated as

$$\mathbf{e}_3{}^{\mathbf{c}} = \frac{\mathbf{e}_1{}^{\mathbf{c}} \times \boldsymbol{y}_{avg}}{\left|\mathbf{e}_1{}^{\mathbf{c}} \times \boldsymbol{y}_{avg}\right|} \qquad (\text{Eq. } 2.153)$$

where:

- $\mathbf{e}_1{}^{\mathbf{c}} \times \boldsymbol{y}_{avg} = \mathbf{Spin}(\mathbf{e}_1{}^{\mathbf{c}})\boldsymbol{y}_{avg} = -\mathbf{Spin}(\boldsymbol{y}_{avg})\mathbf{e}_1{}^{\mathbf{c}}$ (Eq. 2.154)
- $\mathbf{e}_1{}^{\mathbf{c}} \times \boldsymbol{y}_{avg} \quad or \quad \left(\varepsilon_{\mathrm{ijk}}\mathbf{e}_1{}^{\mathbf{c}}{}_{\mathrm{j}} y_{avg}{}_{\mathrm{k}}\right)\mathbf{e}_{\mathrm{i}}{}^{\mathbf{c}}$ (Eq. 2.155)

in which,

- i is representative of represents the direction 3 for $\mathbf{e}_3{}^{\mathbf{c}}$.
- j is representative represents the direction 1 for $\mathbf{e}_1{}^{\mathbf{c}}$.
- k is representative of represents the direction 2 for y_{avg}.

Equation 2.155 is expressed as

$$\left(\varepsilon_{312}\mathbf{e}_1{}^{\mathbf{c}}{}_1 y_{avg}{}_2\right)\mathbf{e}_3{}^{\mathbf{c}} = y_{avg}{}_2\mathbf{e}_3{}^{\mathbf{c}} \qquad (\text{Eq. } 2.156)$$

From Eq. 2.155 and Eq. 2.156 ,

$$y_{avg_2} = \left|\mathbf{e}_1{}^{\mathbf{c}} \times \boldsymbol{y}_{avg}\right| \qquad \text{(Eq. 2.157)}$$

Using Eq. 2.150 and Eq. 2.153 based on, the co-rotational basis vector along direction 2 in the element frame is given by

$$\mathbf{e}_2{}^{\mathbf{c}} = -\mathbf{e}_1{}^{\mathbf{c}} \times \mathbf{e}_3{}^{\mathbf{c}} \qquad \text{(Eq. 2.158)}$$

2.6.3.4 Variation of the co-rotational basis vectors

From Eq. 2.150, the variation of $\mathbf{e}_1{}^{\mathbf{c}}$ in the element frame is given by

$$\delta\mathbf{e}_1{}^{\mathbf{c}} = \frac{\delta\mathbf{x}^{\mathrm{e}}{}_{\mathrm{q}} - \delta\mathbf{x}^{\mathrm{e}}{}_{\mathrm{p}}}{\mathrm{L}} - \frac{\mathbf{x}^{\mathrm{e}}{}_{\mathrm{q}} - \mathbf{x}^{\mathrm{e}}{}_{\mathrm{p}}}{\mathrm{L}^2}\delta\mathrm{L}$$

$$\delta\mathbf{e}_1{}^{\mathbf{c}} = \frac{\delta\mathbf{x}^{\mathrm{e}}{}_{\mathrm{q}} - \delta\mathbf{x}^{\mathrm{e}}{}_{\mathrm{p}}}{\mathrm{L}} - \frac{\mathbf{x}^{\mathrm{e}}{}_{\mathrm{q}} - \mathbf{x}^{\mathrm{e}}{}_{\mathrm{p}}}{\mathrm{L}^2}\left(\left(\mathbf{x}^{\mathrm{e}}{}_{\mathrm{q}} - \mathbf{x}^{\mathrm{e}}{}_{\mathrm{p}}\right)^T\left(\delta\mathbf{x}^{\mathrm{e}}{}_{\mathrm{q}} - \delta\mathbf{x}^{\mathrm{e}}{}_{\mathrm{p}}\right)\right)$$

$$\delta\mathbf{e}_1{}^{\mathbf{c}} = \frac{\delta\mathbf{u}^{\mathrm{e}}{}_{\mathrm{q}} - \delta\mathbf{u}^{\mathrm{e}}{}_{\mathrm{p}}}{\mathrm{L}} - \frac{\mathbf{x}^{\mathrm{e}}{}_{\mathrm{q}} - \mathbf{x}^{\mathrm{e}}{}_{\mathrm{p}}}{\mathrm{L}^2}\left(\left(\mathbf{x}^{\mathrm{e}}{}_{\mathrm{q}} - \mathbf{x}^{\mathrm{e}}{}_{\mathrm{p}}\right)^T\left(\delta\mathbf{u}^{\mathrm{e}}{}_{\mathrm{q}} - \delta\mathbf{u}^{\mathrm{e}}{}_{\mathrm{p}}\right)\right)$$

$$\delta\mathbf{e}_1{}^{\mathbf{c}} = \frac{\delta\mathbf{u}^{\mathrm{e}}{}_{\mathrm{q}} - \delta\mathbf{u}^{\mathrm{e}}{}_{\mathrm{p}}}{\mathrm{L}}\left(\mathbf{I} - \frac{\mathbf{x}^{\mathrm{e}}{}_{\mathrm{q}} - \mathbf{x}^{\mathrm{e}}{}_{\mathrm{p}}}{\mathrm{L}^2}\left(\mathbf{x}^{\mathrm{e}}{}_{\mathrm{q}} - \mathbf{x}^{\mathrm{e}}{}_{\mathrm{p}}\right)^T\right)$$

$$\delta\mathbf{e}_1{}^{\mathbf{c}} = \frac{\delta\mathbf{u}^{\mathrm{e}}{}_{\mathrm{q}} - \delta\mathbf{u}^{\mathrm{e}}{}_{\mathrm{p}}}{\mathrm{L}}\left(\mathbf{I} - \mathbf{e}_1{}^{\mathbf{c}}\mathbf{e}_1{}^{\mathbf{c}T}\right) \qquad \text{(Eq. 2.159)}$$

In the co-rotational frame, the basis vector along direction 1 is given by

$$\mathbf{e}_1{}^{\mathbf{c}} = [1 \quad 0 \quad 0]^T \qquad \text{(Eq. 2.160)}$$

From Eq. 2.159 and Eq. 2.160, the variation of $\mathbf{e_1}^{\mathbf{c}}$ in the co-rotational frame is given by

$$\delta \mathbf{e_1}^{\mathbf{c}} = \frac{\delta \mathbf{u}^{\mathrm{e}}{}_{\mathrm{q}} - \delta \mathbf{u}^{\mathrm{e}}{}_{\mathrm{p}}}{\mathrm{L}} \left(\mathbf{I} - \mathbf{e_1}^{\mathbf{c}} \mathbf{e_1}^{\mathbf{c}T} \right) = \begin{bmatrix} 0 \\ \dfrac{\delta \mathbf{u_2}^{\mathrm{e}}{}_{\mathrm{q}} - \delta \mathbf{u_2}^{\mathrm{e}}{}_{\mathrm{p}}}{\mathrm{L}} \\ \dfrac{\delta \mathbf{u_3}^{\mathrm{e}}{}_{\mathrm{q}} - \delta \mathbf{u_3}^{\mathrm{e}}{}_{\mathrm{p}}}{\mathrm{L}} \end{bmatrix} \qquad \text{(Eq. 2.161)}$$

From Eq. 2.153, the variation of $\mathbf{e_3}^{\mathbf{c}}$ in the element frame is given by

$$\delta \mathbf{e_3}^{\mathbf{c}} = \frac{\delta \mathbf{e_1}^{\mathbf{c}} \times \boldsymbol{y}_{avg} + \mathbf{e_1}^{\mathbf{c}} \times \delta \boldsymbol{y}_{avg}}{\left| \mathbf{e_1}^{\mathbf{c}} \times \boldsymbol{y}_{avg} \right|} + \frac{\mathbf{e_1}^{\mathbf{c}} \times \boldsymbol{y}_{avg}}{\left| \mathbf{e_1}^{\mathbf{c}} \times \boldsymbol{y}_{avg} \right|^2} \delta \left| \mathbf{e_1}^{\mathbf{c}} \times \boldsymbol{y}_{avg} \right|$$

$$\delta \mathbf{e_3}^{\mathbf{c}} = \frac{-\mathbf{Spin}(\boldsymbol{y}_{avg}) \delta \mathbf{e_1}^{\mathbf{c}} + \mathbf{Spin}(\mathbf{e_1}^{\mathbf{c}}) \delta \boldsymbol{y}_{avg}}{\left| \mathbf{e_1}^{\mathbf{c}} \times \boldsymbol{y}_{avg} \right|} + \frac{\mathbf{e_1}^{\mathbf{c}} \times \boldsymbol{y}_{avg}}{\left| \mathbf{e_1}^{\mathbf{c}} \times \boldsymbol{y}_{avg} \right|} \frac{\delta \left| \mathbf{e_1}^{\mathbf{c}} \times \boldsymbol{y}_{avg} \right|}{\left| \mathbf{e_1}^{\mathbf{c}} \times \boldsymbol{y}_{avg} \right|}$$

$$\delta \mathbf{e_3}^{\mathbf{c}} = \frac{-\mathbf{Spin}(\boldsymbol{y}_{avg}) \delta \mathbf{e_1}^{\mathbf{c}} + \mathbf{Spin}(\mathbf{e_1}^{\mathbf{c}}) \delta \boldsymbol{y}_{avg}}{\left| \mathbf{e_1}^{\mathbf{c}} \times \boldsymbol{y}_{avg} \right|} + \mathbf{e_3}^{\mathbf{c}} \frac{\delta \left| \mathbf{e_1}^{\mathbf{c}} \times \boldsymbol{y}_{avg} \right|}{\left| \mathbf{e_1}^{\mathbf{c}} \times \boldsymbol{y}_{avg} \right|}$$

$$\delta \mathbf{e_3}^{\mathbf{c}} = \frac{-\mathbf{Spin}(\boldsymbol{y}_{avg}) \delta \mathbf{e_1}^{\mathbf{c}} + \mathbf{Spin}(\mathbf{e_1}^{\mathbf{c}}) \delta \boldsymbol{y}_{avg}}{y_{avg_2}} + \mathbf{e_3}^{\mathbf{c}} \frac{\delta y_{avg_2}}{y_{avg_2}} \qquad \text{(Eq. 2.162)}$$

In the co-rotational frame, the basis vector along direction 3 is given by

$$\mathbf{e_3}^{\mathbf{c}} = [0 \quad 0 \quad 1]^T \qquad \text{(Eq. 2.163)}$$

From Eq. 2.162 and Eq. 2.163, the variation of $\mathbf{e}_3{}^{\mathbf{c}}$ in the co-rotational frame is given by

$$\delta\mathbf{e}_3{}^{\mathbf{c}} = \frac{1}{y_{avg_2}}\left\{\begin{bmatrix} 0 & y_{avg_3} & -y_{avg_2} \\ -y_{avg_3} & 0 & y_{avg_1} \\ y_{avg_2} & -y_{avg_1} & 0 \end{bmatrix}\begin{bmatrix} 0 \\ \dfrac{\delta\mathbf{u}_2{}^{\mathrm{e}}{}_{\mathrm{q}} - \delta\mathbf{u}_2{}^{\mathrm{e}}{}_{\mathrm{p}}}{\mathrm{L}} \\ \dfrac{\delta\mathbf{u}_3{}^{\mathrm{e}}{}_{\mathrm{q}} - \delta\mathbf{u}_3{}^{\mathrm{e}}{}_{\mathrm{p}}}{\mathrm{L}} \end{bmatrix} + \begin{bmatrix} 0 & 0 & 0 \\ 0 & 0 & -1 \\ 0 & 1 & 0 \end{bmatrix}\begin{bmatrix} \delta y_{avg_1} \\ \delta y_{avg_2} \\ \delta y_{avg_3} \end{bmatrix}\right\} + \begin{bmatrix} 0 \\ 0 \\ 1 \end{bmatrix}\frac{\delta y_{avg_2}}{y_{avg_2}}$$

$$\delta\mathbf{e}_3{}^{\mathbf{c}} = \frac{1}{y_{avg_2}}\left\{\begin{bmatrix} \left(\dfrac{\delta\mathbf{u}_2{}^{\mathrm{e}}{}_{\mathrm{q}} - \delta\mathbf{u}_2{}^{\mathrm{e}}{}_{\mathrm{p}}}{\mathrm{L}}\right)y_{avg_3} - \left(\dfrac{\delta\mathbf{u}_2{}^{\mathrm{e}}{}_{\mathrm{q}} - \delta\mathbf{u}_2{}^{\mathrm{e}}{}_{\mathrm{p}}}{\mathrm{L}}\right)y_{avg_2} \\ \left(\dfrac{\delta\mathbf{u}_3{}^{\mathrm{e}}{}_{\mathrm{q}} - \delta\mathbf{u}_3{}^{\mathrm{e}}{}_{\mathrm{p}}}{\mathrm{L}}\right)y_{avg_1} \\ -\left(\dfrac{\delta\mathbf{u}_2{}^{\mathrm{e}}{}_{\mathrm{q}} - \delta\mathbf{u}_2{}^{\mathrm{e}}{}_{\mathrm{p}}}{\mathrm{L}}\right)y_{avg_1} \end{bmatrix} + \begin{bmatrix} 0 \\ -\delta y_{avg_3} \\ \delta y_{avg_2} \end{bmatrix}\right\} + \begin{bmatrix} 0 \\ 0 \\ \dfrac{\delta y_{avg_2}}{y_{avg_2}} \end{bmatrix}$$

$$\delta\mathbf{e}_3{}^{\mathbf{c}} = \frac{1}{y_{avg_2}}\begin{bmatrix} \left(\dfrac{\delta\mathbf{u}_2{}^{\mathrm{e}}{}_{\mathrm{q}} - \delta\mathbf{u}_2{}^{\mathrm{e}}{}_{\mathrm{p}}}{\mathrm{L}}\right)y_{avg_3} - \left(\dfrac{\delta\mathbf{u}_2{}^{\mathrm{e}}{}_{\mathrm{q}} - \delta\mathbf{u}_2{}^{\mathrm{e}}{}_{\mathrm{p}}}{\mathrm{L}}\right)y_{avg_2} \\ \left(\dfrac{\delta\mathbf{u}_3{}^{\mathrm{e}}{}_{\mathrm{q}} - \delta\mathbf{u}_3{}^{\mathrm{e}}{}_{\mathrm{p}}}{\mathrm{L}}\right)y_{avg_1} - \delta y_{avg_3} \\ -\left(\dfrac{\delta\mathbf{u}_2{}^{\mathrm{e}}{}_{\mathrm{q}} - \delta\mathbf{u}_2{}^{\mathrm{e}}{}_{\mathrm{p}}}{\mathrm{L}}\right)y_{avg_1} + \delta y_{avg_2} + \dfrac{\delta y_{avg_2}}{y_{avg_2}} \end{bmatrix} \qquad \text{(Eq. 2.164)}$$

2.6.3.5 Variation of the transformation matrix between the co-rotational and element frames

In Eq. 2.140, the variation of the frame transformation matrix from the co-rotational frame to the element frame in the element frame is described by

$$\delta\boldsymbol{\Omega}_{\mathbf{E}_c^e} = \mathbf{Spin}(\delta\boldsymbol{\omega}_E{}^e) = \delta\mathbf{E}_c^e(\mathbf{E}_c^e)^T$$

In matrix form using Eq. 2.124, Eq. 2.140 can be written as

$$\begin{bmatrix} \delta\mathbf{e}_1{}^{cT} \\ \delta\mathbf{e}_2{}^{cT} \\ \delta\mathbf{e}_3{}^{cT} \end{bmatrix} [\mathbf{e}_1{}^c \quad \mathbf{e}_2{}^c \quad \mathbf{e}_3{}^c] = \begin{bmatrix} \delta\mathbf{e}_1{}^{cT}\mathbf{e}_1{}^c & \delta\mathbf{e}_1{}^{cT}\mathbf{e}_2{}^c & \delta\mathbf{e}_1{}^{cT}\mathbf{e}_3{}^c \\ \delta\mathbf{e}_2{}^{cT}\mathbf{e}_1{}^c & \delta\mathbf{e}_2{}^{cT}\mathbf{e}_2{}^c & \delta\mathbf{e}_2{}^{cT}\mathbf{e}_3{}^c \\ \delta\mathbf{e}_3{}^{cT}\mathbf{e}_1{}^c & \delta\mathbf{e}_3{}^{cT}\mathbf{e}_2{}^c & \delta\mathbf{e}_3{}^{cT}\mathbf{e}_3{}^c \end{bmatrix} \quad \text{(Eq. 2.165)}$$

From Table 2.1 and Eq. 2.140, the variation of the frame transformation matrix from the co-rotational frame to the element frame in the co-rotational frame is described by

$$(\mathbf{E}_c^e)^T\mathbf{Spin}(\delta\boldsymbol{\omega}_E{}^e)\mathbf{E}_c^e = (\mathbf{E}_c^e)^T\delta\mathbf{E}(\mathbf{E}_c^e)^T\mathbf{E}_c^e = (\mathbf{E}_c^e)^T\delta\mathbf{E}_c^e \quad \text{(Eq 2.166)}$$

In the co-rotational frame, the basis vectors are given by

$$\mathbf{e}_1{}^{\mathbf{c}} = [1 \quad 0 \quad 0]^T$$

$$\mathbf{e}_2{}^{\mathbf{c}} = [0 \quad 1 \quad 0]^T \quad \text{(Eq. 2.167)}$$

$$\mathbf{e}_3{}^{\mathbf{c}} = [0 \quad 0 \quad 1]^T$$

By using the above basis vectors in the co-rotational frame, Eq. 2.166 can be given by and the spin tensor of the variation of the axial vector $\boldsymbol{\omega}_{\mathrm{E}}{}^{\mathrm{e}}$ in Eq. 2.140 can by replaced by

$$\mathbf{Spin}(\delta\boldsymbol{\omega}_{\mathrm{E}}{}^{\mathrm{e}}) = (\mathbf{E}_{\mathrm{c}}^{\mathrm{e}})^{\mathrm{T}}\delta\mathbf{E}_{\mathrm{c}}^{\mathrm{e}} \qquad \text{(Eq. 2.168)}$$

In matrix form, using Eq. 2.124, Eq. 2.168 can be expressed as

$$\begin{bmatrix} \mathbf{e}_1{}^{\mathrm{c}\mathrm{T}} \\ \mathbf{e}_2{}^{\mathrm{c}\mathrm{T}} \\ \mathbf{e}_3{}^{\mathrm{c}\mathrm{T}} \end{bmatrix} [\delta\mathbf{e}_1{}^{\mathrm{c}} \quad \delta\mathbf{e}_2{}^{\mathrm{c}} \quad \delta\mathbf{e}_3{}^{\mathrm{c}}] = \begin{bmatrix} \mathbf{e}_1{}^{\mathrm{c}\mathrm{T}}\delta\mathbf{e}_1{}^{\mathrm{c}} & \mathbf{e}_1{}^{\mathrm{c}\mathrm{T}}\delta\mathbf{e}_2{}^{\mathrm{c}} & \mathbf{e}_1{}^{\mathrm{c}\mathrm{T}}\delta\mathbf{e}_3{}^{\mathrm{c}} \\ \mathbf{e}_2{}^{\mathrm{c}\mathrm{T}}\delta\mathbf{e}_1{}^{\mathrm{c}} & \mathbf{e}_2{}^{\mathrm{c}\mathrm{T}}\delta\mathbf{e}_2{}^{\mathrm{c}} & \mathbf{e}_2{}^{\mathrm{c}\mathrm{T}}\delta\mathbf{e}_3{}^{\mathrm{c}} \\ \mathbf{e}_3{}^{\mathrm{c}\mathrm{T}}\delta\mathbf{e}_1{}^{\mathrm{c}} & \mathbf{e}_3{}^{\mathrm{c}\mathrm{T}}\delta\mathbf{e}_2{}^{\mathrm{c}} & \mathbf{e}_3{}^{\mathrm{c}\mathrm{T}}\delta\mathbf{e}_3{}^{\mathrm{c}} \end{bmatrix} \qquad \text{(Eq. 2.169)}$$

Furthermore, the right-hand side in Eq. 2.169 may be expressed as

$$\begin{bmatrix} \mathbf{e}_1{}^{\mathrm{c}\mathrm{T}}\delta\mathbf{e}_1{}^{\mathrm{c}} & \mathbf{e}_1{}^{\mathrm{c}\mathrm{T}}\delta\mathbf{e}_2{}^{\mathrm{c}} & \mathbf{e}_1{}^{\mathrm{c}\mathrm{T}}\delta\mathbf{e}_3{}^{\mathrm{c}} \\ \mathbf{e}_2{}^{\mathrm{c}\mathrm{T}}\delta\mathbf{e}_1{}^{\mathrm{c}} & \mathbf{e}_2{}^{\mathrm{c}\mathrm{T}}\delta\mathbf{e}_2{}^{\mathrm{c}} & \mathbf{e}_2{}^{\mathrm{c}\mathrm{T}}\delta\mathbf{e}_3{}^{\mathrm{c}} \\ \mathbf{e}_3{}^{\mathrm{c}\mathrm{T}}\delta\mathbf{e}_1{}^{\mathrm{c}} & \mathbf{e}_3{}^{\mathrm{c}\mathrm{T}}\delta\mathbf{e}_2{}^{\mathrm{c}} & \mathbf{e}_3{}^{\mathrm{c}\mathrm{T}}\delta\mathbf{e}_3{}^{\mathrm{c}} \end{bmatrix} = \begin{bmatrix} 0 & -\delta\omega_{\mathbf{E}_3}{}^{\mathrm{e}} & \delta\omega_{\mathbf{E}_2}{}^{\mathrm{e}} \\ \delta\omega_{\mathbf{E}_3}{}^{\mathrm{e}} & 0 & -\delta\omega_{\mathbf{E}_1}{}^{\mathrm{e}} \\ -\delta\omega_{\mathbf{E}_2}{}^{\mathrm{e}} & \delta\omega_{\mathbf{E}_1}{}^{\mathrm{e}} & 0 \end{bmatrix} \qquad \text{(Eq. 2.170)}$$

Then, from Eq. 2.170, the variation of the axial vector $\boldsymbol{\omega}_{\mathrm{E}}{}^{\mathrm{e}}$ can be is given by

$$\delta\boldsymbol{\omega}_{\mathrm{E}}{}^{\mathrm{e}} = \begin{bmatrix} \delta\omega_{\mathbf{E}_1}{}^{\mathrm{e}} \\ \delta\omega_{\mathbf{E}_2}{}^{\mathrm{e}} \\ \delta\omega_{\mathbf{E}_3}{}^{\mathrm{e}} \end{bmatrix} = \begin{bmatrix} -\mathbf{e}_2{}^{\mathrm{c}\mathrm{T}}\delta\mathbf{e}_3{}^{\mathrm{c}} \\ -\mathbf{e}_3{}^{\mathrm{c}\mathrm{T}}\delta\mathbf{e}_1{}^{\mathrm{c}} \\ \mathbf{e}_2{}^{\mathrm{c}\mathrm{T}}\delta\mathbf{e}_1{}^{\mathrm{c}} \end{bmatrix} \qquad \text{(Eq. 2.171)}$$

From Eq. 2.160, Eq. 2.161, Eq. 2.163 , Eq. 2.164, and Eq. 2.167,

$$\delta\boldsymbol{\omega}_{\mathrm{E}}{}^{\mathrm{e}} = \begin{bmatrix} -\mathbf{e}_2{}^{\mathrm{c}\mathrm{T}}\delta\mathbf{e}_3{}^{\mathrm{c}} \\ -\mathbf{e}_3{}^{\mathrm{c}\mathrm{T}}\delta\mathbf{e}_1{}^{\mathrm{c}} \\ \mathbf{e}_2{}^{\mathrm{c}\mathrm{T}}\delta\mathbf{e}_1{}^{\mathrm{c}} \end{bmatrix} = \begin{bmatrix} -\dfrac{1}{y_{avg_2}}\left(\left(\dfrac{\delta\mathbf{u}_3{}^{\mathrm{e}}{}_{\mathrm{q}} - \delta\mathbf{u}_3{}^{\mathrm{e}}{}_{\mathrm{p}}}{\mathrm{L}}\right)y_{avg_1} - \delta y_{avg_3}\right) \\ \dfrac{\delta\mathbf{u}_3{}^{\mathrm{e}}{}_{\mathrm{p}} - \delta\mathbf{u}_3{}^{\mathrm{e}}{}_{\mathrm{q}}}{\mathrm{L}} \\ \dfrac{\delta\mathbf{u}_2{}^{\mathrm{e}}{}_{\mathrm{q}} - \delta\mathbf{u}_2{}^{\mathrm{e}}{}_{\mathrm{p}}}{\mathrm{L}} \end{bmatrix} \quad \text{(Eq. 2.172)}$$

where:

$$\delta\boldsymbol{y}_{avg} = \frac{\delta\mathbf{e}_2{}^{\mathrm{p}} + \delta\mathbf{e}_2{}^{\mathrm{q}}}{2} \quad \text{(Eq. 2.173)}$$

$$\mathbf{Spin}\left(\delta\boldsymbol{\omega}_{\mathrm{p}}{}^{\mathrm{e}}\right) = \delta\mathbf{e}_2{}^{\mathrm{p}}\mathbf{e}_2{}^{\mathrm{p}\mathrm{T}} \quad \text{(Eq. 2.174)}$$

$$\delta\mathbf{e}_2{}^{\mathrm{p}} = \mathbf{Spin}\left(\delta\boldsymbol{\omega}_{\mathrm{p}}{}^{\mathrm{e}}\right)\mathbf{e}_2{}^{\mathrm{p}} = \begin{bmatrix} 0 & -\delta\omega_{\mathrm{p}_3}{}^{\mathrm{e}} & \delta\omega_{\mathrm{p}_2}{}^{\mathrm{e}} \\ \delta\omega_{\mathrm{p}_3}{}^{\mathrm{e}} & 0 & -\delta\omega_{\mathrm{p}_1}{}^{\mathrm{e}} \\ -\delta\omega_{\mathrm{p}_2}{}^{\mathrm{e}} & \delta\omega_{\mathrm{p}_1}{}^{\mathrm{e}} & 0 \end{bmatrix}\begin{bmatrix} \mathbf{e}_2{}^{\mathrm{p}}{}_1 \\ \mathbf{e}_2{}^{\mathrm{p}}{}_2 \\ \mathbf{e}_2{}^{\mathrm{p}}{}_3 \end{bmatrix}$$

$$= \begin{bmatrix} -\delta\omega_{\mathrm{p}_3}{}^{\mathrm{e}}\mathbf{e}_2{}^{\mathrm{p}}{}_2 + \delta\omega_{\mathrm{p}_2}{}^{\mathrm{e}}\mathbf{e}_2{}^{\mathrm{p}}{}_3 \\ \delta\omega_{\mathrm{p}_3}{}^{\mathrm{e}}\mathbf{e}_2{}^{\mathrm{p}}{}_1 - \delta\omega_{\mathrm{p}_1}{}^{\mathrm{e}}\mathbf{e}_2{}^{\mathrm{p}}{}_3 \\ -\delta\omega_{\mathrm{p}_2}{}^{\mathrm{e}}\mathbf{e}_2{}^{\mathrm{p}}{}_1 + \delta\omega_{\mathrm{p}_1}{}^{\mathrm{e}}\mathbf{e}_2{}^{\mathrm{p}}{}_2 \end{bmatrix} \quad \text{(Eq. 2.175)}$$

$$\mathbf{Spin}\left(\delta\boldsymbol{\omega}_{\mathrm{q}}{}^{\mathrm{c}}\right) = \delta\mathbf{e}_2{}^{\mathrm{q}}\mathbf{e}_2{}^{\mathrm{q}\mathrm{T}} \quad \text{(Eq .2.176)}$$

$$\delta\mathbf{e}_2{}^{\mathrm{q}} = \mathbf{Spin}\left(\delta\boldsymbol{\omega}_{\mathrm{q}}{}^{\mathrm{e}}\right)\mathbf{e}_2{}^{\mathrm{q}} = \begin{bmatrix} 0 & -\delta\omega_{\mathrm{q}_3}{}^{\mathrm{e}} & \delta\omega_{\mathrm{q}_2}{}^{\mathrm{e}} \\ \delta\omega_{\mathrm{q}_3}{}^{\mathrm{e}} & 0 & -\delta\omega_{\mathrm{q}_1}{}^{\mathrm{e}} \\ -\delta\omega_{\mathrm{q}_2}{}^{\mathrm{e}} & \delta\omega_{\mathrm{q}_1}{}^{\mathrm{e}} & 0 \end{bmatrix}\begin{bmatrix} \mathbf{e}_2{}^{\mathrm{q}}{}_1 \\ \mathbf{e}_2{}^{\mathrm{q}}{}_2 \\ \mathbf{e}_2{}^{\mathrm{q}}{}_3 \end{bmatrix}$$

$$= \begin{bmatrix} -\delta\omega_{\mathrm{q}_3}{}^{\mathrm{e}}\mathbf{e}_2{}^{\mathrm{q}}{}_2 + \delta\omega_{\mathrm{q}_2}{}^{\mathrm{e}}\mathbf{e}_2{}^{\mathrm{q}}{}_3 \\ \delta\omega_{\mathrm{q}_3}{}^{\mathrm{e}}\mathbf{e}_2{}^{\mathrm{q}}{}_1 - \delta\omega_{\mathrm{q}_1}{}^{\mathrm{e}}\mathbf{e}_2{}^{\mathrm{q}}{}_3 \\ -\delta\omega_{\mathrm{q}_2}{}^{\mathrm{e}}\mathbf{e}_2{}^{\mathrm{q}}{}_1 + \delta\omega_{\mathrm{q}_1}{}^{\mathrm{e}}\mathbf{e}_2{}^{\mathrm{q}}{}_2 \end{bmatrix} \quad \text{(Eq. 2.177)}$$

$$\delta \boldsymbol{y}_{avg} = \frac{1}{2}\begin{bmatrix} \left(-\delta\omega_{p_3}{}^{e}\mathbf{e}_2{}^{p}{}_2 + \delta\omega_{p_2}{}^{e}\mathbf{e}_2{}^{p}{}_3\right) + \left(-\delta\omega_{q_3}{}^{e}\mathbf{e}_2{}^{q}{}_2 + \delta\omega_{q_2}{}^{e}\mathbf{e}_2{}^{q}{}_3\right) \\ \left(\delta\omega_{p_3}{}^{e}\mathbf{e}_2{}^{p}{}_1 - \delta\omega_{p_1}{}^{e}\mathbf{e}_2{}^{p}{}_3\right) + \left(\delta\omega_{q_3}{}^{e}\mathbf{e}_2{}^{q}{}_1 - \delta\omega_{q_1}{}^{e}\mathbf{e}_2{}^{q}{}_3\right) \\ \left(-\delta\omega_{p_2}{}^{e}\mathbf{e}_2{}^{p}{}_1 + \delta\omega_{p_1}{}^{e}\mathbf{e}_2{}^{p}{}_2\right) + \left(-\delta\omega_{q_2}{}^{e}\mathbf{e}_2{}^{q}{}_1 + \delta\omega_{q_1}{}^{e}\mathbf{e}_2{}^{q}{}_2\right) \end{bmatrix} \quad \text{(Eq. 2.178)}$$

$$\delta\omega_{\mathbf{E}_1}{}^{e} = \frac{1}{2}\left(\left(-\delta\omega_{p_2}{}^{e}\frac{\mathbf{e}_2{}^{p}{}_1}{y_{avg_2}} + \delta\omega_{p_1}{}^{e}\frac{\mathbf{e}_2{}^{p}{}_2}{y_{avg_2}}\right) + \left(-\delta\omega_{q_2}{}^{e}\frac{\mathbf{e}_2{}^{q}{}_1}{y_{avg_2}} + \delta\omega_{q_1}{}^{e}\frac{\mathbf{e}_2{}^{q}{}_2}{y_{avg_2}}\right)\right)$$

$$-\left(\frac{\delta\mathbf{u}_3{}^{e}{}_q - \delta\mathbf{u}_3{}^{e}{}_p}{\mathrm{L}}\right)\frac{y_{avg_1}}{y_{avg_2}} \quad \text{(Eq. 2.179)}$$

2.7 Co-Rotational Finite Element Formulation

2.7.1 Geometric Nonlinear Formulation

In this research, the geometric nonlinear formulation is based on:

- Total Lagrangian description.
- The principle of virtual displacements to establish equilibrium equations for the deformed configuration.
- The use of the Green-Lagrange finite strain tensor and the work conjugate second Piola-Kirchhoff stress tensor.

2.7.2 Principle of Virtual Work (Weak Form)

The stationary condition of the total potential energy results in equilibrium equation, which is called principle of virtual work. The principle of virtual work is obtained by the variation of the total potential energy. The general principle of virtual work is given by

$$\delta\mathbf{\Pi} = \delta(\mathbf{U} + \mathbf{V}) = 0 \qquad (\text{Eq. } 2.180)$$

or

$$\text{Internal virtual work} = \text{External virtual work}$$

For geometric nonlinear analysis, the principle of virtual work is commonly written in a Lagrangian description since the integration can be performed over a known

volume. Furthermore, the Green-Lagrange strain is relatively simple to compute in the context of this type of formulation.

As the element deformation other than rigid body motion is generated in the co-rotational frame, the principle virtual work is considered within the co-rotational frame. Internal virtual work is given by

$$\delta \mathbf{d}^{c\mathrm{T}} \mathbf{F}^{c} = \int_{V_o} \delta \mathbf{E}^{\mathbf{T}} \mathbf{S} \; dV_o \qquad \text{(Eq. 2.181)}$$

where:

- $\mathbf{F}^{c}$ = Internal force vector of the element in the co-rotational frame.
- $\mathbf{S}$ = The second Piola-Kirchhoff stress tensor.
- $\delta \mathbf{E}^{\mathbf{T}}$ = Virtual Green-Lagrange strain tensor.
- $\delta \mathbf{d}^{c\mathrm{T}}$ = Virtual displacement corresponding virtual Green-Lagrange strain tensor $\delta \mathbf{E}^{\mathbf{T}}$.
- V_o = Volume in reference configuration.

The external virtual work is given by

$$\delta \mathbf{d}^{c\mathrm{T}} \mathbf{Q}^{c} = \int_{V_o} \delta \mathbf{d}^{c\mathrm{T}} \mathbf{f}^{B} \; dV_o + \int_{A_o} \delta \mathbf{d}^{c\mathrm{T}} \mathbf{f}^{S} \; dA_o \qquad \text{(Eq. 2.182)}$$

where:

- $\mathbf{Q}^{c}$ = External force vector of the element in the co-rotational frame.

- $\mathbf{f}^{B}$ = Externally applied force or body force per unit reference volume.
- $\mathbf{f}^{S}$ = Externally applied force per unit reference surface area or stress resultant.
- A_o = Surface area in reference configuration.

If zero body force is assumed, the virtual work in Eq. 2.180 is given by

$$\int_{V_o} \delta\mathbf{E}^{T}\mathbf{S}\ dV_o = \int_{A_o} \delta\mathbf{d}^{c\,T}\mathbf{f}^{S}\ dA_o \qquad \text{or} \qquad \delta\mathbf{d}^{c\,T}\mathbf{F}^{c} = \delta\mathbf{d}^{c\,T}\mathbf{Q}^{c} \qquad \text{(Eq. 2.183)}$$

2.7.3 Finite Element Formulation in the Co-Rotational Frame

The finite element formulation in the co-rotational frame are derived from the principle virtual displacements in Eq. 2.183. The internal virtual work in Eq. 2.183 employs the variation of the Green-Lagrange strain tensor described in Eq. 2.105. The Green-Lagrange strain tensor is derived from the longitudinal displacement $u_o(x)$, the transverse displacements $v_o(x)$ and $w_o(x)$ and twist angle of the cross-section $\emptyset(x)$ at relative to the reference configuration. These displacements are functions of the element longitudinal coordinate *x*. The displacements in each discretized element in the co-rotational frame are characterized by the 9 degrees of freedom shown in Eq. 2.108. To represent the displacement field in each discretized element, the following shape functions are employed.

- Longitudinal displacement: Linear function in the longitudinal coordinate.

$$u_o(x) = \mathbf{N}_u^{T}\mathbf{d}^{c} \qquad \text{(Eq. 2.184)}$$

where:

- $\mathbf{N}_u = [\mathrm{N_e}(x) \quad 0 \quad 0 \quad 0 \quad 0 \quad 0 \quad 0 \quad 0 \quad 0]^{\mathrm{T}}$ (Eq. 2.185)
- $\mathrm{N_e}(x) = \frac{x}{\mathrm{L}} \quad 0 \leq x \leq \mathrm{L}$ (Eq. 2.186)

- Transverse displacement along direction 2: Cubic Hermitian interpolation in terms of the longitudinal coordinate.

$$v_o(x) = \mathbf{N}_v^{\mathrm{T}} \mathbf{d}^{\mathrm{c}} \quad \text{(Eq. 2.187)}$$

Where:

- $\mathbf{N}_v = \left[0 \quad 0 \quad \mathrm{N}_{\theta^{\mathrm{c}}_{2_{\mathrm{p}}}}(x) \quad 0 \quad 0 \quad 0 \quad \mathrm{N}_{\theta^{\mathrm{c}}_{2_{\mathrm{q}}}}(x) \quad 0 \quad 0\right]^{\mathrm{T}}$ (Eq. 2.188)
- $\mathrm{N}_{\theta^{\mathrm{c}}_{2_{\mathrm{p}}}}(x) = x - \frac{2x^2}{\mathrm{L}} + \frac{x^3}{\mathrm{L}^2} \qquad 0 \leq \mathrm{x} \leq \mathrm{L}$ (Eq. 2.189)
- $\mathrm{N}_{\theta^{\mathrm{c}}_{2_{\mathrm{q}}}}(x) = -\frac{x^2}{\mathrm{L}} + \frac{x^3}{\mathrm{L}^2} \qquad 0 \leq \mathrm{x} \leq \mathrm{L}$ (Eq. 2.190)

- Transverse displacement along direction 3: Cubic Hermitian interpolation in the longitudinal coordinate.

$$w_o(x) = \mathbf{N}_w^{\mathrm{T}} \mathbf{d}^{\mathrm{c}} \quad \text{(Eq. 2.191)}$$

where:

- $\mathbf{N}_w = \left[0 \quad 0 \quad 0 \quad \mathrm{N}_{\theta^{\mathrm{c}}_{3_{\mathrm{p}}}}(x) \quad 0 \quad 0 \quad 0 \quad \mathrm{N}_{\theta^{\mathrm{c}}_{3_{\mathrm{q}}}}(x) \quad 0\right]^{\mathrm{T}}$ (Eq. 2.192)
- $\mathrm{N}_{\theta^{\mathrm{c}}_{3_{\mathrm{p}}}}(x) = -\left(x - \frac{2x^2}{\mathrm{L}} + \frac{x^3}{\mathrm{L}^2}\right) \qquad 0 \leq x \leq \mathrm{L}$ (Eq. 2.193)
- $\mathrm{N}_{\theta^{\mathrm{c}}_{3_{\mathrm{q}}}}(x) = -\left(-\frac{x^2}{\mathrm{L}} + \frac{x^3}{\mathrm{L}^2}\right) \qquad 0 \leq x \leq \mathrm{L}$ (Eq. 2.194)

- Twist angle of the cross-section: Cubic Hermitian interpolation in terms of the longitudinal coordinate.

$$\emptyset(x) = \mathbf{N}_{\emptyset}^{\mathrm{T}}\mathbf{d}^{\mathrm{c}} \qquad \text{(Eq. 2.195)}$$

where:

- $\mathbf{N}_{\emptyset} = \begin{bmatrix} 0 & \mathrm{N}_{\theta_{1_p}^{c}}(x) & 0 & 0 & \mathrm{N}_{\phi_p'}(x) & \mathrm{N}_{\theta_{1_q}^{c}}(x) & 0 & 0 & \mathrm{N}_{\phi_q'}(x) \end{bmatrix}^{\mathrm{T}}$ (Eq. 2.196)
  - $\mathrm{N}_{\theta_{1_p}^{c}}(x) = 1 - \frac{3x^2}{\mathrm{L}^2} + \frac{2x^3}{\mathrm{L}^3} \qquad 0 \leq x \leq \mathrm{L}$ (Eq. 2.197)
  - $\mathrm{N}_{\phi_p'}(x) = x - \frac{2x^2}{\mathrm{L}} + \frac{x^3}{\mathrm{L}^2} \qquad 0 \leq x \leq \mathrm{L}$ (Eq. 2.198)
  - $\mathrm{N}_{\theta_{1_q}^{c}}(x) = \frac{3x^2}{\mathrm{L}^2} - \frac{2x^3}{\mathrm{L}^3} \qquad 0 \leq x \leq \mathrm{L}$ (Eq. 2.199)
  - $\mathrm{N}_{\phi_q'}(x) = 1 - \frac{x^2}{\mathrm{L}} + \frac{x^3}{\mathrm{L}^2} \qquad 0 \leq x \leq \mathrm{L}$ (Eq. 2.200)

The variation of the displacements in Eqs. 2.184, 2.187, 2.191, and 2.195 are given by

$$\delta u_o(x) = \mathbf{N}_u^{\mathrm{T}}\delta\mathbf{d}^{\mathrm{c}} \qquad \text{(Eq. 2.201)}$$

$$\delta v_o(x) = \mathbf{N}_v^{\mathrm{T}}\delta\mathbf{d}^{\mathrm{c}} \qquad \text{(Eq. 2.202)}$$

$$\delta w_o(x) = \mathbf{N}_w^{\mathrm{T}}\delta\mathbf{d}^{\mathrm{c}} \qquad \text{(Eq. 2.203)}$$

$$\delta\emptyset(x) = \mathbf{N}_{\emptyset}^{\mathrm{T}}\delta\mathbf{d}^{\mathrm{c}} \qquad \text{(Eq. 2.204)}$$

From Eqs. 2.201 and through2.204, Eq. 2.105 can be written as

$$\delta\mathbf{E} = \mathbf{WV}\underbrace{\begin{bmatrix} N_e' & 0 & 0 & 0 & 0 & 0 & 0 & 0 & 0 \\ 0 & 0 & N_{\theta_{2p}^c}' & 0 & 0 & 0 & N_{\theta_{2q}^c}' & 0 & 0 \\ 0 & 0 & 0 & N_{\theta_{3p}^c}' & 0 & 0 & 0 & N_{\theta_{3q}^c}' & 0 \\ 0 & 0 & N_{\theta_{2p}^c}'' & 0 & 0 & 0 & N_{\theta_{2q}^c}'' & 0 & 0 \\ 0 & 0 & 0 & N_{\theta_{3p}^c}'' & 0 & 0 & 0 & N_{\theta_{3q}^c}'' & 0 \\ 0 & N_{\theta_{1p}^c} & 0 & 0 & N_{\phi_p'} & N_{\theta_{1q}^c} & 0 & 0 & N_{\phi_q'} \\ 0 & N_{\theta_{1p}^c}' & 0 & 0 & N_{\phi_p'}' & N_{\theta_{1q}^c}' & 0 & 0 & N_{\phi_q'}' \\ 0 & N_{\theta_{1p}^c}'' & 0 & 0 & N_{\phi_p'}'' & N_{\theta_{1q}^c}'' & 0 & 0 & N_{\phi_q'}'' \end{bmatrix}}_{\mathbf{B}}\delta\mathbf{d}^c \quad \text{(Eq. 2.205)}$$

$$\delta\mathbf{E} = \mathbf{WVB}\delta\mathbf{d}^c \quad \text{(Eq. 2.206)}$$

where:

- $\mathbf{B} = \begin{bmatrix} N_e' & 0 & 0 & 0 & 0 & 0 & 0 & 0 & 0 \\ 0 & 0 & N_{\theta_{2p}^c}' & 0 & 0 & 0 & N_{\theta_{2q}^c}' & 0 & 0 \\ 0 & 0 & 0 & N_{\theta_{3p}^c}' & 0 & 0 & 0 & N_{\theta_{3q}^c}' & 0 \\ 0 & 0 & N_{\theta_{2p}^c}'' & 0 & 0 & 0 & N_{\theta_{2q}^c}'' & 0 & 0 \\ 0 & 0 & 0 & N_{\theta_{3p}^c}'' & 0 & 0 & 0 & N_{\theta_{3q}^c}'' & 0 \\ 0 & N_{\theta_{1p}^c} & 0 & 0 & N_{\phi_p'} & N_{\theta_{1q}^c} & 0 & 0 & N_{\phi_q'} \\ 0 & N_{\theta_{1p}^c}' & 0 & 0 & N_{\phi_p'}' & N_{\theta_{1q}^c}' & 0 & 0 & N_{\phi_q'}' \\ 0 & N_{\theta_{1p}^c}'' & 0 & 0 & N_{\phi_p'}'' & N_{\theta_{1q}^c}'' & 0 & 0 & N_{\phi_q'}'' \end{bmatrix}$

Using Eq. 2.206, Eq. 2.183 can be given by

$$\int_{V_o} \delta\mathbf{d}^{cT}\mathbf{B}^T\mathbf{V}^T\mathbf{W}^T\mathbf{S}\ dV_o = \int_{A_o} \delta\mathbf{d}^{cT}\mathbf{f}^S\ dA_o \quad \text{(Eq. 2.207)}$$

For arbitrary $\delta\mathbf{d}^{cT}$, Eq. 2.207 results in equilibrium equations and can be given by

$$\delta \mathbf{d}^{c^T} \left\{ \int_{V_o} \mathbf{B}^T \mathbf{V}^T \mathbf{W}^T \mathbf{S} \; dV_o - \int_{A_o} \mathbf{f}^S \; dA_o \right\} = \mathbf{0} \qquad \text{(Eq. 2.208)}$$

From Eq. 2.183 and Eq. 2.208, the internal force vector and the external force vector of the element in the co-rotational frame is given by

$$\mathbf{F}^c = \int_{V_o} \mathbf{B}^T \mathbf{V}^T \mathbf{W}^T \mathbf{S} \; dV_o \qquad \text{(Eq. 2.209)}$$

$$\mathbf{Q}^c = \int_{A_o} \mathbf{f}^S \; dA_o \qquad \text{(Eq. 2.210)}$$

From Eq. 2.209, the second Piola-Kirchhoff stress tensor may be written as

$$\mathbf{S} = \mathbf{C}\mathbf{E} = \mathbf{C}\mathbf{W}\mathbf{V}\mathbf{B}\mathbf{d}^c \qquad \text{(Eq. 2.211)}$$

In Eq. 2.211, the constitutive relation between the second Piola-Kirchhoff stress tensor and the Green-Lagrange strain tensor is given by

$$\mathbf{C} = \begin{bmatrix} E & 0 \\ 0 & G \end{bmatrix} \qquad \text{(Eq. 2.212)}$$

where E is the elastic modulus and G is the shear modulus.

Considering the open section thin-walled beam theory which is the function of the longitudinal direction, the internal force vector of the element in the co-rotational frame in Eq. 2.209 is given by

$$\mathbf{F}^c = \int_0^{L_o} \mathbf{B}^T \mathbf{V}^T \left(\int_{A_o} \mathbf{W}^T \mathbf{S} \; dA_o \right) \; dX_1 = \int_0^{L_o} \mathbf{B}^T \mathbf{V}^T (\mathbf{D}) \; dX_1 \qquad \text{(Eq. 2.213)}$$

where:

- The stress resultant internal force vector in each cross-section is

$$\mathbf{D} = \int_{A_o} \mathbf{W}^T \mathbf{S} \; dA_o = \int_{A_o} \begin{bmatrix} 1 & 0 \\ -y & 0 \\ z & 0 \\ (y^2 + z^2) & 0 \\ \bar{\omega} & 0 \\ \psi & -2\hat{\gamma} \end{bmatrix} \begin{bmatrix} S_{11} \\ S_{1s} \end{bmatrix} \; dA_o \qquad \text{(Eq. 2.214)}$$

$$\mathbf{D} = \begin{bmatrix} \int_{A_o} S_{11} \; dA_o \\ \int_{A_o} -yS_{11} \; dA_o \\ \int_{A_o} zS_{11} \; dA_o \\ \int_{A_o} (y^2 + z^2)S_{11} \; dA_o \\ \int_{A_o} \bar{\omega}S_{11} \; dA_o \\ \int_{A_o} (\psi S_{11} + -2\hat{\gamma}S_{1s}) \; dA_o \end{bmatrix} = \begin{bmatrix} P \\ M_z \\ M_y \\ W \\ B \\ T \end{bmatrix} \qquad \text{(Eq. 2.215)}$$

By inserting Eq. 2.211 into Eq. 2.209, the internal force vector of the element in the co-rotational frame can be given by

$$\mathbf{F}^c = \int_{V_o} \mathbf{B}^T \mathbf{V}^T \mathbf{W}^T \mathbf{S} \; dV_o = \int_{V_o} \mathbf{B}^T \mathbf{V}^T \mathbf{W}^T \mathbf{C} \mathbf{W} \mathbf{V} \mathbf{B} \mathbf{d}^c \; dV_o \qquad \text{(Eq. 2.216)}$$

Considering the cross-section area in reference configuration, Eq. 2.216 can be described by

$$\mathbf{F}^{c} = \int_{0}^{L_o} \mathbf{B}^{T}\mathbf{V}^{T}\left(\int_{A_o} \mathbf{W}^{T}\mathbf{C}\mathbf{W}\ dA_o\right)\mathbf{V}\mathbf{B}\mathbf{d}^{c}\ dX_1 = \int_{0}^{L_o} \mathbf{B}^{T}\mathbf{V}^{T}\mathbf{K}^{s}\mathbf{V}\mathbf{B}\mathbf{d}^{c}\ dX_1 \quad \text{(Eq. 2.217)}$$

where the section tangent stiffness matrix is given by

$$\mathbf{K}^{s} = \int_{A_o} \mathbf{W}^{T}\mathbf{C}\mathbf{W}\ dA_o \quad \text{(Eq. 2.218)}$$

2.7.4 Variation of the Internal Force in the Co-Rotational Frame

In Eq. 2.121, the variation of the internal force within the co-rotational frame results in the elastic stiffness and the geometric stiffness and can be expressed as

$$\delta\mathbf{F}^{c} = \int_{0}^{L_o} (\delta\mathbf{B}^{T}\mathbf{V}^{T}\mathbf{D} + \mathbf{B}^{T}\delta\mathbf{V}^{T}\mathbf{D} + \mathbf{B}^{T}\mathbf{V}^{T}\delta\mathbf{D})\ dX_1 \quad \text{(Eq. 2.219)}$$

In Eq. 2.219, the first term is zero:

$$\delta\mathbf{B}^{T} = \mathbf{0} \rightarrow \delta\mathbf{B}^{T}\mathbf{V}^{T}\mathbf{D} = \mathbf{0} \quad \text{(Eq. 2.220)}$$

In Eq. 2.219, the second term results in geometric stiffness and can be given by

$$\mathbf{B}^{T}\delta\mathbf{V}^{T}\mathbf{D} = \mathbf{B}^{T}\begin{bmatrix} 0 & 0 & 0 & 0 & 0 & 0 \\ \delta v_{o,x} & 0 & 0 & 0 & 0 & 0 \\ \delta w_{o,x} & 0 & 0 & 0 & 0 & 0 \\ 0 & 0 & \delta\emptyset & 0 & 0 & 0 \\ 0 & \delta\emptyset & 0 & 0 & 0 & 0 \\ 0 & \delta w_{o,xx} & \delta v_{o,xx} & 0 & 0 & 0 \\ 0 & 0 & 0 & \delta\emptyset_{,x} & 0 & 0 \\ 0 & 0 & 0 & 0 & 0 & 0 \end{bmatrix}\begin{bmatrix} P \\ M_z \\ M_y \\ W \\ B \\ T_{sv} \end{bmatrix} = \mathbf{B}^{T}\begin{bmatrix} 0 \\ P\delta v_{o,x} \\ P\delta w_{o,x} \\ M_y\delta\emptyset \\ M_z\delta\emptyset \\ M_z\delta w_{o,xx} + M_y\delta v_{o,xx} \\ W\delta\emptyset_{,x} \\ 0 \end{bmatrix}$$

(Eq. 2.221)

$$\mathbf{B}^{\mathrm{T}}\begin{bmatrix} 0 \\ \mathrm{P}\delta v_{o,x} \\ P\delta w_{o,x} \\ \mathrm{M_y}\delta\emptyset \\ \mathrm{M_z}\delta\emptyset \\ \mathrm{M_z}\delta w_{o,xx} + \mathrm{M_y}\delta v_{o,xx} \\ \mathrm{W}\delta\emptyset_{,x} \\ 0 \end{bmatrix} = \mathbf{B}^{\mathrm{T}}\begin{bmatrix} 0 & 0 & 0 & 0 & 0 & 0 & 0 & 0 \\ 0 & 0 & 0 & 0 & 0 & 0 & 0 & 0 \\ 0 & 0 & \mathrm{P} & 0 & 0 & 0 & 0 & 0 \\ 0 & 0 & 0 & 0 & 0 & \mathrm{M_y} & 0 & 0 \\ 0 & 0 & 0 & 0 & 0 & \mathrm{M_z} & 0 & 0 \\ 0 & 0 & 0 & \mathrm{M_y} & \mathrm{M_z} & 0 & 0 & 0 \\ 0 & 0 & 0 & 0 & 0 & 0 & \mathrm{W} & 0 \\ 0 & 0 & 0 & 0 & 0 & 0 & 0 & 0 \end{bmatrix}\begin{bmatrix} \delta u_{o,x} \\ \delta v_{o,x} \\ \delta w_{o,x} \\ \delta v_{o,xx} \\ \delta w_{o,xx} \\ \delta\emptyset \\ \delta\emptyset_{,x} \\ \delta\emptyset_{,xx} \end{bmatrix}$$

(Eq. 2.222)

From Eq. 2.221 and Eq. 2.222, the second term in Eq. 2.219 is given by

$$\mathbf{B}^{\mathrm{T}}\delta\mathbf{V}^{\mathrm{T}}\mathbf{D} = \mathbf{B}^{\mathrm{T}}\mathbf{G}^{\mathrm{c}}\mathbf{B}\delta\mathbf{d}^{\mathrm{c}} \qquad \text{(Eq. 2.223)}$$

where:

- $\mathbf{G}^{\mathrm{c}} = \begin{bmatrix} 0 & 0 & 0 & 0 & 0 & 0 & 0 & 0 \\ 0 & 0 & 0 & 0 & 0 & 0 & 0 & 0 \\ 0 & 0 & \mathrm{P} & 0 & 0 & 0 & 0 & 0 \\ 0 & 0 & 0 & 0 & 0 & \mathrm{M_y} & 0 & 0 \\ 0 & 0 & 0 & 0 & 0 & \mathrm{M_z} & 0 & 0 \\ 0 & 0 & 0 & \mathrm{M_y} & \mathrm{M_z} & 0 & 0 & 0 \\ 0 & 0 & 0 & 0 & 0 & 0 & \mathrm{W} & 0 \\ 0 & 0 & 0 & 0 & 0 & 0 & 0 & 0 \end{bmatrix}$

In Eq 2.219, the third term results in elastic stiffness and can be given by

$$\mathbf{B}^{\mathrm{T}}\mathbf{V}^{\mathrm{T}}\delta\mathbf{D} = \mathbf{B}^{\mathrm{T}}\mathbf{V}^{\mathrm{T}}(\mathbf{K}^{\mathrm{s}}\mathbf{V}\mathbf{B}\delta\mathbf{d}^{\mathrm{c}}) \qquad \text{(Eq. 2.224)}$$

From Eq. 2.220, Eq. 2.223, and Eq. 2.224, the variation of the internal force within co-rotational frame in Eq. 2.219 results in

$$\delta\mathbf{F}^{\mathrm{c}} = \int_0^{\mathrm{L}_o} \left(\mathbf{B}^{\mathrm{T}}\mathbf{G}^{\mathrm{c}}\mathbf{B}\delta\mathbf{d}^{\mathrm{c}} + \mathbf{B}^{\mathrm{T}}\mathbf{V}^{\mathrm{T}}(\mathbf{K}^{\mathrm{s}}\mathbf{V}\mathbf{B}\delta\mathbf{d}^{\mathrm{c}})\right)\, \mathrm{dX}_1 \qquad \text{(Eq. 2.225)}$$

For finite increments, Eq. 2.225 can be given by

$$\Delta\mathbf{F}^{\mathrm{c}} = \mathbf{K}^{\mathrm{c}}\Delta\mathbf{d}^{\mathrm{c}} \qquad \text{(Eq. 2.226)}$$

where:

- $\mathbf{K}^{\mathrm{c}} = \int_0^{\mathrm{L}_o}\left(\mathbf{B}^{\mathrm{T}}\mathbf{G}^{\mathrm{c}}\mathbf{B} + \mathbf{B}^{\mathrm{T}}\mathbf{V}^{\mathrm{T}}\mathbf{K}^{\mathrm{s}}\mathbf{V}\mathbf{B}\right)\ \mathrm{dX}_1$

2.7.5 Section Tangent Stiffness Matrix

The element section tangent stiffness is given by Eq. 2.218. From Eq. 2.104 and 2.212, the section tangent stiffness in Lagrange description can be expressed by a closed form as

$$\mathbf{K}^{\mathrm{s}} = \mathrm{E}\begin{bmatrix} \int_{\mathrm{A}_o}\mathrm{dA}_o & \int_{\mathrm{A}_o}-y\mathrm{dA}_o & \int_{\mathrm{A}_o}z\mathrm{dA}_o & \int_{\mathrm{A}_o}r^2\mathrm{dA}_o & \int_{\mathrm{A}_o}\bar{\omega}\mathrm{dA}_o & \int_{\mathrm{A}_o}\psi\mathrm{dA}_o \\ & \int_{\mathrm{A}_o}y^2\mathrm{dA}_o & \int_{\mathrm{A}_o}-yz\mathrm{dA}_o & \int_{\mathrm{A}_o}-yr^2\mathrm{dA}_o & \int_{\mathrm{A}_o}-y\bar{\omega}\mathrm{dA}_o & \int_{\mathrm{A}_o}-y\psi\mathrm{dA}_o \\ & & \int_{\mathrm{A}_o}z^2\mathrm{dA}_o & \int_{\mathrm{A}_o}zr^2\mathrm{dA}_o & \int_{\mathrm{A}_o}z\bar{\omega}\mathrm{dA}_o & \int_{\mathrm{A}_o}z\psi\mathrm{dA}_o \\ & \boldsymbol{Symmetry} & & \int_{\mathrm{A}_o}r^4\mathrm{dA}_o & \int_{\mathrm{A}_o}r^2\bar{\omega}\mathrm{dA}_o & \int_{\mathrm{A}_o}r^2\psi\mathrm{dA}_o \\ & & & & \int_{\mathrm{A}_o}\bar{\omega}^2\mathrm{dA}_o & \int_{\mathrm{A}_o}\bar{\omega}\psi\mathrm{dA}_o \\ & & & & & \int_{\mathrm{A}_o}(\psi^2+\frac{4\mathrm{G}\hat{\gamma}^2}{\mathrm{E}})\mathrm{dA}_o \end{bmatrix}$$

(Eq. 2.227)

where:

- $r^2 = y^2 + z^2$

Figure 2.15 shows the cross-section dimensional variables. Point O on the cross-section is the reference design axis, taken as the mid-depth of the web, at the top flange, or at the bottom flange. Point S is the shear center of the cross-section. The cross-section shear center is employed for the calculation of the components of the section tangent stiffness matrix in the structural analysis.

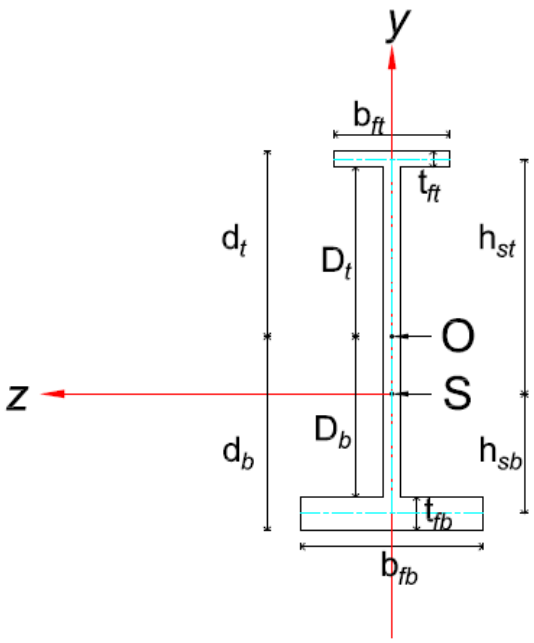

Figure 2.15 Cross-section dimensional variables.

The components of the section tangent stiffness matrix Eq. 2.227 are given by

$K^s{}_{11} = \int_{A_o} dA_o = A_o$: Cross section area.

$K^s{}_{12} = \int_{A_o} -y \; dA_o = -y_c A_o$: First moment of the area about the reference z axis through the shear center.

$$K^s_{13} = \int_{A_o} z \ dA_o = 0$$

$K^s_{14} = \int_{A_o} (y^2 + z^2) \ dA_o = I_y + I_z$: Polar moment of inertia about the shear center.

$$K^s_{15} = \int_{A_o} \bar{\omega} \ dA_o = 0$$

$$K^s_{16} = \int_{A_o} \psi \ dA_o = 0$$

$K^s_{22} = \int_{A_o} y^2 \ dA_o = I_z$: Moment of inertia about the reference z axis through the shear center.

$K^s_{23} = \int_{A_o} -yz dA_o = 0$: Product of inertia about the reference axis.

$$K^s_{24} = \int_{A_o} -y(y^2 + z^2) \ dA_o$$

$$= -b_{ft} t_{ft} \left({D_t}^2 + D_t t_{ft} + {t_{ft}}^2 / 2 \right) h_{ft}$$

$$+ b_{fb} t_{fb} \left({D_b}^2 + D_b t_{fb} + {t_{fb}}^2 / 2 \right) h_{fb} - D t_w \left({D_t}^2 + {D_b}^2 \right) \frac{(D_t - D_b)}{4}$$

$$- \ I_{ft} h_{ft} + I_{fb} h_{fb} - I_{wy} \frac{(D_t - D_b)}{2}$$

$$K^s_{25} = \int_{A_o} -y\bar{\omega} \ dA_o = 0$$

$$K^s_{26} = \int_{A_o} -y\psi \ dA_o = 0$$

$K^s_{33} = \int_{A_o} z^2 \, dA_o = I_y$: Moment of inertia about the reference y axis through the shear center.

$$K^s_{34} = \int_{A_o} z(y^2 + z^2) \, dA_o = 0$$

$$K^s_{35} = \int_{A_o} z\bar{\omega} \, dA_o = 0$$

$$K^s_{36} = \int_{A_o} z\psi \, dA_o = R_t I_{ft} + R_b I_{fb}$$

$$K^s_{44} = \int_{A_o} r^4 \, dA_o$$

$$= b_{ft} \frac{\left(d_t{}^5 - D_t{}^5\right)}{5} + b_{ft}{}^3 \frac{\left(d_t{}^3 - D_t{}^3\right)}{18} + b_{ft}{}^5 \frac{t_{ft}}{80} + b_{fb} \frac{\left(d_b{}^5 - D_b{}^5\right)}{5}$$

$$+ b_{fb}{}^3 \frac{\left(d_b{}^3 - D_b{}^3\right)}{18} + b_{fb}{}^5 \frac{t_{fb}}{80} + t_w \frac{\left(D_t{}^5 + D_b{}^5\right)}{5} + t_w{}^3 \frac{\left(D_t{}^5 + D_b{}^5\right)}{18}$$

$$+ t_w{}^5 \frac{(D_t + D_b)}{80}$$

$$K^s_{45} = \int_{A_o} (y^2 + z^2)\bar{\omega} \, dA_o = 0$$

$$K^s_{46} = \int_{A_o} (y^2 + z^2)\psi \, dA_o = 0$$

$K^s_{55} = \int_{A_o} \bar{\omega}^2 \, dA_o = C_w$: Cross-section warping constant.

$$K^s_{56} = \int_{A_o} \bar{\omega}\psi \, dA_o = -R_t h_{st} I_{ft} + R_b h_{sb} I_{fb}$$

and

$$\mathrm{K^s}_{66} = \int_{\mathrm{A}_o} \left(\psi^2 + \frac{4\mathrm{G}\hat{\gamma}^2}{\mathrm{E}} \right) \mathrm{dA}_o = \mathrm{R}_t{}^2 \mathrm{I}_{ft} + \mathrm{R}_b{}^2 \mathrm{I}_{fb} + \frac{\mathrm{GJ}}{\mathrm{E}}$$

where:

$$\mathrm{R}_t(x) = -2\frac{\mathrm{dh}_{st}(x)}{\mathrm{d}x} - \frac{\mathrm{d}y_s(x)}{\mathrm{d}x} + y_s(x)\frac{\mathrm{db}_{ft}(x)}{\mathrm{d}x}\frac{1}{\mathrm{b}_{ft}(x)}$$

$$\mathrm{R}_b(x) = 2\frac{\mathrm{dh}_{sb}(x)}{\mathrm{d}x} - \frac{\mathrm{d}y_s(x)}{\mathrm{d}x} + y_s(x)\frac{\mathrm{db}_{fb}(x)}{\mathrm{d}x}\frac{1}{\mathrm{b}_{fb}(x)}$$

Based on the solution of the above integral equations, the section tangent stiffness matrix may be expressed as

$$\mathbf{K^s} = \mathrm{E}\begin{bmatrix} \mathrm{A}_o & -y_c\mathrm{A}_o & 0 & (\mathrm{I}_y + \mathrm{I}_z) & 0 & 0 \\ & \mathrm{I}_z & 0 & \mathrm{K^s}_{24} & 0 & 0 \\ & & \mathrm{I}_y & 0 & 0 & \mathrm{R}_t\mathrm{I}_{ft} + \mathrm{R}_b\mathrm{I}_{fb} \\ & & & \mathrm{K^s}_{44} & 0 & 0 \\ & \boldsymbol{Symmetry} & & & \mathrm{C}_w & -\mathrm{R}_t\mathrm{h}_{st}\mathrm{I}_{ft} + \mathrm{R}_b\mathrm{h}_{sb}\mathrm{I}_{fb} \\ & & & & & \mathrm{R}_t{}^2\mathrm{I}_{ft} + \mathrm{R}_b{}^2\mathrm{I}_{fb} + \frac{\mathrm{GJ}}{\mathrm{E}} \end{bmatrix}$$

(Eq. 2.228)

2.7.6 Internal Force Transformations Required for the Projection Operator

The transformation of the internal force vector from the co-rotational frame to the global frame is described by Eq. 2.114. The transformation from the element frame to the

global frame is fixed. The transformation from the co-rotational frame to the element frame is derived below.

The internal force vector in the element frame is given by

$$\mathbf{F}^{e}{}_{m}(\mathbf{u}^{e}, \boldsymbol{\theta}^{e}, \emptyset) = \begin{bmatrix} \mathbf{F}^{e}{}_{mu} \\ \mathbf{F}^{e}{}_{m\theta} \\ \mathbf{F}^{e}{}_{m\emptyset} \end{bmatrix} = \begin{bmatrix} \dfrac{\partial U^{e}}{\partial \mathbf{u}^{e}{}_{m}} \\ \dfrac{\partial U^{e}}{\partial \boldsymbol{\theta}^{e}{}_{m}} \\ \dfrac{\partial U^{e}}{\partial \emptyset_{m}} \end{bmatrix} \qquad m = p, q \qquad (\text{Eq. } 2.229)$$

where:

- U^{e} = Internal energy which is a function of current displacement.
- $\mathbf{F}^{e}$ = Internal force vector in the element frame.
- $\mathbf{u}^{e}$ = Element displacement vector in the element frame.
- $\boldsymbol{\theta}^{e}$ = Rotation vector in the element frame.
- $\emptyset$ = Warping degree of freedom.
- $\mathbf{F}^{e}{}_{u}$= Internal force vector in the element frame, work conjugate to $\mathbf{u}^{e}$.
- $\mathbf{F}^{e}{}_{\theta}$ = Internal force vector in the element frame, work conjugate to $\boldsymbol{\theta}^{e}$.
- $\mathbf{F}^{e}{}_{\emptyset}$ = Internal force vector in the element frame, work conjugate to $\emptyset$.

The internal force vector in the co-rotational frame is given by

$$\mathbf{F}^{c}{}_{m}(\mathbf{u}^{c},\boldsymbol{\theta}^{c},\emptyset)=\begin{bmatrix}\mathbf{F}^{c}{}_{mu}\\ \mathbf{F}^{c}{}_{m\theta}\\ \mathbf{F}^{c}{}_{m\emptyset}\end{bmatrix}=\begin{bmatrix}\dfrac{\partial U^{e}}{\partial \mathbf{u}^{c}{}_{m}}\\ \dfrac{\partial U^{e}}{\partial \boldsymbol{\theta}^{c}{}_{m}}\\ \dfrac{\partial U^{e}}{\partial \emptyset_{m}}\end{bmatrix}\qquad m=p,q \qquad \text{(Eq. 2.230)}$$

where:

- $\mathbf{F}^{c}$ = Internal force vector in the co-rotational frame.
- $\mathbf{u}^{c}$ = Element displacement vector in the co-rotational frame.
- $\boldsymbol{\theta}^{c}$ = Rotation vector in the co-rotational frame.
- $\mathbf{F}^{c}{}_{u}$= Internal force vector in the co-rotational frame, work conjugate to $\mathbf{u}^{c}$..
- $\mathbf{F}^{c}{}_{\theta}$ = Internal force vector in the co-rotational frame, work conjugate to $\boldsymbol{\theta}^{c}$.
- $\mathbf{F}^{c}{}_{\emptyset}$ = Internal force vector in the co-rotational frame, work conjugate to $\emptyset$.

From Eq. 2.229 and Eq. 2.230, the relationship between the internal force vector in the element frame and in the co-rotational frame is described by chain rule and given by

$$\mathbf{F}^{e}{}_{m}(\mathbf{u}^{e},\boldsymbol{\theta}^{e},\emptyset)=\begin{bmatrix}\dfrac{\partial U^{e}}{\partial \mathbf{u}^{e}{}_{m}}\\ \dfrac{\partial U^{e}}{\partial \boldsymbol{\theta}^{e}{}_{m}}\\ \dfrac{\partial U^{e}}{\partial \emptyset_{m}}\end{bmatrix}=\sum_{n=p}^{q}\begin{bmatrix}\dfrac{\partial \mathbf{u}^{c}{}_{n}}{\partial \mathbf{u}^{e}{}_{m}} & \dfrac{\partial \boldsymbol{\theta}^{c}{}_{n}}{\partial \mathbf{u}^{e}{}_{m}} & 0\\ \dfrac{\partial \mathbf{u}^{c}{}_{n}}{\partial \boldsymbol{\theta}^{e}{}_{m}} & \dfrac{\partial \boldsymbol{\theta}^{c}{}_{n}}{\partial \boldsymbol{\theta}^{e}{}_{m}} & 0\\ 0 & 0 & 1\end{bmatrix}\begin{bmatrix}\dfrac{\partial U^{e}}{\partial \mathbf{u}^{c}{}_{n}}\\ \dfrac{\partial U^{e}}{\partial \boldsymbol{\theta}^{c}{}_{n}}\\ \dfrac{\partial U^{e}}{\partial \emptyset_{n}}\end{bmatrix}=\sum_{n=p}^{q}\mathbf{J}^{e}{}_{mn}\,\mathbf{F}^{c}{}_{n}(\mathbf{u}^{c},\boldsymbol{\theta}^{c},\emptyset)$$

(Eq. 2.231)

where:

- $\mathbf{J}^{e}{}_{mn}$ = Jacobian matrix from the co-rotational frame to the element frame.

Using the components and basis vector, Eq. 2.231 can be expressed as

$$\mathbf{F}_k{}^e{}_m(\mathbf{u}^e, \boldsymbol{\theta}^e, \emptyset)\mathbf{e}_k{}^e{}_m = \sum_{n=p}^{q} \mathbf{J}^e{}_{mn}\, \mathbf{F}_k{}^c{}_n(\mathbf{u}^c, \boldsymbol{\theta}^c, \emptyset)\mathbf{e}_k{}^c{}_n \qquad k = 1,2,3 \quad \text{(Eq. 2.232)}$$

where:

$\mathbf{F}_k{}^e$ = The components of the internal force vector in the element frame.

$\mathbf{e}_k{}^e$ = Basis vector in the element frame.

$\mathbf{F}_k{}^c$ = The components of the internal force vector in the co-rotational frame.

$\mathbf{e}_k{}^c$ = Basis vector in the co-rotational frame.

By taking the dot product of the basis vector in the element frame on both sides of Eq. 2.232, one obtains

$$\mathbf{F}_k{}^e{}_m(\mathbf{u}^e, \boldsymbol{\theta}^e, \emptyset)\mathbf{e}_k{}^e{}_m \cdot \mathbf{e}_t{}^e{}_m = \sum_{n=p}^{q} \mathbf{J}^e{}_{mn}\, \mathbf{F}_k{}^c{}_n(\mathbf{u}^c, \boldsymbol{\theta}^c, \emptyset)\mathbf{e}_k{}^c{}_n \cdot \mathbf{e}_t{}^e{}_m \qquad \text{(Eq. 2.233)}$$

Equation 2.233 can be expressed further as

$$\mathbf{F}_t{}^e{}_m(\mathbf{u}^e, \boldsymbol{\theta}^e, \emptyset) = \mathbf{e}_t{}^e{}_m \cdot \mathbf{e}_k{}^c{}_n \sum_{n=p}^{q} \mathbf{J}^e{}_{mn}\, \mathbf{F}_k{}^c{}_n(\mathbf{u}^c, \boldsymbol{\theta}^c, \emptyset) \qquad \text{(Eq. 2.234)}$$

where: m and n are independent indices.

$$\begin{cases} \mathbf{e}_t{}^e{}_m \cdot \mathbf{e}_k{}^c{}_n = 0 & \text{if } m \neq n \\ \mathbf{e}_t{}^e{}_m \cdot \mathbf{e}_k{}^c{}_n = E_{tk}{}^e_c & \text{if } m = n \end{cases}$$

By chain rule, the Jacobian matrix is obtained as

$$\mathbf{J}^{e}{}_{mn} = \begin{bmatrix} \frac{\partial \mathbf{u}^{c}{}_{n}}{\partial \mathbf{u}^{e}{}_{m}} & \frac{\partial \boldsymbol{\theta}^{c}{}_{n}}{\partial \mathbf{u}^{e}{}_{m}} & 0 \\ \frac{\partial \mathbf{u}^{c}{}_{n}}{\partial \boldsymbol{\theta}^{e}{}_{m}} & \frac{\partial \boldsymbol{\theta}^{c}{}_{n}}{\partial \boldsymbol{\theta}^{e}{}_{m}} & 0 \\ 0 & 0 & 1 \end{bmatrix} = \begin{bmatrix} \frac{\partial \mathbf{u}^{c}{}_{n}}{\partial \mathbf{u}^{e}{}_{m}} & \frac{\partial \boldsymbol{\theta}^{c}{}_{n}}{\partial \mathbf{u}^{e}{}_{m}} \frac{\partial \boldsymbol{\omega}^{c}{}_{n}}{\partial \boldsymbol{\omega}^{c}{}_{n}} & 0 \\ \frac{\partial \mathbf{u}^{c}{}_{n}}{\partial \boldsymbol{\theta}^{e}{}_{m}} \frac{\partial \boldsymbol{\omega}^{e}{}_{m}}{\partial \boldsymbol{\omega}^{e}{}_{m}} & \frac{\partial \boldsymbol{\theta}^{c}{}_{n}}{\partial \boldsymbol{\theta}^{e}{}_{m}} \frac{\partial \boldsymbol{\omega}^{e}{}_{m}}{\partial \boldsymbol{\omega}^{e}{}_{m}} \frac{\partial \boldsymbol{\omega}^{c}{}_{n}}{\partial \boldsymbol{\omega}^{c}{}_{n}} & 0 \\ 0 & 0 & 1 \end{bmatrix} \quad \text{(Eq. 2.236)}$$

Furthermore, the Jacobian matrix in Eq. 2.236 can be decomposed into the form

$$\mathbf{J}^{e}{}_{mn} = \begin{bmatrix} \frac{\partial \mathbf{u}^{c}{}_{n}}{\partial \mathbf{u}^{e}{}_{m}} & \frac{\partial \boldsymbol{\theta}^{c}{}_{n}}{\partial \mathbf{u}^{e}{}_{m}} & 0 \\ \frac{\partial \mathbf{u}^{c}{}_{n}}{\partial \boldsymbol{\theta}^{e}{}_{m}} & \frac{\partial \boldsymbol{\theta}^{c}{}_{n}}{\partial \boldsymbol{\theta}^{e}{}_{m}} & 0 \\ 0 & 0 & 1 \end{bmatrix} = \begin{bmatrix} \mathbf{I} & 0 & 0 \\ 0 & \frac{\partial \boldsymbol{\omega}^{e}{}_{m}}{\partial \boldsymbol{\theta}^{e}{}_{m}} & 0 \\ 0 & 0 & 1 \end{bmatrix} \begin{bmatrix} \frac{\partial \mathbf{u}^{c}{}_{n}}{\partial \mathbf{u}^{e}{}_{m}} & \frac{\partial \boldsymbol{\omega}^{c}{}_{n}}{\partial \mathbf{u}^{e}{}_{m}} & 0 \\ \frac{\partial \mathbf{u}^{c}{}_{n}}{\partial \boldsymbol{\omega}^{e}{}_{m}} & \frac{\partial \boldsymbol{\omega}^{c}{}_{n}}{\partial \boldsymbol{\omega}^{e}{}_{m}} & 0 \\ 0 & 0 & 1 \end{bmatrix} \begin{bmatrix} \mathbf{I} & 0 & 0 \\ 0 & \frac{\partial \boldsymbol{\theta}^{c}{}_{n}}{\partial \boldsymbol{\omega}^{c}{}_{n}} & 0 \\ 0 & 0 & 1 \end{bmatrix}$$

(Eq. 2.237)

where:

- $\begin{bmatrix} \mathbf{I} & 0 & 0 \\ 0 & \frac{\partial \boldsymbol{\omega}^{e}{}_{m}}{\partial \boldsymbol{\theta}^{e}{}_{m}} & 0 \\ 0 & 0 & 1 \end{bmatrix}$: Jacobian matrix between the rotation vector and the axial vector in the element frame.
- $\begin{bmatrix} \frac{\partial \mathbf{u}^{c}{}_{n}}{\partial \mathbf{u}^{e}{}_{m}} & \frac{\partial \boldsymbol{\omega}^{c}{}_{n}}{\partial \mathbf{u}^{e}{}_{m}} & 0 \\ \frac{\partial \mathbf{u}^{c}{}_{n}}{\partial \boldsymbol{\omega}^{e}{}_{m}} & \frac{\partial \boldsymbol{\omega}^{c}{}_{n}}{\partial \boldsymbol{\omega}^{e}{}_{m}} & 0 \\ 0 & 0 & 1 \end{bmatrix}$: Projection matrix.
- $\begin{bmatrix} \mathbf{I} & 0 & 0 \\ 0 & \frac{\partial \boldsymbol{\theta}^{c}{}_{n}}{\partial \boldsymbol{\omega}^{c}{}_{n}} & 0 \\ 0 & 0 & 1 \end{bmatrix}$: Jacobian matrix between the rotation vector and the axial vector in the co-rotational frame.

The relationship between the rotation vector and the axial vector is given by

$$\frac{\partial \boldsymbol{\theta}}{\partial \boldsymbol{\omega}} = \mathbf{I} - \frac{1}{2}\boldsymbol{\Theta} + \frac{1 - \frac{1}{2}\theta \cot\left(\frac{\theta}{2}\right)}{\theta^2}\boldsymbol{\Theta}^2 \qquad \text{(Eq. 2.238)}$$

where:

- $\theta = \sqrt{{\theta_1}^2 + {\theta_2}^2 + {\theta_3}^2}$: The magnitude of the rotation vector

As shown in Eq. 2.114, Eq. 2.234 can be given by

$$\mathbf{F}^{\mathrm{e}}(\mathbf{u}^{\mathrm{e}}, \boldsymbol{\theta}^{\mathrm{e}}, \emptyset) = \mathbf{U}^{\mathrm{e}}\mathbf{P}^{\mathrm{T}}\mathbf{M}\mathbf{F}^{\mathrm{c}}(\mathbf{u}^{\mathrm{c}}, \boldsymbol{\theta}^{\mathrm{c}}, \emptyset) \qquad \text{(Eq. 2.235)}$$

where:

- $\mathbf{U}^{\mathrm{e}} = \mathbf{e}_{\mathrm{t}}{}^{\mathrm{e}}{}_{\mathrm{m}} \cdot \mathbf{e}_{\mathrm{k}}{}^{\mathrm{c}}{}_{\mathrm{n}}$: Coordinate transformation from the co-rotational frame to the element frame.
- $\mathbf{U}^{\mathrm{e}}\mathbf{P}^{\mathrm{T}} = \begin{bmatrix} \frac{\partial \mathbf{u}^{\mathrm{c}}{}_{\mathrm{n}}}{\partial \mathbf{u}^{\mathrm{e}}{}_{\mathrm{m}}} & \frac{\partial \boldsymbol{\omega}^{\mathrm{c}}{}_{\mathrm{n}}}{\partial \mathbf{u}^{\mathrm{e}}{}_{\mathrm{m}}} & 0 \\ \frac{\partial \mathbf{u}^{\mathrm{c}}{}_{\mathrm{n}}}{\partial \boldsymbol{\omega}^{\mathrm{e}}{}_{\mathrm{m}}} & \frac{\partial \boldsymbol{\omega}^{\mathrm{c}}{}_{\mathrm{n}}}{\partial \boldsymbol{\omega}^{\mathrm{e}}{}_{\mathrm{m}}} & 0 \\ 0 & 0 & 1 \end{bmatrix}$: Projection matrix in the element frame.
- $\mathbf{M}$ = Mapping that gives the reduction in the degrees of freedom from the element frame to the co-rotational frame).

2.7.7 Projection Tensor

The projection tensor is given by

$$\mathbf{U}^{\mathrm{e}}\mathbf{P}_{\mathrm{mn}}{}^{\mathrm{T}} = \begin{bmatrix} \dfrac{\partial \mathbf{u}^{\mathrm{c}}{}_{\mathrm{n}}}{\partial \mathbf{u}^{\mathrm{e}}{}_{\mathrm{m}}} & \dfrac{\partial \boldsymbol{\omega}^{\mathrm{c}}{}_{\mathrm{n}}}{\partial \mathbf{u}^{\mathrm{e}}{}_{\mathrm{m}}} & 0 \\ \dfrac{\partial \mathbf{u}^{\mathrm{c}}{}_{\mathrm{n}}}{\partial \boldsymbol{\omega}^{\mathrm{e}}{}_{\mathrm{m}}} & \dfrac{\partial \boldsymbol{\omega}^{\mathrm{c}}{}_{\mathrm{n}}}{\partial \boldsymbol{\omega}^{\mathrm{e}}{}_{\mathrm{m}}} & 0 \\ 0 & 0 & 1 \end{bmatrix} \qquad \mathrm{m}\ \&\ \mathrm{n} = \mathrm{p}, \mathrm{q} \qquad \text{(Eq. 2.239)}$$

The projection tensor is defined in the element frame. Thus, the variation of the displacement vectors and the variation of the axial vectors in the element frame are employed:

$$\frac{\partial \mathbf{u}^{\mathrm{c}}{}_{\mathrm{n}}}{\partial \mathbf{u}^{\mathrm{e}}{}_{\mathrm{m}}} = \frac{\left(\mathbf{Spin}(\mathbf{x}^{\mathrm{e}}{}_{\mathrm{n}} - \mathbf{x}^{\mathrm{e}}{}_{\mathrm{o}})\delta\boldsymbol{\omega}_{\mathrm{E}}{}^{e} + (\delta\mathbf{x}^{\mathrm{e}}{}_{\mathrm{n}} - \delta\mathbf{x}^{\mathrm{e}}{}_{\mathrm{o}})\right)}{\partial \mathbf{u}^{\mathrm{e}}{}_{\mathrm{m}}} \qquad \text{(Eq. 2.240)}$$

$$\frac{\partial \boldsymbol{\omega}^{\mathrm{c}}{}_{\mathrm{n}}}{\partial \mathbf{u}^{\mathrm{e}}{}_{\mathrm{m}}} = \frac{\delta\boldsymbol{\omega}^{\mathrm{e}}{}_{\mathrm{n}} - \delta\boldsymbol{\omega}_{\mathrm{E}}{}^{\mathrm{e}}}{\partial \mathbf{u}^{\mathrm{e}}{}_{\mathrm{m}}} \qquad \text{(Eq. 2.241)}$$

$$\frac{\partial \mathbf{u}^{\mathrm{c}}{}_{\mathrm{n}}}{\partial \boldsymbol{\omega}^{\mathrm{e}}{}_{\mathrm{m}}} = \frac{\left(\mathbf{Spin}(\mathbf{x}^{\mathrm{e}}{}_{\mathrm{n}} - \mathbf{x}^{\mathrm{e}}{}_{\mathrm{o}})\delta\boldsymbol{\omega}_{\mathrm{E}}{}^{e} + (\delta\mathbf{x}^{\mathrm{e}}{}_{\mathrm{n}} - \delta\mathbf{x}^{\mathrm{e}}{}_{\mathrm{o}})\right)}{\partial \boldsymbol{\omega}^{\mathrm{e}}{}_{\mathrm{m}}} \qquad \text{(Eq. 2.242)}$$

$$\frac{\partial \boldsymbol{\omega}^{\mathrm{c}}{}_{\mathrm{n}}}{\partial \boldsymbol{\omega}^{\mathrm{e}}{}_{\mathrm{m}}} = \frac{\delta\boldsymbol{\omega}^{\mathrm{e}}{}_{\mathrm{n}} - \delta\boldsymbol{\omega}_{\mathrm{E}}{}^{\mathrm{e}}}{\partial \boldsymbol{\omega}^{\mathrm{e}}{}_{\mathrm{m}}} \qquad \text{(Eq. 2.243)}$$

The variation of the axial vector $\boldsymbol{\omega}_{\mathrm{E}}{}^{\mathrm{e}}$ in Eq. 2.172 is given by

$$\delta\boldsymbol{\omega}_{\mathrm{E}}{}^{\mathrm{e}} = \begin{bmatrix} -\mathbf{e}_2{}^{\mathrm{c}\mathrm{T}}\delta\mathbf{e}_3{}^{\mathrm{c}} \\ -\mathbf{e}_3{}^{\mathrm{c}\mathrm{T}}\delta\mathbf{e}_1{}^{\mathrm{c}} \\ \mathbf{e}_2{}^{\mathrm{c}\mathrm{T}}\delta\mathbf{e}_1{}^{\mathrm{c}} \end{bmatrix} = \begin{bmatrix} -\dfrac{1}{y_{avg_2}}\left(\left(\dfrac{\delta\mathbf{u}_3{}^{\mathrm{e}}{}_{\mathrm{q}} - \delta\mathbf{u}_3{}^{\mathrm{e}}{}_{\mathrm{p}}}{\mathrm{L}}\right)y_{avg_1} - \delta y_{avg_3}\right) \\ \dfrac{\delta\mathbf{u}_3{}^{\mathrm{e}}{}_{\mathrm{p}} - \delta\mathbf{u}_3{}^{\mathrm{e}}{}_{\mathrm{q}}}{\mathrm{L}} \\ \dfrac{\delta\mathbf{u}_2{}^{\mathrm{e}}{}_{\mathrm{q}} - \delta\mathbf{u}_2{}^{\mathrm{e}}{}_{\mathrm{p}}}{\mathrm{L}} \end{bmatrix}$$

From Eqs. 2.240, 2.241, 2.242, 2.243, and 2.172, the closed form of the projection matrix is given by

$$\mathbf{P}(\mathbf{U}^{\mathrm{e}})^{\mathrm{T}} = \begin{bmatrix} 0 & 0 & 0 & 0 & 0 & 0 & 0 & 0 & 0 & 0 & 0 & 0 & 0 & 0 \\ 0 & 0 & 0 & 0 & 0 & 0 & 0 & 0 & 0 & 0 & 0 & 0 & 0 & 0 \\ 0 & 0 & 0 & 0 & 0 & 0 & 0 & 0 & 0 & 0 & 0 & 0 & 0 & 0 \\ 0 & 0 & \mathrm{P}_{43} & \mathrm{P}_{44} & \mathrm{P}_{45} & 0 & 0 & 0 & 0 & \mathrm{P}_{410} & \mathrm{P}_{411} & \mathrm{P}_{412} & 0 & 0 \\ 0 & 0 & -\frac{1}{\mathrm{L}} & 0 & 1 & 0 & 0 & 0 & 0 & \frac{1}{\mathrm{L}} & 0 & 0 & 0 & 0 \\ 0 & \frac{1}{\mathrm{L}} & 0 & 0 & 0 & 1 & 0 & 0 & -\frac{1}{\mathrm{L}} & 0 & 0 & 0 & 0 & 0 \\ 0 & 0 & 0 & 0 & 0 & 0 & 1 & 0 & 0 & 0 & 0 & 0 & 0 & 0 \\ -1 & 0 & 0 & 0 & 0 & 0 & 0 & 1 & 0 & 0 & 0 & 0 & 0 & 0 \\ 0 & 0 & 0 & 0 & 0 & 0 & 0 & 0 & 0 & 0 & 0 & 0 & 0 & 0 \\ 0 & 0 & 0 & 0 & 0 & 0 & 0 & 0 & 0 & 0 & 0 & 0 & 0 & 0 \\ 0 & 0 & \mathrm{P}_{103} & \mathrm{P}_{104} & \mathrm{P}_{105} & 0 & 0 & 0 & 0 & \mathrm{P}_{1010} & \mathrm{P}_{1011} & \mathrm{P}_{1012} & 0 & 0 \\ 0 & 0 & -\frac{1}{\mathrm{L}} & 0 & 0 & 0 & 0 & 0 & 0 & \frac{1}{\mathrm{L}} & 0 & 1 & 0 & 0 \\ 0 & \frac{1}{\mathrm{L}} & 0 & 0 & 0 & 0 & 0 & 0 & -\frac{1}{\mathrm{L}} & 0 & 0 & 0 & 1 & 0 \\ 0 & 0 & 0 & 0 & 0 & 0 & 0 & 0 & 0 & 0 & 0 & 0 & 0 & 1 \end{bmatrix}$$

(Eq. 2.244)

where:

$$\mathrm{P}_{43} = -\frac{y_{avg_1}}{\mathrm{L}y_{avg_2}} = \mathrm{P}_{103}$$

$$\mathrm{P}_{44} = 1 - \frac{\mathbf{e}_2{}^{\mathrm{p}}{}_2}{2y_{avg_2}}$$

$$\mathrm{P}_{45} = \frac{\mathbf{e}_2{}^{\mathrm{p}}{}_1}{2y_{avg_2}} = \mathrm{P}_{105}$$

$$\mathrm{P}_{410} = \frac{y_{avg_1}}{\mathrm{L}y_{avg_2}} = \mathrm{P}_{1010}$$

$$P_{411} = -\frac{\mathbf{e}_2{}^{q}{}_2}{2y_{avg_2}}$$

$$P_{412} = \frac{\mathbf{e}_2{}^{q}{}_1}{2y_{avg_2}} = P_{1012}$$

$$P_{104} = -\frac{\mathbf{e}_2{}^{p}{}_2}{2y_{avg_2}}$$

$$P_{1011} = 1 - \frac{\mathbf{e}_2{}^{q}{}_2}{2y_{avg_2}}$$

2.7.8 Variation in the Internal Force Vector due to a Variation in the Element Displacements $\delta\mathbf{U}^{e}$

In Eq. 2.121, the variation of the internal force vector corresponding to the global frame is given by

$$\delta\mathbf{F}^{g} = \mathbf{U}^{g}\delta\mathbf{U}^{e}\mathbf{P}^{T}\mathbf{M}\mathbf{F}^{c} + \mathbf{U}^{g}\mathbf{U}^{e}\delta\mathbf{P}^{T}\mathbf{M}\mathbf{F}^{c} + \mathbf{U}^{g}\mathbf{U}^{e}\mathbf{P}^{T}\mathbf{M}\delta\mathbf{F}^{c}$$

The first term in Eq. 2.121 can be expressed as

$$\mathbf{U}^{g}\delta\mathbf{U}^{e}\mathbf{P}^{T}\mathbf{M}\mathbf{F}^{c} = \mathbf{U}^{g}\mathrm{diag}(\delta\mathbf{E}_{c}^{e})\mathbf{P}^{T}\mathbf{M}\mathbf{F}^{c} \qquad \text{(Eq 2.245)}$$

Furthermore, the variation of the spin tensor of $\boldsymbol{\omega}_{E}{}^{e}$ is given by

$$\delta\boldsymbol{\Omega}_{\mathbf{E}_c^e} = \mathbf{Spin}(\delta\boldsymbol{\omega}_{E}{}^{e}) = \delta\mathbf{E}_{c}^{e}(\mathbf{E}_{c}^{e})^{T} \qquad \text{(Eq 2.246)}$$

From Eq. 2.246, Eq. 2.245 can be given by

$$\mathbf{U}^{g}\delta\mathbf{U}^{e}\mathbf{P}^{T}\mathbf{M}\mathbf{F}^{c} = \mathbf{U}^{g}\begin{bmatrix} \mathbf{Spin}(\delta\boldsymbol{\omega}_{E}{}^{e}) & \mathbf{0} & 0 & \mathbf{0} & \mathbf{0} & 0 \\ \mathbf{0} & \mathbf{Spin}(\delta\boldsymbol{\omega}_{E}{}^{e}) & 0 & \mathbf{0} & \mathbf{0} & 0 \\ 0 & 0 & 0 & 0 & 0 & 0 \\ \mathbf{0} & \mathbf{0} & 0 & \mathbf{Spin}(\delta\boldsymbol{\omega}_{E}{}^{e}) & \mathbf{0} & 0 \\ \mathbf{0} & \mathbf{0} & 0 & \mathbf{0} & \mathbf{Spin}(\delta\boldsymbol{\omega}_{E}{}^{e}) & 0 \\ 0 & 0 & 0 & 0 & 0 & 0 \end{bmatrix}\mathbf{U}^{e}\mathbf{P}^{T}\mathbf{M}\mathbf{F}^{c}$$

(Eq 2.247)

With respect to internal force vector in the element frame, Eq. 2.247 can be expressed as

$$\mathbf{U}^{g}\delta\mathbf{U}^{e}\mathbf{P}^{T}\mathbf{M}\mathbf{F}^{c} = \mathbf{U}^{g}\begin{bmatrix} \mathbf{Spin}(\delta\boldsymbol{\omega}_{E}{}^{e}) & \mathbf{0} & 0 & \mathbf{0} & \mathbf{0} & 0 \\ \mathbf{0} & \mathbf{Spin}(\delta\boldsymbol{\omega}_{E}{}^{e}) & 0 & \mathbf{0} & \mathbf{0} & 0 \\ 0 & 0 & 0 & 0 & 0 & 0 \\ \mathbf{0} & \mathbf{0} & 0 & \mathbf{Spin}(\delta\boldsymbol{\omega}_{E}{}^{e}) & \mathbf{0} & 0 \\ \mathbf{0} & \mathbf{0} & 0 & \mathbf{0} & \mathbf{Spin}(\delta\boldsymbol{\omega}_{E}{}^{e}) & 0 \\ 0 & 0 & 0 & 0 & 0 & 0 \end{bmatrix}\mathbf{F}^{e}$$

(Eq 2.248)

In Eq. 2.248, the internal force vector in the element frame $\mathbf{F}^{e}$ is mapped to the internal force vector in the co-rotational frame $\mathbf{F}^{c}$ in Eq. 2.109, where:

$$\mathbf{F}^{c} = \begin{Bmatrix} \mathrm{P} & \mathrm{M}_{1_p}^{c} & \mathrm{M}_{3_p}^{c} & \mathrm{M}_{2_p}^{c} & \mathrm{B}_{p} & \mathrm{M}_{1_q}^{c} & \mathrm{M}_{3_q}^{c} & \mathrm{M}_{2_q}^{c} & \mathrm{B}_{q} \end{Bmatrix}^{T}$$

$$\mathbf{F}^{e} = \begin{Bmatrix} \mathrm{F}_{1_p}^{e} & \mathrm{F}_{2_p}^{e} & \mathrm{F}_{3_p}^{e} & \mathrm{M}_{1_p}^{e} & \mathrm{M}_{2_p}^{e} & \mathrm{M}_{3_p}^{e} & \mathrm{B}_{p} & \mathrm{F}_{1_q}^{e} & \mathrm{F}_{2_q}^{e} & \mathrm{F}_{3_q}^{e} & \mathrm{M}_{1_q}^{e} & \mathrm{M}_{2_q}^{e} & \mathrm{M}_{3_q}^{e} & \mathrm{B}_{q} \end{Bmatrix}^{T}$$

$$\mathbf{F}^{e} = \begin{Bmatrix} -\mathrm{P} & -\mathrm{V}_{y} & -\mathrm{V}_{z} & \mathrm{M}_{1_p}^{c} & \mathrm{M}_{2_p}^{c} & \mathrm{M}_{3_p}^{c} & \mathrm{B}_{p} & \mathrm{P} & \mathrm{V}_{y} & \mathrm{V}_{z} & \mathrm{M}_{1_q}^{c} & \mathrm{M}_{2_q}^{c} & \mathrm{M}_{3_q}^{c} & \mathrm{B}_{q} \end{Bmatrix}^{T}$$

(Eq. 2.249)

where:

- $M_{1_p}^c + M_{1_q}^c = 0$ (Eq. 2.250)
- $V_y = \frac{-\left(M_{3_p}^c + M_{3_q}^c\right)}{L}$ (Eq. 2.251)
- $V_z = \frac{\left(M_{2_p}^c + M_{2_q}^c\right)}{L}$ (Eq. 2.252)

In terms of the components of the internal force vector in the element frame, Eq. 2.248 can be written as

$$\mathbf{U}^g \delta \mathbf{U}^e \mathbf{P}^T \mathbf{M} \mathbf{F}^c = \mathbf{U}^g \begin{bmatrix} \mathbf{Spin}(\delta \boldsymbol{\omega}_E{}^e) & \mathbf{0} & 0 & \mathbf{0} & \mathbf{0} & 0 \\ \mathbf{0} & \mathbf{Spin}(\delta \boldsymbol{\omega}_E{}^e) & 0 & \mathbf{0} & \mathbf{0} & 0 \\ 0 & 0 & 0 & 0 & 0 & 0 \\ \mathbf{0} & \mathbf{0} & 0 & \mathbf{Spin}(\delta \boldsymbol{\omega}_E{}^e) & \mathbf{0} & 0 \\ \mathbf{0} & \mathbf{0} & 0 & \mathbf{0} & \mathbf{Spin}(\delta \boldsymbol{\omega}_E{}^e) & 0 \\ 0 & 0 & 0 & 0 & 0 & 0 \end{bmatrix} \begin{bmatrix} \mathbf{F}^e{}_{pu} \\ \mathbf{F}^e{}_{p\theta} \\ \mathbf{F}^e{}_{p\emptyset} \\ \mathbf{F}^e{}_{qu} \\ \mathbf{F}^e{}_{q\theta} \\ \mathbf{F}^e{}_{q\emptyset} \end{bmatrix}$$

(Eq. 2.253)

$$\mathbf{U}^g \delta \mathbf{U}^e \mathbf{P}^T \mathbf{M} \mathbf{F}^c = \mathbf{U}^g \begin{bmatrix} \mathbf{Spin}(\delta \boldsymbol{\omega}_E{}^e)\mathbf{F}^e{}_{pu} \\ \mathbf{Spin}(\delta \boldsymbol{\omega}_E{}^e)\mathbf{F}^e{}_{p\theta} \\ 0 \\ \mathbf{Spin}(\delta \boldsymbol{\omega}_E{}^e)\mathbf{F}^e{}_{qu} \\ \mathbf{Spin}(\delta \boldsymbol{\omega}_E{}^e)\mathbf{F}^e{}_{q\theta} \\ 0 \end{bmatrix} = \mathbf{U}^g \begin{bmatrix} -\mathbf{Spin}\left(\mathbf{F}^e{}_{pu}\right) \\ -\mathbf{Spin}\left(\mathbf{F}^e{}_{p\theta}\right) \\ 0 \\ -\mathbf{Spin}\left(\mathbf{F}^e{}_{qu}\right) \\ -\mathbf{Spin}\left(\mathbf{F}^e{}_{q\theta}\right) \\ 0 \end{bmatrix} \delta \boldsymbol{\omega}_E{}^e$$

(Eq. 2.254)

$$\delta \boldsymbol{\omega}_E{}^e = \frac{\delta \boldsymbol{\omega}_E{}^e}{\partial \mathbf{d}^e} \delta \mathbf{d}^e = \begin{bmatrix} \frac{\delta \boldsymbol{\omega}_E{}^e}{\partial \mathbf{u}^e{}_p} & \frac{\delta \boldsymbol{\omega}_E{}^e}{\partial \boldsymbol{\omega}^e{}_p} & \frac{\delta \boldsymbol{\omega}_E{}^e}{\partial \emptyset_p} & \frac{\delta \boldsymbol{\omega}_E{}^e}{\partial \mathbf{u}^e{}_q} & \frac{\delta \boldsymbol{\omega}_E{}^e}{\partial \boldsymbol{\omega}^e{}_q} & \frac{\delta \boldsymbol{\omega}_E{}^e}{\partial \emptyset_q} \end{bmatrix} \delta \mathbf{d}^e$$

$$\frac{\delta\boldsymbol{\omega}_{\mathrm{E}}{}^{\mathrm{e}}}{\partial\mathbf{d}^{\mathrm{e}}}=\begin{bmatrix} 0 & 0 & \dfrac{y_{avg_1}}{\mathrm{L}y_{avg_2}} & \dfrac{1}{2}\dfrac{\mathbf{e}_2{}^{\mathrm{p}}{}_2}{y_{avg_2}} & \dfrac{-1}{2}\dfrac{\mathbf{e}_2{}^{\mathrm{p}}{}_1}{y_{avg_2}} & 0 & 0 & 0 & 0 & \dfrac{-y_{avg_1}}{\mathrm{L}y_{avg_2}} & \dfrac{1}{2}\dfrac{\mathbf{e}_2{}^{\mathrm{q}}{}_2}{y_{avg_2}} & \dfrac{-1}{2}\dfrac{\mathbf{e}_2{}^{\mathrm{q}}{}_1}{y_{avg_2}} & 0 & 0 \\ 0 & 0 & \dfrac{1}{\mathrm{L}} & 0 & 0 & 0 & 0 & 0 & 0 & \dfrac{-1}{\mathrm{L}} & 0 & 0 & 0 & 0 \\ 0 & \dfrac{-1}{\mathrm{L}} & 0 & 0 & 0 & 0 & 0 & 0 & \dfrac{1}{\mathrm{L}} & 0 & 0 & 0 & 0 & 0 \end{bmatrix}$$

(Eq. 2.255)

The first term in Eq 2.121is given by

$$\mathbf{U}^{\mathrm{g}}\delta\mathbf{U}^{\mathrm{e}}\mathbf{P}^{\mathrm{T}}\mathbf{M}\mathbf{F}^{\mathrm{c}}=\mathbf{U}^{\mathrm{g}}\mathbf{K}_{\mathrm{g1}}\delta\mathbf{d}^{\mathrm{e}} \qquad \text{(Eq. 2.256)}$$

where:

$$\mathbf{K}_{\mathrm{g1}}=\begin{bmatrix} -\mathbf{Spin}\left(\mathbf{F}^{\mathrm{e}}{}_{\mathrm{pu}}\right) \\ -\mathbf{Spin}\left(\mathbf{F}^{\mathrm{e}}{}_{\mathrm{p}\theta}\right) \\ 0 \\ -\mathbf{Spin}\left(\mathbf{F}^{\mathrm{e}}{}_{\mathrm{qu}}\right) \\ -\mathbf{Spin}\left(\mathbf{F}^{\mathrm{e}}{}_{\mathrm{q}\theta}\right) \\ 0 \end{bmatrix}\begin{bmatrix} \dfrac{\delta\boldsymbol{\omega}_{\mathrm{E}}{}^{\mathrm{e}}}{\partial\mathbf{u}^{\mathrm{e}}{}_{\mathrm{p}}} & \dfrac{\delta\boldsymbol{\omega}_{\mathrm{E}}{}^{\mathrm{e}}}{\partial\boldsymbol{\omega}^{\mathrm{e}}{}_{\mathrm{p}}} & \dfrac{\delta\boldsymbol{\omega}_{\mathrm{E}}{}^{\mathrm{e}}}{\partial\emptyset_{\mathrm{p}}} & \dfrac{\delta\boldsymbol{\omega}_{\mathrm{E}}{}^{\mathrm{e}}}{\partial\mathbf{u}^{\mathrm{e}}{}_{\mathrm{q}}} & \dfrac{\delta\boldsymbol{\omega}_{\mathrm{E}}{}^{\mathrm{e}}}{\partial\boldsymbol{\omega}^{\mathrm{e}}{}_{\mathrm{q}}} & \dfrac{\delta\boldsymbol{\omega}_{\mathrm{E}}{}^{\mathrm{e}}}{\partial\emptyset_{\mathrm{q}}} \end{bmatrix}$$

From Eq. 2.249 and Eq. 2.255, Eq. 2.256 is obtained as

$$\mathbf{K}_{g1} =$$

$$\begin{bmatrix}
0 & \frac{-V_y}{L} & \frac{-V_z}{L} & 0 & 0 & 0\,0\,0 & \frac{V_y}{L} & \frac{V_z}{L} & 0 & 0 & 0\,0 \\
0 & \frac{P}{L} & \frac{V_z y_{avg_1}}{L y_{avg_2}} & \frac{V_z}{2}\frac{{e_2}^p{}_2}{y_{avg_2}} & \frac{-V_z}{2}\frac{{e_2}^p{}_1}{y_{avg_2}} & 0\,0\,0 & \frac{-P}{L} & \frac{-V_z y_{avg_1}}{L y_{avg_2}} & \frac{V_z}{2}\frac{{e_2}^q{}_2}{y_{avg_2}} & \frac{-V_z}{2}\frac{{e_2}^q{}_1}{y_{avg_2}} & 0\,0 \\
0\,0 & \left(\frac{P}{L} - \frac{V_y y_{avg_1}}{L y_{avg_2}}\right) & \frac{-V_y}{2}\frac{{e_2}^p{}_2}{y_{avg_2}} & \frac{V_y}{2}\frac{{e_2}^p{}_1}{y_{avg_2}} & 0\,0\,0 & 0 & -\left(\frac{P}{L} - \frac{V_y y_{avg_1}}{L y_{avg_2}}\right) & \frac{-V_y}{2}\frac{{e_2}^q{}_2}{y_{avg_2}} & \frac{V_y}{2}\frac{{e_2}^q{}_1}{y_{avg_2}} & 0\,0 \\
0 & \frac{M^c_{2p}}{L} & \frac{M^c_{3p}}{L} & 0 & 0 & 0\,0\,0 & \frac{-M^c_{2p}}{L} & \frac{-M^c_{3p}}{L} & 0 & 0 & 0\,0 \\
0 & \frac{-M^c_{1p}}{L} & \frac{-M^c_{3p} y_{avg_1}}{L y_{avg_2}} & \frac{-M^c_{3p}}{2}\frac{{e_2}^p{}_2}{y_{avg_2}} & \frac{M^c_{3p}}{2}\frac{{e_2}^p{}_1}{y_{avg_2}} & 0\,0\,0 & \frac{M^c_{1p}}{L} & \frac{M^c_{3p} y_{avg_1}}{L y_{avg_2}} & \frac{-M^c_{3p}}{2}\frac{{e_2}^q{}_2}{y_{avg_2}} & \frac{M^c_{3p}}{2}\frac{{e_2}^q{}_1}{y_{avg_2}} & 0\,0 \\
0\,0 & \left(\frac{-M^c_{1p}}{L} + \frac{M^c_{2p} y_{avg_1}}{L y_{avg_2}}\right) & \frac{M^c_{2p}}{2}\frac{{e_2}^p{}_2}{y_{avg_2}} & \frac{-M^c_{2p}}{2}\frac{{e_2}^p{}_1}{y_{avg_2}} & 0\,0\,0 & 0 & \left(\frac{M^c_{1p}}{L} - \frac{M^c_{2p} y_{avg_1}}{L y_{avg_2}}\right) & \frac{M^c_{2p}}{2}\frac{{e_2}^q{}_2}{y_{avg_2}} & \frac{-M^c_{2p}}{2}\frac{{e_2}^q{}_1}{y_{avg_2}} & 0\,0 \\
0\,0 & 0 & 0 & 0 & 0\,0\,0 & 0 & 0 & 0 & 0 & 0\,0 \\
0 & \frac{V_y}{L} & \frac{V_z}{L} & 0 & 0 & 0\,0\,0 & \frac{-V_y}{L} & \frac{-V_z}{L} & 0 & 0 & 0\,0 \\
0 & \frac{-P}{L} & \frac{-V_z y_{avg_1}}{L y_{avg_2}} & \frac{-V_z}{2}\frac{{e_2}^p{}_2}{y_{avg_2}} & \frac{V_z}{2}\frac{{e_2}^p{}_1}{y_{avg_2}} & 0\,0\,0 & \frac{P}{L} & \frac{V_z y_{avg_1}}{L y_{avg_2}} & -\frac{V_z}{2}\frac{{e_2}^q{}_2}{y_{avg_2}} & \frac{-V_z}{2}\frac{{e_2}^q{}_1}{y_{avg_2}} & 0\,0 \\
0\,0 & -\left(\frac{P}{L} - \frac{V_y y_{avg_1}}{L y_{avg_2}}\right) & \frac{V_y}{2}\frac{{e_2}^p{}_2}{y_{avg_2}} & \frac{-V_y}{2}\frac{{e_2}^p{}_1}{y_{avg_2}} & 0\,0\,0 & 0 & \left(\frac{P}{L} - \frac{V_y y_{avg_1}}{L y_{avg_2}}\right) & \frac{V_y}{2}\frac{{e_2}^q{}_2}{y_{avg_2}} & \frac{V_y}{2}\frac{{e_2}^q{}_1}{y_{avg_2}} & 0\,0 \\
0 & \frac{M^c_{2q}}{L} & \frac{M^c_{3q}}{L} & 0 & 0 & 0\,0\,0 & \frac{-M^c_{2q}}{L} & \frac{-M^c_{3q}}{L} & 0 & 0 & 0\,0 \\
0 & \frac{M^c_{1q}}{L} & \frac{-M^c_{3q} y_{avg_1}}{L y_{avg_2}} & \frac{-M^c_{3q}}{2}\frac{{e_2}^p{}_2}{y_{avg_2}} & \frac{M^c_{3q}}{2}\frac{{e_2}^p{}_1}{y_{avg_2}} & 0\,0\,0 & \frac{-M^c_{1q}}{L} & \frac{M^c_{3q} y_{avg_1}}{L y_{avg_2}} & \frac{-M^c_{3q}}{2}\frac{{e_2}^q{}_2}{y_{avg_2}} & \frac{M^c_{3q}}{2}\frac{{e_2}^q{}_1}{y_{avg_2}} & 0\,0 \\
0\,0 & \left(\frac{M^c_{1q}}{L} + \frac{M^c_{2q} y_{avg_1}}{L y_{avg_2}}\right) & \frac{M^c_{2q}}{2}\frac{{e_2}^p{}_2}{y_{avg_2}} & \frac{-M^c_{2q}}{2}\frac{{e_2}^p{}_1}{y_{avg_2}} & 0\,0\,0 & 0 & \left(\frac{-M^c_{1q}}{L} - \frac{M^c_{2q} y_{avg_1}}{L y_{avg_2}}\right) & \frac{M^c_{2q}}{2}\frac{{e_2}^q{}_2}{y_{avg_2}} & \frac{-M^c_{2q}}{2}\frac{{e_2}^q{}_1}{y_{avg_2}} & 0\,0 \\
0\,0 & 0 & 0 & 0 & 0\,0\,0 & 0 & 0 & 0 & 0 & 0\,0
\end{bmatrix}$$

(Eq 2.257)

2.7.9 Variation in the Internal Force Vector due to the Variation of the Projection Operator $\delta\mathbf{P}^T$

In Eq. 2.121, the variation of the internal force vector corresponding to the global frame is given by

$$\delta\mathbf{F}^g = \mathbf{U}^g\delta\mathbf{U}^e\mathbf{P}^T\mathbf{M}\mathbf{F}^c + \mathbf{U}^g\mathbf{U}^e\delta\mathbf{P}^T\mathbf{M}\mathbf{F}^c + \mathbf{U}^g\mathbf{U}^e\mathbf{P}^T\mathbf{M}\delta\mathbf{F}^c$$

The second term in Eq. 2.121 is

$$\mathbf{U}^{g}\mathbf{U}^{e}\delta\mathbf{P}^{T}\mathbf{M}\mathbf{F}^{c} \qquad \text{(Eq. 2.258)}$$

From Eq. 2.109 and Eq. 2.119, the following equation can be developed:

$$\mathbf{M}\mathbf{F}^{c} = \left\{0 \;\; 0 \;\; 0 \;\; M^{c}_{1_p} \;\; M^{c}_{2_p} \;\; M^{c}_{3_p} \;\; B_p \;\; P \;\; 0 \;\; 0 \;\; M^{c}_{1_q} \;\; M^{c}_{2_q} \;\; M^{c}_{3_q} \;\; B_q\right\}^{T} \qquad \text{(Eq. 2.259)}$$

The variation of the projection matrix in the element frame is given by

$$\delta\mathbf{P}(\mathbf{U}^{e})^{T} =$$

$$\begin{bmatrix}
0 & 0 & 0 & 0 & 0 & 0 & 0 & 0 & 0 & 0 & 0 & 0 & 0 & 0 \\
0 & 0 & 0 & 0 & 0 & 0 & 0 & 0 & 0 & 0 & 0 & 0 & 0 & 0 \\
0 & 0 & 0 & 0 & 0 & 0 & 0 & 0 & 0 & 0 & 0 & 0 & 0 & 0 \\
0 & 0 & \delta P_{43} & \delta P_{44} & \delta P_{45} & 0 & 0 & 0 & 0 & \delta P_{410} & \delta P_{411} & \delta P_{412} & 0 & 0 \\
0 & 0 & -\delta\left(\frac{1}{L}\right) & 0 & 0 & 0 & 0 & 0 & 0 & \delta\left(\frac{1}{L}\right) & 0 & 0 & 0 & 0 \\
0 & \delta\left(\frac{1}{L}\right) & 0 & 0 & 0 & 0 & 0 & 0 & -\delta\left(\frac{1}{L}\right) & 0 & 0 & 0 & 0 & 0 \\
0 & 0 & 0 & 0 & 0 & 0 & 0 & 0 & 0 & 0 & 0 & 0 & 0 & 0 \\
0 & 0 & 0 & 0 & 0 & 0 & 0 & 0 & 0 & 0 & 0 & 0 & 0 & 0 \\
0 & 0 & 0 & 0 & 0 & 0 & 0 & 0 & 0 & 0 & 0 & 0 & 0 & 0 \\
0 & 0 & 0 & 0 & 0 & 0 & 0 & 0 & 0 & 0 & 0 & 0 & 0 & 0 \\
0 & 0 & \delta P_{103} & \delta P_{104} & \delta P_{105} & 0 & 0 & 0 & 0 & \delta P_{1010} & \delta P_{1011} & \delta P_{1012} & 0 & 0 \\
0 & 0 & -\delta\left(\frac{1}{L}\right) & 0 & 0 & 0 & 0 & 0 & 0 & \delta\left(\frac{1}{L}\right) & 0 & 0 & 0 & 0 \\
0 & \delta\left(\frac{1}{L}\right) & 0 & 0 & 0 & 0 & 0 & 0 & -\delta\left(\frac{1}{L}\right) & 0 & 0 & 0 & 0 & 0 \\
0 & 0 & 0 & 0 & 0 & 0 & 0 & 0 & 0 & 0 & 0 & 0 & 0 & 0
\end{bmatrix}$$

(Eq. 2.260)

From Eq. 2.259 and Eq. 2.260,

$$\mathbf{U}^{e}\delta\mathbf{P}^{T}\mathbf{M}\mathbf{F}^{c} = \begin{Bmatrix} 0 \\ \delta\left(\frac{1}{L}\right)\left(M_{3_p}^{c} + M_{3_q}^{c}\right) \\ M_{1_p}^{c}\delta P_{43} + M_{1_q}^{c}\delta P_{103} - \delta\left(\frac{1}{L}\right)\left(M_{2_p}^{c} + M_{2_q}^{c}\right) \\ M_{1_p}^{c}\delta P_{44} + M_{1_q}^{c}\delta P_{104} \\ M_{1_p}^{c}\delta P_{45} + M_{1_q}^{c}\delta P_{105} \\ 0 \\ 0 \\ 0 \\ -\delta\left(\frac{1}{L}\right)\left(M_{3_p}^{c} + M_{3_q}^{c}\right) \\ M_{1_p}^{c}\delta P_{410} + M_{1_q}^{c}\delta P_{1010} + \delta\left(\frac{1}{L}\right)\left(M_{2_p}^{c} + M_{2_q}^{c}\right) \\ M_{1_p}^{c}\delta P_{411} + M_{1_q}^{c}\delta P_{1011} \\ M_{1_p}^{c}\delta P_{412} + M_{1_q}^{c}\delta P_{1012} \\ 0 \\ 0 \end{Bmatrix} \qquad \text{(Eq. 2.261)}$$

where:

$$\delta P_{43} = -\frac{1}{L}\delta\left(\frac{y_{avg_1}}{y_{avg_2}}\right) + \frac{\delta L}{L^2}\left(\frac{y_{avg_1}}{y_{avg_2}}\right) = \delta P_{103}$$

$$\delta P_{44} = \frac{1}{2}\delta\left(\frac{\mathbf{a}_{2_2}}{y_{avg_2}}\right) = \delta P_{104}$$

$$\delta P_{45} = \frac{1}{2}\delta\left(\frac{\mathbf{a}_{2_1}}{y_{avg_2}}\right) = \delta P_{105}$$

$$\delta P_{410} = \frac{1}{L}\delta\left(\frac{y_{avg_1}}{y_{avg_2}}\right) - \frac{\delta L}{L^2}\left(\frac{y_{avg_1}}{y_{avg_2}}\right) = \delta P_{1010}$$

$$\delta P_{411} = -\frac{1}{2}\delta\left(\frac{\mathbf{b}_{2_2}}{y_{avg_2}}\right) = \delta P_{1011}$$

$$\delta P_{412} = \frac{1}{2}\delta\left(\frac{\mathbf{b}_{2_1}}{y_{avg_2}}\right) = \delta P_{1012}$$

From Eq. 2.250, Eq. 2.261 can be expressed as

$$\mathbf{U}^{e}\delta\mathbf{P}^{T}\mathbf{M}\mathbf{F}^{c} = \begin{Bmatrix} 0 \\ \delta\left(\frac{1}{L}\right)\left(M^{c}_{3_p} + M^{c}_{3_q}\right) \\ -\delta\left(\frac{1}{L}\right)\left(M^{c}_{2_p} + M^{c}_{2_q}\right) \\ 0 \\ 0 \\ 0 \\ 0 \\ 0 \\ -\delta\left(\frac{1}{L}\right)\left(M^{c}_{3_p} + M^{c}_{3_q}\right) \\ \delta\left(\frac{1}{L}\right)\left(M^{c}_{2_p} + M^{c}_{2_q}\right) \\ 0 \\ 0 \\ 0 \\ 0 \end{Bmatrix} \qquad \text{(Eq. 2.262)}$$

In Eq. 2.151, the current element length is given by

$$L = \sqrt{\left(\mathbf{x}^{e}{}_{q} - \mathbf{x}^{e}{}_{p}\right)^{T}\left(\mathbf{x}^{e}{}_{q} - \mathbf{x}^{e}{}_{p}\right)}$$

The variation of the inverse of the current element length may be written as

$$\delta\left(\frac{1}{L}\right) = \frac{-\delta L}{L^2} = \frac{\left(\mathbf{x}^{e}{}_{q} - \mathbf{x}^{e}{}_{p}\right)^{T}\left(\delta\mathbf{x}^{e}{}_{q} - \delta\mathbf{x}^{e}{}_{p}\right)}{L^2} = \frac{-\left(\delta\mathbf{u}_1{}^{e}{}_{q} - \delta\mathbf{u}_1{}^{e}{}_{p}\right)}{L^2} \qquad \text{(Eq. 2.263)}$$

Then, Eq. 2.262 can be expressed as

$$\mathbf{U}^{e}\delta\mathbf{P}^{T}\mathbf{M}\mathbf{F}^{c}=\begin{Bmatrix}0\\ \frac{\left(\delta\mathbf{u}_1{}^{e}{}_{q}-\delta\mathbf{u}_1{}^{e}{}_{p}\right)}{L^{2}}\left(M^{c}_{3_p}+M^{c}_{3_q}\right)\\ -\frac{\left(\delta\mathbf{u}_1{}^{e}{}_{q}-\delta\mathbf{u}_1{}^{e}{}_{p}\right)}{L^{2}}\left(M^{c}_{2_p}+M^{c}_{2_q}\right)\\ 0\\0\\0\\0\\0\\ -\frac{\left(\delta\mathbf{u}_1{}^{e}{}_{q}-\delta\mathbf{u}_1{}^{e}{}_{p}\right)}{L^{2}}\left(M^{c}_{3_p}+M^{c}_{3_q}\right)\\ \frac{\left(\delta\mathbf{u}_1{}^{e}{}_{q}-\delta\mathbf{u}_1{}^{e}{}_{p}\right)}{L^{2}}\left(M^{c}_{2_p}+M^{c}_{2_q}\right)\\0\\0\\0\\0\end{Bmatrix} \qquad \text{(Eq. 2.264)}$$

From Eq. 2.251 and Eq. 2.252, Eq. 2.264 can be expressed as

$$\mathbf{U}^{e}\delta\mathbf{P}^{T}\mathbf{M}\mathbf{F}^{c}=\begin{Bmatrix}0\\ \left(\delta\mathbf{u}_1{}^{e}{}_{q}-\delta\mathbf{u}_1{}^{e}{}_{p}\right)\frac{V_y}{L}\\ \left(\delta\mathbf{u}_1{}^{e}{}_{q}-\delta\mathbf{u}_1{}^{e}{}_{p}\right)\frac{V_z}{L}\\0\\0\\0\\0\\0\\ \left(\delta\mathbf{u}_1{}^{e}{}_{p}-\delta\mathbf{u}_1{}^{e}{}_{q}\right)\frac{V_y}{L}\\ \left(\delta\mathbf{u}_1{}^{e}{}_{p}-\delta\mathbf{u}_1{}^{e}{}_{q}\right)\frac{V_z}{L}\\0\\0\\0\\0\end{Bmatrix} \qquad \text{(Eq. 2.265)}$$

With respect to the variation of the displacement in the element frame, Eq. 2.265 can be expressed as

$$\mathbf{U}^{\mathrm{e}}\delta\mathbf{P}^{\mathrm{T}}\mathbf{M}\mathbf{F}^{\mathrm{c}} = \mathbf{K}_{\mathrm{g2}}\delta\mathbf{d}^{\mathrm{e}} \qquad \text{(Eq. 2.266)}$$

$$\mathbf{K}_{\mathrm{g2}} = \begin{bmatrix} 0 & 0 & 0 & 0 & 0 & 0 & 0 & 0 & 0 & 0 & 0 & 0 & 0 & 0 \\ \frac{-V_y}{L} & 0 & 0 & 0 & 0 & 0 & 0 & \frac{V_y}{L} & 0 & 0 & 0 & 0 & 0 & 0 \\ \frac{-V_z}{L} & 0 & 0 & 0 & 0 & 0 & 0 & \frac{V_z}{L} & 0 & 0 & 0 & 0 & 0 & 0 \\ 0 & 0 & 0 & 0 & 0 & 0 & 0 & 0 & 0 & 0 & 0 & 0 & 0 & 0 \\ 0 & 0 & 0 & 0 & 0 & 0 & 0 & 0 & 0 & 0 & 0 & 0 & 0 & 0 \\ 0 & 0 & 0 & 0 & 0 & 0 & 0 & 0 & 0 & 0 & 0 & 0 & 0 & 0 \\ 0 & 0 & 0 & 0 & 0 & 0 & 0 & 0 & 0 & 0 & 0 & 0 & 0 & 0 \\ 0 & 0 & 0 & 0 & 0 & 0 & 0 & 0 & 0 & 0 & 0 & 0 & 0 & 0 \\ \frac{V_y}{L} & 0 & 0 & 0 & 0 & 0 & 0 & \frac{-V_y}{L} & 0 & 0 & 0 & 0 & 0 & 0 \\ \frac{V_z}{L} & 0 & 0 & 0 & 0 & 0 & 0 & \frac{-V_z}{L} & 0 & 0 & 0 & 0 & 0 & 0 \\ 0 & 0 & 0 & 0 & 0 & 0 & 0 & 0 & 0 & 0 & 0 & 0 & 0 & 0 \\ 0 & 0 & 0 & 0 & 0 & 0 & 0 & 0 & 0 & 0 & 0 & 0 & 0 & 0 \\ 0 & 0 & 0 & 0 & 0 & 0 & 0 & 0 & 0 & 0 & 0 & 0 & 0 & 0 \\ 0 & 0 & 0 & 0 & 0 & 0 & 0 & 0 & 0 & 0 & 0 & 0 & 0 & 0 \end{bmatrix} \delta\mathbf{d}^{\mathrm{e}}$$

Then, the second term in Eq. 2.121 is given by

$$\mathbf{U}^{\mathrm{g}}\mathbf{U}^{\mathrm{e}}\delta\mathbf{P}^{\mathrm{T}}\mathbf{M}\mathbf{F}^{\mathrm{c}} = \mathbf{U}^{\mathrm{g}}\,\mathbf{K}_{\mathrm{g2}}\delta\mathbf{d}^{\mathrm{e}} \qquad \text{(Eq. 2.267)}$$

From Eq. 2.113 through Eq. 2.267, Eq. 2.121 is

$$\delta\mathbf{F}^{\mathrm{g}} = \mathbf{U}^{\mathrm{g}}\left(\frac{\mathbf{K}_{\mathrm{g1}} + \mathbf{K}_{\mathrm{g1}}{}^{\mathrm{T}}}{\mathbf{2}} + \frac{\mathbf{K}_{\mathrm{g2}} + \mathbf{K}_{\mathrm{g2}}{}^{\mathrm{T}}}{\mathbf{2}} + \mathbf{U}^{\mathrm{e}}\mathbf{P}^{\mathrm{T}}\mathbf{M}\left(\int_0^{L_o}\left(\mathbf{B}^{\mathrm{T}}\mathbf{G}^{\mathrm{c}}\mathbf{B} + \mathbf{B}^{\mathrm{T}}\mathbf{V}^{\mathrm{T}}\mathbf{K}^{\mathrm{s}}\mathbf{V}\mathbf{B}\right)\mathrm{d}X_1\right)\mathbf{M}^{\mathrm{T}}\mathbf{P}(\mathbf{U}^{\mathrm{e}})^{\mathrm{T}}\right)(\mathbf{U}^{\mathrm{g}})^{\mathrm{T}}\delta\mathbf{d}^{\mathrm{g}}$$

2.7.10 Load Height Effect of Transverse Loads

2.7.10.1 Load height concept

The finite element analysis based on open section thin-walled beam theory employs one reference axis. This axis is the cross-section shear center in this research. In a physical structure, the load and displacement boundary conditions do not always correspond to the shear center. As shown in Figure 2.17, the loads can be located away from the shear center.

In Figure 2.16 (a), the external work is determined by applying the external force at the shear center. In Figure 2.16 (b), the external work is determined by applying the external force at an arbitrary point considering the eccentricity of the applied loads, which results in additional work. Point O in Figure 2.16 is the center of rotation of the cross-section, wherever that might be. The load height effect at the cross-section can be explained by the eccentricity. As shown in Figure 2.16 (a), the longitudinal displacement Eq. 2.89 along the shear center is given by

$$u_1 = u = u_o - y\alpha_z - z\alpha_y + \bar{\omega}\emptyset_{,x}$$

where:

- $\alpha_z = v_{o,x}\, cos\, \emptyset + w_{o,x} sin\emptyset$
- $\alpha_y = w_{o,x}\, cos\, \emptyset - v_{o,x} sin\emptyset$
- $\bar{\omega} = \int_s \left(y_{,s} \cdot z - z_{,s} \cdot y\right) ds$

The transverse displacements considering the eccentricity may be expressed as

$$\begin{Bmatrix} u_2 \\ u_3 \end{Bmatrix} = \begin{Bmatrix} v \\ w \end{Bmatrix} = \begin{bmatrix} \cos\emptyset & -\sin\emptyset \\ \sin\emptyset & \cos\emptyset \end{bmatrix} \begin{Bmatrix} e_y \\ e_z \end{Bmatrix} + \begin{Bmatrix} v_o \\ w_o \end{Bmatrix} - \begin{Bmatrix} e_y \\ e_z \end{Bmatrix} \quad \text{(Eq. 2.268)}$$

$$v = v_o + e_y \cos\emptyset - e_z sin\emptyset - e_y = v_o - z sin\emptyset - e_y(1 - cos\,\emptyset) \quad \text{(Eq. 2.269)}$$

$$w = w_o + e_y \sin\emptyset + e_z cos\emptyset - e_z = w_o + e_y sin\emptyset - e_z(1 - cos\,\emptyset) \quad \text{(Eq. 2.270)}$$

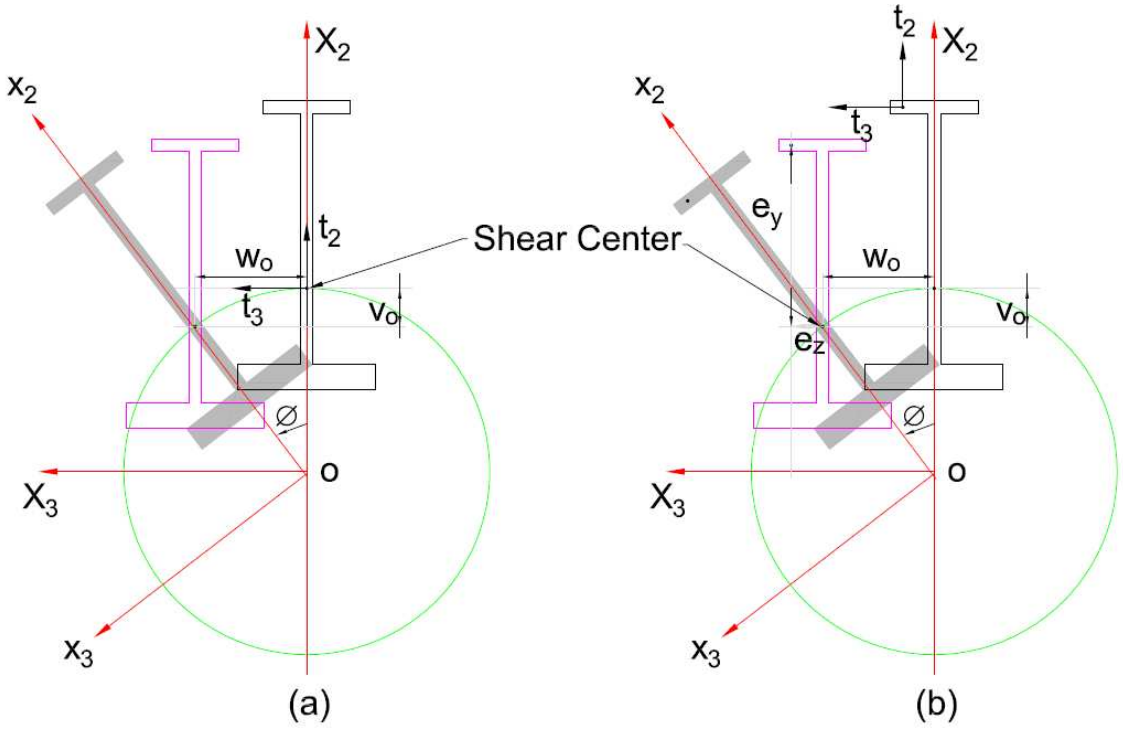

Figure2.16 (a) External work of the cross-section at shear center and (b) External work of the cross-section considering eccentricity.

The total external work is then given by

$$\mathbf{W} = \mathbf{W}_o + \mathbf{W}_h \quad \text{(Eq. 2.271)}$$

where:

- The external work done by applying the external force at the shear center is

$$\mathbf{W}_{\mathrm{o}} = \int_{\mathrm{S}_{x0}} \mathrm{t}_x(0)u(0)\ dydz + \int_{\mathrm{S}_{x\mathrm{L}}} \mathrm{t}_x(\mathrm{L})u(\mathrm{L})\ dydz + \int_{\mathrm{S}_y} \mathrm{t}_y v_o\ dzdx + \int_{\mathrm{S}_z} \mathrm{t}_z w_o\ dydx$$

(Eq. 2.272)

- With respect to applied force in direction 2 or y-direction within the element frame, the external work done by applying the external force at an arbitrary point and considering the load eccentricity is

$$\mathbf{W}_{\mathrm{h}} = -\int_{\mathrm{S}_y} \mathrm{t}_y \mathrm{e}_y(1 - cos\,\emptyset)\ dzdx - \int_{\mathrm{S}_y} \mathrm{t}_y \mathrm{e}_z\, sin\,\emptyset\ dzdx \qquad \text{(Eq. 2.273)}$$

where:

- $\mathrm{t}_x(x)$ = Traction in x-direction or direction 1.
- $\mathrm{t}_y(x)$ = Traction in y-direction or direction 2.
- $\mathrm{t}_z(x)$ = Traction in z-direction or direction 3.
- S_{x0} = Surface area perpendicular to x-direction at $x = 0$.
- $\mathrm{S}_{x\mathrm{L}}$= Surface area perpendicular to x-direction at $x = \mathrm{L}$.
- S_y = Surface area perpendicular to y-direction.
- S_z = Surface area perpendicular to z-direction.
- e_y = Eccentricity in y-direction.
- e_z = Eccentricity in z-direction.

2.7.10.2 Contributions to the external virtual work

The variation of the total external virtual work in Eq. 2.271 is

$$\delta \mathbf{W} = \delta \mathbf{W}_{\mathrm{o}} + \delta \mathbf{W}_{\mathrm{h}} \qquad \text{(Eq. 2.274)}$$

where:

- The variation of the external virtual work for loading at the shear center is

$$\delta \mathbf{W}_{\mathrm{o}} = \int_{S_{x0}} \mathrm{t}_x(0)\delta u(0)\, dydz + \int_{S_{xL}} \mathrm{t}_x(\mathrm{L})\delta u(L)\, dydz + \int_{S_y} \mathrm{t}_y \delta v_o \; dzdx$$

$$+ \int_{S_z} \mathrm{t}_z \delta w_o \; dydx \qquad \text{(Eq. 2.275)}$$

and

- The variation of the external virtual work due to the load eccentricity is

$$\delta \mathbf{W}_{\mathrm{h}} = -\int_{S_y} \mathrm{t}_y \mathrm{e}_y \sin\emptyset\delta\emptyset \; dzdx - \int_{S_y} \mathrm{t}_y \mathrm{e}_z \cos\emptyset\delta\emptyset \; dzdx \qquad \text{(Eq. 2.276)}$$

where the variation of the longitudinal displacement is given by

$$\delta u = \delta u_o - y\left(\delta v_{o,x}\cos\emptyset - v_{o,x}\sin\emptyset\delta\emptyset + \delta w_{o,x}\sin\emptyset + w_{o,x}\cos\emptyset\delta\emptyset\right)$$

$$- z(\delta w_{o,x}\cos\emptyset - w_{o,x}\cos\emptyset\,\delta\emptyset - \delta v_{o,x}\sin\emptyset - v_{o,x}\cos\emptyset\delta\emptyset) + \bar{\omega}\delta\emptyset_{,x}$$

(Eq. 2.277)

As shown in Figure 2.17, the forces can be applied at the two end cross-sections (Surface $x = 0$ and surface $x = \mathrm{L}$), and the side surfaces (Surface y and Surface z) within the element frame.

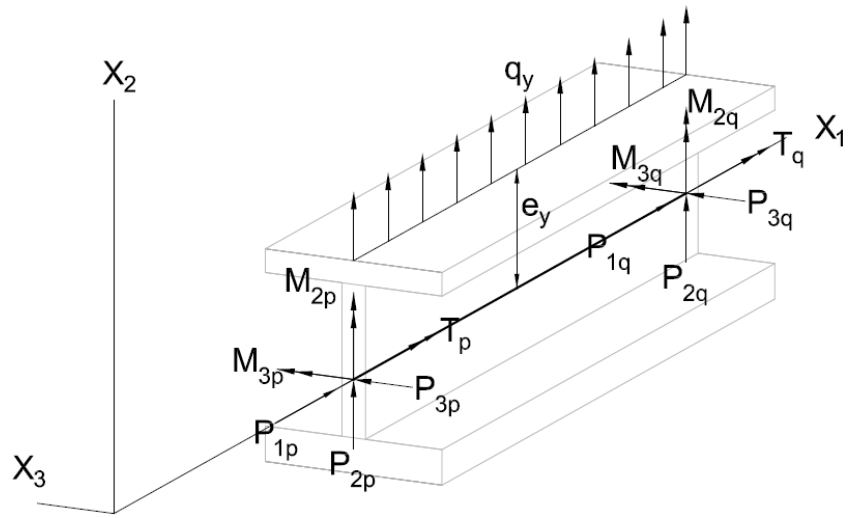

Figure 2.17 Concept of element forces at two end nodes and load-height effects.

The contributions of these different element applied forces are as follows.

- <u>Surface $x = 0$</u>

$$\int_{S_{x0}} \mathrm{t}_x(0)\delta u(0)\, dydz = \mathrm{t}_x(0)\delta u(0)\mathrm{A}_0 = \mathrm{P}_{1\mathrm{p}}\delta u(0) \qquad (\mathrm{Eq.}\ 2.278)$$

$$\mathrm{P}_{1\mathrm{p}}\delta u(0) = \mathrm{P}_{1\mathrm{p}}\Big\{\delta u_o(0)$$
$$- y(0)\Big(\delta v_{o,x}(0)\cos\emptyset(0) - v_{o,x}(0)\sin\emptyset(0)\delta\emptyset(0) + \delta w_{o,x}(0)\sin\emptyset(0)$$
$$+ w_{o,x}(0)\cos\emptyset(0)\delta\emptyset(0)\Big)$$
$$- z(0)\Big(\delta w_{o,x}(0)\cos\emptyset(0) - w_{o,x}(0)\cos\emptyset(0)\delta\emptyset(0)$$
$$- \delta v_{o,x}(0)\sin\emptyset(0) - v_{o,x}(0)\cos\emptyset(0)\delta\emptyset(0)\Big) + \bar{\omega}(0)\delta\emptyset_{,x}(0)\Big\}$$

(Eq. 2.279)

$\mathrm{P}_{1\mathrm{p}}\delta u(0) =$

$\mathrm{P}_{1\mathrm{p}}\delta u_o(0)$: Axial load contribution to the external virtual work

$-\mathrm{M}_{3\mathrm{p}}\Big(\delta v_{o,x}(0)\cos\emptyset(0) - v_{o,x}(0)\sin\emptyset(0)\delta\emptyset(0) + \delta w_{o,x}(0)\sin\emptyset(0) + w_{o,x}(0)\cos\emptyset(0)\delta\emptyset(0)\Big)$: z axis bending moment contribution to the external virtual work

$-\mathrm{M}_{2\mathrm{p}}\Big(\delta w_{o,x}(0)\cos\emptyset(0) - w_{o,x}(0)\cos\emptyset(0)\delta\emptyset(0) - \delta v_{o,x}(0)\sin\emptyset(0) - v_{o,x}(0)\cos\emptyset(0)\delta\emptyset(0)\Big)$: y axis bending moment contribution to the external virtual work

$\mathrm{P}_{1\mathrm{p}}\bar{\omega}(0)\delta\emptyset_{,x}(0)$: Bi-moment contribution to the external virtual work

(Eq. 2.280)

- Surface $x = \mathrm{L}$

$$\int_{S_{xL}} \mathrm{t}_x(\mathrm{L})\delta u(\mathrm{L})\, dydz = \mathrm{t}_x(\mathrm{L})\delta u(\mathrm{L})\mathrm{A}_\mathrm{L} = \mathrm{P}_{1\mathrm{q}}\delta u(\mathrm{L}) \qquad \text{(Eq. 2.281)}$$

$$\begin{aligned}\mathrm{P}_{1\mathrm{q}}\delta u(\mathrm{L}) = \mathrm{P}_{1\mathrm{q}}\Big\{&\delta u_o(\mathrm{L}) \\ &- y(\mathrm{L})\Big(\delta v_{o,x}(\mathrm{L})\cos\emptyset(\mathrm{L}) - v_{o,x}(\mathrm{L})\sin\emptyset(\mathrm{L})\delta\emptyset(\mathrm{L}) + \delta w_{o,x}(\mathrm{L})sin\emptyset(\mathrm{L}) \\ &+ w_{o,x}(\mathrm{L})cos\emptyset(\mathrm{L})\delta\emptyset(\mathrm{L})\Big) \\ &- z(\mathrm{L})\Big(\delta w_{o,x}(\mathrm{L})\cos\emptyset(\mathrm{L}) - w_{o,x}(\mathrm{L})\cos\emptyset(\mathrm{L})\delta\emptyset(\mathrm{L}) - \delta v_{o,x}(\mathrm{L})sin\emptyset(\mathrm{L}) \\ &- v_{o,x}(\mathrm{L})cos\emptyset(\mathrm{L})\delta\emptyset(\mathrm{L})\Big) + \bar{\omega}(\mathrm{L})\delta\emptyset_{,x}(\mathrm{L})\Big\} \qquad \text{(Eq. 2.282)}\end{aligned}$$

$\mathrm{P}_{1\mathrm{q}}\delta u(\mathrm{L}) =$

$\mathrm{P}_{1\mathrm{q}}\delta u_o(\mathrm{L})$: Axial load contribution to the external virtual work

$-\mathrm{M}_{3\mathrm{q}}\Big(\delta v_{o,x}(\mathrm{L})\cos\emptyset(\mathrm{L}) - v_{o,x}(\mathrm{L})\sin\emptyset(\mathrm{L})\delta\emptyset(\mathrm{L}) + \delta w_{o,x}(\mathrm{L})sin\emptyset(\mathrm{L}) + w_{o,x}(\mathrm{L})cos\emptyset(\mathrm{L})\delta\emptyset(\mathrm{L})\Big)$: z axis bending moment contribution to the external virtual work

$-\mathrm{M}_{2\mathrm{q}}\Big(\delta w_{o,x}(\mathrm{L})\cos\emptyset(\mathrm{L}) - w_{o,x}(\mathrm{L})\cos\emptyset(\mathrm{L})\delta\emptyset(\mathrm{L}) - \delta v_{o,x}(\mathrm{L})sin\emptyset(\mathrm{L}) - v_{o,x}(\mathrm{L})cos\emptyset(\mathrm{L})\delta\emptyset(\mathrm{L})\Big)$: y axis bending moment contribution to the external virtual work

$\mathrm{P}_{1\mathrm{q}}\bar{\omega}(\mathrm{L})\delta\emptyset_{,x}(\mathrm{L})$: Bi-moment contribution to the external virtual work

(Eq. 2.283)

- Surface y: Transverse distributed load in the direction, contribution to the external virtual work

$$\int_{S_y} \mathrm{t}_y \delta v_o \; dzdx = \mathrm{P}_{2\mathrm{p}} \delta v_o(0) + \mathrm{P}_{2\mathrm{q}} \delta v_o(\mathrm{L}) + \int_0^{\mathrm{L}} \mathrm{q}_y \delta v_o \; dx \qquad \text{(Eq. 2.284)}$$

- Surface z: Transverse distributed load in the z direction, contribution to the external virtual work

$$\int_{S_z} \mathrm{t}_z \delta w_o \; dydx = \mathrm{P}_{3\mathrm{p}} \delta w_o(0) + \mathrm{P}_{3\mathrm{q}} \delta w_o(\mathrm{L}) \qquad \text{(Eq. 2.285)}$$

- Load height: Applied twisting moment contribution to the external virtual work in Eq. 2.276 is given by

$$\delta \mathbf{W}_{\mathrm{h}} = -\int_{S_y} \mathrm{t}_y \mathrm{e}_y \, sin\, \emptyset \delta \emptyset \, dzdx - \int_{S_y} \mathrm{t}_y \mathrm{e}_z cos \emptyset \delta \emptyset \; dzdx$$

If the load height along direction 2 within the element frame and small twist are only considered, Eq. 2.276 is given by

- Two end cross-sections (Surface $x = 0$ and Surface $x = \mathrm{L}$)

$$\delta \mathbf{W}_{\mathrm{h1}} = -\int_{S_y} \mathrm{t}_y \mathrm{e}_y \emptyset \delta \emptyset \; dzdx = -\left(\mathrm{P}_{2\mathrm{p}} \mathrm{e}_y \emptyset(0) \delta \emptyset(0) + \mathrm{P}_{2\mathrm{q}} \mathrm{e}_y \emptyset(\mathrm{L}) \delta \emptyset(\mathrm{L}) \right) \qquad \text{(Eq. 2.286)}$$

where:

- $e_z = 0$ due to load height only along y-direction.
- The shape function of the twist at surface $x = 0$ and surface $x = \mathrm{L}$ from Eq. 2.195 within the co-rotational frame can be given as

$$\emptyset(0) = \mathbf{N}_{\emptyset 0}^{\mathrm{T}} \mathbf{d}^{\mathrm{c}} \qquad \text{(Eq. 2.287)}$$

$$\emptyset(\mathrm{L}) = \mathbf{N}_{\emptyset \mathrm{L}}^{\mathrm{T}} \mathbf{d}^{\mathrm{c}} \qquad \text{(Eq. 2.288)}$$

where:

$$\mathbf{N}_{\emptyset}(0) = \mathbf{N}_{\emptyset 0} = [0 \quad 1 \quad 0 \quad 0 \quad 0 \quad 0 \quad 0 \quad 0 \quad 1]^{\mathrm{T}} \qquad \text{(Eq. 2.289)}$$

$$\mathbf{N}_{\emptyset}(\mathrm{L}) = \mathbf{N}_{\emptyset \mathrm{L}} = [0 \quad 0 \quad 0 \quad 0 \quad 0 \quad 1 \quad 0 \quad 0 \quad 1]^{\mathrm{T}} \qquad \text{(Eq. 2.290)}$$

From Eqs. 2.287 through 2.290, Eq. 2.286 within the co-rotational frame can be formulated by

$$\delta \mathbf{W}_{\mathrm{h1}}{}^{\mathrm{c}} = -\left(\mathrm{P}_{2\mathrm{p}} \mathrm{e}_y \delta \mathbf{d}^{\mathrm{c}\,\mathrm{T}} \mathbf{N}_{\emptyset}(0) \mathbf{N}_{\emptyset}^{\mathrm{T}}(0) \mathbf{d}^{\mathrm{c}} + \mathrm{P}_{2\mathrm{q}} \mathrm{e}_y \delta \mathbf{d}^{\mathrm{c}\,\mathrm{T}} \mathbf{N}_{\emptyset}(\mathrm{L}) \mathbf{N}_{\emptyset}^{\mathrm{T}}(\mathrm{L}) \mathbf{d}^{\mathrm{c}}\right) \qquad \text{(Eq. 2.291)}$$

The stiffness matrix representing the load height effect by two end cross-section within the co-rotational frame can be derived as

$$\begin{aligned} \delta \mathbf{W}_{\mathrm{h1}}{}^{\mathrm{c}} &= -\delta \mathbf{d}^{\mathrm{c}\,\mathrm{T}} \left(\mathrm{P}_{2\mathrm{p}} \mathrm{e}_y \mathbf{N}_{\emptyset}(0) \mathbf{N}_{\emptyset}^{\mathrm{T}}(0) + \mathrm{P}_{2\mathrm{q}} \mathrm{e}_y \mathbf{N}_{\emptyset}(\mathrm{L}) \mathbf{N}_{\emptyset}^{\mathrm{T}}(\mathrm{L})\right) \mathbf{d}^{\mathrm{c}} \\ &= -\delta \mathbf{d}^{\mathrm{c}\,\mathrm{T}} \mathbf{K}_{\mathrm{h1}}{}^{\mathrm{c}} \mathbf{d}^{\mathrm{c}} \end{aligned} \qquad \text{(Eq. 2.292)}$$

where:

$$\mathbf{K}_{\mathrm{h1}}{}^{\mathrm{c}}=\begin{bmatrix} 0 & 0 & 0 & 0 & 0 & 0 & 0 & 0 & 0 \\ 0 & \mathrm{P_{2p}}e_y & 0 & 0 & 0 & 0 & 0 & 0 & \mathrm{P_{2p}}e_y \\ 0 & 0 & 0 & 0 & 0 & 0 & 0 & 0 & 0 \\ 0 & 0 & 0 & 0 & 0 & 0 & 0 & 0 & 0 \\ 0 & 0 & 0 & 0 & 0 & 0 & 0 & 0 & 0 \\ 0 & 0 & 0 & 0 & 0 & \mathrm{P_{2q}}e_y & 0 & 0 & \mathrm{P_{2q}}e_y \\ 0 & 0 & 0 & 0 & 0 & 0 & 0 & 0 & 0 \\ 0 & 0 & 0 & 0 & 0 & 0 & 0 & 0 & 0 \\ 0 & \mathrm{P_{2p}}e_y & 0 & 0 & 0 & \mathrm{P_{2q}}e_y & 0 & 0 & \mathrm{P_{2p}}e_y + \mathrm{P_{2q}}e_y \end{bmatrix} \quad \text{(Eq. 2.293)}$$

- Along the longitudinal direction

$$\delta\mathbf{W}_{\mathrm{h2}} = -\int_{S_y} \mathrm{t}_y \mathrm{e}_y \emptyset\delta\emptyset \; dzdx = -\int_{\mathrm{L}} \mathrm{q}_y \mathrm{e}_y \emptyset(x) \; \delta\emptyset(x)dx \quad \text{(Eq. 2.294)}$$

where:

- $\mathrm{e}_z = 0$ and small $\emptyset$
- Shape function of the twist from Eq. 2.195 can be given by

$$\emptyset(x) = \mathbf{N}_{\emptyset}^{\mathrm{T}}\mathbf{d}^{\mathrm{c}}$$

where:

$$\mathbf{N}_{\emptyset} = \begin{bmatrix} 0 & \mathrm{N}_{\theta_{1\mathrm{p}}^{\mathrm{c}}}(x) & 0 & 0 & \mathrm{N}_{\phi_{\mathrm{p}}'}(x) & \mathrm{N}_{\theta_{1\mathrm{q}}^{\mathrm{c}}}(x) & 0 & 0 & \mathrm{N}_{\phi_{\mathrm{q}}'}(x) \end{bmatrix}^{\mathrm{T}}$$

- $\mathrm{N}_{\theta_{1\mathrm{p}}^{\mathrm{c}}}(x) = 1 - \frac{3x^2}{\mathrm{L}^2} + \frac{2x^3}{\mathrm{L}^3} \qquad 0 \leq \mathrm{x} \leq \mathrm{L}$
- $\mathrm{N}_{\phi_{\mathrm{p}}'}(x) = x - \frac{2x^2}{\mathrm{L}} + \frac{x^3}{\mathrm{L}^2} \qquad 0 \leq \mathrm{x} \leq \mathrm{L}$
- $\mathrm{N}_{\theta_{1\mathrm{q}}^{\mathrm{c}}}(x) = \frac{3x^2}{\mathrm{L}^2} - \frac{2x^3}{\mathrm{L}^3} \qquad 0 \leq \mathrm{x} \leq \mathrm{L}$
- $\mathrm{N}_{\phi_{\mathrm{q}}'}(x) = 1 - \frac{x^2}{\mathrm{L}} + \frac{x^3}{\mathrm{L}^2} \qquad 0 \leq \mathrm{x} \leq \mathrm{L}$

From Eq. 2.195, Eq. 2.294 within the co-rotational frame can be formulated as

$$\delta \mathbf{W}_{\mathrm{h2}}{}^{\mathrm{c}} = -\int_{\mathrm{L}} \mathrm{q}_y \mathrm{e}_y \delta \mathbf{d}^{\mathrm{c}\mathrm{T}} \mathbf{N}_{\emptyset} \mathbf{N}_{\emptyset}^{\mathrm{T}} \mathbf{d}^{\mathrm{c}} \, dx \qquad \text{(Eq. 2.295)}$$

The stiffness matrix including the load height effect along the longitudinal within the co-rotational frame is derived as

$$\delta \mathbf{W}_{\mathrm{h2}}{}^{\mathrm{c}} = -\delta \mathbf{d}^{\mathrm{c}\mathrm{T}} \int_{\mathrm{L}} \mathrm{q}_y \mathrm{e}_y \mathbf{N}_{\emptyset} \mathbf{N}_{\emptyset}^{\mathrm{T}} \, dx \, \mathbf{d}^{\mathrm{c}} = -\delta \mathbf{d}^{\mathrm{c}\mathrm{T}} \int_{\mathrm{L}} \mathbf{K}_{\mathrm{h2}}{}^{\mathrm{c}} \, dx \, \mathbf{d}^{\mathrm{c}} \qquad \text{(Eq. 2.296)}$$

where:

$$\mathbf{K}_{\mathrm{h2}}{}^{\mathrm{c}} =$$

$$\mathrm{q}_y \mathrm{e}_y \begin{bmatrix} 0 & 0 & 0 & 0 & 0 & 0 & 0 & 0 & 0 \\ 0 & \left(\mathrm{N}_{\theta_{1\mathrm{p}}^{\mathrm{c}}}(x)\right)^2 & 0 & 0 & \mathrm{N}_{\theta_{1\mathrm{p}}^{\mathrm{c}}}(x)\mathrm{N}_{\phi_{\mathrm{p}}'}(x) & \mathrm{N}_{\theta_{1\mathrm{p}}^{\mathrm{c}}}(x)\mathrm{N}_{\theta_{1\mathrm{q}}^{\mathrm{c}}}(x) & 0 & 0 & \mathrm{N}_{\theta_{1\mathrm{p}}^{\mathrm{c}}}(x)\mathrm{N}_{\phi_{\mathrm{q}}'}(x) \\ 0 & 0 & 0 & 0 & 0 & 0 & 0 & 0 & 0 \\ 0 & 0 & 0 & 0 & 0 & 0 & 0 & 0 & 0 \\ 0 & \mathrm{N}_{\theta_{1\mathrm{p}}^{\mathrm{c}}}(x)\mathrm{N}_{\phi_{\mathrm{p}}'}(x) & 0 & 0 & \left(\mathrm{N}_{\phi_{\mathrm{p}}'}(x)\right)^2 & \mathrm{N}_{\phi_{\mathrm{p}}'}(x)\mathrm{N}_{\theta_{1\mathrm{q}}^{\mathrm{c}}}(x) & 0 & 0 & \mathrm{N}_{\phi_{\mathrm{p}}'}(x)\mathrm{N}_{\phi_{\mathrm{q}}'}(x) \\ 0 & \mathrm{N}_{\theta_{1\mathrm{p}}^{\mathrm{c}}}(x)\mathrm{N}_{\theta_{1\mathrm{q}}^{\mathrm{c}}}(x) & 0 & 0 & \mathrm{N}_{\phi_{\mathrm{p}}'}(x)\mathrm{N}_{\theta_{1\mathrm{q}}^{\mathrm{c}}}(x) & \left(\mathrm{N}_{\theta_{1\mathrm{q}}^{\mathrm{c}}}(x)\right)^2 & 0 & 0 & \mathrm{N}_{\theta_{1\mathrm{q}}^{\mathrm{c}}}(x)\mathrm{N}_{\phi_{\mathrm{q}}'}(x) \\ 0 & 0 & 0 & 0 & 0 & 0 & 0 & 0 & 0 \\ 0 & 0 & 0 & 0 & 0 & 0 & 0 & 0 & 0 \\ 0 & \mathrm{N}_{\theta_{1\mathrm{p}}^{\mathrm{c}}}(x)\mathrm{N}_{\phi_{\mathrm{q}}'}(x) & 0 & 0 & \mathrm{N}_{\phi_{\mathrm{p}}'}(x)\mathrm{N}_{\phi_{\mathrm{q}}'}(x) & \mathrm{N}_{\theta_{1\mathrm{q}}^{\mathrm{c}}}(x)\mathrm{N}_{\phi_{\mathrm{q}}'}(x) & 0 & 0 & \left(\mathrm{N}_{\phi_{\mathrm{q}}'}(x)\right)^2 \end{bmatrix}$$

(Eq. 2.297)

Additional external work by load height effects in the global frame is given by

$$\delta \mathbf{W}_{\mathrm{h}} = -\delta \mathbf{d}^{\mathrm{g}\mathrm{T}} \mathbf{U}^{\mathrm{g}} \mathbf{U}^{\mathrm{e}} \mathbf{P}^{\mathrm{T}} \mathbf{M} \left(\mathbf{K}_{\mathrm{h1}}{}^{\mathrm{c}} + \int_{\mathrm{L}} \mathbf{K}_{\mathrm{h2}}{}^{\mathrm{c}} \, dx \right) \mathbf{M}^{\mathrm{T}} \mathbf{P} (\mathbf{U}^{\mathrm{e}})^{\mathrm{T}} (\mathbf{U}^{\mathrm{g}})^{\mathrm{T}} \mathbf{d}^{\mathrm{g}} \qquad \text{(Eq. 2.298)}$$

Load height results in twisting moment. There is no projection effect $\mathbf{P} = \mathbf{I}$ since load height is generated within the cross-section.

Then, the stiffness matrix including the load height effect in the global frame is given by

$$\mathbf{K}_{\mathrm{h}}{}^{\mathrm{g}} = \mathbf{U}^{\mathrm{g}}\mathbf{U}^{\mathrm{e}}\mathbf{M}\left(\mathbf{K}_{\mathrm{h1}}{}^{\mathrm{c}} + \int_{\mathrm{L}} \mathbf{K}_{\mathrm{h2}}{}^{\mathrm{c}} dx\right)\mathbf{M}^{\mathrm{T}}(\mathbf{U}^{\mathrm{e}})^{\mathrm{T}}(\mathbf{U}^{\mathrm{g}})^{\mathrm{T}} \qquad \text{(Eq. 2.299)}$$

where:

$\mathbf{U}^{\mathrm{g}}$: Coordinate transformation of the displacement and the internal force from the element frame to the global frame.

$\mathbf{U}^{\mathrm{e}}$: Coordinate transformation of the displacement and the internal force from the co-rotational frame to the element frame.

$\mathbf{P}$: Projection between the element frame and the co-rotational frame, which removes the element rigid body motions. The projection matrix may be described in the element frame for the co-rotational frame.

Considering the load height effect, the variation of the internal force vector in Eq. 2.121 is

$$\delta\mathbf{F}^{\mathrm{g}} + \mathbf{K}_{\mathrm{h}}{}^{\mathrm{g}}\mathbf{d}^{\mathrm{g}} = \mathbf{U}^{\mathrm{g}}\delta\mathbf{U}^{\mathrm{e}}\mathbf{P}^{\mathrm{T}}\mathbf{M}\mathbf{F}^{\mathrm{c}} + \mathbf{U}^{\mathrm{g}}\mathbf{U}^{\mathrm{e}}\delta\mathbf{P}^{\mathrm{T}}\mathbf{M}\mathbf{F}^{\mathrm{c}} + \mathbf{U}^{\mathrm{g}}\mathbf{U}^{\mathrm{e}}\mathbf{P}^{\mathrm{T}}\mathbf{M}\delta\mathbf{F}^{\mathrm{c}}$$
$$+ \mathbf{U}^{\mathrm{g}}\mathbf{U}^{\mathrm{e}}\mathbf{M}\left(\mathbf{K}_{\mathrm{h1}}{}^{\mathrm{c}} + \int_{\mathrm{L}} \mathbf{K}_{\mathrm{h2}}{}^{\mathrm{c}} dx\right)\mathbf{M}^{\mathrm{T}}(\mathbf{U}^{\mathrm{e}})^{\mathrm{T}}(\mathbf{U}^{\mathrm{g}})^{\mathrm{T}}\mathbf{d}^{\mathrm{g}} \qquad \text{(Eq. 2.300)}$$

From Eqs. 2.225, 2.256, 2.267, and 2.299, the variation of the internal force vector including the load height effect in Eq. 2.300 is

$$\delta\mathbf{F}^{g} + \mathbf{K}_{h}{}^{g}\mathbf{d}^{g} = \mathbf{U}^{g}\left(\frac{\mathbf{K}_{g1} + \mathbf{K}_{g1}{}^{T}}{\mathbf{2}}\right)(\mathbf{U}^{g})^{T}\mathbf{d}^{g} + \mathbf{U}^{g}\left(\frac{\mathbf{K}_{g2} + \mathbf{K}_{g2}{}^{T}}{\mathbf{2}}\right)(\mathbf{U}^{g})^{T}\mathbf{d}^{g}$$
$$+ \mathbf{U}^{g}\mathbf{U}^{e}\mathbf{P}^{T}\mathbf{M}\left(\int_{0}^{L_o}\left(\mathbf{B}^{T}\mathbf{G}^{c}\mathbf{B} + \mathbf{B}^{T}\mathbf{V}^{T}\mathbf{K}^{s}\mathbf{V}\mathbf{B}\right)dX_1\right)\mathbf{M}^{T}\mathbf{P}(\mathbf{U}^{e})^{T}(\mathbf{U}^{g})^{T}\mathbf{d}^{g}$$
$$+ \mathbf{U}^{g}\mathbf{U}^{e}\mathbf{M}\left(\mathbf{K}_{h1}{}^{c} + \int_{0}^{L_o}\mathbf{K}_{h2}{}^{c}\,dX_1\right)\mathbf{M}^{T}(\mathbf{U}^{e})^{T}(\mathbf{U}^{g})^{T}\mathbf{d}^{g} \qquad \text{(Eq. 2.301)}$$

2.7.11 Bracing and Support Height Effects

2.7.11.1 Modeling of bracing and support height effects using rigid offsets

As shown in Figure 2.18, boundary conditions and support conditions can be located away from the shear center. Since open section thin-walled beam theory assumes that there is no distortion of the cross-section profile, bracing and support height effects can be represented by rigid links. In Figure 2.18, the rigid link for a support is shown as d_s and the rigid link for a bracing is shown as d_b.

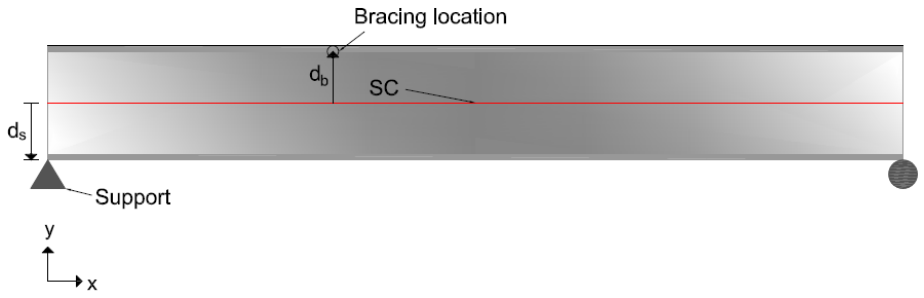

Figure 2.18 Modeling of bracing and support height effects using rigid offsets.

2.7.11.2 Rigid offsets for bracing and support height effects

Rigid offsets for representation of bracing and support height effects are formulated only along the 2 or y-direction in this research within the element frame. In addition, they are formulated only at the element ends. That is, a node needs to be inserted at any location where the lateral displacements are constrained in the 3 direction by bracing at a given height or where lateral displacements are constrained in the 2 direction by supports.

Figure 2.19 (a) shows the master node and slave node degrees of freedom of the cross-section of the start node p. Figure 2.19 (b) shows master node and slave node degrees of freedom of the cross-section of the end node q.

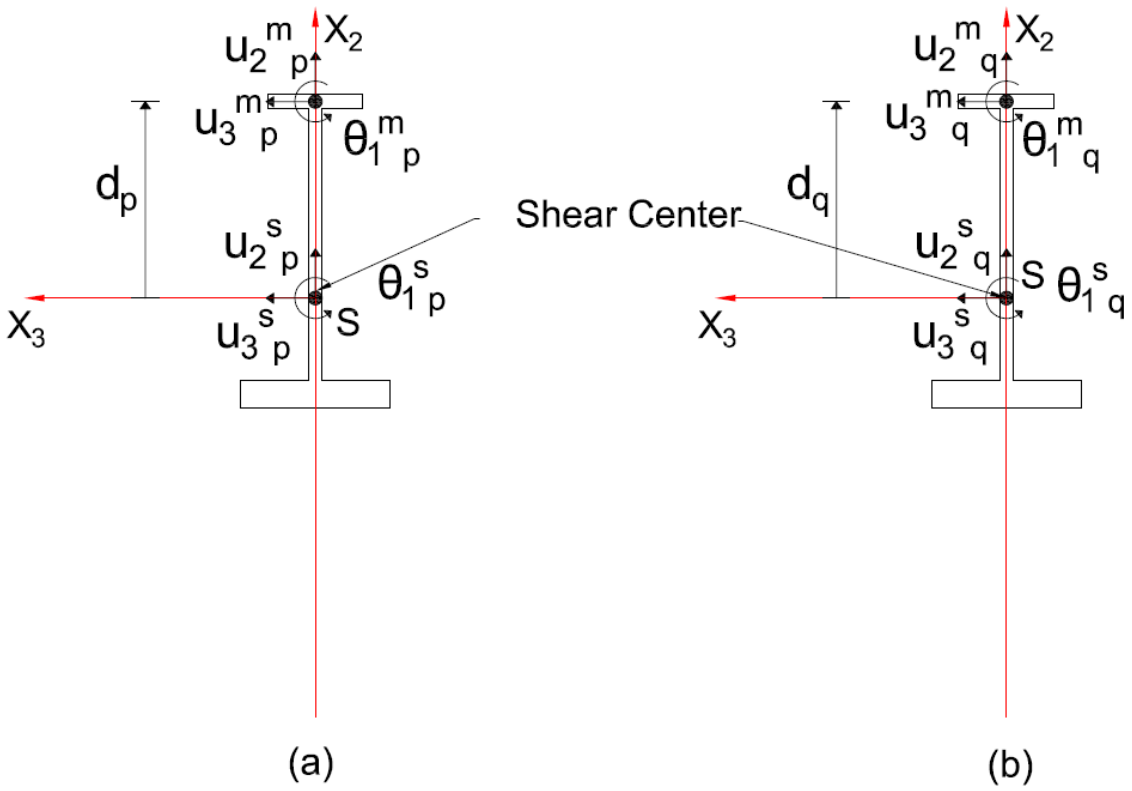

Figure 2.19 Degrees of freedom of master and slave nodes for rigid offsets.

Rigid offset with the rigid link d_p and d_q for bracing or/and support height can be formulated in the element frame. Master nodes are located at the support and/or the brace points. Slave nodes are located at the shear center. In the Total Lagrangian description, the displacements of the slave nodes

$$\mathbf{d}^{es} = \left\{ u_{1_p}^{e\ s}\ u_{2_p}^{e\ s}\ u_{3_p}^{e\ s}\ \theta_{1_p}^{e\ s}\ \theta_{2_p}^{e\ s}\ \theta_{3_p}^{e\ s}\ \phi_p'^{\,s}\ u_{1_q}^{e\ s}\ u_{2_q}^{e\ s}\ u_{3_q}^{e\ s}\ \theta_{1_q}^{e\ s}\ \theta_{2_q}^{e\ s}\ \theta_{3_q}^{e\ s}\ \phi_q'^{\,s} \right\}^T$$

(Eq. 2.302)

can be expressed by displacements of the master nodes

$$\mathbf{d}^{em} = \left\{ u_{1_p}^{e\ m} u_{2_p}^{e\ m} u_{3_p}^{e\ m} \theta_{1_p}^{e\ m} \theta_{2_p}^{e\ m} \theta_{3_p}^{e\ m} \phi_p'^{\,m} u_{1_q}^{e\ m} u_{2_q}^{e\ m} u_{3_q}^{e\ m} \theta_{1_q}^{e\ m} \theta_{2_q}^{e\ m} \theta_{3_q}^{e\ m} \phi_q'^{\,m} \right\}^T$$

(Eq. 2.303)

by the following relationships:

$$u_{3_p}^{e\ s} = u_{3_p}^{e\ m} - d\theta_{1_p}^{e\ m} \quad \text{(Eq. 2.304)}$$

$$u_{3_q}^{e\ s} = u_{3_q}^{e\ m} - d\theta_{1_q}^{e\ m} \quad \text{(Eq. 2.305)}$$

From Eqs. 2.304 and 2.305, the variation in the displacement between slave nodes and master nodes is described as

$$\delta\mathbf{d}^{es} = \mathbf{R}^d \delta\mathbf{d}^{em} \quad \text{(Eq. 2.306)}$$

where:

- Rigid offset matrix in the element frame.

$$\mathbf{R}^{\mathrm{d}} = \begin{bmatrix} 1 & 0 & 0 & 0 & 0 & 0 & 0 & 0 & 0 & 0 & 0 & 0 & 0 \\ 0 & 1 & 0 & 0 & 0 & 0 & 0 & 0 & 0 & 0 & 0 & 0 & 0 \\ 0 & 0 & 1 & -\mathrm{d} & 0 & 0 & 0 & 0 & 0 & 0 & 0 & 0 & 0 \\ 0 & 0 & 0 & 1 & 0 & 0 & 0 & 0 & 0 & 0 & 0 & 0 & 0 \\ 0 & 0 & 0 & 0 & 1 & 0 & 0 & 0 & 0 & 0 & 0 & 0 & 0 \\ 0 & 0 & 0 & 0 & 0 & 1 & 0 & 0 & 0 & 0 & 0 & 0 & 0 \\ 0 & 0 & 0 & 0 & 0 & 0 & 1 & 0 & 0 & 0 & 0 & 0 & 0 \\ 0 & 0 & 0 & 0 & 0 & 0 & 0 & 1 & 0 & 0 & 0 & 0 & 0 \\ 0 & 0 & 0 & 0 & 0 & 0 & 0 & 0 & 1 & -\mathrm{d} & 0 & 0 & 0 \\ 0 & 0 & 0 & 0 & 0 & 0 & 0 & 0 & 0 & 1 & 0 & 0 & 0 \\ 0 & 0 & 0 & 0 & 0 & 0 & 0 & 0 & 0 & 0 & 1 & 0 & 0 \\ 0 & 0 & 0 & 0 & 0 & 0 & 0 & 0 & 0 & 0 & 0 & 1 & 0 \\ 0 & 0 & 0 & 0 & 0 & 0 & 0 & 0 & 0 & 0 & 0 & 0 & 1 \end{bmatrix} \qquad \text{(Eq. 2.307)}$$

The load height effect in Eq. 2.299 is independent of the rigid offset in Eq. 2.307. Considering the rigid offset, the variation of the internal force vector including the load height effect in Eq. 2.301 is given by

$$\begin{aligned} \delta\mathbf{F}^{\mathrm{g}} + \mathbf{K}_{\mathrm{h}}{}^{\mathrm{g}}\mathbf{d}^{\mathrm{g}} = {} & \mathbf{U}^{\mathrm{g}}\left(\mathbf{R}^{\mathrm{d}}\right)^{\mathrm{T}}\left(\frac{\mathbf{K}_{\mathrm{g1}} + \mathbf{K}_{\mathrm{g1}}{}^{\mathrm{T}}}{\mathbf{2}}\right)\mathbf{R}^{\mathrm{d}}(\mathbf{U}^{\mathrm{g}})^{\mathrm{T}}\mathbf{d}^{\mathrm{g}} \\ & + \mathbf{U}^{\mathrm{g}}\left(\mathbf{R}^{\mathrm{d}}\right)^{\mathrm{T}}\left(\frac{\mathbf{K}_{\mathrm{g2}} + \mathbf{K}_{\mathrm{g2}}{}^{\mathrm{T}}}{\mathbf{2}}\right)\mathbf{R}^{\mathrm{d}}(\mathbf{U}^{\mathrm{g}})^{\mathrm{T}}\mathbf{d}^{\mathrm{g}} \\ & + \mathbf{U}^{\mathrm{g}}\left(\mathbf{R}^{\mathrm{d}}\right)^{\mathrm{T}}\mathbf{U}^{\mathrm{e}}\mathbf{P}^{\mathrm{T}}\mathbf{M}\left(\int_0^{L_o}\left(\mathbf{B}^{\mathrm{T}}\mathbf{G}^{\mathrm{c}}\mathbf{B}\right.\right. \\ & \left.\left. + \mathbf{B}^{\mathrm{T}}\mathbf{V}^{\mathrm{T}}\mathbf{K}^{\mathrm{s}}\mathbf{V}\mathbf{B}\right)\mathrm{d}X_1\right)\mathbf{M}^{\mathrm{T}}\mathbf{P}(\mathbf{U}^{\mathrm{e}})^{\mathrm{T}}\mathbf{R}^{\mathrm{d}}(\mathbf{U}^{\mathrm{g}})^{\mathrm{T}}\mathbf{d}^{\mathrm{g}} \\ & + \mathbf{U}^{\mathrm{g}}\mathbf{U}^{\mathrm{e}}\mathbf{M}\left(\mathbf{K}_{\mathrm{h1}}{}^{\mathrm{c}} + \int_0^{L_o}\mathbf{K}_{\mathrm{h2}}{}^{\mathrm{c}}\mathrm{d}X_1\right)\mathbf{M}^{\mathrm{T}}(\mathbf{U}^{\mathrm{e}})^{\mathrm{T}}(\mathbf{U}^{\mathrm{g}})^{\mathrm{T}}\mathbf{d}^{\mathrm{g}} \end{aligned} \qquad \text{(Eq. 2.308)}$$

2.7.12 Use of Tapered Elements to Address Steps in Cross-Section

In general, steps in the member flange thickness, flange width and web thickness are relatively common. Changes in the flange thickness or width result in changes in the shear center. This is illustrated in Figure 2.20. Finite element analysis requires one more element to connect the discontinuity in shear center which results in computational error. As shown in Figure 2.21, transition of flange width results in discontinuity of warping. The warping continuously follows tapering shape due to redundancy of area. The only solution is to use a taper over a short length. Currently, there is no guidance for the length to be used in providing this taper.

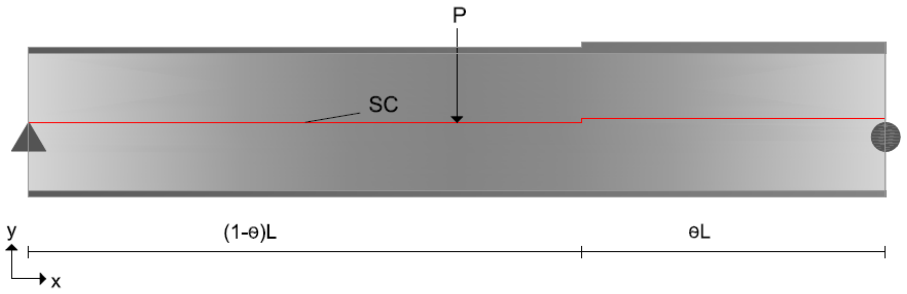

Figure 2.20 Variation of flange thickness and the effect on the shear center in a non-prismatic I beam

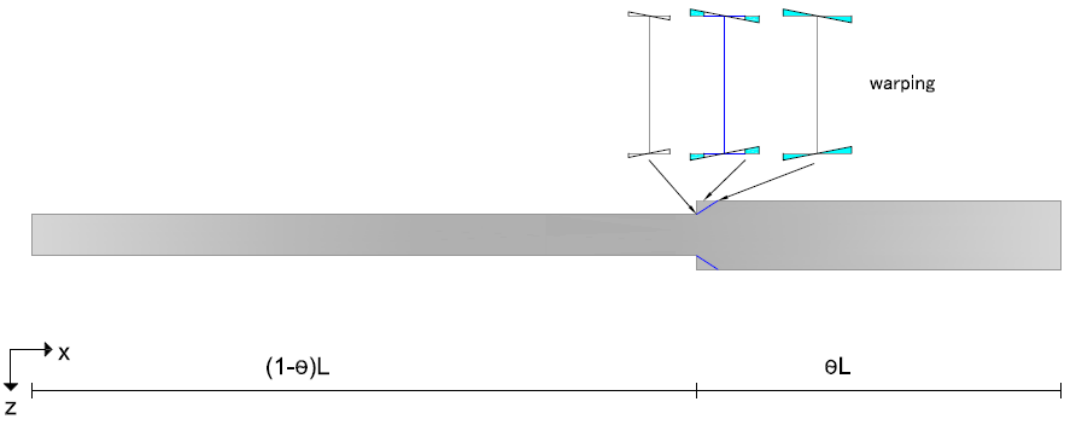

Figure 2.21 Variation of flange width

A slope equal to 1:1 is selected to address the appropriate tapering short length to address steps in the flange thickness or flange width. In SABRE2, the shear center difference at the stepped location is taken to be the same as the tapering length. For the verification of the tapering length for a transition in flange thickness, the lateral torsional buckling multipliers from SABRE2 are compared to those from a 3D Shell FEA solution. In Figure 2.20, the dimensions are: top flange $6\text{in} \times 0.5\text{in}$ and $6\text{in} \times 1\text{in}$, bottom flange $6\text{in} \times 0.5\text{in}$throughout the length of the beam, and web $23.5\text{in} \times 0.374\text{in}$. The member length is$\text{L} = 20\text{ft}$ is employed. For the 3D Shell modeling, stiffeners are used at the support and loading locations to prevent stress concentrations

From Table 2.3 and Table 2.4, the 3D finite element analysis based on open section thin-walled beam theory has good agreement with the 3D shell finite element analysis.

Table 2.3 Load $\text{P} = 1\text{kip}$ in Figure 2.20 with respect to transition length factor.

Θ	SABRE 2	3D Shell
0.1	34.493	35.382
0.2	36.7103	36.878
0.3	39.0838	38.563
0.4	41.876	41.112
0.5	45.7637	46.111
1	60.4313	60.783

where:

- Θ = Transition length factor.

Table 2.4 Load P = −1kip in Figure 2.20 with respect to transition length factor.

Θ	SABRE 2	3D Shell
0.1	34.1264	34.938
0.2	35.3283	36.074
0.3	36.2076	37.355
0.4	37.3384	38.505
0.5	39.5556	39.707
1	51.3883	50.95

2.8 SABRE2

The finite element formulation developed in the previous sections is implemented in a software tool named SABRE2 in this research. MATLAB is employed as the underlying platform for SABRE2. As shown in Figure 2.22 through 2.31, SABRE2 provides an easy-to-use graphical user-interface.

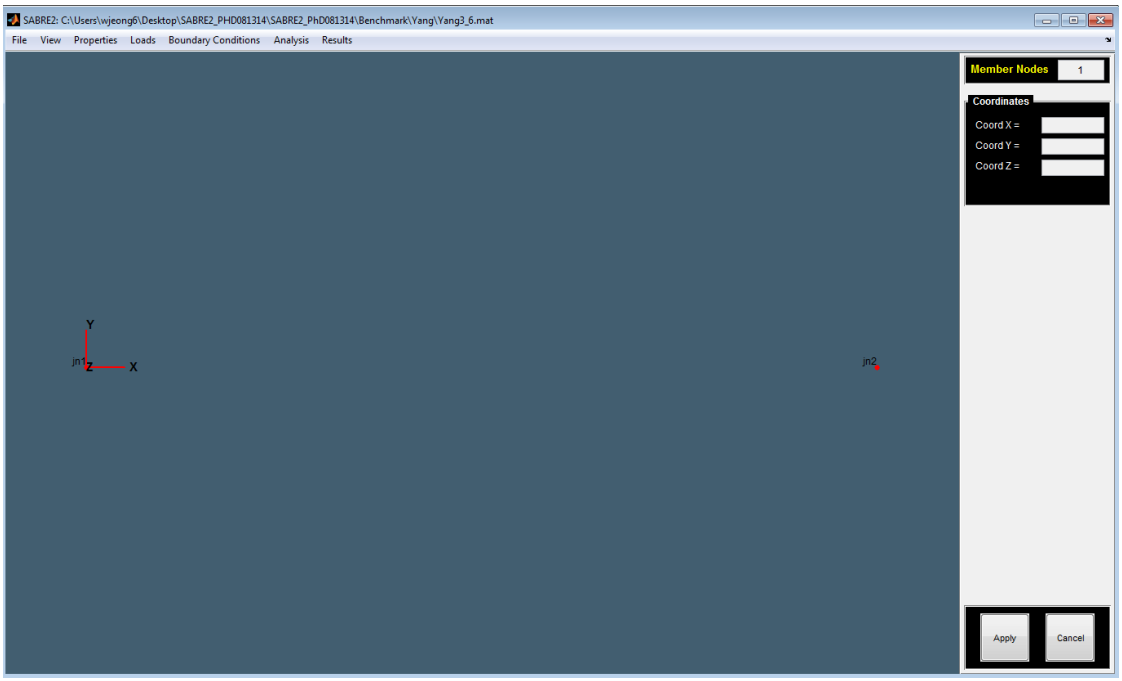

Figure 2.22 Screenshot of SABRE2 for the definition of joint nodes.

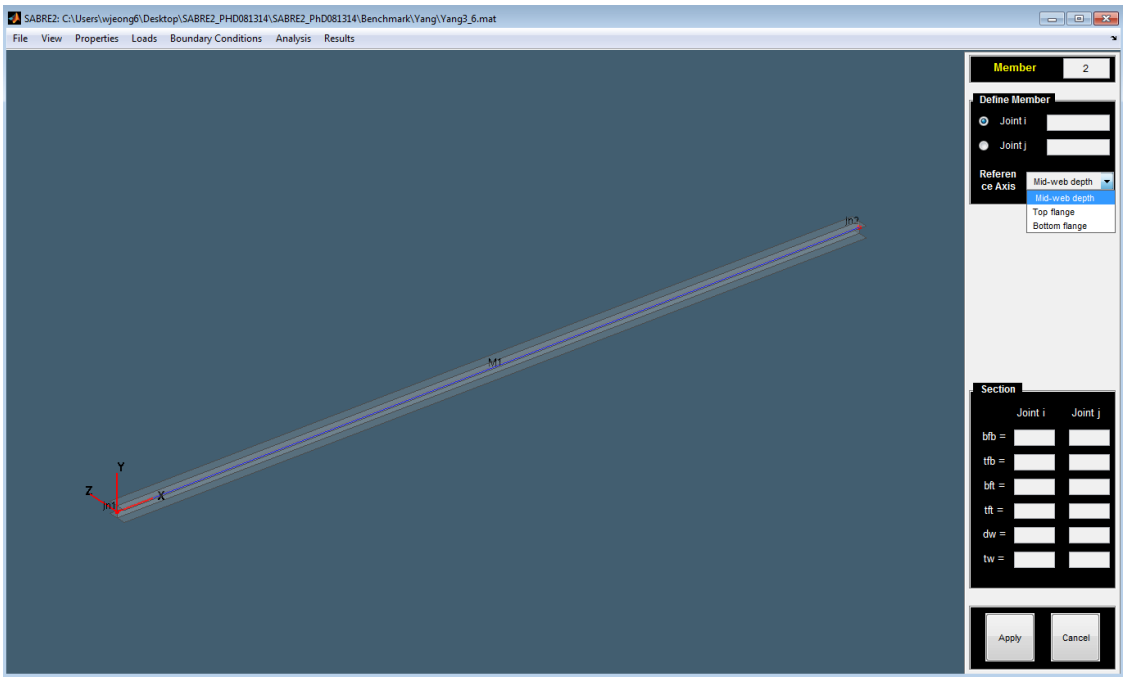

Figure 2.23 Screenshot of SABRE2 for the definition of members.

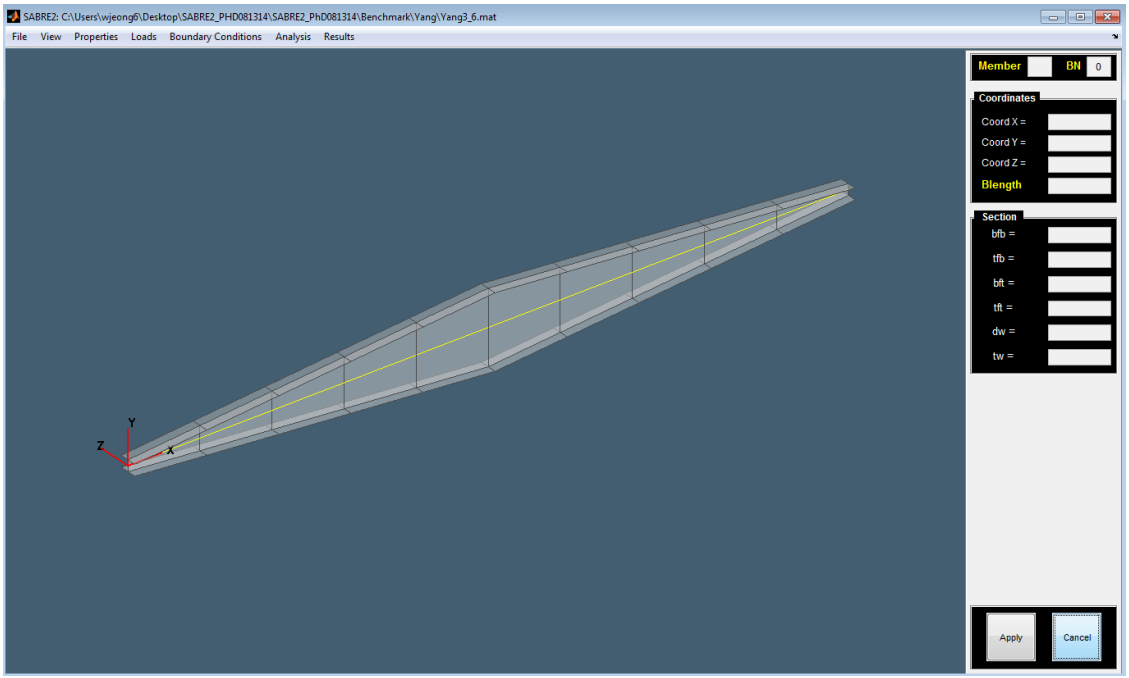

Figure 2.24 Screenshot of SABRE2 for bracing locations.

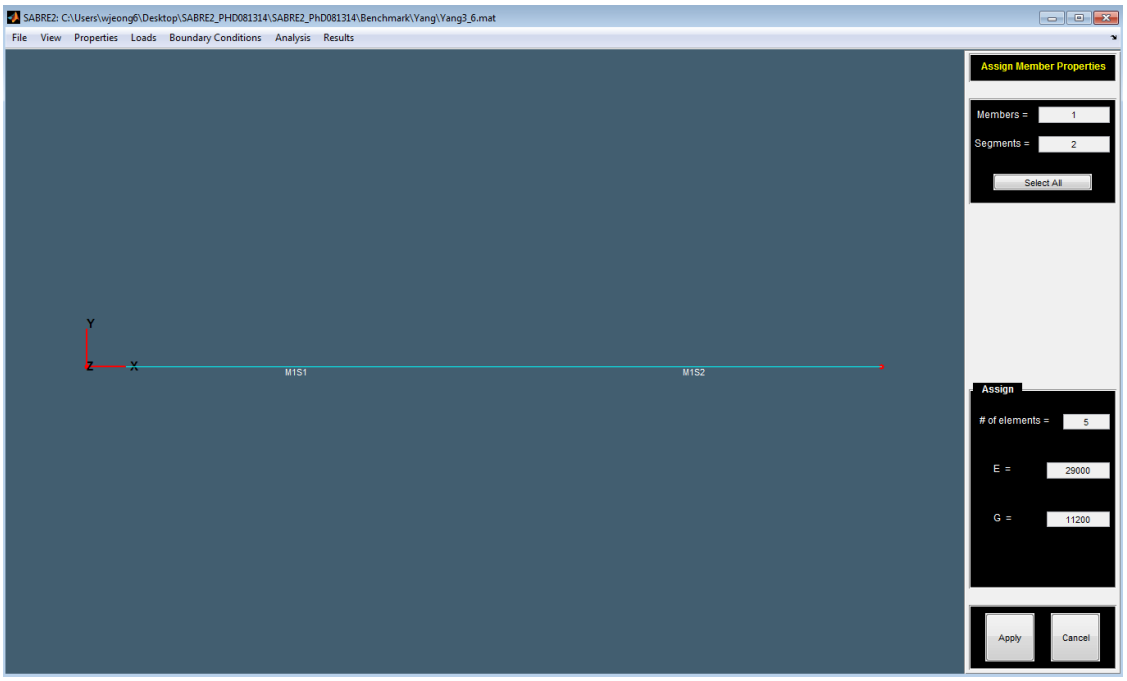

Figure 2.25 Screenshot of SABRE2 for material properties and the number of elements.

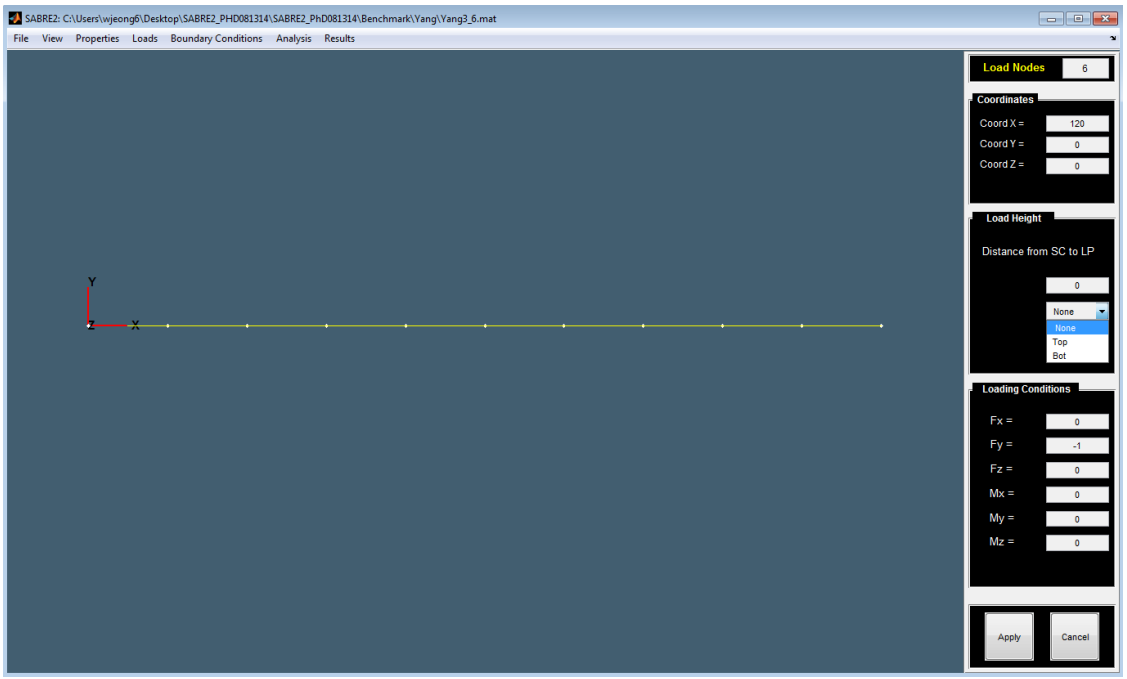

Figure 2.26 Screenshot of SABRE2 for point loads.

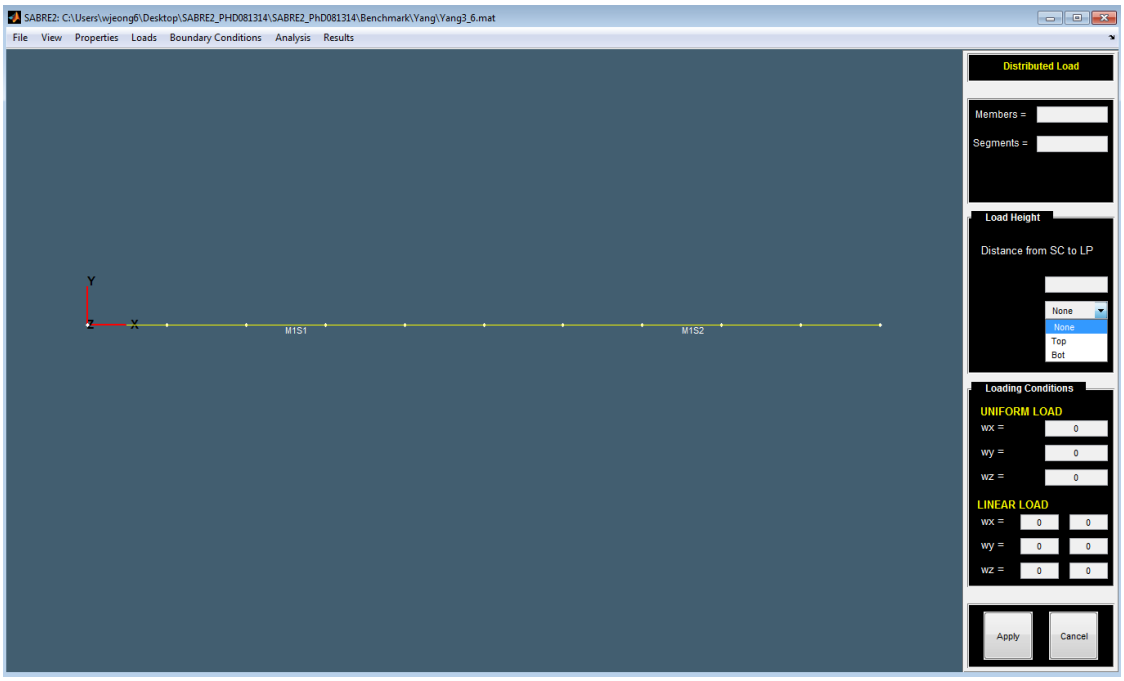

Figure 2.27 Screenshot of SABRE2 for distributed loads.

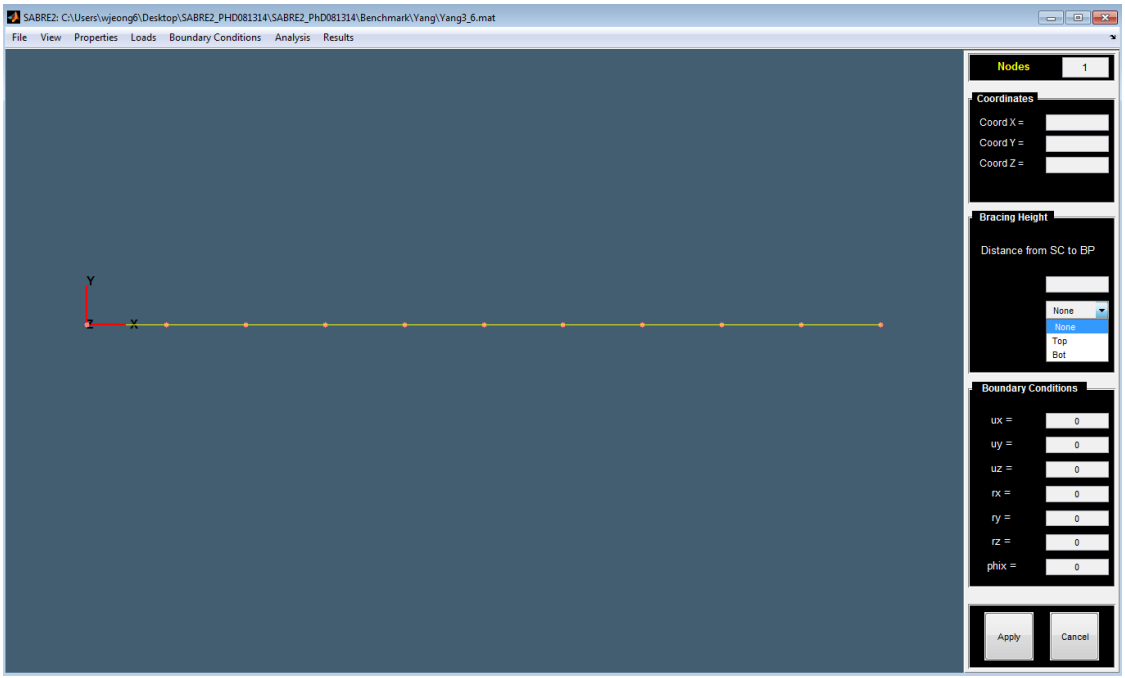

Figure 2.28 Screenshot of SABRE2 for boundary and bracing conditions.

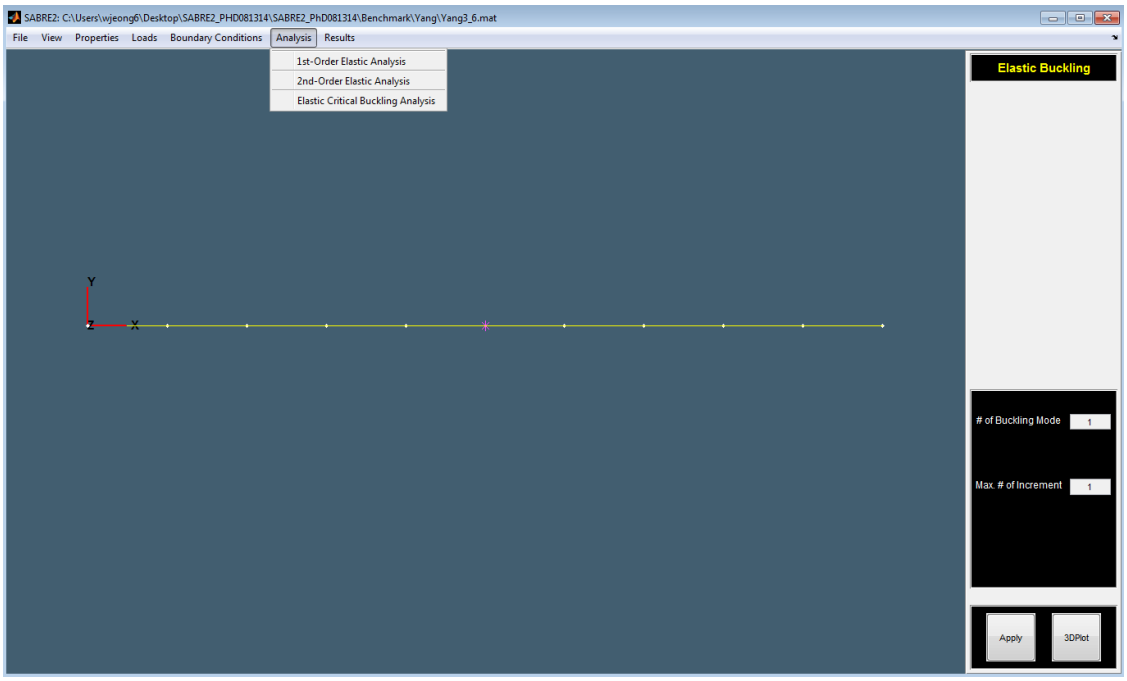

Figure 2.29 Screenshot of SABRE2 for analysis.

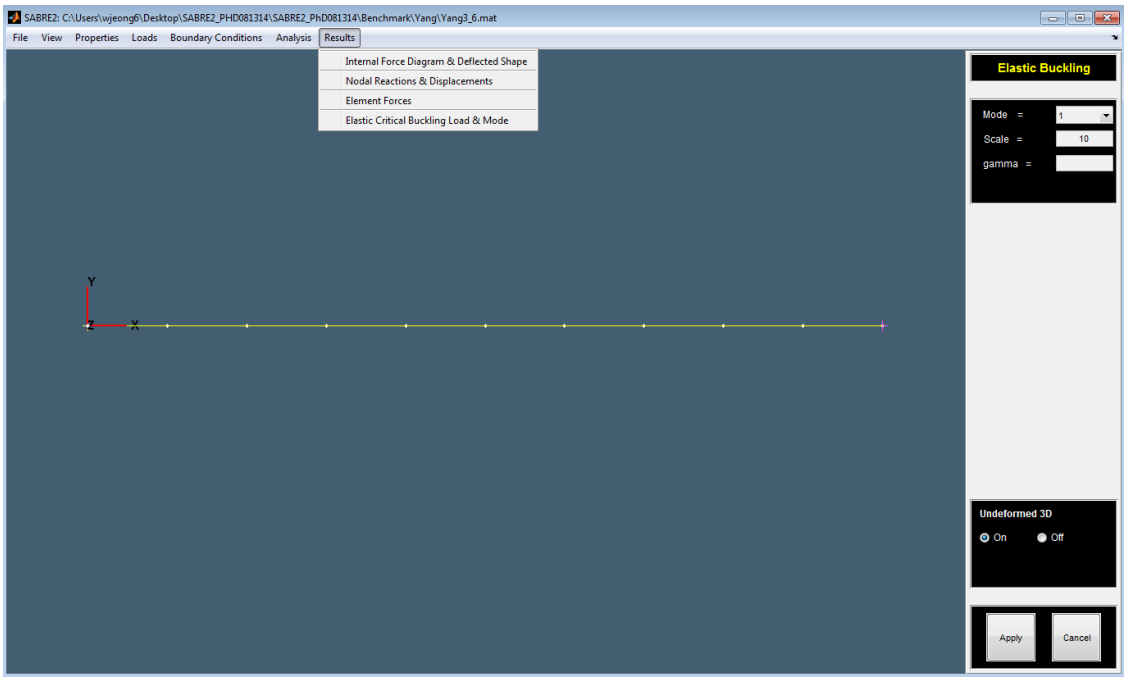

Figure 2.30 Screenshot of SABRE2 for results.

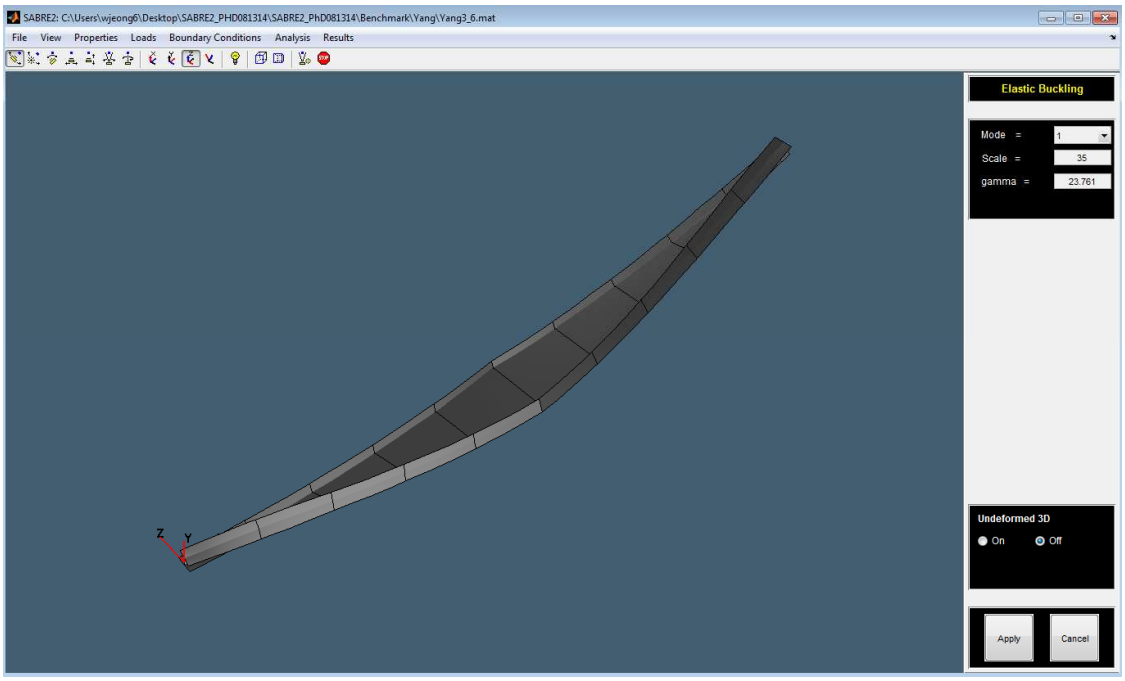

Figure 2.31 Screenshot of SABRE2 for deformed buckled geometry.

The SABRE2 problem definition and the analysis solution proceed as follows:

1) The start and end joint nodes are defined for each member as shown in Figure 2.22.
2) Members including section properties are defined between the joint nodes. As shown in Figure 2.23, the user can define a design axis, which is a straight reference axis (top flange, bottom flange or mid-web depth) used to locate the nonprismatic member in space.
3) The locations of transitions in the cross section (steps, taper changes), concentrated load points, and bracing points are defined as shown in Figure 2.24.

4) The number of elements and material properties are assigned for each segment as shown in Figure 2.25.
5) General loadings including load height are defined as shown in Figure 2.26 and 2.27.
6) Boundary and bracing conditions including rigid offsets are defined as shown in Figure 2.28.
7) The analysis procedure – first-order elastic, second-order elastic, or elastic buckling analysis – is selected as shown in Figure 2.29.
8) The desired analysis results (nodal displacements, member force diagram or 3D elastic buckling modes) are selected for display using an efficient graphical user-interface, as shown in Figure 2.30. An illustration of the deformed buckled geometry including warping is shown in Figure 2.31.

2.9 Benchmark Problems

This section provides a number of benchmark problems that serve to illustrate and validate the beam FEA capabilities developed in this research.

A steel modulus of elasticity of $E = 29000\text{ksi}$ and a shear modulus of elasticity $G = 11200\text{ksi}$ are employed throughout the solutions. Units of kips and inches are employed throughout. In each of the benchmark problems using SABRE2, the constrained *degrees of freedom* at support or bracing locations are indicated by a list $(u, v, w, \theta_x, \theta_x, \theta_x, \theta_x')$ in which the numeral **1** for a given dof indicates a fixed or constrained dof, and the numeral **0** indicates that the dof is free.

To check the 3D finite element analysis using SABRE2 results, the critical lateral-torsional buckling moment exact solution which is defined by Galambos and Surovek (2005) is employed. The exact solution explains singly- or doubly- symmetric cross-section, prismatic member under simply-supported and uniform bending moment loading and is described in Eq. 2.309.

$$M_{cr} = \frac{\pi^2 E I_y G J}{L^2}\left[\frac{\beta_z}{2GJ} + \sqrt{\left(\frac{\beta_z}{2GJ}\right)^2 + \frac{L^2}{\pi^2 E I_y G J}\left(\frac{\pi^2 E C_w}{L^2 G J} + 1\right)}\right] \quad \text{(Eq. 2.309)}$$

Where,

- I_y= Out-of-plane moment of inertia, in^4.
- J = Torsional constant, in^4.
- β_z = Singly-symmetric parameter,in.
- C_w = Warping constant, in^6.

2.9.1 Simply-Supported I Beam

2.9.1.1 Variation of member lengths

The elastic buckling loads for a simply-supported I beam under pure bending are analyzed to validate SABRE2 and are compared with the exact solution of Eq. 2.309. For the validation, various member lengths with respect to different cross-sections are analyzed using eight elements. In Figure 2.32, the member lengths are 200in, 400in, 600in, 800in, and 1000in. The cross-sections are W21x93, W24x207, and W40x294.

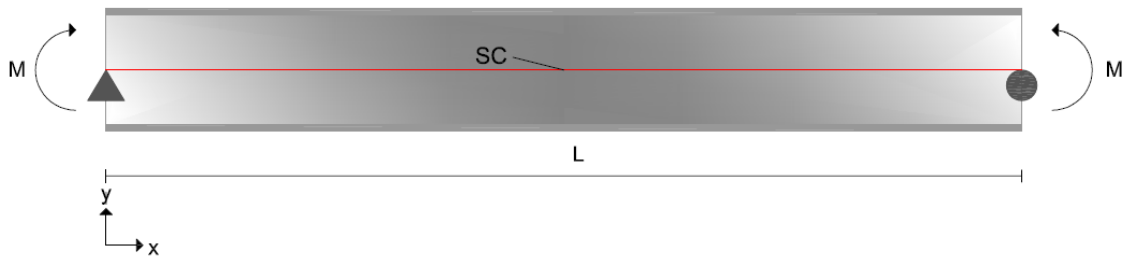

Figure 2.32 Simply-supported I beam under pure bending moment.

In Tables 2.5 through 2.7, the elastic critical buckling loads are shown with respect to various member lengths for W21x93, W24x207, and W40x294. From the tables, the results using 8 elements compared to the exact solutions of Eq. 2.309 show 0.499~0.739% differences, which indicate that the beam finite element provides an accurate representation of the analytical solutions for this basic case.

Table 2.5 Elastic critical buckling loads with respect to member length for a **W21x93**.

	Exact solution	FEA solution	Error (%)
Buckling load (kips·in) L = 200in	9369.9	9323.3	-0.497
Buckling load (kips·in) L = 400in	3624.8	3601.6	-0.640
Buckling load (kips·in) L = 600in	2261.6	2246.1	-0.685
Buckling load (kips·in) L = 800in	1653.6	1641.8	-0.709
Buckling load (kips·in) L = 1000in	1306.8	1297.3	-0.723

Table 2.6 Elastic critical buckling loads with respect to member length for a **W24x207**

	Exact solution	FEA solution	Error (%)
Buckling load (kips·in) L = 200in	64250	63929	-0.496
Buckling load (kips·in) L = 400in	23860	23704	-0.638
Buckling load (kips·in) L = 600in	14660	14557	-0.687
Buckling load (kips·in) L = 800in	10650	10571	-0.714
Buckling load (kips·in) L = 1000in	8386.0	8324.5	-0.732

Table 2.7 Elastic critical buckling loads with respect to member length for a **W40x294**

	Exact solution	FEA solution	Error (%)
Buckling load (kips·in) L = 200in	94120	93654	-0.496
Buckling load (kips·in) L = 400in	33320	33106	-0.637
Buckling load (kips·in) L = 600in	20060	19924	-0.686
Buckling load (kips·in) L = 800in	14440	14337	-0.711
Buckling load (kips·in) L = 1000in	11320	11238	-0.726

2.9.1.2 Kitipornchai's singly-symmetric members

Figure 2.33 shows a simply-supported I beam under moment gradient loading. The parameter β indicates the fraction of the left-end moment applied at the right end. For β< 1, the beam is subjected to a moment gradient loading which is applied to shear center (SC in Figure 2.33). For the analysis, member length is 600in and the cross-section dimensions are shown in Table 2.8. Using the same basic configuration shown in Figure 2.33, the converged critical buckling modes such as rotation of cross-section and out-of-plane displacement for mono-symmetric members are studied in this section. The degree of the beam cross-section mono-symmetry is described by the parameter

$$\rho = \frac{I_{ytop}}{I_{ytop} + I_{ybot}} \qquad \text{(Eq 2.309)}$$

and the specific cross-sections having the different degrees of mono-symmetry are shown in Figure 2.34.

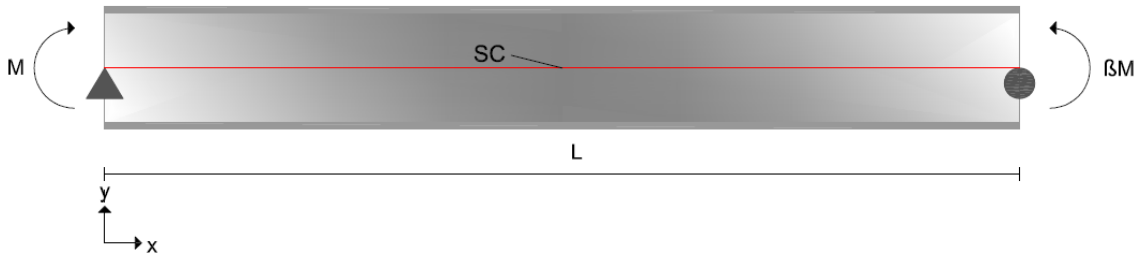

Figure 2.33 Simply-supported I beam under moment gradient loading.

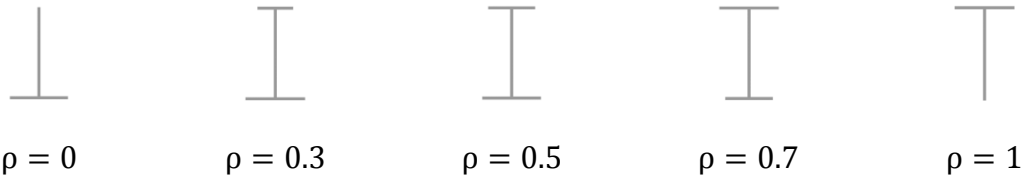

Figure 2.34 Cross-section shaving different degrees of mono-symmetry ρ

Kitipornchai (1986) investigated the elastic lateral buckling of simply supported singly-symmetric prismatic I-beams under moment gradient. He used a finite integral method and the Rayleigh-Ritz energy approach to obtain independent solutions. The paper shows the elastic buckling moments depend on the degree of the beam single-symmetry as well as the nature of the moment gradient loadings. To compare with the results from Kitpornchai (1986), various moment gradient loading factors β are studied as shown in Figure 2.35. The critical buckling modes are illustrated in Figure 2.35. These results are visually identical to the results provided by Kitipornchai. The twist rotations and lateral displacements are affected by the moment gradient loading factor β and the mono-symmetry factor ρ.

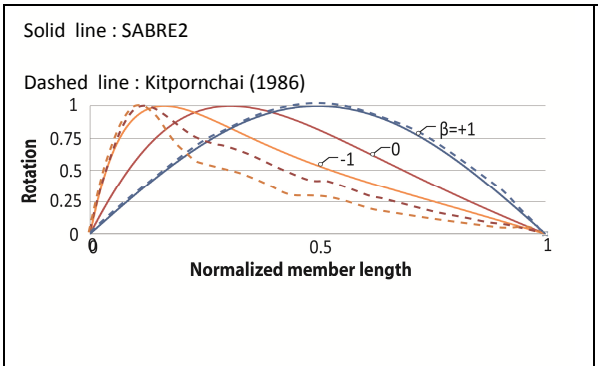

Rotation (ρ = 0)

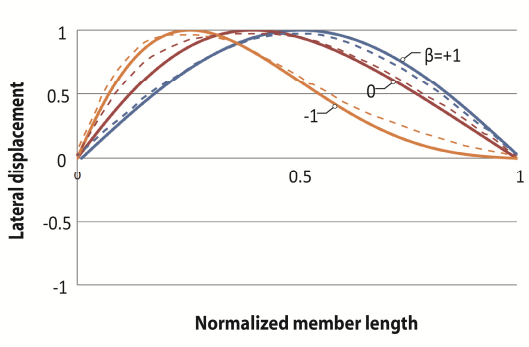

Lateral displacement (ρ = 0)

Figure 2.35 Elastic critical buckling modes for singly-symmetric I beams subjected to moment gradient loadings (continued)

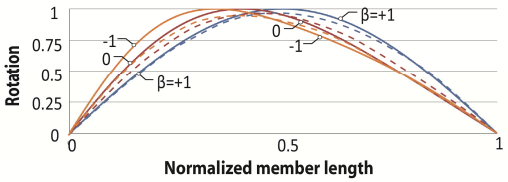

Rotation ($\rho = 0.3$)

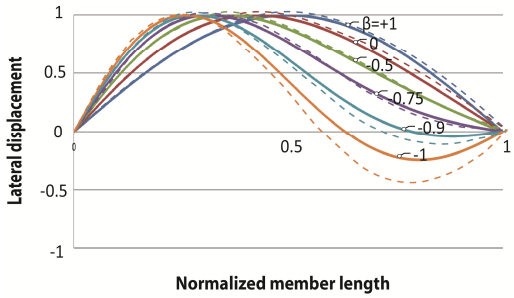

Lateral displacement ($\rho = 0.3$)

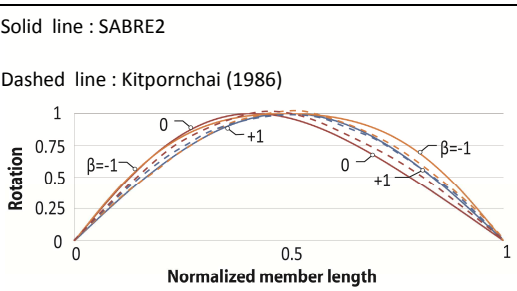

Rotation ($\rho = 0.5$)

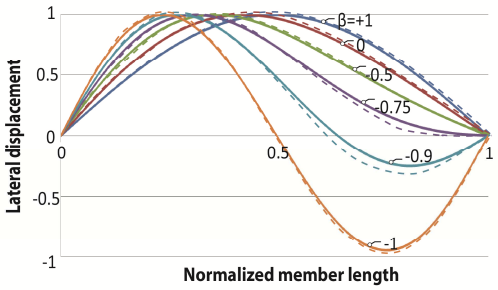

Lateral displacement ($\rho = 0.5$)

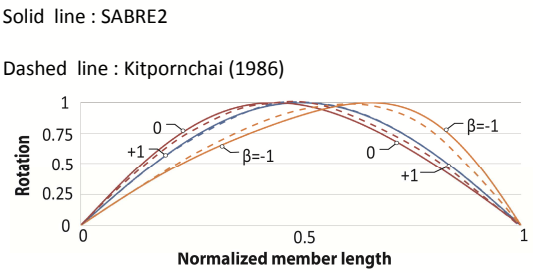

Rotation ($\rho = 0.7$)

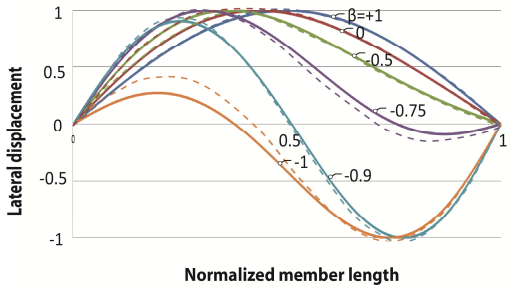

Lateral displacement ($\rho = 0.7$)

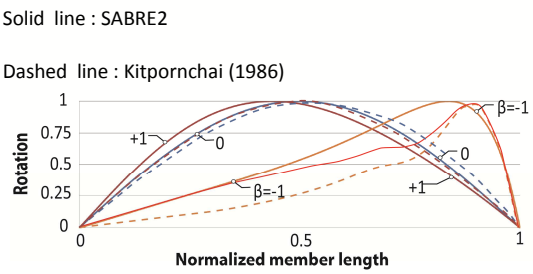

Rotation ($\rho = 1$)

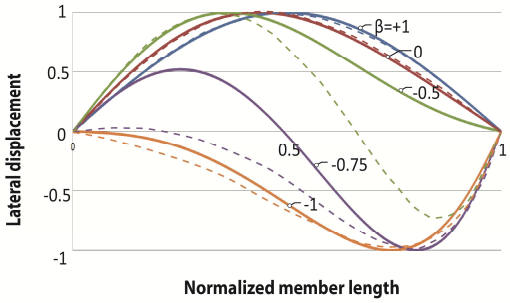

Lateral displacement ($\rho = 1$)

Figure 2.35 Elastic critical buckling modes for singly-symmetric I beams subjected to moment gradient loadings

Table 2.8 Member dimensions for the simply-supported singly-symmetric member

	b_{ft}	t_{ft}	b_{fb}	t_{fb}	h	t_w
$\rho = 0$	$0.580in$	$0.580in$	$8.420in$	$0.930in$	$20.09in$	$0.580in$
$\rho = 0.3$	$8.420in$	$0.930in$	$11.17in$	$0.930in$	$19.74in$	$0.580in$
$\rho = 0.5$	$8.420in$	$0.930in$	$8.420in$	$0.930in$	$19.74in$	$0.580in$
$\rho = 0.7$	$11.170in$	$0.930in$	$8.420in$	$0.930in$	$19.74in$	$0.580in$
$\rho = 1$	$8.420in$	$0.930in$	$0.580in$	$0.580in$	$20.09in$	$0.580in$

The elastic critical buckling loads are shown in Table 2.9. If the mono-symmetric factors are smaller than 0.5, the critical buckling loads are increased as the moment gradient loading factor becomes -1. If the mono-symmetric factors are greater than 0.5, the maximum critical loads are generated as the moment gradient loading factor becomes 0.

Table 2.9 Elastic critical buckling loads (M_{cr}) with respect to the moment gradient loading factor β and the mono-symmetry factor ρ. (kip · in)

	$\beta = 1$	$\beta = 0$	$\beta = -0.5$	$\beta = -0.75$	$\beta = -0.9$	$\beta = -1$
$\rho = 0$	917.0	1057	1789	1895	1947	1977
$\rho = 0.3$	2710	4808	6391	7152	7505	7645
$\rho = 0.5$	2262	4064	5491	6094	6185	6006
$\rho = 0.7$	3659	6660	9070	9485	8615	7766
$\rho = 1$	1548	2815	3684	2781	2268	2010

2.9.1.3 Members with multiple unbraced lengths

As an example of lateral torsional buckling of members with multiple unbraced lengths, a simply-supported beam having one intermediate lateral brace location, subdividing the beam into two unequal unbraced lengths in Figure 2.36, and a second beam having two intermediate lateral brace locations in Figure 2.37, subdividing the beam into three unbraced lengths, are studied. For the analysis, member length is 600in and the cross-section is W21x93.

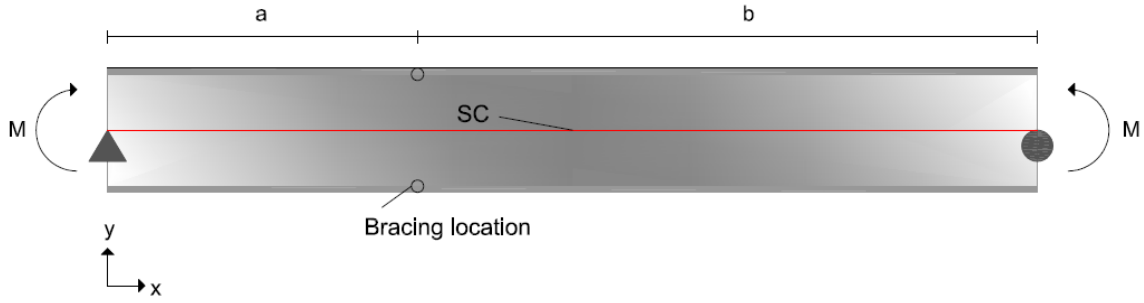

Figure 2.36 Simply-supported two-spans (unbraced length) W21x93 under moment gradient loading

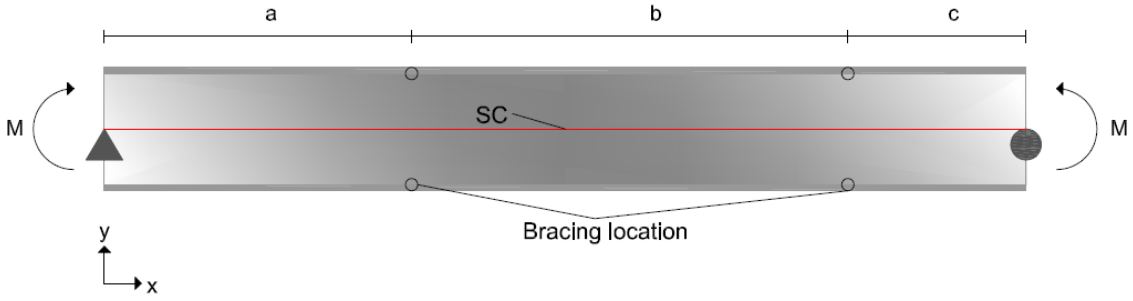

Figure 2.37 Simply-supported three-spans (unbraced length) W21x93 under moment gradient loading

To investigate the effects of bracings for the elastic lateral torsional buckling strength, different bracing locations are modeled and the critical buckling loads and the critical buckling modes such as rotation of cross-section and out-of-plane displacement are analyzed. For bracing conditions, both the lateral displacement and the twisting of the section are prevented at the brace locations. The bracing condition in SABRE2 is described by:

- Bracing :$(\mathrm{u}, \mathrm{v}, \mathrm{w}, \theta_x, \theta_x, \theta_x, \theta_x') = (0,0,1,1,0,0,0)$

The converged critical buckling modes are described in Figure 2.38 for the case with one intermediate brace location and in Figure 2.39 for the case with two intermediate brace locations. The buckling rotations and lateral displacement are affected by the number and the location of the brace points.

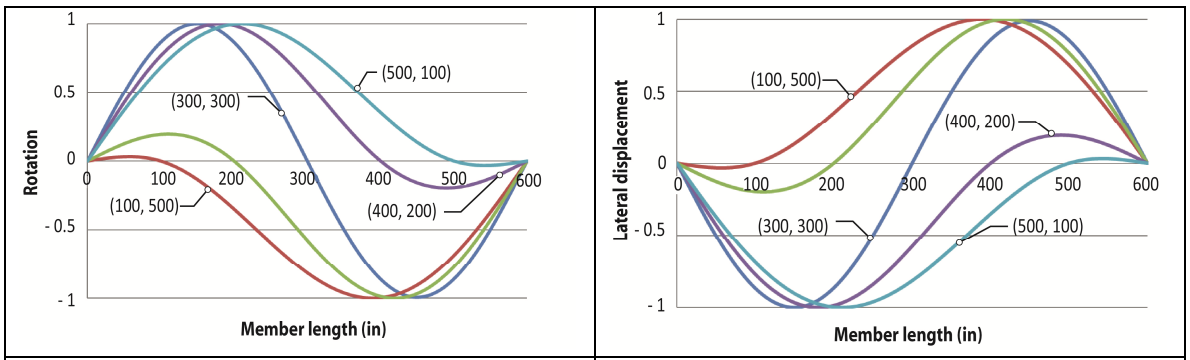

Rotation	Lateral displacement

Figure 2.38 Elastic critical buckling modes for member composed of two unbraced lengths

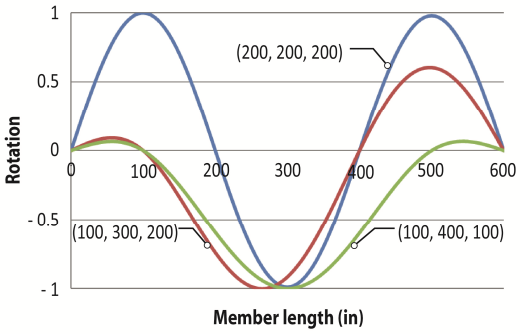

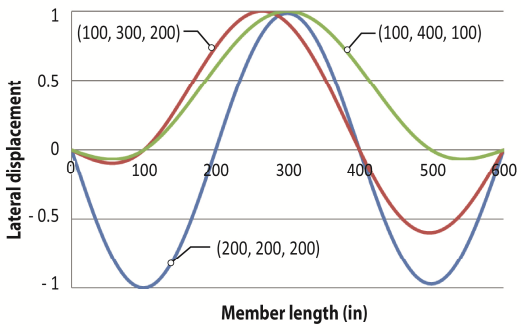

Rotation	Lateral displacement

Figure 2.39 Elastic critical buckling modes for member composed of three unbraced lengths

In Table 2.10 and Table 2.11, the elastic buckling loads are investigated. The largest critical buckling load is generated under equal unbraced lengths and the smallest critical buckling load is generated under shortest unbraced lengths.

Table 2.10 Elastic critical buckling loads for a member composed of two unbraced lengths

	(300,300)	(100,500)	(200,400)	(400,200)	(500,100)
$M_{cr}(kips \cdot in)$	5236	3977	4708	4683	3954

Table 2.11 Elastic critical buckling loads for a member composed of three unbraced lengths

	(200,200,200)	(100,300,200)	(100,400,100)
$M_{cr}(kips \cdot in)$	9369	8289	7350

2.9.2 Web Tapered Members

2.9.2.1 Yang and Yau & Andrade and Camotim simply-supported web-tapered member

Figure 2.40 shows a simply-supported I-beam having a tapered web depth. The input information for this benchmark in SABRE2 is as follows:

- Doubly symmetric and web tapered member
- Boundary Conditions
  - Support1 : $(\mathrm{u}, \mathrm{v}, \mathrm{w}, \theta_x, \theta_x, \theta_x, \theta_x') = (1,1,1,1,0,0,0)$
  - Support2 : $(\mathrm{u}, \mathrm{v}, \mathrm{w}, \theta_x, \theta_x, \theta_x, \theta_x') = (0,1,1,1,0,0,0)$

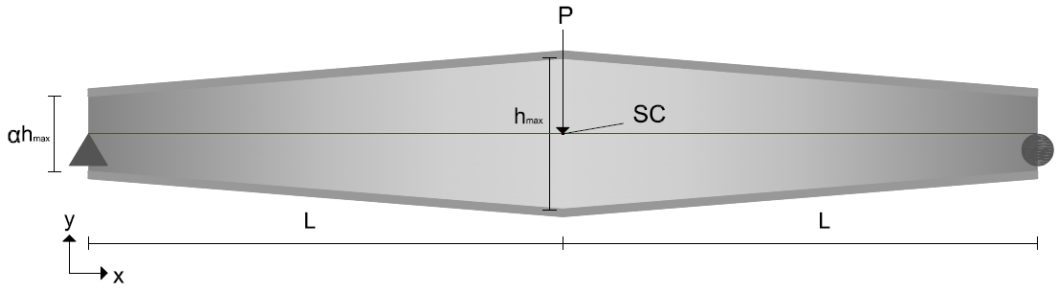

Figure 2.40 Simply-supported web tapered I beam under point loading at mid-span.

The elastic lateral torsional buckling load for Model 1 in Figure 2.41 and Model 2 in Figure 2.42 is reported as a function of the tapering factor α in Table 2.12 and Table 2.13. Model 1 and 10 elements which are consistent with Yang and Yau's analyses (1987) are employed for SABRE2-1. Model 2 which are consistent with the Chang (2006)

solution are employed for SABRE2-2 under converged elements. The results from the current research show good agreement with Yang and Yau's and Chang's results. Andrade and Camotim's result, which employs a Rayleigh-Ritz approach and sinusoidal shape functions for lateral torsional buckling analysis, gives a slightly higher buckling load than the solution from this research as well as the solution from Chang (2006). This is particularly the case when the tapering factor α is 0.3.

Table 2.12 Member dimensions for the simply-supported web-tapered member

	b_{ft} and b_{fb}	t_{ft} and t_{fb}	h_{max}	t_w	L
Model 1	$5.984in$	$0.512in$	$24.016in$	$0.374in$	$120.079in$
Model 2	$6in$	$0.5in$	$24in$	$0.374in$	$120in$

where:

- Model 1 : These are the dimensions for this problem used by Yang and Yau (1987). The results from the current research, based on these dimensions, are labeled as SABRE2-1.
- Model 2 : These are the dimensions for this problem used by Andrade and Camotim (2005). The results from the current research, based on these dimensions, are labeled as SABRE2-2. In addition, the results for this problem are obtained from the Chang (2006).

Table 2.13 Member dimensions for the simply-supported web-tapered member

α	0.1	0.15	0.2	0.3	0.4	0.5	0.6	0.7	0.8	0.9	1
$h_{max} + t_f$	2.9	4.1	5.3	7.7	10.1	12.5	14.9	17.3	19.7	22.1	24.5

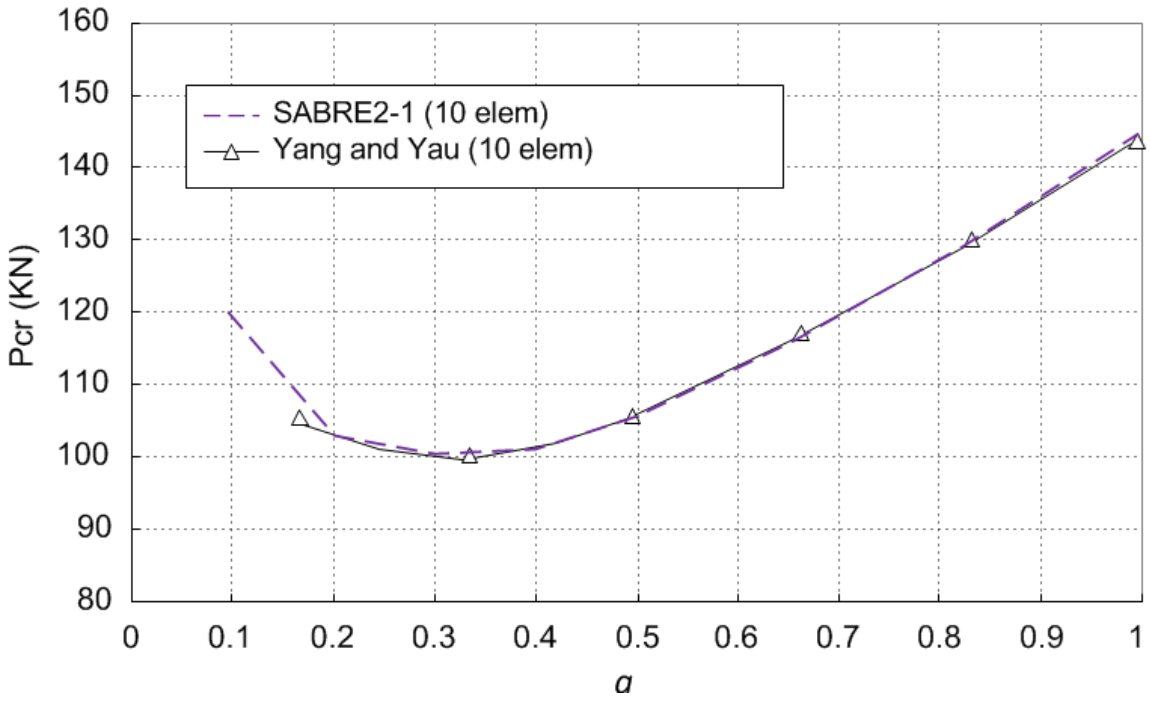

Figure 2.41 Elastic critical buckling loads of Model 1 with respect to tapering factor α

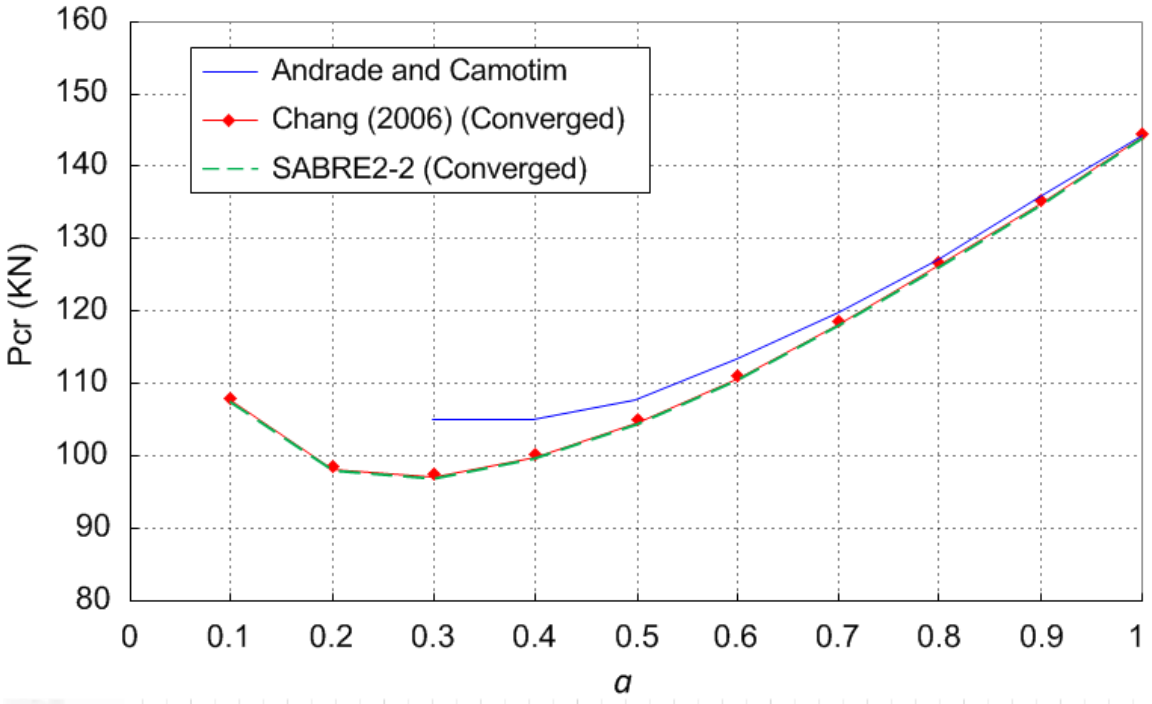

Figure 2.42 Elastic critical buckling loads of Model 2 with respect to tapering factor α

In Figure 2.43, SABRE2 is compared with 3D finite element analysis using shell elements and open section thin-walled beam using stepped elements. MASTAN2 (2013) and StabLab (2013) are employed to analyze the web tapered member in Figure 2.40 using stepped elements. MASTAN2 (2013) is structural analysis software limited to prismatic and doubly-symmetric member. StabLab (2013) is structural analysis software touted for analysis of singly-or doubly- symmetric and tapered members. MASTAN2 (2013) is used to model the member using stepped elements with average depth of both ends of the elements and with the smallest depth of both ends of the elements. StabLab (2013) for the tapering member analysis gives close agreement with MASTAN2 (2013) using stepped elements with the smallest depth of both ends of the elements. The shell finite element analysis is the most rigorous of all the solutions presented in the plot. Comparison of the StabLab and MASTAN solutions to the shell finite element solution shows clearly that the use of stepped prismatic elements generally gives incorrect results for lateral-torsional buckling of tapered members. However, SABRE2 shows very good agreement with 3D shell model of the tapering member for all values of the tapering factor.

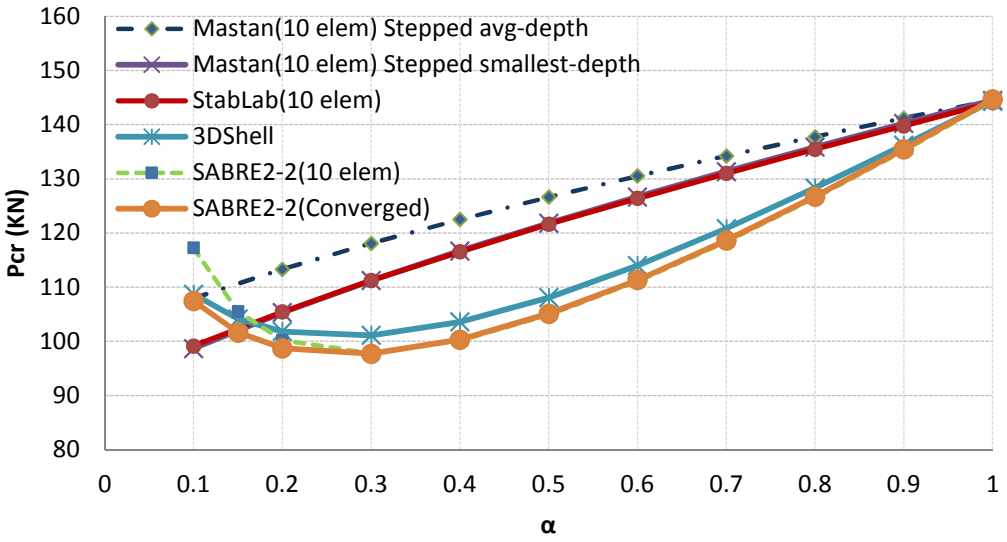

Figure 2.43 3D Finite element analysis using shell elements and open section thin-walled beam theory.

2.9.2.2 Simply-supported member with a single web-taper

Single side web tapered members are widely employed in many instances of structural design due to the convenience of the construction. Figure 2.44 shows the bottom flange single side web-tapered member under downward point loading at its mid-span. Figure 2.45 shows a top flange single side web-tapered member under downward point loading at its mid-span. SABRE2 is analyzed using Model 2 in Table 2.12 and ten elements

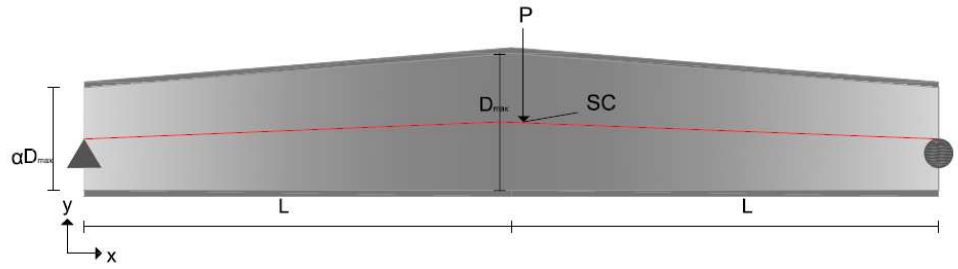

Figure 2.44 Bottom flange single side web-tapered simply-supported I beam under point loading at mid-span

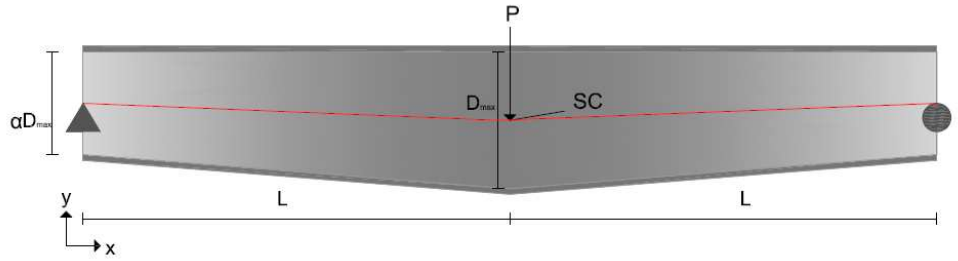

Figure 2.45 Top flange single side web-tapered simply-supported I beam under point loading at mid-span

For the validation of the SABRE2 solutions, finite element analysis using shell elements are compared with the SABRE2 analysis. Transverse stiffeners $(\text{width}, \text{thickness}) = (2.813\text{in}, 0.7\text{in})$ at boundaries and loading location are included in the shell finite element model. Inverted arch effect is consistent with the top flange single side web-tapered members in Figure 2.45. Arch effect is consistent with the bottom flange single side web-tapered members in Figure 2.44. As shown in Figure 2.43 and in Figure 2.46, the elastic critical buckling loads with respect to tapering factor α for single side web-tapered members and double side web-tapered members have very good

agreement between finite element using shell elements and SABRE2. Top flange single side web-tapered members under downward point loading at mid-span have much larger critical buckling load than double side web-tapered members as tapering parameter α decreases. Bottom flange single side web-tapered members under downward point loading at mid-span have much smaller critical buckling load than double side web-tapered members as the tapering parameter α decreases.

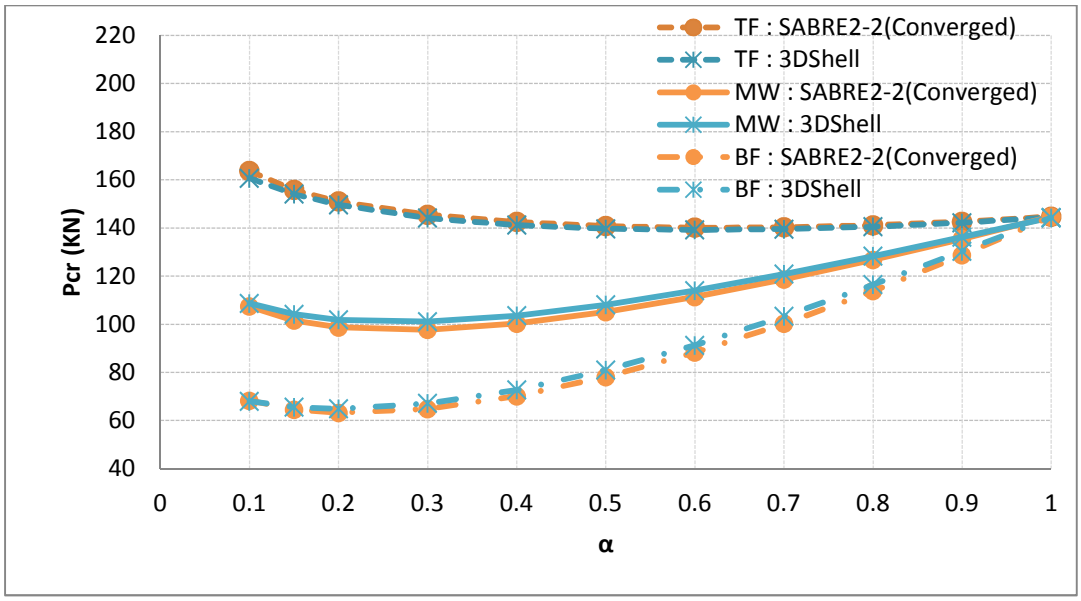

Figure 2.46 Elastic critical buckling load with respect to tapering factor α for single side web-tapered simply-supported member.

where:

- TF = Top flange in Figure 2.45
- MW = Mid-web depth in Figure 2.40
- BF = Bottom flange in Figure 2.44

2.9.2.3 Load height and rigid offset effects

In many cases, the physical loads and supports can be applied to the top flange or bottom flange of the member. Bracing can be placed at the top or bottom of web. For the verification of the SABRE2 capabilities for solving these problems, a simply-supported I beam under point loading at mid-span with W21x93 is studied. In Figure 2.47, off-axis lateral bracing at mid-span are simulated based on rigid-offset. For the analysis, member length of 600in and 8 elements are employed.

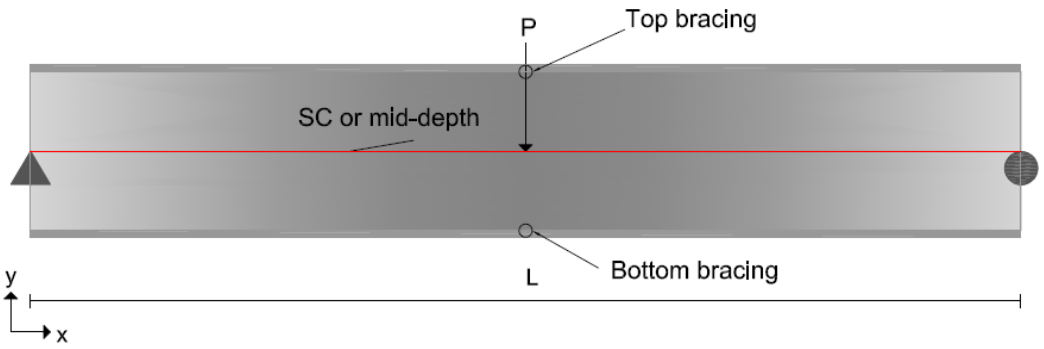

Figure 2.47 Simply-supported I beam under point loading at mid-span with W21x93

Table 2.14 Load height and rigid offset under load P=1kip

	Load Point	Bracing Point	LRF 1	LRF 2
Case1	Mid-depth	Both flange	61.92 kip	63.75 kip
Case2	Mid-depth	Top flange	61.91 kip	63.74 kip
Case3	Mid-depth	Bottom flange	29.94 kip	29.94 kip
Case4	Top flange	Both flange	61.92 kip	63.68 kip
Case5	Top flange	Top flange	61.91 kip	63.66 kip
Case6	Top flange	Bottom flange	19.86 kip	19.83 kip
Case7	Bottom flange	Both flange	61.93 kip	63.82 kip
Case8	Bottom flange	Top flange	61.92 kip	63.81 kip
Case9	Bottom flange	Bottom flange	55.56 kip	55.69 kip

where:

- LRF 1: Finite element analysis using formulated load height and rigid offsets for bracing and support height effects.
- LRF 2: Finite element analysis using additional transverse “stub” elements for load height and bracing location.
- Case1 : Load height effect is not included but lateral torsional bracing at mid-depth are included.
- Case2 : Load height effect is not included but lateral bracing at top flange is included.
- Case3 : Load height effect is not included but lateral bracing at bottom flange is included.
- Case4 : Load height effect at top flange is included but lateral torsional bracing at mid-depth is included.
- Case5 : Load height effect at top flange is included but lateral bracing at top flange is included.
- Case6 : Load height effect at top flange is included but lateral bracing at bottom flange is included.
- Case7 : Load height effect at bottom flange is included but lateral torsional bracing at mid-depth is included.
- Case8 : Load height effect at bottom flange is included but lateral bracing at top flange is included.
- Case9 : Load height effect at bottom flange is included but lateral bracing at bottom flange is included.

The SABRE2 solution (LRF 1) including the formulation of load height and rigid offset is compared with a SABRE2 solution (LRF 2) in which transverse "stub" beam elements are inserted between the shear center and the constraint position at the locations of the loading and bracing. Table 2.14 shows the elastic critical buckling loads with respect to load height and rigid offset. The formulated SABRE2 (LRF 1) has good agreements with SABRE2 including transverse stub elements. As shown in Table 2.14, load height and rigid offset can affect the critical buckling load.

The consideration of load height and bracing height effects for a large number of concentrated transverse loads and brace points is studied using the AISC roof girder example (AISC 2002) shown in Figures 2.48 through 2.50. The results from the SABRE2 formulation considering load height and rigid offsets to the brace points is compared with a SABRE2 solution conducted by adding transverse stub elements at the locations of the loads and the bracing, similar to the above solutions. For this analysis, a prismatic cross-section is used having a top and bottom flange width of 6 in, a top and bottom flange thickness of 0.375 in, a web depth of 24 in, and a web thickness of 0.149 in. Fourteen elements are employed to model the full length of the member, with one element between each of the purlin locations in Figure 2.48.

Table 2.15 shows that the formulated SABRE2 solution has good agreement with the solution where additional transverse stub elements are used for uniform loads and multiple bracings. SABRE2 including formulation of load-height and rigid offset can be very efficient and exact to calculate critical buckling loads since modeling time can be reduced and warping along web depth in case of adding additional elements for load-height and rigid-offset can be removed.

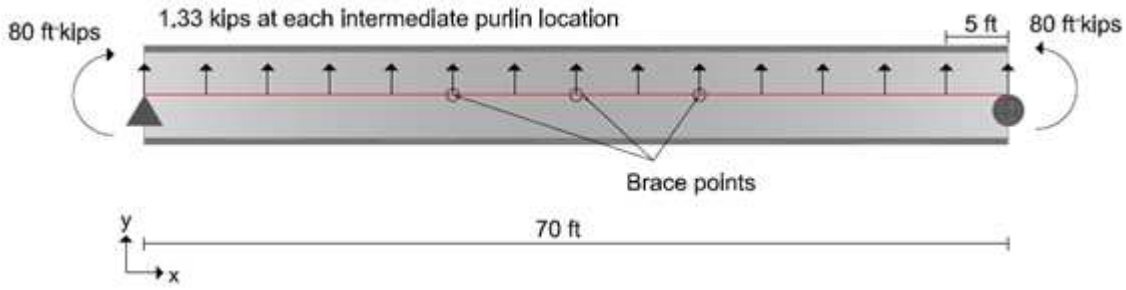

Figure 2.48 Simply-supported I beam subjected to distributed loading under lateral torsional bracing at mid-depth.

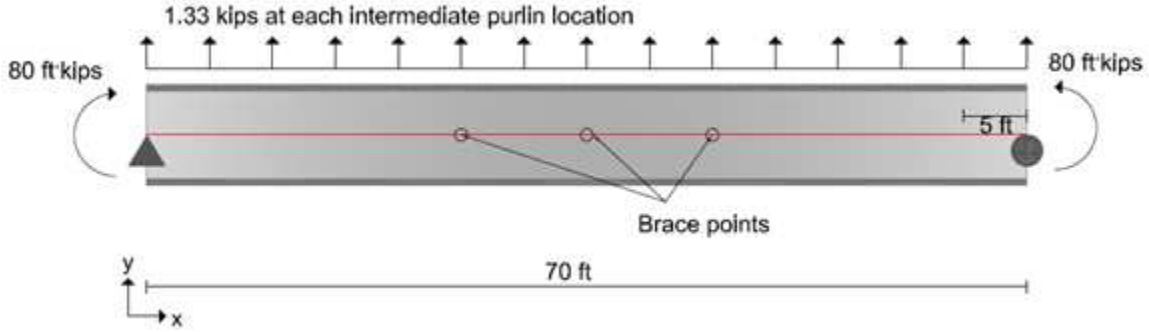

Figure 2.49 Simply-supported I beam subjected to distributed loading under load height effects and lateral torsional bracing at mid-depth.

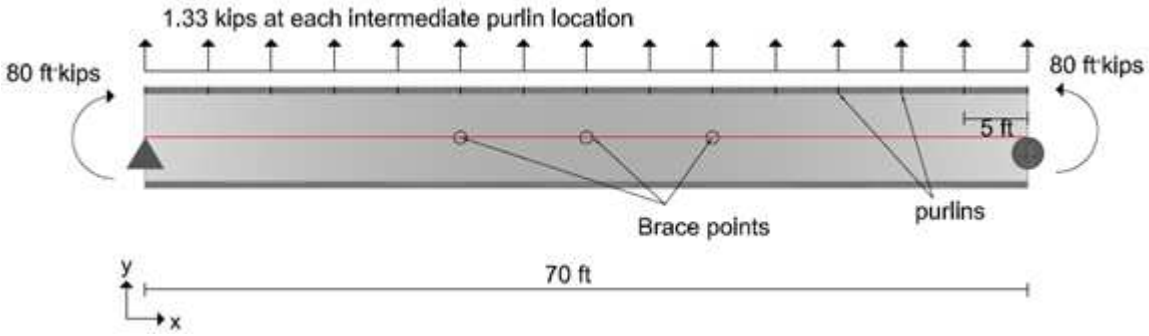

Figure 2.50 Simply-supported I beam subjected to distributed loading under load height effects, lateral bracing at purlin locations (top flange), and lateral torsional bracing at mid-depth.

Table 2.15 Results considering load height for the AISC (2002) roof girder example

	LRF 1	LRF 2
AISCRafterExample	2.237	2.287
AISCRafterExampleLH	2.637	2.684
AISCRafterExampleLHLR	2.974	3.018
AISCRafterExampleLTBO	2.501	2.545

where:

- LRF 1: Finite element analysis using formulated load height and rigid offsets for bracing and support height effects.
- LRF 2: Finite element analysis using additional transverse stub elements for load height and bracing location.
- AISCRafterExample: As shown in Figure 2.48, load height effects are not included but lateral torsional bracing at mid-depth are included.
- AISCRafterExampleLH: As shown in Figure 2.49, load height effects are included and lateral torsional bracing at mid-depth are included.
- AISCRafterExampleLHLR: As shown in Figure 2.50, load height effects, lateral bracing at top flange, and lateral torsional bracing at mid-web depth are included.
- AISCRafterExampleLTBO: As shown in Figure 2.49, load height effects are included and torsional only bracing at mid-depth are included.

2.9.3 L-frame

For frame analysis, the proper formulation and implementation of the element for 3D rotations and moments must be verified. To demonstrate the correctness of the formulation pertaining to finite rotation effects and the proper linearization of these effects, the L-frame problem presented in this section is very useful. The model in Figure 2.51 is selected from Yang (1984). The same rectangular cross-section along the entire members is employed. Point load $P = 1N$ is applied to the free end and the other end is set up fixed boundaries. The material properties which are the Young's elastic modulus $E = 71{,}240\ N/mm^2$ and the Poisson's ratio $\nu = 0.3$ are employed. For the simulation, 10 elements are employed for SABRE2, Yang, and MASTAN2 (2013).

As shown in Table 2.16, the solution obtained from SABRE2 is close agreement with Yang (1984) and MASTAN2 (2013), which indicates that the element 3D rotations and moments are properly formulated and implemented.

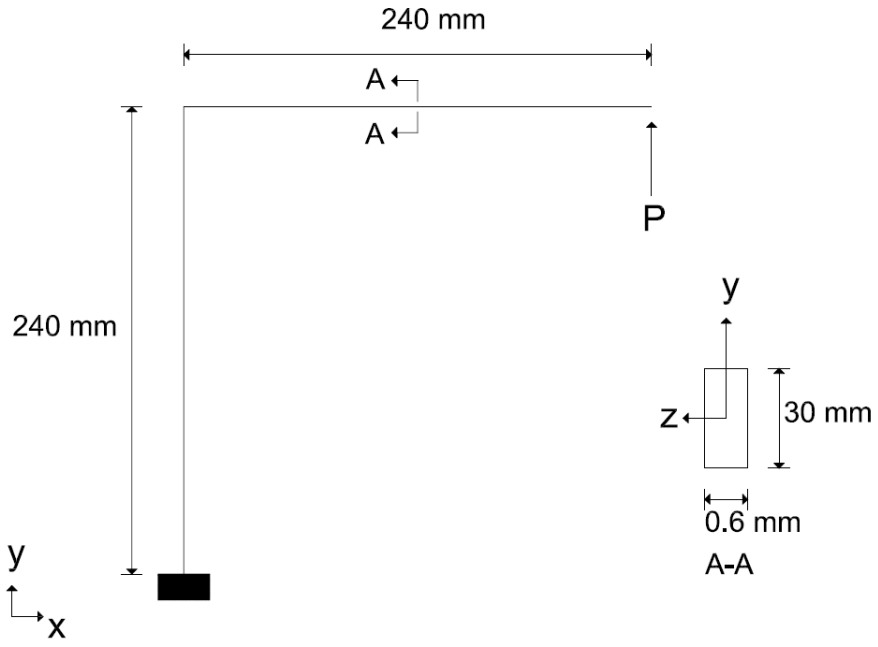

Figure 2.51 L-shaped frame subjected to a tip load.

Table 2.16 The critical buckling load for L-frame using different finite element analysis

	SABRE2	Yang (1984)	MASTAN2 (2013)
P_{cr} (N)	1.093	1.087	1.093

CHAPTER 3

AUTOMATIC OPTIMIZED MEMBER AND FRAME DESIGN

3.1 Background

The member design for a general nonprismatic geometry requires the selection of section sizes and their variation along the member length, including single or multiple web tapers in the cross-section, as well as the determination of brace point locations, which establishes the member unbraced lengths. Currently, the optimized design for these types of members typically is performed essentially by trial and error methods. Although some manufacturers and software providers have proprietary algorithms for achieving designs, the optimized design of frames composed of general nonprismatic members has been largely unexplored in academic research.

In the current research, the development of an automatic algorithmic means for optimization of nonprismatic member designs under general loadings based on minimum cost is studied. One of the areas of complexity of the problem is the relatively large number of variables such as the web-taper angle or angles, member section sizes (top and bottom flange width, top and bottom flange thickness, web depth, and web thickness), the location of braces, and the number of unbraced lengths. For the optimization, the current research investigates the application of Genetic Algorithms to this design optimization problem.

3.2 Literature Review

For automatic optimized steel design using Genetic Algorithms (GA), Chen (1997) developed and implemented a methodology for automated design of discrete structural systems using a Genetic Algorithm as an automated design tool. The AISC-ASD (AISC 1989) design code was employed to illustrate the design methodology considering sizing, shape and topology optimal designs of structural framed systems subjected to static and dynamic loads. Chen's investigation was limited to rolled wide flange section member designs using elastic analysis.

Erbatur, et al. (2000) presented the development of a computer-based systematic approach for discrete optimal design of planar and space frames. The main characteristic of the solution methodology was the use of a genetic algorithm (GA) as the optimizer. The paper was limited to the investigation doubly symmetric prismatic members.

Hayalioglu (2000) presented a genetic algorithm (GA) for the optimum design of geometrically non-linear elastic-plastic steel frames with discrete design variables. The design variables were selected from practically available sets of rolled steel sections. This investigation was also limited only to prismatic members.

Gil and Andreu (2001) presented a method for the identification of the optimum shape and cross-sections of a planar truss structures under stress and geometrical constraints. The methodology combined a full stress design optimization with a conjugate gradient optimization.

Gero, et al. (2005) showed the implementation of an elitist genetic algorithm that, when applied to steel structures, was able to obtain structural elements with minimum

weight and satisfy the safety factors or coefficients (ultimate limit states) of the applicable building code. However, these authors only considered the optimized design of prismatic members.

Gero, et al. (2006) developed an elitist genetic algorithm (GA) which was compared with common commercial solutions for complex structural optimization. The genetic algorithm was tuned and improved to obtain structural elements of minimum weight that satisfied the ultimate limit states of the applicable building code. Subsequently, the same spatial structures were optimized using a commercial structural analysis program. Finally, the cost and weight improvement obtained using the genetic algorithm was discussed. Gero, et al. (2006) limited their investigation to prismatic members.

Degertekin, et al. (2008) presented algorithms for the optimum design of geometrically nonlinear steel space frames using a tabu search and genetic algorithm. Their Tabu search utilized the features of short-term memory facility (tabu list) and aspiration criteria. Their genetic algorithm employed reproduction, crossover and mutation operators. The design algorithms focused only on minimum weight frames composed of suitable sections from a standard set of steel sections such as the ASTM wide-flange (W) shapes.

Although there is a large body of literature pertaining to the analysis and design of web-tapered I-section members, as reflected in the annotated literature review provided by AISC/MBMA Design Guide 25 (DG25) (Kaehler et al., 2011), automatic optimized design including the rigorous calculation of lateral torsional buckling loads for general

nonprismatic members has not been pursued to the knowledge of the author. The major contributions of the current research are:

1) Refinement of finite element analysis approaches for calculation of the buckling loads of general geometries under general loadings by handling load height, multiple brace and support locations, and 3D elastic buckling modes.
2) Proper application of the elastic buckling analysis capabilities to members with multiple bracing locations.
3) Recommendation of updates to DG25 procedures.
4) Combination of rigorous buckling solution capabilities with Genetic Algorithms to achieve optimized designs of a complex structural engineering problem based on cost.

3.3 Application of 3D FEA Capabilities to Handle Multiple Brace Locations (Design against Lateral Torsion Buckling)

Current practice for the design of braced column and beam members commonly involves design based on K = 1, i.e., based on the assumption of idealized torsionally and flexurally simply-supported end conditions. This approach neglects the effects of continuity across the brace point locations. The continuity effects can have either a positive or negative influence on the strength of a given unbraced segment. For the most critical unbraced lengths, the continuity effects generally tend to increase the strength. Eigenvalue buckling analysis can be employed to account for these continuity effects. However, for a member composed of a large number of unbraced lengths, eigenvalue buckling analysis can improperly penalize less critical unbraced lengths when applied to all the unbraced lengths in a single analysis of the entire member or overall structural system. This is because, for a given buckling analysis model and buckling limit state, the eigenvalue buckling analysis gives only one value for γ_e for the entire model. Unbraced lengths remote from the actual critical unbraced lengths, and which are participating little either positively or negatively in the actual buckling mode, are assigned a γ_e associated with the critical segment.

In the physical structure, the stability failure actually tends to localize in the most highly stressed unbraced length, with little participation from the non-adjacent unbraced lengths. In current practice, this behavior has been addressed typically by the use of subassembly models and using idealized assumptions about the boundary conditions at the interface between the subassemblies and the remainder of the structure. The most

commonly used and recognized example of this sort is the application of column effective length factor alignment charts.

Accurate assessment of the true interaction between the different unbraced lengths would require a comprehensive full nonlinear load-deflection analysis of the geometrically imperfect structure. The current research seeks to take advantage of the continuity effects captured from an accurate eigenvalue buckling analysis without improperly penalizing non-adjacent unbraced lengths. This is achieved by focusing on a model involving a given unbraced length under consideration along with each of its adjacent unbraced lengths. The idealized assumption of torsionally and flexurally simply-supported conditions is moved "one segment away" from the ends of a given unbraced length when it is under evaluation. The above approach leads to a more accurate approximation of the member stability effects than the current common practice of assuming torsionally and flexurally simply-supported conditions immediately at the ends of a given unbraced length.

Figure 3.1 shows a member having multiple unbraced lengths. The buckling strength multipliers γ_{e} and γ_{eLTB} need to be calculated for each of these lengths. These are labeled as γ_{e1} and γ_{eLTB1} to γ_{en} and γ_{eLTBn} in the figure, where n is the total number of unbraced lengths. For the unbraced lengths at the member ends, the buckling analysis is conducted using a subassembly containing the end unbraced length and the adjacent interior unbraced length. This is shown for the first unbraced length by Figure 3.1(b). For the interior unbraced lengths, the bucking analysis to determine the buckling strength multipliers includes the unbraced length under consideration and the adjacent unbraced

segments on each side of this length. This is shown for the second and third unbraced legths by Figures 3.1(c) and (d).

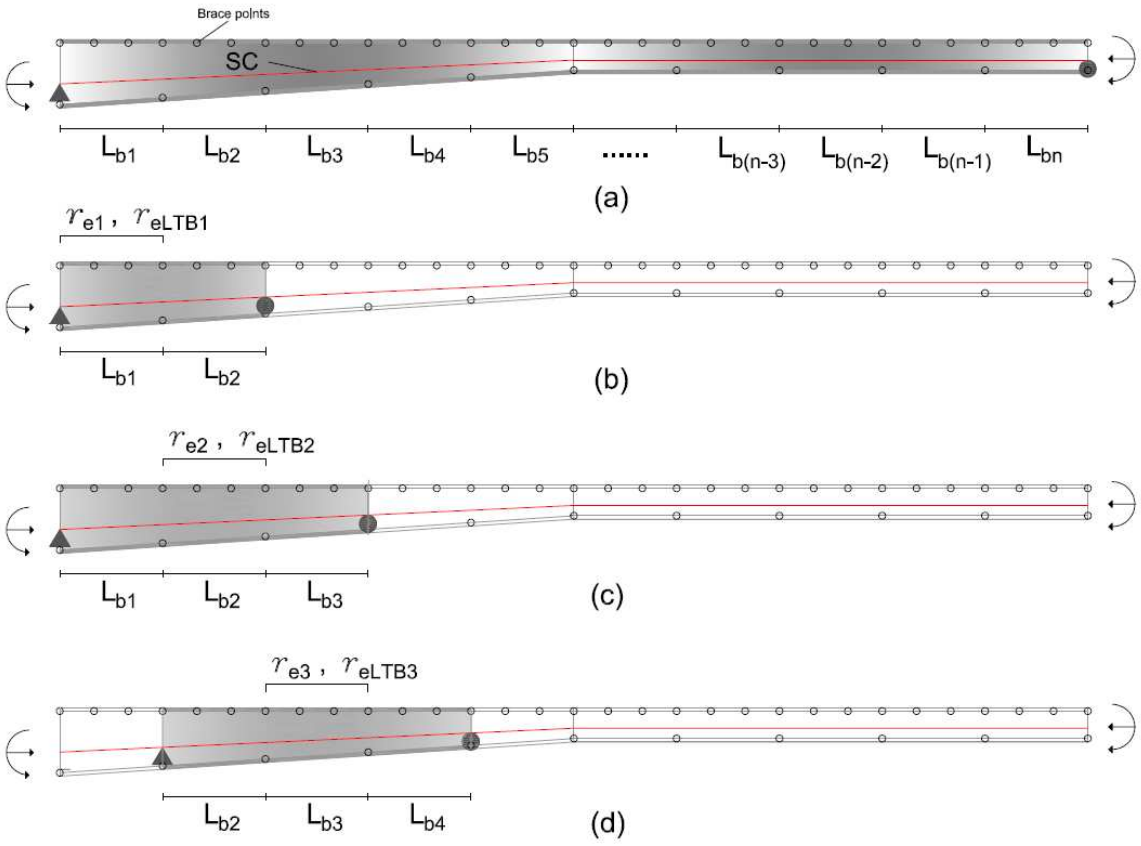

Figure 3.1 Concept of 3D FEA capabilities to handle multiple brace locations.

3.4 Overview of DG25 Approach

In the following section, the limits of applicability of DG25 are reviewed. Next, the DG25 provisions are studied and updated provisions pertaining to the application of a new unified effective area approach for determining the resistance of members in concentric axial compression are recommended that tie more explicitly to the direct calculation of γ_e values from calculation tools and account more accurately for slender element cross-section effects based on 2016 updates to the AISC Specification. Finally, corresponding examples are presented that compare to the solutions from the updated DG25 and from SABRE2 to the current DG25,.

3.4.1 Limits of Applicability of DG25

For an optimized design using Genetic Algorithms, the maximum and minimum values of genes such as the web-taper angle or angles, member section dimensions (top and bottom flange width, top and bottom flange thickness, web depth, and web thickness), the location of braces, and the number of unbraced lengths have to be decided. In this work, the search ranges for the genes are set based on the current DG25 limits:

1) Yield stress, $F_y \leq 55$ ksi
2) Homogeneous members only, i.e., all plates composed of steel must have the same yield strength.
3) Linear or piecewise linear web tapered members.
4) Web taper angle,α_{WT} : between zero and 15^0
5) Thickness of each flange is greater than or equal to the web thickness.

6) Flange slenderness ratio: $\frac{b_f}{2t_f} \leq 18$

7) Flange width $b_f \geq \frac{h}{7}$ throughout each unbraced length L_b,except that if $L_b \leq 1.1 r_t \sqrt{E/F_y}$,$b_f \geq \frac{h}{9}$

8) The web slenderness (without transverse stiffeners or with stiffeners at $a/h > 1.5$) must satisfy:

$$\frac{h}{t_w} \leq \frac{0.40E}{F_y} \leq 260$$

9) Web slenderness (with transverse stiffeners at $a/h \leq 1.5$) must satisfy:

$$\frac{h}{t_w} \leq 12\sqrt{\frac{E}{F_y}}$$

where:

- α_{WT} : Web taper angle.
- b_f : Flange width, in.
- t_f : Flange thickness, in.
- t_w : Web thickness, in.
- h : Web depth, in.
- E : modulus of elasticity, ksi.
- F_y : Yield stress, ksi.
- r_t : Radius of gyration of the flange in flexural compression plus one third of the web area in compression due to the application of major axis bending moment alone, calculated using the largest section depth within the length under consideration, in.

3.4.2 Recommended Updates to the DG25 Provisions for Axial Compression

In this section, updates to DG25 are recommended that implement the new AISC (2016) provisions as well as accommodate rigorous calculation of γ_e values to improve the determination of member axial compressive resistances. For members with multiple unbraced lengths, the elastic buckling multiplier γ_e can be calculated rigorously by eigenvalue buckling analysis using the concept of Section 3.3. In each unbraced length, the most critical buckling limit state (out-of-plane flexural buckling, torsional buckling, flexural-torsional buckling, or constrained-axis torsional buckling) is captured by the smallest elastic buckling multiplier using finite element analysis. The updates to DG25 procedures are :

Step 1) Calculate γ_e considering all the potential buckling limit states. The governing γ_e is the smallest eigenvalue from the general eigenvalue buckling calculations conducted from a model of each unbraced length and its adjacent unbraced lengths, as discussed in Section 3.3.

Step 2) Calculate f_r and $F_e = \gamma_e f_r$ at the potentially critical cross-sections. The critical cross-section is generally either the one that has the largest $f_r / F_y(A_e/A_g)$ or the smallest A_e/A_g. The variables f_r and F_e vary due to changes in the internal axial force P_r as well as changes in the gross area A_g along the member length. The locations that need to be checked generally include positions:

- At the ends of the length under consideration.
- At the smaller cross-section at a plate transition.

- At a step in the axial load.
- At a location where $h/t_w = 131$ (this is the web slenderness at which the flange local buckling coefficient k_c first reaches its minimum specified value)

Step 3) Calculate F_{cr} at the potentially critical cross-sections:

- When $\frac{F_y}{F_e} \leq 2.25$

$$F_{cr} = \left[0.658^{\frac{F_y}{F_e}}\right] F_y \qquad (\text{AISC 2016 Prov. E7} - 2)$$

- When $\frac{F_y}{F_e} > 2.25$

$$F_{cr} = 0.877 F_e \qquad (\text{AISC 2016 Prov. E7} - 3)$$

Step 4) Calculate the effective width b_e for each of the cross-section elements and the corresponding effective area A_e of potentially critical cross-sections.

When $\lambda \leq \lambda_r \sqrt{\frac{F_y}{F_{cr}}}$

$$b_e = b \qquad (\text{AISC 2016 Prov. E7} - 2)$$

When $\lambda > \lambda_r \sqrt{\frac{F_y}{F_{cr}}}$

$$b_e = b \left[1 - c_1 \sqrt{\frac{F_{el}}{F_{cr}}}\right] \sqrt{\frac{F_{el}}{F_{cr}}} \qquad (\text{AISC 2016 Prov. E7} - 3)$$

where:

$$F_{el} = \left(c_2 \frac{\lambda_r}{\lambda}\right)^2 F_y \qquad (\text{AISC 2016 Prov. E7} - 4)$$

where:

- b = Width of the element (for flanges this is b_f, for web this is d_w), in.
- c_1 = Effective width imperfection adjustment factor determined from the AISC (2016) Table E7-1 which is shown as Table 3.1.
- $c_2 = \frac{\left(1-\sqrt{1-4c_1}\right)}{2c_1}$
- λ = Width-to-thickness ratio for the elements as determined in AISC (2010) Table B4.1a.
- λ_r = limiting width-to-thickness ratio as determined in AISC (2010) Table B4.1a.
- F_{el} = Elastic local buckling stress, ksi.

Table 3.1 AISC (2016) Table E7-1

Case	Slender Element	c_1	c_2
(a)	Stiffened elements except flanges of square and rectangular sections of uniform thickness	0.18	1.31
(b)	Flanges of square and rectangular sections of uniform thickness	0.20	1.38
(c)	All other elements	0.22	1.49

$$A_e = b_{eft}t_{ft} + b_{ew}t_w + b_{efb}t_{fb} \qquad (Eq3.1)$$

where:

- A_e : Summation of the effective areas of the cross-section based on reduced effective widths, b_e.

Step 5) Calculate the nominal compressive strength P_n and the strength ratio $\frac{P_u}{\emptyset P_n}$ at each of the potentially critical cross-sections. The largest value of $\frac{P_u}{\emptyset P_n}$ is the governing value.

where:

- $P_n = F_{cr}A_e$ (AISC 2016 Prov. E7 − 1)

3.4.3 Flexure

The nominal flexural strength, M_n, shall be the lower value obtained according to the applicable limit states. In DG25, tapered beams are subject to the same limit states as prismatic members, that is, the strength is the lowest of that determined for any of the following applicable limit states:

a. Compression flange yielding will be included in Lateral-torsional buckling
b. Lateral-torsional buckling (LTB)
c. Compression flange local buckling (FLB)
d. Tension flange yielding (TFY)

Tension flange rupture is not considered in this research. For the flexure limit state, if sufficient lateral and/or torsional bracing is not provided, the limit states result in out-of-plane (lateral) bending displacement and twisting of a cross-section. This strength limit state is called Lateral Torsional Buckling (LTB), which can be assessed more rigorously by computational tools such as SABRE2.

3.4.3.1 Web plastification factor in compression, R_{pc}

R_{pc} is the effective cross-section plastic shape factor, limited by compression, for cross sections with compact or noncompact webs. This term is used to adjust the flexural strength to account for the favorable effect of web plastification in cross sections with nonslender web elements. The value of R_{pc} ranges from 1.0 for sections with slender webs to $\frac{M_p}{M_{yc}}$ for compact shapes. Using the section properties at the cross section under consideration, calculate R_{pc} as :

For $\lambda_w \leq \lambda_{pw}$,

$$R_{pc} = \frac{M_p}{M_{yc}} \qquad (\text{DG25 } 5.4-4)$$

For $\lambda_{rw} > \lambda_w > \lambda_{pw}$,

$$R_{pc} = \left[\frac{M_p}{M_{yc}} - \left(\frac{M_p}{M_{yc}} - 1\right)\left(\frac{\lambda_w - \lambda_{pw}}{\lambda_{rw} - \lambda_{pw}}\right)\right] \leq \frac{M_p}{M_{yc}} \qquad (\text{DG25 } 5.4-5)$$

For $\lambda_w \geq \lambda_{rw}$, or $\frac{I_{yc}}{I_y} \leq 0.23$

$$R_{pc} = 1.0 \leq \frac{M_p}{M_{yc}}$$

where:

- $M_p = F_y Z_x \leq 1.6 F_y S_{xc}$: Plastic moment, kip · in.
- $M_{yc} = F_y S_{xc}$: Yielding moment in compression, kip · in.
- S_{xc} = The gross section modulus to the extreme fiber of the compression flange.

- $\lambda_w = \frac{h_c}{t_w}$: Width to thickness ratio of web.
- $\lambda_{pw} = 3.76\sqrt{\frac{E}{F_y}}$ For doubly symmetric sections from 2010 Spec. Table B4.1.
- $\lambda_{pw} = \frac{\frac{h_c}{h_p}\sqrt{\frac{E}{F_y}}}{\left(0.54\frac{M_p}{M_{ymin}} - 0.09\right)^2} \leq \lambda_{rw}$ For singly symmetric sections from 2010 Spec. Table B4.1.
- $\lambda_{rw} = 5.70\sqrt{\frac{E}{F_y}}$ For a noncompact web from 2010 Spec. Table B4.1.
- h_c : Twice the distance from the cross-section centroid toe the inside face of the compression flange, in.
- h_p : Twice the distance from the plastic neutral axis to the inside face of the compression flange, in.

3.4.3.2 Web bend buckling factor, R_{pg}

R_{pg} is the bending strength reduction factor for cross sections with slender webs. This term reduces the nominal flexural strength to account for the weakening effect of web bend buckling and subsequent post-buckling behavior involving load shedding, to the flanges. This strength reduction is the result of local buckling of the web in the compression region. The value of R_{pg} is 1.0 for sections with compact or noncompact webs and less than 1.0 for sections with slender webs. Using the section properties at the cross section under consideration,

For $\lambda_w \leq \lambda_{rw}$,

$$R_{pg} = 1.0$$

For $\lambda_w > \lambda_{rw}$,

$$R_{pg} = 1.0 - \frac{a_w}{1{,}200 + 300a_w}\left(\lambda_w - 5.70\sqrt{\frac{E}{F_y}}\right) \leq 1.0 \quad (\text{DG25 } 5.4-6)$$

where:

- $a_w = \frac{h_c t_w}{b_{fc} t_{fc}} \leq 10.0$

3.4.3.3 Lateral-torsional buckling (LTB)

The provisions for lateral-torsional buckling are modified versions of the AISC (2010) provisions to account for the influence of nonprismatic member geometry. In this work, the LTB strength is checked in a manner similar to the handling of axial compression buckling in Section 3.3. This procedure takes into account both the LTB behavior and the behavior represented by the web bend buckling and plastification factors, R_{pc} and R_{pg}.

The lateral-torsional buckling limit state is checked for each unbraced length. The nominal lateral-torsional buckling strength, M_{nLTB}, is calculated as follows:

Step 1) Calculate the elastic lateral-torsional buckling multiplier, γ_{eLTB}, using finite element analysis for each unbraced length. The adjacent unbraced lengths are included in these buckling analysis models in the same manner as discussed in Section 3.3.

Step 2) At sampling locations along the unbraced length, determine the nominal flexural strength, M_{nLTB}, as a function of the ratio $\frac{\gamma_{eLTB} f_r}{F_y}$, where the compression flange flexural stress f_r typically is considered a several locations, as discussed in DG25 (the location associated with the largest value of f_r usually governs):

a. If $\frac{\gamma_{eLTB} f_r}{F_y} \geq \frac{\pi^2}{1.1^2} = 8.2$, the lateral-torsional buckling limit state does not apply.

b. If $8.2 > \frac{\gamma_{eLTB} f_r}{F_y} > \frac{F_L}{F_y}$, calculate the inelastic nominal lateral-torsional buckling strength

$$M_{nLTB} = R_{pc} R_{pg} M_{yc} \left[1 - \left(1 - \frac{F_L}{R_{pc} F_y} \right) \left(\frac{\pi \sqrt{\frac{F_y}{\gamma_{eLTB} f_r}} - 1.1}{\pi \sqrt{\frac{F_y}{F_L}} - 1.1} \right) \right]$$

$$\leq R_{pc} R_{pg} M_{yc} \qquad \text{(DG25 Eq. } 5.4-16\text{)}$$

c. If $\frac{\gamma_{eLTB} f_r}{F_y} \leq \frac{F_L}{F_y}$, calculate the elastic lateral-torsional buckling nominal

For members with slender webs

$$M_{nLTB} = R_{pg} \gamma_{eLTB} f_r S_{xc} \qquad \text{(DG25 Eq. } 5.4-17\text{)}$$

For other members,

$$M_{nLTB} = \gamma_{eLTB} f_r S_{xc} \qquad (DG25\ Eq.\ 5.4-18)$$

Step 3) Calculate the nominal flexural strength M_n and the strength ratio $\frac{M_u}{\emptyset M_n}$ corresponding to each of the sampling locations along the unbraced length. The largest value of $\frac{M_u}{\emptyset M_n}$ is the governing value.

3.4.4 Combined Flexure and Axial Force for Doubly and Singly-Symmetric Members

Force-based combined strength check of the doubly and singly symmetric members is given by:

If $\frac{P_r}{P_c} \geq 0.2$,

$$\frac{P_r}{P_c} + \frac{8}{9}\left(\frac{M_{rx}}{M_{cx}} + \frac{M_{ry}}{M_{cy}}\right) \leq 1.0 \qquad (DG25\ 5.5-1a)$$

If $\frac{P_r}{P_c} < 0.2$,

$$\frac{P_r}{2P_c} + \left(\frac{M_{rx}}{M_{cx}} + \frac{M_{ry}}{M_{cy}}\right) \leq 1.0 \qquad (DG25\ 5.5-1b)$$

where:

- P_r : Required axial strength,kips.
- P_c : Available axial strength,kips; $= \emptyset_c P_n$ for LRFD.

- M_{rx} : Required flexural strength about x-axis, kip · in.
- M_{ry} : Required flexural strength about y-axis, kip · in.
- M_{cx} : Available flexural strength about x-axis, kip · in, $= \emptyset_b M_{nx}$ for LRFD.
- M_{cy} : Available flexural strength about y-axis, kip · in, $= \emptyset_b M_{ny}$ for LRFD.
- $\emptyset_c$: Resistance factor for compression; =0.9.
- $\emptyset_b$: Resistance factor for flexure; =0.9.

3.4.5 DG25 Examples for Tapered Member Design

In this section, the solutions using the recommended updated DG25 procedures, which involve the new unified effective approach for determining the column axial compressive resistance and the buckling γ_e values determined from SABRE2, are compared to the current DG25 solutions.

3.4.5.1 Doubly-symmetric tapered member subjected to axial compression

In this section, the compressive strength of the member shown in Figure 3.2 is evaluated using the updated DG25 provisions, the use of SABRE2, and the recommended handling of multiple unbraced lengths. The linearly web tapered member is subjected to applied compressive load $P = 11.3$ kips. In Table 3.2, the member section properties are listed at the potential critical locations.

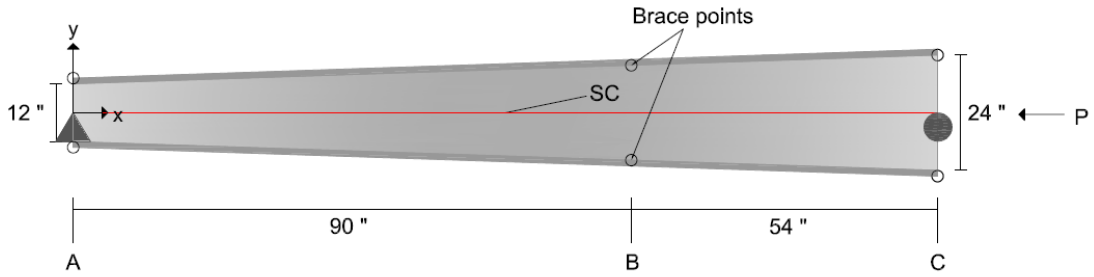

Figure 3.2 Simply-supported linearly web tapered I beam under compression.

For the eigenvalue buckling analysis using SABRE2, 8 elements are employed. The required material and geometric properties are :

- Material Properties:

- $F_y = 55$ ksi

- Geometric Properties:

- Doubly symmetric member:

- Member and segment length are given by:

  i. $L_{AB} = L_{byAB} = L_{bzAB} = 90$ in : Segment AB

  ii. $L_{BC} = L_{byBC} = L_{bzBC} = 54$ in : Segment BC

  iii. $L = L_{bx} = L_{AB} + L_{BC} = 144$ in : Entire member

Table 3.2 Employed section properties for doubly-symmetric tapered member subjected to axial compression

	Location A	CR Location	Location B	Location C
b_{fb} or b_{ft}	6.000in	6.000in	6.000in	6.000in
t_{fb} or t_{ft}	0.250in	0.250in	0.250in	0.250in
t_w	0.125in	0.125in	0.125in	0.125in
h	12.00in	16.33in	19.50in	24.00in
I_x	130.6 in^4	251.4 in^4	369.8 in^4	585.1 in^4
I_y	9.000 in^4	9.000 in^4	9.000 in^4	9.000 in^4
A_g	4.500in^2	5.040in^2	5.440in^2	6.000in^2

where:

- b_{fb} = Bottom flange width.
- b_{ft} =Top flange width.
- t_{fb} = Bottom flange thickness.
- t_{ft} =Tension flange width.

The updated DG25 procedures are then:

Step 1) The calculated elastic buckling multiplier γ_e using SABRE2 is given by

$$\gamma_e = 39.71$$

Step2) f_r and $F_e = \gamma_e f_r$ at all the potentially critical cross-sections are shown in Table 3.3.

Table 3.3 Stresses at all the potentially critical cross-sections for doubly-symmetric tapered member subjected to axial compression

	Location A	CR Location	Location B	Location C
f_r	2.511	2.242	2.078	1.883
$F_e = \gamma_e f_r$	99.71	89.01	82.52	74.78
$\frac{F_y}{\gamma_e f_r}$	0.552	0.618	0.667	0.735

Step 3) F_{cr} at all the potentially critical cross-sections are calculated based on Table 3.3 and are shown in Table 3.4.

Table 3.4 Critical stresses at all the potentially critical cross-sections for doubly-symmetric tapered member subjected to axial compression

	Location A	CR Location	Location B	Location C
F_{cr}	43.65 ksi	42.46 ksi	41.60 ksi	40.42 ksi

Step 4) The effective width b_e for each of the cross-section elements and the corresponding effective area A_e at each of the potentially critical cross-sections using Table 3.4 are shown in Table 3.5 through 3.7, where:

- b_{ef} : The reduced effective flange width, and
- b_{ew} : The reduced effective web depth.

Table 3.5 Reduced effective flange widths for doubly-symmetric tapered member subjected to axial compression

	Location A	CR Location	Location B	Location C
$\lambda_{rf}\sqrt{\frac{F_y}{F_{cr}}}$	10.54	9.900	10.00	10.14
b_{ef}	5.580 in	5.369 in	5.403 in	5.452 in

Table 3.6 The reduced effective web depth for doubly-symmetric tapered member subjected to axial compression

	Location A	CR Location	Location B	Location C
$\lambda_{rw}\sqrt{\frac{F_y}{F_{cr}}}$	38.40	38.94	39.34	39.91
b_{ew}	5.687 in	5.920 in	6.050 in	6.206 in

Table 3.7 The reduced effective area for doubly-symmetric tapered member subjected to axial compression

	Location A	CR Location	Location B	Location C
A_e	$3.502\ in^2$	$3.424\ in^2$	$3.458\ in^2$	$3.502\ in^2$

Step 5) The nominal compressive strength P_n and the strength ratio $\frac{P_u}{\emptyset P_n}$ at each of the potentially critical cross-sections using Table 3.7 are shown in Table 3.8.

Table 3.8 The strength ratio for entire member for doubly-symmetric tapered member subjected to axial compression

	Location A	CR Location	Location B	Location C
$\phi_c P_{nM} = \phi_c F_{cr} A_e$	137.6 kips	130.8 kips	129.5 kips	127.4kips
$\frac{P_r}{\phi_c P_{nM}}$	0.082	0.086	0.087	**0.089**

3.4.5.2 Doubly-symmetric tapered member subjected to flexure

In this section, the flexural strength of the member shown in Figure 3.3 is evaluated using the DG25 Provisions with the calculation of γ_{eLTB} from SABRE2. Linearly web tapered member is subjected to applied moment $M = -1800\ \text{kip} \cdot \text{in}$. Flexural strength design is investigated using Table 3.9 through 3.14.

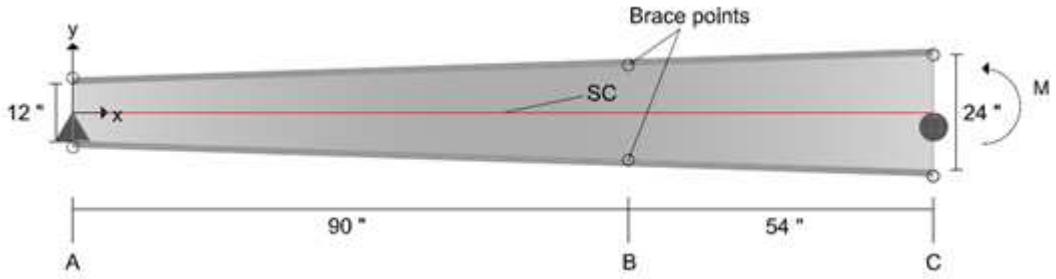

Figure 3.3 Simply-supported linearly web tapered I beam under flexure.

For the analysis, eight elements are employed and the required material and geometric properties are :

- Material Properties

- $F_y = 55$ ksi

- $F_u = 70$ ksi

- Geometric Properties

- Doubly symmetric member is subject to:

- Member and segment length are given by:

i. $L_{AB} = L_{byAB} = L_{bzAB} = 90$ in : Segment AB

ii. $L_{BC} = L_{byBC} = L_{bzBC} = 54$ in : Segment BC

iii. $L = L_{bx} = L_{AB} + L_{BC} = 144$ in : Entire Member

Table 3.9 Employed section properties for doubly-symmetric tapered member subjected to flexure (continued)

	Location A	Mid-span of segment AB	Location B	Mid-span of segment BC	Location C
b_{fc} or b_{ft}	6.000in	6.000in	6.000in	6.000in	6.000in
t_{fc} or t_{ft}	0.250in	0.250in	0.250in	0.250in	0.250in
t_w	0.125in	0.125in	0.125in	0.125in	0.125in
h	12.00in	15.75in	19.50in	21.75in	24.00in
d	12.50in	16.25in	20.00in	22.25in	24.50in
h_o	12.25in	16.00in	19.75in	22.00in	24.25in
A_g	4.500in^2	4.970in^2	5.440in^2	5.720in^2	6.000in^2
y_{bar}	6.250in	8.130in	10.00in	11.13in	12.25in
I_x	130.6 in^4	232.7 in^4	369.8 in^4	470.2 in^4	585.1 in^4
S_{xc}	20.89 in^3	28.64 in^3	36.98 in^3	42.26 in^3	47.76 in^3
S_{xt}	20.89 in^3	28.64 in^3	36.98 in^3	42.26 in^3	47.76 in^3

Table 3.9 Employed section properties for doubly-symmetric tapered member subjected to flexure

I_{yc}	$4.500in^4$	$4.500in^4$	$4.500in^4$	$4.500in^4$	$4.500in^4$
I_{yt}	$4.500in^4$	$4.500in^4$	$4.500in^4$	$4.500in^4$	$4.500in^4$
I_y	$9.000in^4$	$9.000in^4$	$9.000in^4$	$9.000in^4$	$9.000in^4$
h_{cp}	6.000in	7.880in	9.750in	10.88in	12.00in
Z_x	$22.88\ in^3$	$31.75\ in^3$	$41.51\ in^3$	$47.78\ in^3$	$54.38\ in^3$
h_c	12.00in	15.75in	19.50in	21.75in	24.00in
h_p	12.00in	15.75in	19.50in	21.75in	24.00in

Table 3.10 Strengths and stresses for doubly-symmetric tapered member subjected to flexure

	Location A	Mid-span of segment AB	Location B	Mid-span of segment BC	Location C
M_r	$0.000kip \cdot in$	$562.5kip \cdot in$	$1125kip \cdot in$	$1462.5kip \cdot in$	$1800kip \cdot in$
f_r	0.000 ksi	19.64 ksi	30.42 ksi	34.60 ksi	37.69 ksi
M_y	$1149kip \cdot in$	$1575kip \cdot in$	$2034kip \cdot in$	$2325kip \cdot in$	$2627kip \cdot in$
M_p	$1258kip \cdot in$	$1746kip \cdot in$	$2283kip \cdot in$	$2628kip \cdot in$	$2991kip \cdot in$

Table 3.11 Flange limiting width to thickness ratios for doubly-symmetric tapered member subjected to flexure

	Location A	Mid-span of segment AB	Location B	Mid-span of segment BC	Location C
λ_f	12.00	12.00	12.00	12.00	12.00
k_c	0.410	0.360	0.350	0.350	0.350
F_L	38.50 ksi	38.50 ksi	38.50 ksi	38.50 ksi	38.50 ksi
λ_{rf}	16.66	15.56	15.43	15.43	15.43
λ_{pf}	8.730	8.730	8.730	8.730	8.730
Flange	Noncompact	Noncompact	Noncompact	Noncompact	Noncompact

Table 3.12 Web limiting width to thickness ratios for doubly-symmetric tapered member subjected to flexure

	Location A	Mid-span of segment AB	Location B	Mid-span of segment BC	Location C
λ_w	96.00	126.0	156.0	174.0	192.0
λ_{rw}	131.0	131.0	131.0	131.0	131.0
λ_{pw}	86.34	86.34	86.34	86.34	86.34
Web	Noncompact	Noncompact	Slender	Slender	Slender

Table 3.13 Web plastification factor in compression, R_{pc} for doubly-symmetric tapered member subjected to flexure

	Location A	Mid-span of segment AB	Location B	Mid-span of segment BC	Location C
R_{pc}	1.074	1.012	1.000	1.000	1.000

Table 3.14 Web bend buckling factor, R_{pg} for doubly-symmetric tapered member subjected to flexure

	Location A	Mid-span of segment AB	Location B	Mid-span of segment BC	Location C
a_w	1.000	1.313	1.625	1.813	2.000
R_{pg}	1.000	1.000	0.976	0.955	0.932

For flexural design, the general procedure in DG25 is employed:

Step 1) The elastic lateral-torsional buckling multiplier, γ_{eLTB}, using SABRE2, and using the recommended multiple unbraced length approach discussed in Section 3.3 is :

$$\gamma_{eLTB} = 5.687$$

Step 2) At the different sampling locations along the entire length, the nominal lateral torsional flexural strength, M_{nLTB}, is shown in Table 3.15.

Table 3.15 The nominal lateral torsional flexural strength for doubly-symmetric tapered member subjected to flexure

	Location A	Mid-span of segment AB	Location B	Mid-span of segment BC	Location C
$\frac{\gamma_{eLTB} f_r}{F_y}$	0.000	2.030	3.150	3.580	3.900
$\frac{F_L}{F_y}$	0.700	0.700	0.700	0.700	0.700
$M_{n\,LTBAB}$	$0 kip \cdot in$	$1390 kip \cdot in$	$1834 kip \cdot in$	$2080 kip \cdot in$	$2313 kip \cdot in$

Step 3) The nominal flexural strength M_n and the strength ratio $\frac{M_u}{\emptyset M_n}$ for lateral torsional buckling and flange local buckling are shown in Table 3.16 and Table 3.17. The largest value of $\frac{M_u}{\emptyset M_n}$ is the governing value.

Table 3.16 The strength ratio for lateral torsional buckling for doubly-symmetric tapered member subjected to flexure

	Location A	Mid-span of segment AB	Location B	Mid-span of segment BC	Location C
$M_{n\ LTBAB}$	0kip · in	1390kip · in	1834kip · in	2080kip · in	2313kip · in
$\frac{M_r}{\phi_b M_{n\ LTBAB}}$	0	0.450	0.682	0.781	**0.845**

Table 3.17 The strength ratio for compression flange local buckling for doubly-symmetric tapered member subjected to flexure

	Location A	Mid-span of segment AB	Location B	Mid-span of segment BC	Location C
$M_{n\ FLB}$	1057kip · in	1359kip · in	1694kip · in	1895kip · in	2090kip · in
$\frac{M_r}{\phi_b M_{n\ FLB}}$	0	0.460	0.738	0.858	**0.957**

From Table 3.16 and 3.17, flexural strength for doubly-symmetric web-tapered member in Figure 3.3 is governed by the compression flange local buckling at Location C.

3.4.5.3 Combined axial compression and flexure for doubly symmetric tapered member

Combined axial compression and flexure for doubly symmetric tapered member is investigated. Results based on the recommended updates to DG25 are compared to the current DG25 results.

Recommended updates to DG25

From Table 3.8, the governing axial compression strength ratios are 0.0870 at Location B for segment AB and 0.089 at Location C for segment BC. The compression flange local buckling governs the flexure. The governing flexural strength ratios are 0.738 at Location B (FLB) for segment AB and 0.957 at Location C (FLB) for segment BC. From the governing strength ratio, the combined strength ratios of flexure and axial compression for each unbraced length are :

a) Segment AB

Since $\frac{P_r}{P_c} < 0.2$

$$\frac{P_r}{2P_c} + \left(\frac{M_{rx}}{M_{cx}} + \frac{M_{ry}}{M_{cy}}\right) = \frac{0.087}{2} + (0.738 + 0) = 0.781 \leq 1.0$$

b) Segment BC

Since $\frac{P_r}{P_c} < 0.2$

$$\frac{P_r}{2P_c} + \left(\frac{M_{rx}}{M_{cx}} + \frac{M_{ry}}{M_{cy}}\right) = \frac{0.089}{2} + (0.957 + 0) = 1.00 \leq 1.0$$

Current DG25 Results

DG25 assumes torsionally simply supported boundary condition to calculate the equivalent elastic critical buckling in each unbraced length. As shown in Figure 3.2 and 3.3, two unbraced length are assumed, which result in investigating combined unity check in each unbraced using different elastic critical buckling loads.

a) Segment AB

As shown in Table 3.18, the governing axial compression strength ratio using DG 25 is 0.0901 at CR Location.

Table 3.18 The strength ratio of axial compression for segment AB using DG25

	Location A	CR Location	Location B
$\frac{P_r}{\phi_c P_{nL}}$	0.0723	0.0749	0.0742
$\frac{P_r}{\phi_c P_{nAB}}$	0.0879	**0.0901**	0.0879

where:

- P_{nL}= The nominal strength of axial compression for entire member
- P_{nAB}= The nominal strength of axial compression for segment AB

From Table 3.19, flexural strength for doubly-symmetric web-tapered segment AB using DG25 is governed by the compression flange local buckling at Location B.

Table 3.19 The strength ratio of flexure for segment AB using DG25

	Location A	Mid-span of segment AB	Location B
$\frac{M_r}{\phi_b M_{n\ LTBAB}}$	0	0.392	0.630
$\frac{M_r}{\phi_b M_{n\ FLB}}$	0	0.460	**0.738**

where:

- $M_{n\ LTBAB}$= The nominal lateral torsional buckling strength for segment AB
- $M_{n\ FLB}$= The nominal compression flange local buckling strength

Combined axial compression and flexural strength ratio is:

Since $\frac{P_r}{P_c} < 0.2$

$$\frac{P_r}{2P_c} + \left(\frac{M_{rx}}{M_{cx}} + \frac{M_{ry}}{M_{cy}}\right) = \frac{0.0901}{2} + (0.738 + \mathbf{0}) = 0.783 \leq 1.0$$

b) Segment BC

As shown in Table 3.20, the governing axial compression strength ratio using DG 25 is 0.0796 at Location B.

Table 3.20 The strength ratio of axial compression for segment BC using DG25

	Location B	Location C
$\frac{P_r}{\phi_c P_{nL}}$	0.0742	0.0734
$\frac{P_r}{\phi_c P_{nBC}}$	**0.0796**	0.0788

where:

- P_{nBC}= The nominal strength of axial compression for segment BC

From Table 3.21, the flexural strength for the doubly-symmetric web-tapered segment BC using DG25 is governed by the compression flange local buckling at Location C.

Table 3.21 The strength ratio of flexure for segment BC using DG25

	Location B	Mid-span of segment BC	Location C
$\frac{M_r}{\phi_b M_{n\ LTBBC}}$	0.630	0.732	0.817
$\frac{M_r}{\phi_b M_{n\ FLB}}$	0.738	0.858	**0.957**

where:

- $M_{n\ LTBBC}$= The nominal lateral torsional buckling strength for segment BC

The combined axial compression and flexural strength ratio is:

Since $\frac{P_r}{P_c} < 0.2$

$$\frac{P_r}{2P_c} + \left(\frac{M_{rx}}{M_{cx}} + \frac{M_{ry}}{M_{cy}}\right) = \frac{0.0796}{2} + (0.957 + \mathbf{0}) = 0.997 \leq 1.0$$

The updated DG25 provisions employ one elastic buckling strength for the entire member in this example (since the member has only two unbraced lengths), while DG25 employs a separately calculated elastic buckling strength for each unbraced length. However, since the doubly-symmetric tapered member in Figure 3.4 is governed by the compression flange local buckling in both DG25 and updated DG25, the flexural strength of updated DG25 provisions is the same as that of DG25. The updated DG25 provisions employ one elastic buckling strength for entire member using the recommended multiple unbraced length approach. DG25 employs two elastic buckling strengths for entire member, which results in the different axial compression strength between updated DG25 and the current DG25.

3.4.5.4 Singly-symmetric tapered member subjected to axial compression

The compressive strength of the member shown in Figure 3.4 is evaluated using updated DG25 Provisions, including the calculation of γ_e from SABRE2. The linearly web tapered member is subjected to applied load $P = 11.3$ kips. In Table 3.22, section properties are calculated at possible critical location.

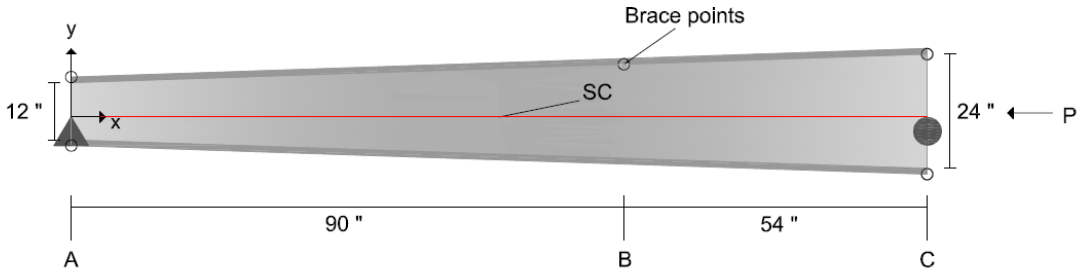

Figure 3.4 Simply-supported singly-symmetric web tapered I beam under compression.

For the analysis, eight elements are employed and the required material and geometric properties are :

- Material Properties:

- $F_y = 55$ ksi

- Geometric Properties:

- Member and segment length are given by:

  i. $L_{AB} = L_{byAB} = 90$ in : Segment AB

  ii. $L_{BC} = L_{byBC} = 54$ in : Segment BC

  iii. $L = L_{bx} = L_{bz} = L_{AB} + L_{BC} = 144$ in : Entire Member

Table 3.22 Employed section properties for the singly-symmetric web tapered I beam under compression

	Location A	CR Location	Location B	Location C
b_{fb} or b_{ft}	6.000in	6.000in	6.000in	6.000in
t_{fb}	0.219in	0.219in	0.219in	0.219in
t_{ft}	0.313in	0.313in	0.313in	0.313in
t_w	0.125in	0.125in	0.125in	0.125in
h	12.00in	16.33in	19.50in	24.00in
y_{bar}	6.970in	9.290in	10.97in	13.33in
A_g	$4.690in^2$	$5.230in^2$	$5.630in^2$	$6.190in^2$
I_x	135.4 in^4	260.7 in^4	383.2 in^4	605.9 in^4

where,

- y_{bar} : Distance from compression (top) flange to centroid

The updated DG25 procedures are then:

Step 1) The calculated elastic buckling multiplier γ_e using SABRE2 including bracing point at top of the flange is given by

$$\gamma_e = 13.58$$

Step2) f_r and $F_e = \gamma_e f_r$ at all the potentially critical cross-sections are shown in Table 3.23.

Table 3.23 Stresses at all the potentially critical cross-sections for the singly-symmetric web tapered I beam under compression

	Location A	CR Location	Location B	Location C
f_r	2.511	2.242	2.078	1.883
$F_e = \gamma_e f_r$	34.11	30.45	28.23	25.58
$\frac{F_y}{\gamma_e f_r}$	1.612	1.806	1.948	2.149

Step 3) F_{cr} at all the potentially critical cross-sections are calculated based on Table 3.23 and are shown in Table 3.24.

Table 3.24 Critical stresses at all the potentially critical cross-sections for the singly-symmetric web tapered I beam under compression

	Location A	CR Location	Location B	Location C
F_{cr}	28.00 ksi	25.82 ksi	24.33 ksi	22.36 ksi

Step 4) The effective width b_e for each of the cross-section elements and the corresponding effective area A_e at each of the potentially critical cross-sections using Table 3.24 are shown in Table 3.25 through 3.27.

Table 3.25 The reduced effective flange width for the singly-symmetric web tapered I beam under compression

	Location A	CR Location	Location B	Location C
$\lambda_{rf}\sqrt{\frac{F_y}{F_{cr}}}$	13.16	12.68	13.07	13.63
b_{eft}	6.000 in	6.000 in	6.000 in	6.000 in
b_{efb}	6.000 in	6.000 in	6.000 in	6.000 in

where,

- b_{eft} : The reduced effective top flange width for entire member
- b_{efb} : The reduced effective bottom flange width for entire member

Table 3.26 The reduced effective web depth for the singly-symmetric web tapered I beam under compression

	Location A	CR Location	Location B	Location C
$\lambda_{rw}\sqrt{\frac{F_y}{F_{cr}}}$	47.95	49.92	51.43	53.65
b_{ew}	6.916 in	7.428 in	7.757 in	8.195 in

Table 3.27 The reduced effective area for the singly-symmetric web tapered I beam under compression

	Location A	CR Location	Location B	Location C
A_e	3.860 in^2	3.930 in^2	3.970 in^2	3.020 in^2

Step 5) The nominal compressive strength P_n and the strength ratio $\frac{P_u}{\emptyset P_n}$ at each of the potentially critical cross-sections using Table 3.27 are shown in Table 3.28.

Table 3.28 The strength ratio for entire member for the singly-symmetric web tapered I beam under compression

	Location A	CR Location	Location B	Location C
$\phi_c P_n = \phi_c F_{cr} A_e$	97.27 kips	91.33 kips	86.93 kips	60.80kips
$\frac{P_r}{\phi_c P_n}$	0.116	0.124	0.130	0.186

3.4.5.5 Singly-symmetric tapered member subjected to flexure

The flexural strength of the member shown in Figure 3.5 is evaluated using the DG25 provisions along with the calculation of γ_{eLTB} using SABRE2. The linearly web tapered member is subjected to applied moment $M = -1800\ \text{kip} \cdot \text{in}$. Flexural strength design is investigated using Table 3.29 through 3.34 and is given by:

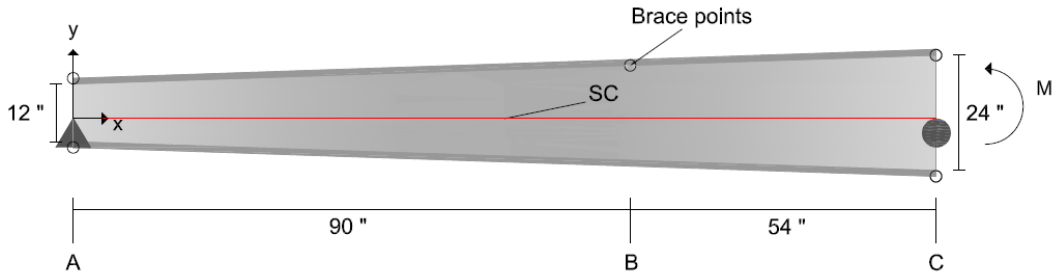

Figure 3.5 Simply-supported singly-symmetric web tapered I beam under flexure.

For the analysis, eight elements are employed and the required material and geometric properties are :

- Material Properties

- $F_y = 55$ ksi

- $F_u = 70$ ksi

- Geometric Properties

- Singly symmetric member:

- Member and segment length are given by:

  i. $L_{AB} = L_{byAB} = 90$ in : Segment AB

  ii. $L_{BC} = L_{byBC} = 54$ in : Segment BC

  iii. $L = L_{bx} = L_{bz} = L_{AB} + L_{BC} = 144$ in : Entire member

Table 3.29 Employed section properties for singly-symmetric tapered member subjected to flexure (continued)

	Location A	Mid-span of a member	Location B	Location C
b_{fc} or b_{ft}	6.000in	6.000in	6.000in	6.000in
t_{fc}	0.313in	0.313in	0.313in	0.313in
t_{ft}	0.219in	0.219in	0.219in	0.219in
t_w	0.125in	0.125in	0.125in	0.125in
h	12.00in	18.00in	19.50in	24.00in
d	12.53in	18.53in	20.03in	24.53in
h_o	12.27in	18.27in	19.77in	24.27in
A_g	$4.690in^2$	$5.440in^2$	$5.630in^2$	$6.190in^2$

Table 3.29 Employed section properties for singly-symmetric tapered member subjected to flexure

y_{bar}	5.560in	8.350in	9.060in	11.20in
I_x	135.4 in^4	321.9 in^4	383.2 in^4	605.9 in^4
S_{xc}	24.35 in^3	38.53 in^3	42.29 in^3	54.11 in^3
S_{xt}	19.43 in^3	31.63 in^3	34.93 in^3	45.44 in^3
I_{yc}	5.630in^4	5.630in^4	5.630in^4	5.630in^4
I_{yt}	3.940in^4	3.940in^4	3.940in^4	3.940in^4
I_y	9.560in^4	9.570in^4	9.570in^4	9.570in^4
h_{cp}	3.750in	6.750in	7.500in	9.750in
Z_x	23.43 in^3	38.62 in^3	42.76 in^3	56.05 in^3
h_c	10.50in	16.08in	17.50in	21.77in
h_p	7.500in	13.50in	15.00in	19.50in

Table 3.30 Strengths and stresses for singly-symmetric tapered member subjected to flexure

	Location A	Mid-span of a member	Location B	Location C
M_r	0.000kip · in	900.0kip · in	1125kip · in	1800kip · in
f_r	0.000 ksi	23.36 ksi	26.60 ksi	33.27 ksi
M_{yc}	1339kip · in	2119kip · in	2326kip · in	2976kip · in
M_{yt}	1069kip · in	1740kip · in	1921kip · in	2499kip · in
M_y	1069kip · in	1740kip · in	1921kip · in	2499kip · in
M_p	1289kip · in	2124kip · in	2352kip · in	3083kip · in

Table 3.31 Flange limiting width to thickness ratios for singly-symmetric tapered member subjected to flexure

	Location A	Mid-span of a member	Location B	Location C
λ_f	9.600	9.600	9.600	9.600
k_c	0.410	0.350	0.350	0.350
F_L	38.50 ksi	38.50 ksi	38.50 ksi	38.50 ksi
λ_{rf}	16.66	15.43	15.43	15.43
λ_{pf}	8.730	8.730	8.730	8.730
Flange	Noncompact	Noncompact	Noncompact	Noncompact

Table 3.32 Web limiting width to thickness ratios for singly-symmetric tapered member subjected to flexure

	Location A	Mid-span of a member	Location B	Location C
λ_w	83.97	128.7	140.0	174.2
λ_{rw}	131.0	131.0	131.0	131.0
λ_{pw}	102.0	84.40	82.12	77.23
Web	Compact	Noncompact	Slender	Slender

Table 3.33 Web plastification factor in compression, R_{pc} for singly-symmetric tapered member subjected to flexure

	Location A	Mid-span of a member	Location B	Location C
R_{pc}	0.962	1.000	1.000	1.000

Table 3.34 Web bend buckling factor,R_{pg} for singly-symmetric tapered member subjected to flexure

	Location A	Mid-span of a member	Location B	Location C
a_w	0.700	1.072	1.167	1.451
R_{pg}	1.000	1.000	0.993	0.962

For flexural design, the general procedure in DG25 is employed and is given by:

Step 1) The elastic lateral-torsional buckling multiplier, γ_{eLTB}, using finite element analysis (SABRE2) is :

$$\gamma_{eLTB} = 5.077$$

Step 2) At sampling locations along the entire length, the nominal lateral torsional flexural strength, M_{nLTB}, is shown in Table 3.35.

Table 3.35 The nominal lateral torsional flexural strength for singly-symmetric tapered member subjected to flexure

	Location A	Mid-span of a member	Location B	Location C
$\frac{\gamma_{eLTB} f_r}{F_y}$	0.000	2.156	2.455	3.071
$\frac{F_L}{F_y}$	0.700	0.700	0.700	0.700
$M_{n\,LTB}$	$0.000 kip \cdot in$	$1870 kip \cdot in$	$2074 kip \cdot in$	$2638 kip \cdot in$

Step 3) The nominal flexural strength M_n and the strength ratio $\frac{M_u}{\emptyset M_n}$ for lateral torsional buckling, flange local buckling, and top flange yielding are shown in Table 3.36 and Table 3.38. The largest value of $\frac{M_u}{\emptyset M_n}$ is the governing value.

Table 3.36 The strength ratio for lateral torsional buckling for singly-symmetric tapered member subjected to flexure

	Location A	Mid-span of a member	Location B	Location C
$M_{n\,LTB}$	$0.000 kip \cdot in$	$1870 kip \cdot in$	$2074 kip \cdot in$	$2638 kip \cdot in$
$\frac{M_r}{\phi_b M_{n\,LTB}}$	0.000	0.535	0.602	**0.758**

Table 3.37 The strength ratio for compression flange local buckling for singly-symmetric tapered member subjected to flexure

	Location A	Mid-span of a member	Location B	Location C
$M_{n\,FLB}$	$1250 kip \cdot in$	$2036 kip \cdot in$	$2220 kip \cdot in$	$2750 kip \cdot in$
$\frac{M_r}{\phi_b M_{n\,FLB}}$	0.000	0.491	0.563	**0.727**

Table 3.38 The strength ratio for top flange yielding for singly-symmetric tapered member subjected to flexure

	Location A	Mid-span of a member	Location B	Location C
$M_{n\,TFY}$	$1289 kip \cdot in$	$1758 kip \cdot in$	$1921 kip \cdot in$	$2499 kip \cdot in$
$\frac{M_r}{\phi_b M_{n\,TFY}}$	0.000	0.569	0.651	**0.800**

From Table 3.36 and 3.38, flexural strength for singly-symmetric linearly web-tapered member in Figure 3.5 is governed by the compression flange local buckling at Location C.

3.4.5.6 Combined axial compression and flexure for singly-symmetric tapered member

Combined axial compression and flexure for singly-symmetric linearly tapered member is investigated. Results from the recommended updated DG25 provisions are compared with current DG25 results.

<u>Updates to DG25 Provisions</u>

As shown in Table 3.28, the governing axial compression strength ratio is located at Location C and has the value of 0.186. From Table 3.36 through 3.38, the governing flexural strength ratio is located at Location C and is 0.8 which is generated by the top flange yielding. Using those axial compression and flexural strength ratio, combined unity is given by:

Since $\frac{P_r}{P_c} < 0.2$

$$\frac{P_r}{2P_c} + \left(\frac{M_{rx}}{M_{cx}} + \frac{M_{ry}}{M_{cy}}\right) = \frac{0.186}{2} + (0.800 + \mathbf{0}) = 0.893 \leq 1.0$$

Current DG25 Results

In this section, a DG25 singly-symmetric linearly tapered example is considered. Torsional simply supported boundary condition and top flange lateral bracing condition at Location B are employed to calculate the equivalent elastic critical buckling. The solutions of the example are calculated using DG25 linearly web-tapered procedure and are described in Table 3.39 and Table 3.40.

Table 3.39 The strength ratio of axial compression for a member using DG25

	Location A	CR Location	Location B	Location C
$\frac{P_r}{\phi_c P_{nL}}$	0.0615	**0.0629**	0.0624	0.0617
$\frac{P_r}{\phi_c P_{nCAT}}$	0.1030	**0.1037**	0.1032	0.1026
$\frac{P_r}{\phi_c P_{nAB}}$	0.0767	**0.0778**	0.0773	-
$\frac{P_r}{\phi_c P_{nBC}}$	-	-	**0.0673**	0.0667

Table 3.40 The strength ratio of flexure for a member using DG25

	Location A	Mid-span of a member	Location B	Location C
$\frac{M_r}{\phi_b M_{n\,LTB}}$	0.000	0.723	0.728	**0.751**
$\frac{M_r}{\phi_b M_{n\,FLB}}$	0.000	0.491	0.563	**0.727**
$\frac{M_r}{\phi_b M_{n\,TFY}}$	0.000	0.569	0.651	**0.800**

Since $\frac{P_r}{P_c} < 0.2$

$$\frac{P_r}{2P_c} + \left(\frac{M_{rx}}{M_{cx}} + \frac{M_{ry}}{M_{cy}}\right) = \frac{0.1037}{2} + (0.800 + \mathbf{0}) = 0.852 \leq 1.0$$

For singly-symmetric linearly tapered example, the updated DG25 and the current DG25 are analyzed using an entire member for axial compression and flexure. However, the difference in the calculation of the elastic critical buckling strength causes the difference in the governing location and the nominal axial strength. For flexure, the governing flexural strengths are the same in each other since top flange yielding controls the design.

From the previous results based on doubly symmetric linearly tapered member having bracing at Location B in Figure 3.2 and singly symmetric linearly tapered member having top flange only lateral bracing at Location B in Figure 3.4, updated DG 25 provisions employing the recommended multiple bracing location concept and the elastic buckling multiplier of SABRE2 are investigated and compared with the current DG25. From the comparison, the results show good agreement.

In the following section for automatic optimized design, the algorithms are investigated using the updated DG25, the recommended multiple bracing location concepts, and SABRE2.

3.5 Genetic Algorithms

3.5.1 Concept of Genetic Algorithms

Genetic Algorithms (GA) is one of the stochastic searching methods for optimization. Figure 3.6 shows the concept of machine learning Genetic Algorithms. In this research, GA is employed to enable an automatic optimized design algorithmic means.

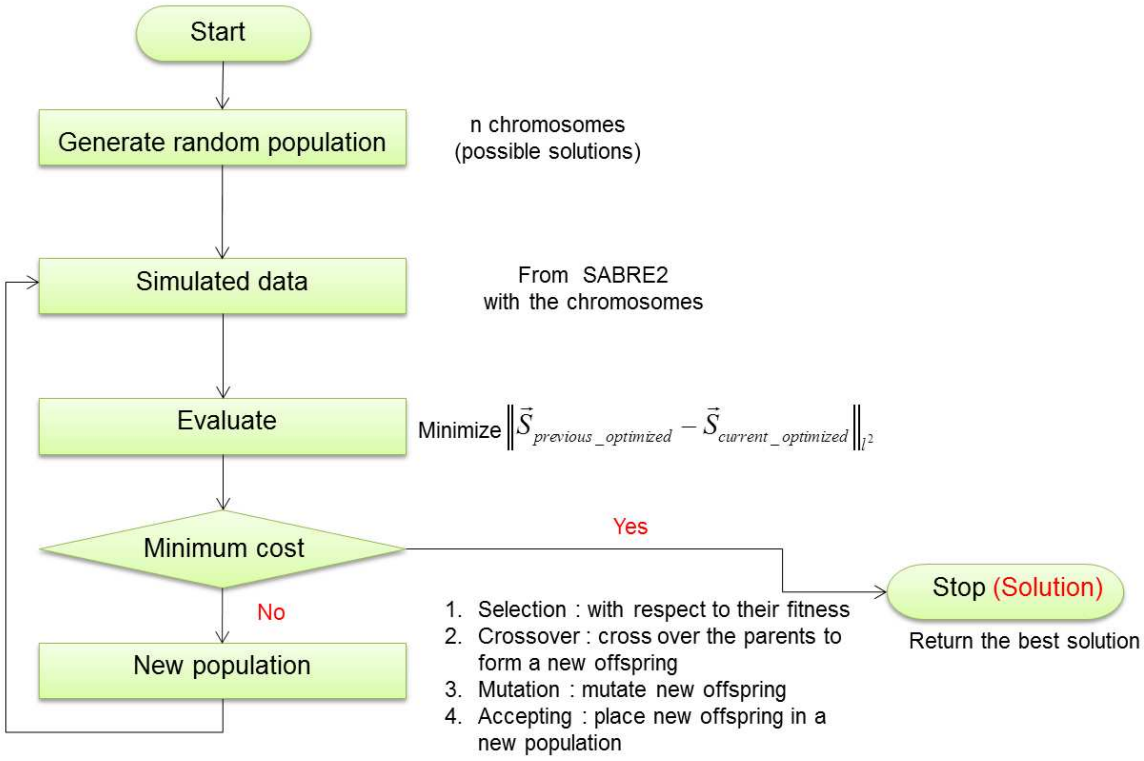

Figure 3.6 Concept of Genetic Algorithms

Member design is to select cross-section properties under given external loads and geometries so that the cross-section will be considered to be calculated and defined as unknown variables (genes) in Genetic Algorithms. The unknown variables such as flange

thickness, flange width, web depth, web thickness, nonprismatic (web tapering) factor, bracing points and brace spacing in member design are randomly generated in Genetic Algorithms. The first randomly generated “individuals” (possible solutions) which are composed of “genes” are called “parents”. Using the “parents” and considering updated DG25 provisions, the system will select the several “parents” (individuals) with respect to their fitness which is defined in Eq. 3.2.

$$\text{Minimize } \left\| \vec{S}_{previous_{optimized}} - \vec{S}_{current_{optimized}} \right\|_2^2 \qquad \text{(Eq. 3.2)}$$

Using the selected “parents” (individuals), “Crossover”, “Mutation”, and “Accepting” will be applied to generate next generations which are called “offspring”. Using the new offspring and considering updated DG25 provisions, the several offspring (possible solutions) with respect to their fitness will be selected and employed as parents for next generation. The machine learning algorithm will result in one converged value which will be the best solution in member design problem on the basis of minimum cost.

3.5.2 Terminology of Genetic Algorithms

General terminology of Genetic Algorithm can be given by:

1) Search space

- Population = The group of chromosomes or individual. As shown in Figure 3.7, the search space is composed of total chromosomes or individual.
- Chromosome or individual = For this research, possible design is representative of the chromosome.
- Genes = The characteristics of the chromosome. For this research, cross-section properties such as top and bottom flange width and thickness, web depth, tapering parameter, bracing points within cross-section, and bracing locations along a member.
- Population size = The number of chromosomes or individuals.
- Search range = Minimum and maximum values for each gene. For this research, design limitation of DG25 and user defined minimum and maximum values are employed.

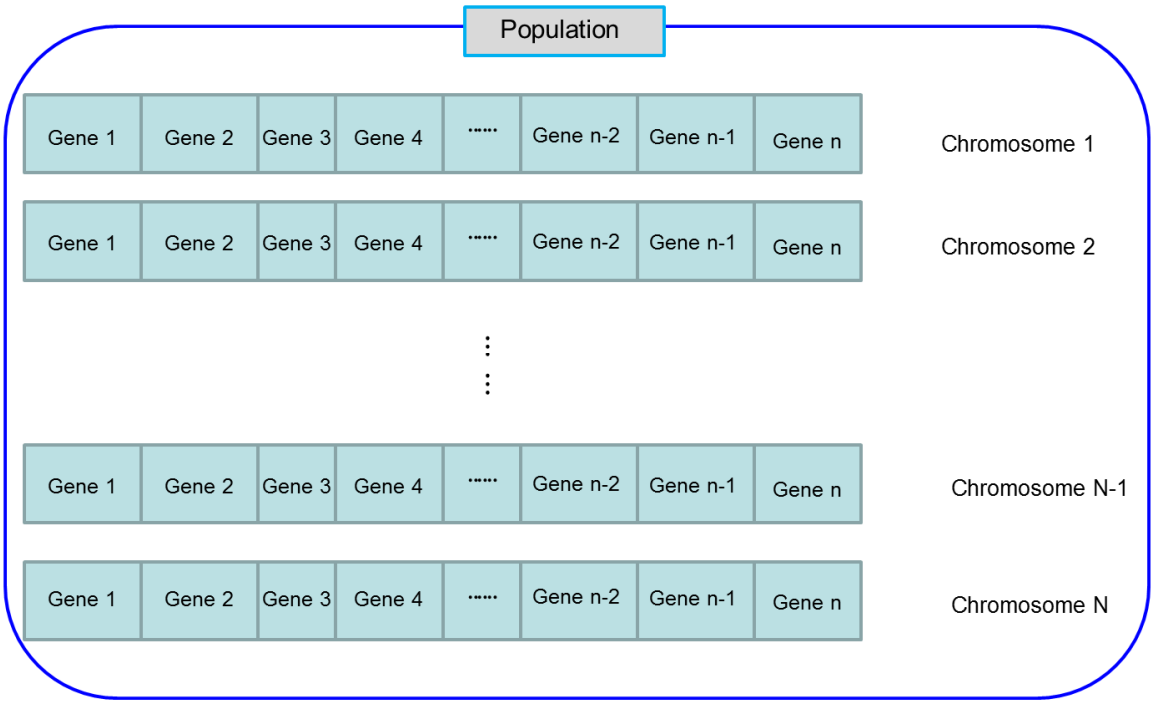

Figure 3.7 Concept of search space

2) Production

- Generation = The act of producing the different level of population.
- Parents = Chromosomes in the current generation.
- Offspring = Chromosomes in the next generation.

2) Genetic operators

Three basic genetic operators – selection, crossover, accepting, and mutation- are performed to produce the chromosomes from the current generation to child generation that become fitter in the simulated evolution process.

- Selection = Selection is a process in which a mating pool of chromosomes in the current generation is chosen in a certain way to reproduce the offspring according to the fitness values of the chromosomes of the current generation. This operator is designed to improve the average quality of the population by giving individuals of higher fitness to be copied to produce the new individuals of chromosomes in the offspring generation. The quality of an individual in the current generation is measured by its fitness value through the evaluation of the fitness function. Once a chromosome has been selected for production, it enters into a mating pool that is a tentative new population ready for further Genetic Algorithms.
  - Uniform selection
  - Roulette selection
  - Tournament selection

- Crossover = Crossover is an operation to exchange part of the genes in the chromosomes of two parents in the mating pool to create new individuals for the offspring generation. First members of the chromosomes in the mating pool are mated at random. Next, using one of the following schemes to generate new chromosomes.

  - One-point crossover scheme : A crossover operator randomly selects a crossover point within a chromosome. As shown in Figure 3.8, two chromosomes are interchanged at this point to produce two new offspring.

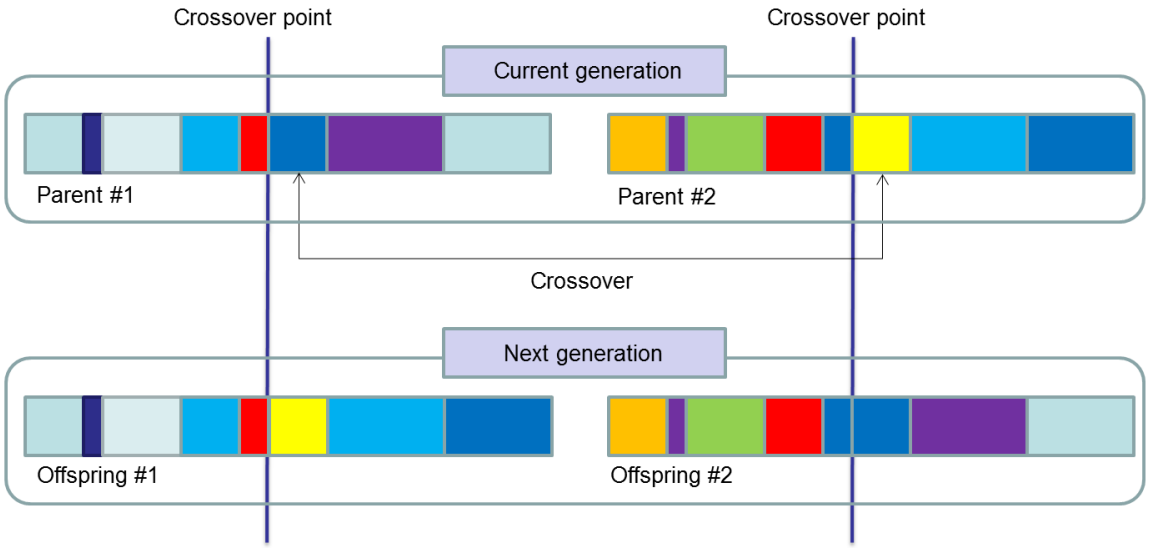

Figure 3.8 Concept of one point crossover

- Multipoint crossover scheme : a crossover operator randomly selects a number of crossover points within a chromosome. As shown in Figure 3.9, the genes in the chromosomes of the two parents are interchanged between these points to produce two new offspring.

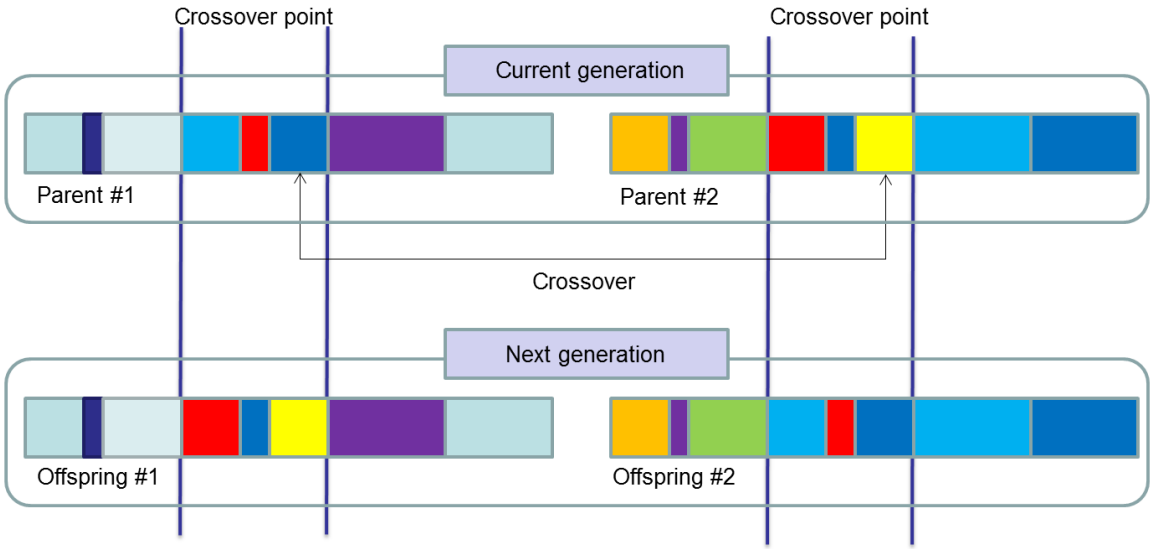

Figure 3.9 Concept of two points crossover

- Uniform crossover scheme : As uniform crossover operator decides which parent will contribute each of the genes in the offspring chromosomes with a given probability at the gene bit level rather than at the gene segment level. In the uniform crossover strategy, the crossover positions are predefined in a mask. All the chromosomes in a population are uniformly crossed over the same position. If the probability is 0.5 in Figure 3.10, half of the gene bits in the offspring will come from parent 1 and the other half will come from parent 2. Predefined mask with probability 0.5 randomly can be generated.

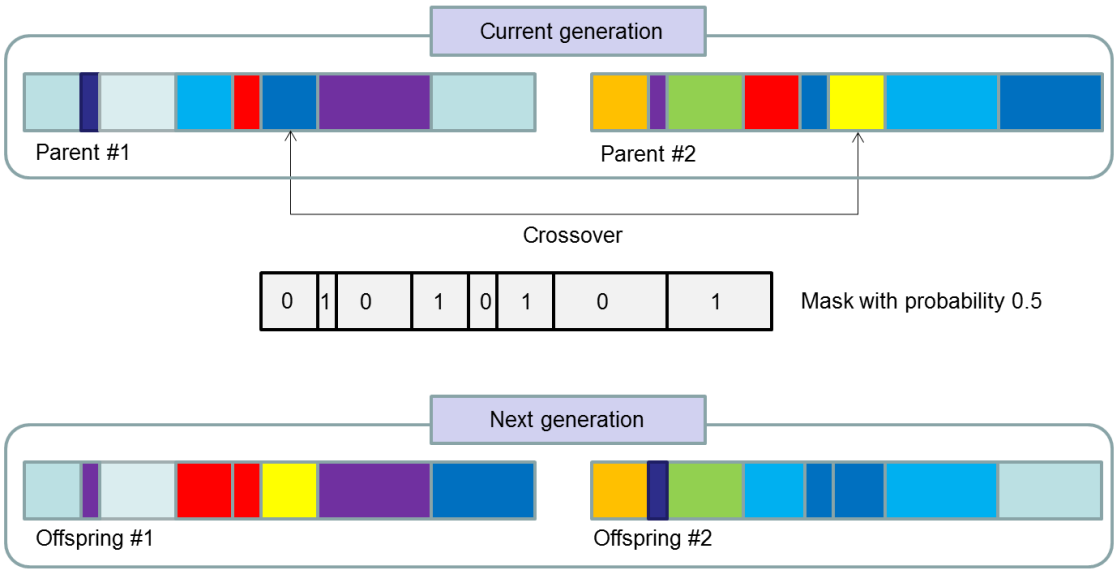

Figure 3.10 Concept of uniform crossover

- Mutation : The mutation operator is designed so that one or more of the chromosome's genes can be mutated at a small probability as shown in Figure

3.11. The goal of the mutation operator is to prevent the genetic population from converging to a local minimum and to introduce some new possible solutions to the generation. Without mutation, the population would rapidly become uniform.

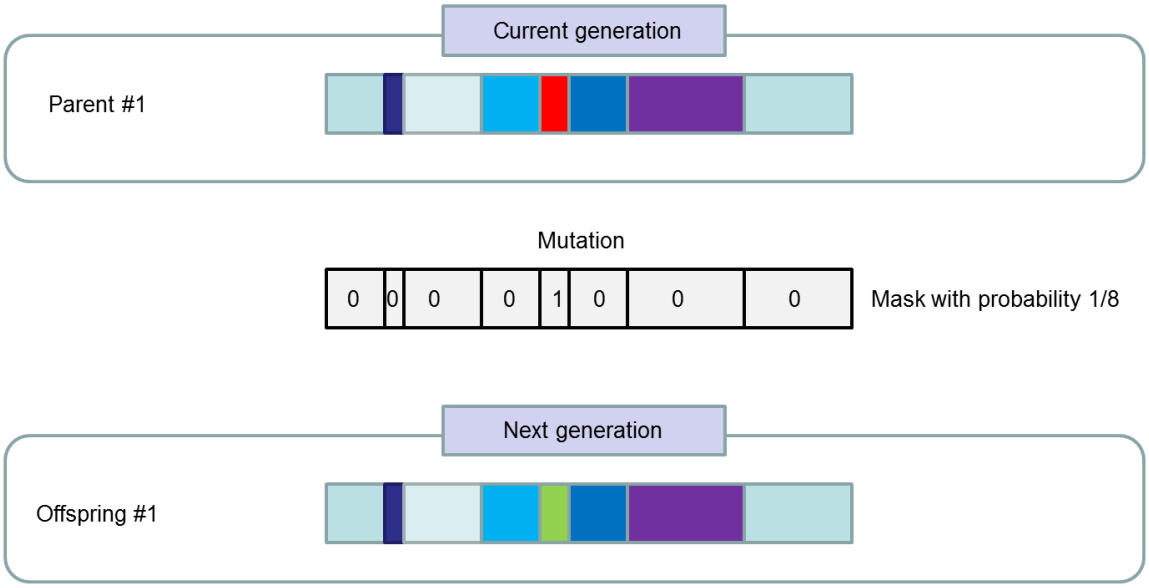

Figure 3.11 Concept of mutation

- Accepting – New offspring from selection, crossover, and mutation are placed in a new population (chromosomes)

3.5.3 Fitness and elitist selection

A fitness function is an objective function employed to rank each chromosome for the selection of the next generation. Prior to the above three basic operator, elitism selects the best chromosomes considering fitness ranking. The selected best chromosomes are descended without changing the gene property. Fitness is "***cost function***" in this research.

Cost in large open space, stadiums, or bridge girders includes manufacturing cost, construction cost, transportation cost, steel weight, etc. Cost function will be various dependent on construction fields. The current research focuses on developing an optimization algorithmic means using Genetic Algorithms based on ***total minimum equivalent weight*** from a cross-section dimensions, tapering angle or angles, and bracings. Bracing cost is considered in the fitness function by assigning equivalent weight. If a cost function in each field is defined and given, the optimization algorithmic means can be easily changed.

3.6 Optimized Design

3.6.1 Optimized Design

Figure 3.12 shows an automatic optimized design procedure. Prior to automatic optimized design, material properties, boundary and bracing conditions, multiple loading, member or frame geometries are initially set up. The number of population, the number of generation, the number of elitists, user defined search range, mutation probability, selection types, crossover types are the set up.

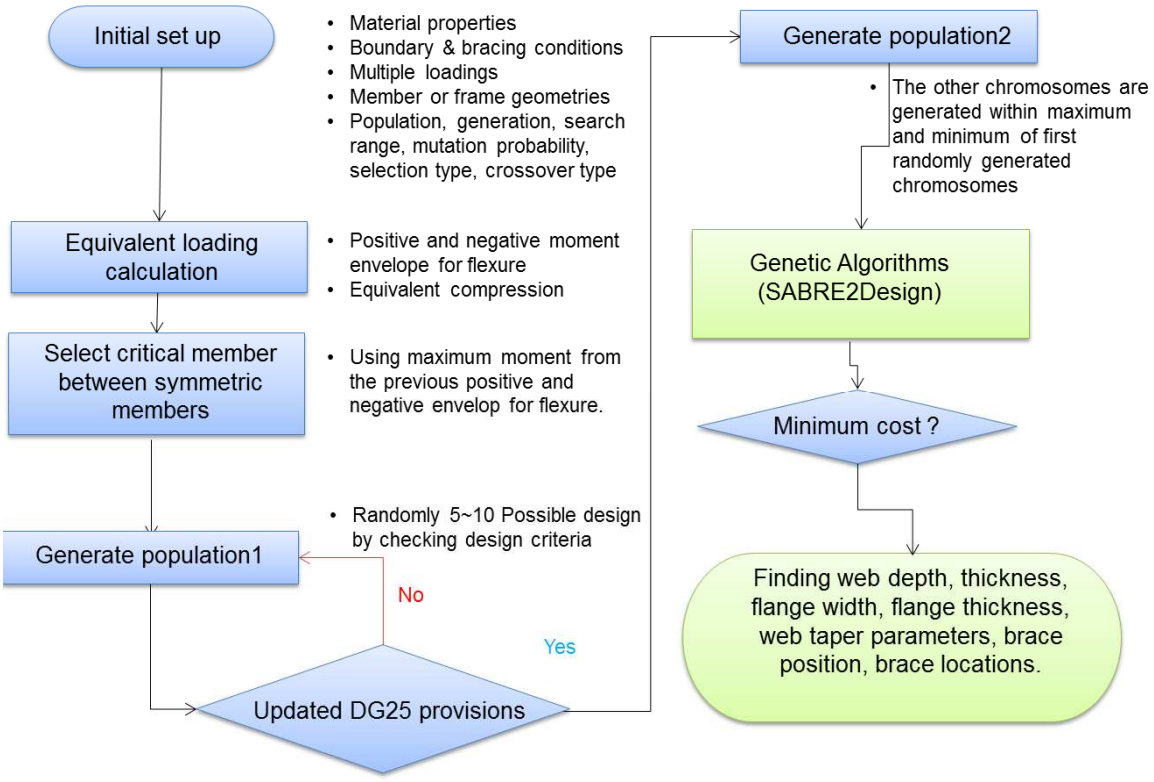

Figure 3.12 Automatic optimized design procedure

On the basis of a given external loads and a given geometry, equivalent loadings from multiple loadings are automatically calculated. The equivalent loadings have positive moment envelop, negative moment envelop, and axial compression. Using the

equivalent loadings and initially defined properties are employed to select possible solutions in Genetic Algorithms (GA).

A Genetic Algorithms (GA) will first randomly generate 5~10 chromosomes composed of unknown variables (called “genes”) such as flange thickness, flange width, web depth, web thickness, nonprismatic (web tapering) factor, bracing points, and brace spacing. Using the unknown variables and 3D Finite Element Analysis software SABRE2, the elastic buckling strength multiplier γ_e and γ_{eLTB} for a general prismatic- or nonprismatic geometry, doubly- or singly- symmetric cross-section subjected to positive and negative moment envelop will be calculated based on update DG25 provisions. Using the calculated elastic buckling strength multiplier $\gamma_e$and γ_{eLTB}, axial compression and flexural strength design are investigated. From shear force and displacement calculation, shear strength and serviceability are investigated. If the prior design criteria are not satisfied, penalty is applied to the chromosome, which is omitted in next generation. From initial 5~10 randomly generated chromosomes, the other chromosomes are selected for selection, crossover, accepting, and mutation. On the basis of the satisfied unknown variables for the updated DG25, several “individuals” which are composed of unknown variables (genes) are selected considering total minimum cost. The selected individuals which are possible solutions are employed for the next generation of Genetic Algorithms.

In Genetic Algorithms, “crossover” to form new “offspring” which are composed of unknown variables (genes), “mutation” to mutate new offspring (new unknown variable from the previous unknown variables), and “accepting” to place new offspring in a new population is applied to generate new genes. Using the generated new offspring,

SABRE2 is employed to calculate member forces, member displacements, and elastic buckling loads. Figure 6 summarizes how an optimized “individual” is obtained which is the best solution considering the total minimum cost on the basis of the “elitism”. The machine learning Genetic Algorithms for automatic optimized general non-prismatic member design will search the best solution (individual) which is composed of “genes” such as flange thickness, flange width, web depth, web thickness, non-prismatic (web tapering) parameters, bracing locations, and brace spacing.

3.6.2 SABRE2Design

Using the recommended automatic design procedure, automatic optimized design software which is called SABRE2Design is developed. Screenshots of SABRE2Design for initial set up of clear-span frame design are shown in Figure 3.13 through 3.20.

Figure 3.13 Screenshot of SABRE2Design for the definition of joint nodes.

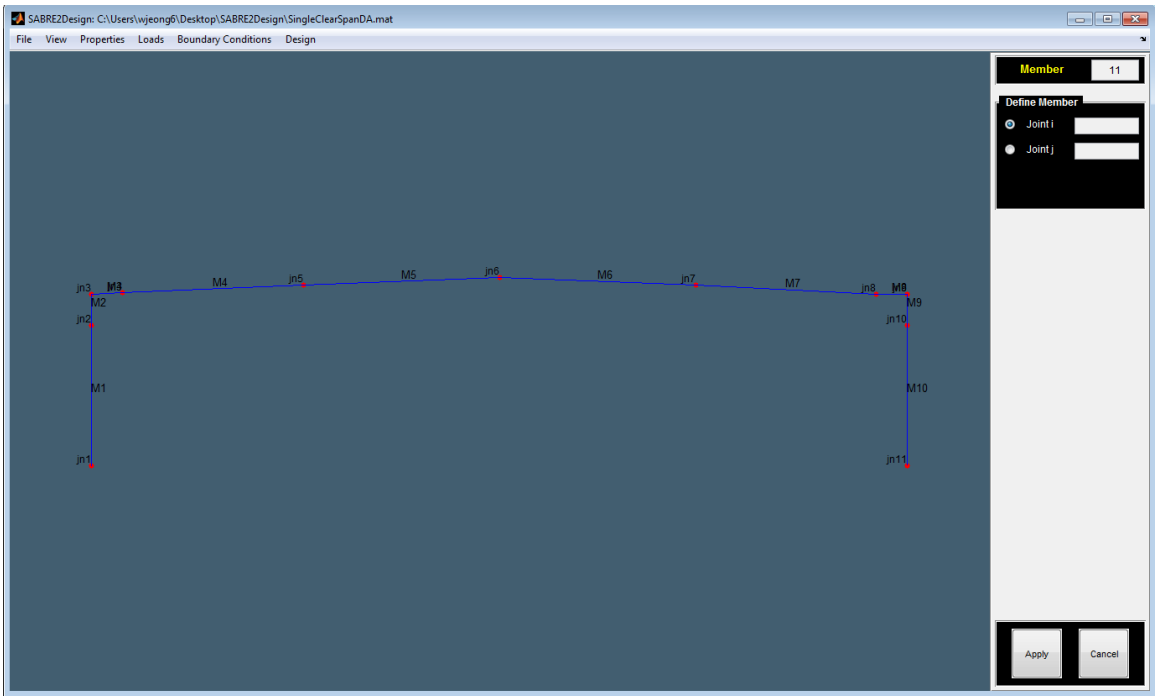

Figure 3.14 Screenshot of SABRE2Design for the definition of members.

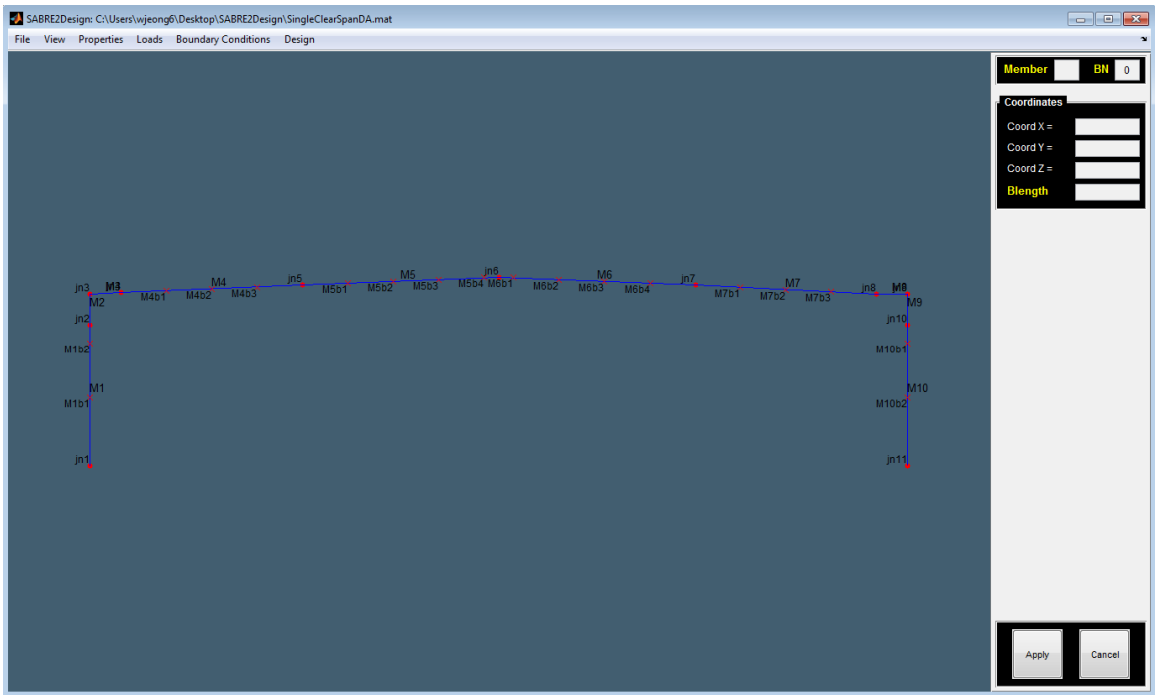

Figure 3.15 Screenshot of SABRE2Design for bracing locations.

Figure 3.16 Screenshot of SABRE2Design for material properties and the number of elements.

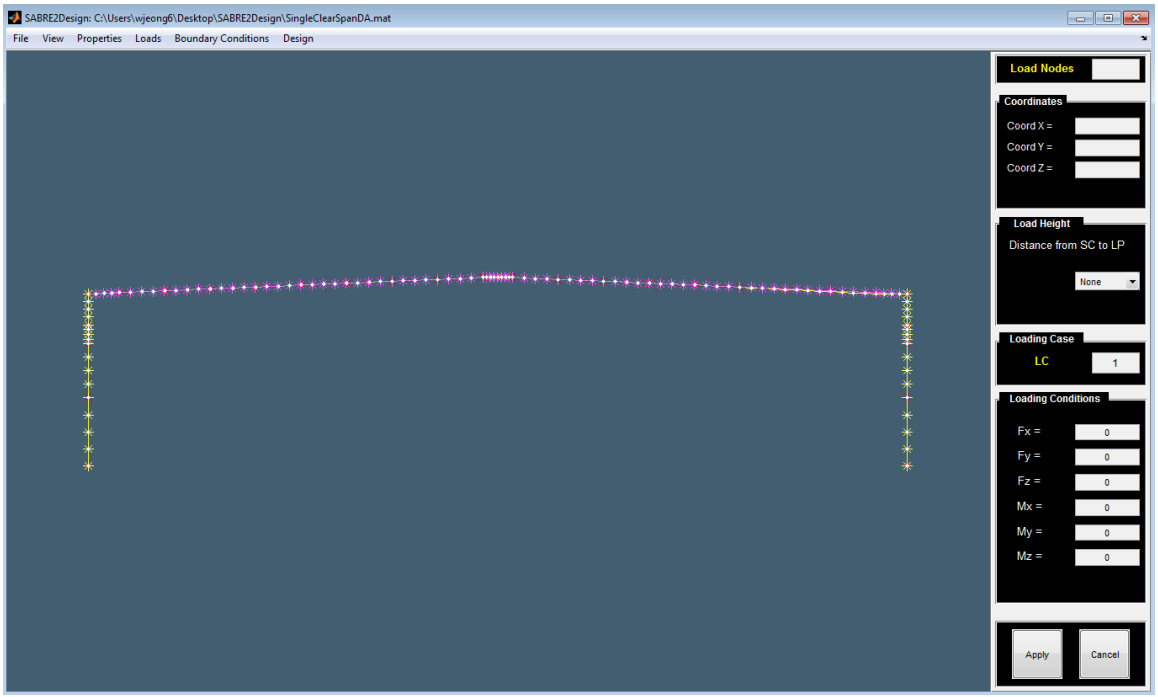

Figure 3.17 Screenshot of SABRE2Design for point loads.

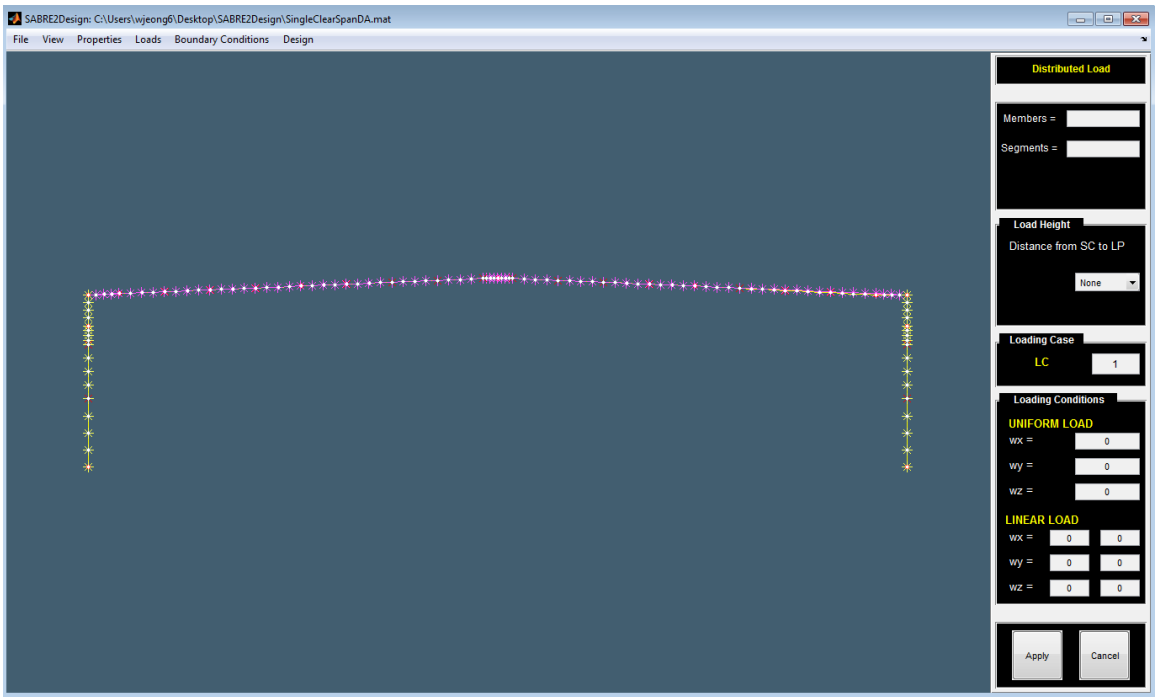

Figure 3.18 Screenshot of SABRE2Design for distributed loads.

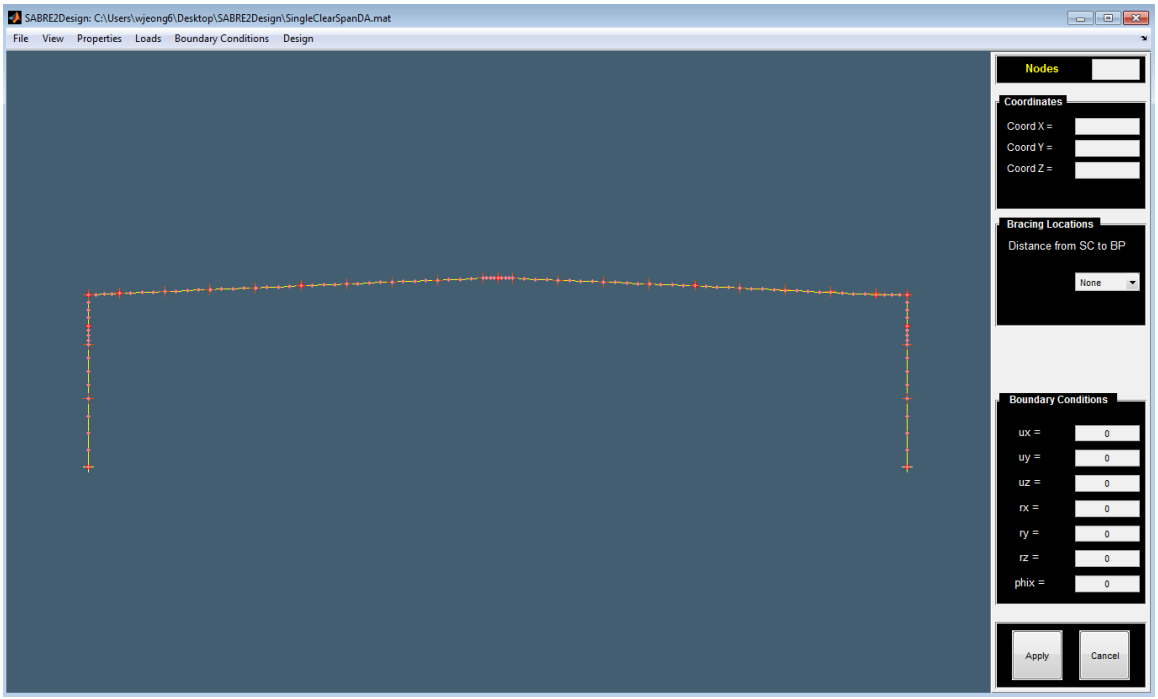

Figure 3.19 Screenshot of SABRE2Design for boundary and bracing conditions.

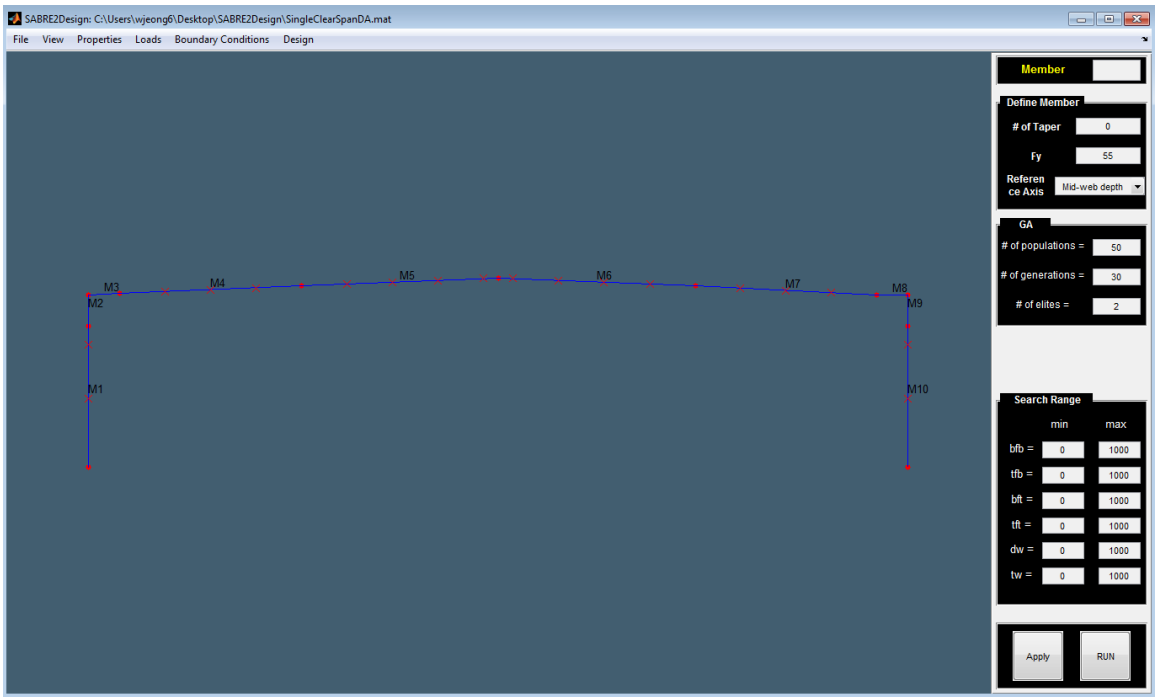

Figure 3.20 Screenshot of SABRE2Design for design.

The procedures to employ SABRE2Desitgn are:

1) Joint nodes which are start and end nodes for each member are defined as shown in Figure 3.13.
2) Members using joint nodes are defined as shown in Figure 3.14.
3) Bracings for possible purlin or girt locations are defined as shown in Figure 3.15.
4) The number of elements and material properties are assigned for each segment as shown in Figure 3.16.
5) Multiple general loading combinations are defined as shown in Figure 3.17 and 3.18.
6) Boundary and bracing conditions are defined as shown in Figure 3.19.

7) Set up design parameters such as the number of taper, yield stress, reference design axis, the number of populations, the number of generations, the number of elites, and search range for each gene and start to design as shown in Figure 3.20.

SABRE2Design is employed for the following benchmark problems

3.6.3 Search Range for Each Gene

The objective of this research is to find top flange width, top flange thickness, bottom flange width, bottom flange thickness, web thickness, web depth, web tapering angle, web tapering location, bracing points, and bracing locations which are called genes, and number of bracing, bracing location. To characterize the genes, the DG25 limits of applicability given in Section 3.4.1 are employed. In DG25, practical web-tapered members produced by American manufacturers often have noncompact or slender webs and flanges (Kaehler et al., 2011). Thus, the following equations are added to the above limits.

Slender web:

$$t_w \geq 1.49\sqrt{\frac{E}{F_y}} \qquad \text{(Eq. 3.3)}$$

In the ANSI/AISC 360-10 Specification, structural plate products are described as sheet, strip or bar material. For the structural plates, the preferred discrete incremental dimensions are:

- Thickness : $\frac{1}{16}$ in increments if $t \leq \frac{3}{8}$

- Thickness : $\frac{1}{8}$ in increments if $\frac{3}{8} < t \leq 1$
- Thickness : $\frac{1}{4}$ in increments if $1 < t$
- Width : The current extreme width for sheared plate is 200 in
- Width : the preferred increments is $\frac{1}{4}$ in

Based on the preferred increments of thickness and with for structural plates, SABRE2Design is employing discrete increments of :

- Flange width : $\frac{1}{4}$ in increments
- Flange thickness : $\frac{1}{16}$ in increments
- Web depth : $\frac{1}{4}$ in increments
- Web thickness : $\frac{1}{32}$ in increments

For web thickness, as $\frac{1}{32}$ in increments are widely employed, SABRE2Design has the same increments.

For optimized design of structural member or frame, linearly web-tapered members are widely employed. Moreover, during manufacturing the web-tapered members, web-tapering angles are selected to minimize the steel plate loss using SABRE2Design, which is described in Figure 3.21. Linearly tapered web plates can be nested to minimize scrap. Based on specific plate having width D, SABRE2Design can design optimized member design which results in reducing the steel loss without.

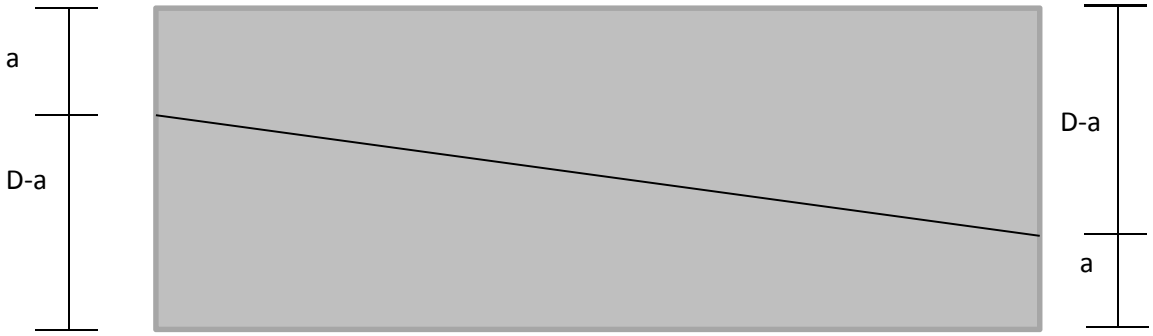

Figure 3.21 Concept of manufacturing web-tapering members.

3.7 Benchmark Problems

3.7.1 DG25 Member Examples

In this section, an automatic optimized member design is conducted using the overall geometry and loading from one of the DG25 examples. The top and bottom flange width and thickness, web thickness, web depth, bracing points, and tapering angle are designed using SABRE2Design. The required input parameters such as member length, applied load, boundary conditions, one-side lateral bracing locations are described in Figure 3.22.

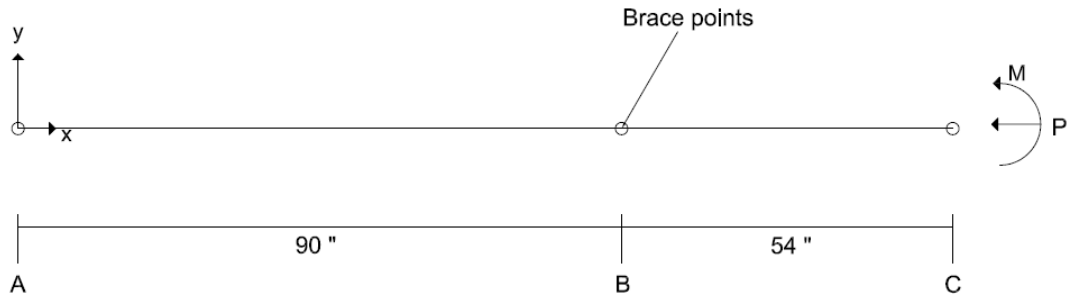

Figure 3.22 DG25 Examples.

Input parameters

In Figure 3.22, the specific input parameters are:

- Entire member length : 144in
- Bracing point :one-side lateral bracing at 90in from left support (A)

- Moment load : $\mathrm{M} = -1800\ \mathrm{kip \cdot in}$
- Axial compression : $\mathrm{M} = -11.3\ \mathrm{kip}$
- Boundary conditions
  - Support A : $(\mathrm{u, v, w}, \theta_x, \theta_x, \theta_x, \theta_x') = (1,1,1,1,0,0,0)$
  - Support C : $(\mathrm{u, v, w}, \theta_x, \theta_x, \theta_x, \theta_x') = (0,1,1,1,0,0,0)$
- Initial bracing condition
  - Support B : $(\mathrm{u, v, w}, \theta_x, \theta_x, \theta_x, \theta_x') = (0,0,1,0,0,0,0)$

The other required input parameter, material properties are:

- $\mathrm{F_y} = 55\ \mathrm{ksi}$
- $\mathrm{F_u} = 70\ \mathrm{ksi}$
- $\mathrm{E} = 29000\ \mathrm{ksi}$
- $\mathrm{G} = 21000\ \mathrm{ksi}$

User defined search range of the unknown values, genes in SABRE2Design are:

- Bottom flange width: $\mathrm{b_{fb}} = 4\ \mathrm{in} \sim 1000\mathrm{in}$
- Bottom flange thickness: $\mathrm{t_{fb}} = 0\ \mathrm{in} \sim 5/16\mathrm{in}$
- Top flange width: $\mathrm{b_{ft}} = 4\ \mathrm{in} \sim 1000\mathrm{in}$
- Top flange thickness: $\mathrm{t_{ft}} = 0\ \mathrm{in} \sim 5/16\mathrm{in}$
- Web depth: $\mathrm{d_w} = 10\ \mathrm{in} \sim 1000\mathrm{in}$
- Web thickness: $\mathrm{t_w} = 1/32\ \mathrm{in} \sim 8/16\mathrm{in}$

The genes were randomly generated within the user defined search range and DG25 limits. The discrete random generations were employed.

The Genetic Algorithms parameters to design the DG25 examples using SABRE2Design are:

- Number of population : 40
- Number of generation : 30
- Number of elites : 3
- Uniform selection
- Uniform crossover

For the member design using SABRE2Design, each both sides bracing has equivalent weight of 30 lb.

Output design

In Table 3.41, if bracing equivalent weight is considered, top flange only lateral bracing is selected since the bracing equivalent weight is large enough to affect the optimized design. However, if bracing equivalent weight is not considered, top and bottom flange are laterally braced since as many as bracing results in increasing the elastic critical buckling load.

Table 3.41 Optimized member design results

	b_{fb}	t_{fb}	b_{ft}	t_{ft}	t_w	d_{wA}	d_{wC}	Bracing points
C1	6.25 in	0.219 in	4.25 in	0.156 in	0.156 in	10.75 in	29.50 in	Top
C2	6.25 in	0.219in	4.00 in	0.156 in	0.156 in	10.75 in	30.35in	Top
C3	5.00 in	0.219 in	4.00 in	0.156 in	0.156 in	11.50 in	28.50 in	Top and Bot
C4	5.00 in	0.219 in	4.75 in	0.156 in	0.156 in	10.75 in	28.25 in	Top and Bot

where:

- C1 : Top flange is only laterally braced at the intermediate brace point
- C2 : The selection of laterally bracing point at bottom flange is flexible considering bracing equivalent weight.
- C3 : Top flange and bottom flange are always laterally at the intermediate brace points.
- C4 : The selection of laterally bracing point at bottom flange is flexible without considering bracing equivalent weight.

Comparing with DG25

Optimized design C1 and C2 are equivalent to DG25-2 which is laterally braced at top and bottom flanges. Optimized design C3 and C4 are equivalent to DG25-1 in which top flange is only laterally braced at intermediate point. Total equivalent weight is investigated in each case and compared with the DG25 examples whose cross-section properties are shown in Table 3.42.

Table 3.42 Member properties of DG25 examples

	b_{fb}	t_{fb}	b_{ft}	t_{ft}	t_w	d_{wA}	d_{wC}	Bracing location
DG25-1	6 in	0.250 in	6 in	0.250 in	0.125 in	12 in	24 in	Top and Bot
DG25-2	6 in	0.313in	6 in	0.212 in	0.125 in	12 in	24 in	Top

Total weight of optimized design C1 through C4 and two DG25 examples are:

- Total weight of C1: $C_1 = 209.68$ lb

- Total weight of C2: $C_2 = 210.65$ lb
- Total weight of C3: $C_1 = 225.8$ lb (including one 30lb for both side bracing)
- Total weight of C4: $C_2 = 197.24$ lb
- Total weight of DG25-1: $DG25_1 = 211.68$ lb
- Total weight of DG25-2: $DG25_1 = 217.56$ lb

Optimized design using SABRE2Design shows better design results compared with DG25 example in total equivalent weight.

3.7.2 Clear-Span Frame Design Under LRFD Loadings

Single-span frame example from White and Kim (2006) was automatically designed using SABRE2Design. The example was selected by the authors and the MBMA Steering Group to validate the design provisions. In The general characteristics of the single- or clear- span frame were explained in Figure 3.23.

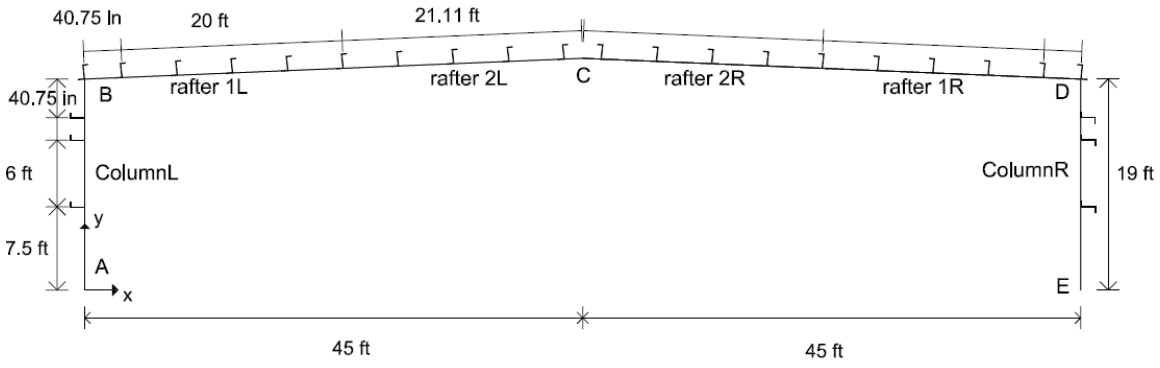

Figure 3.23 White and Kim 2006 Examples

Input parameters

In Figure 3.23, the specific input parameters are:

- 90 ft span
- 19 ft eave height
- $^1/_2 : 12$ roof slope
- 25 ft frame spacing
- 300 ft building length
- The single-span frame is symmetric about its ridge line.
- The single-span frame has simple base conditions.
- The steel minimum yield strength is $F_y = 55$ ksi.
- The steel elastic modulus is $E = 29000$ ksi.
- The span-to-eave height of the single-span frame is selected as a relatively large value (4.74) which results in a relatively large axial thrust in the rafters.
- The $^1/_2 : 12$ roof slope is a practical minimum below which many designers would consider the two rafters in the single-span frame as a single member spanning between the exterior columns.
- The rafters in the single-span frame are considered as two separate members with a length equal to the distance from the knee to the ridge.
- Boundary , eave, and rigid conditions
    - Support A : $(u, v, w, \theta_x, \theta_x, \theta_x, \theta_x') = (1,1,1,1,0,0,0)$
    - Support B : $(u, v, w, \theta_x, \theta_x, \theta_x, \theta_x') = (0,0,1,0,0,0,1)$
    - Support C : $(u, v, w, \theta_x, \theta_x, \theta_x, \theta_x') = (0,0,1,1,0,0,1)$

- Support D : $(\mathrm{u}, \mathrm{v}, \mathrm{w}, \theta_x, \theta_x, \theta_x, \theta_x') = (0,0,1,0,0,0,1)$
- Support E : $(\mathrm{u}, \mathrm{v}, \mathrm{w}, \theta_x, \theta_x, \theta_x, \theta_x') = (1,1,1,1,0,0,0)$

- Double bracing conditions of top of columns and both ends of rafter1
  - $(\mathrm{u}, \mathrm{v}, \mathrm{w}, \theta_x, \theta_x, \theta_x, \theta_x') = (0,0,1,0,0,0,0)$
- Single bracing condition
  - $(\mathrm{u}, \mathrm{v}, \mathrm{w}, \theta_x, \theta_x, \theta_x, \theta_x') = (0,0,1,0,0,0,0)$

Loading

The following factored Load Combination 3 (LC3) loadings from ASCE 7 are considered for the single-span design and are given by:

i. Load Case 1 : $1.2\mathrm{D} + 1.6\mathrm{S}_{\mathrm{unbalanced}} + 0.5\mathrm{W}$

ii. Load Case 2 : $1.2\mathrm{D} + 1.6\mathrm{S}_{\mathrm{unbalanced}}$

iii. Load Case 3 : $1.2\mathrm{D} + 1.6\mathrm{S}_{\mathrm{balanced}} + 0.5\mathrm{W}$

iv. Load Case 4 : $1.2\mathrm{D} + 1.6\mathrm{S}_{\mathrm{balanced}}$

where:

- D : Dead load from ASCE 7 which is shown in Figure 3.24.
- $\mathrm{S}_{\mathrm{unbalanced}}$: The unbalanced snow load condition required by ASCE 7 which is shown in Figure 3.25.
- $\mathrm{S}_{\mathrm{balanced}}$: The balanced (uniform) snow load condition required by ASCE 7 which is shown in Figure 3.26.
- W : Wind load from ASCE 7 which is shown in Figure 3.27.

The magnitudes of the load parameters for the single-span frame design are:

a) Dead Load : D

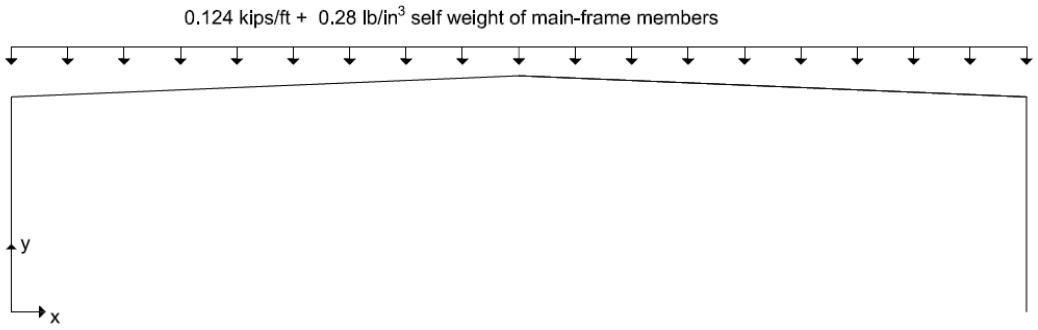

Figure 3.24 Nominal (unfactored) dead loads on projected horizontal area.

b) Unbalanced Snow Load : $S_{unbalanced}$

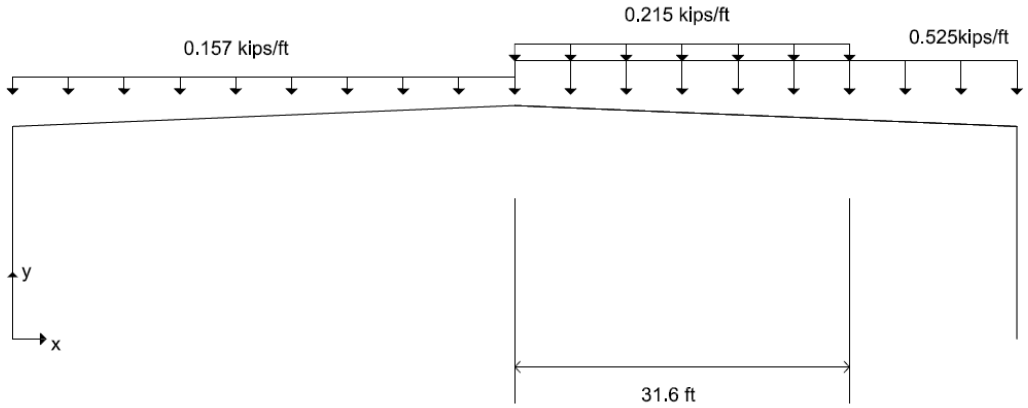

Figure 3.25 Nominal (unfactored) unbalanced snow loads on projected horizontal area. area.

c) Balanced Snow Load : $S_{balanced}$

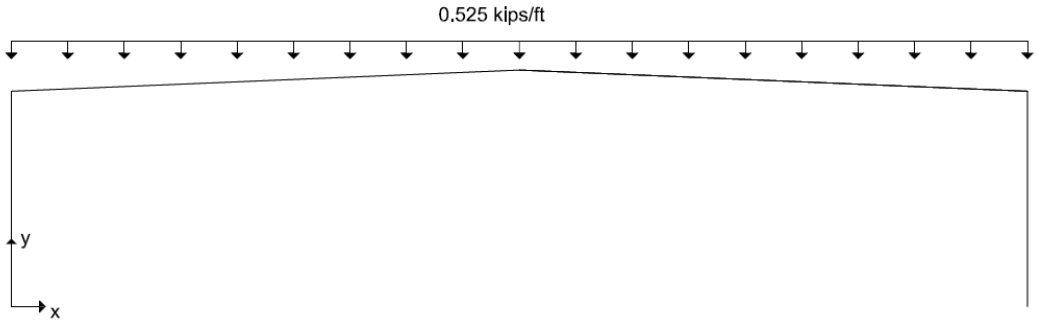

Figure 3.26 Nominal (unfactored) uniform snow loads on projected horizontal area.

d) Wind Load : W

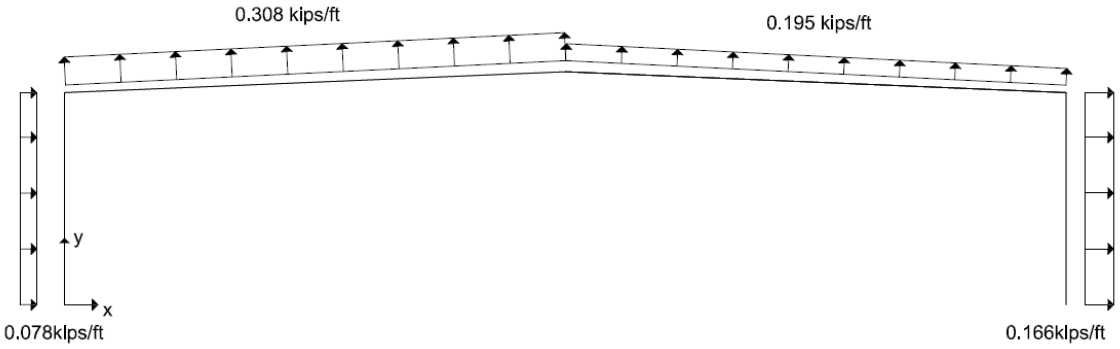

Figure 3.27 Nominal (unfactored) wind design pressures.

User defined search range of the unknown values, genes in SABRE2Design are:

- Bottom flange width: $b_{fb} = 5 \text{ in} \sim 1000\text{in}$
- Bottom flange thickness: $t_{fb} = 0 \text{ in} \sim 12/16\text{in}$

- Top flange width: $b_{ft} = 5$ in ~ 1000in
- Top flange thickness: $t_{ft} = 0$ in $\sim 12/16$in
- Web depth: $d_w = 10$ in ~ 1000in
- Web thickness: $t_w = 4/32$ in $\sim 10/32$in

The genes were randomly generated within the user defined search range and DG25 limits. The discrete random generations were employed.

Genetic Algorithms parameters to design the DG25 examples using SABRE2Design are:

- Number of population : 40
- Number of generation : 30
- Number of elites : 2
- Uniform selection
- Uniform crossover

For the member design using SABRE2Design, each both sides bracing has equivalent weight of 30 lb.

Output design

In Table 3.43, the optimized design for clear-span is suggested under 4 loading cased in Figure 3.24 through 3.27. In column, inside flange was under compression so that inside flange thickness and inside flange width are greater than outside flange thickness and outside flange width. As moment at the top of column is larger than

moment at the bottom of the column, web depths were linearly increased from the bottom of the column to the top of the column.

In rafter1, inside flange was under compression so that inside flange thickness and inside flange width are greater than outside flange thickness and outside flange width. As moment of rafter 1 near column is larger than moment of rafter1 near rafter 2, web depths were linearly increased from near column to near rafter 2.

In rafter2, , outside flange was under compression so that outside flange thickness and outside flange width are greater than inside flange thickness and inside flange width. Moment of rafter 2 near ridge line is larger than moment of rafter2 near rafter 1, web depths were linearly decreased from near ridge line to near rafter 1.

Table 3.43 Optimized frame design results using SABRE2Design

	b_{fi}	t_{fi}	b_{fo}	t_{fo}	t_w	d_{w1}	d_{w2}
Column R	6.820 in	0.344 in	6.290 in	0.281 in	0.281 in	44.00 in	12.25 in
Rafter1L	8.290 in	0.406in	5.540 in	0.344 in	0.281 in	35.25 in	20.75in
Rafter2L	7.000 in	0.219 in	6.750 in	0.376 in	0.188 in	20.75 in	46.50 in

where:

- b_{fi}: Inside flange width
- t_{fi}:Inside flange thickness
- b_{fo}: Outside flange width
- t_{fo}:Outside flange thickness
- d_{w1}: Web depth

- Column : Top
- Rafter 1 : Near column
- Rafter 2: Near rafter1

- d_{w2}: Web depth
  - Column : Bottom
  - Rafter 1 : Near rafter 2
  - Rafter 2: Near ridge line
- Total weight of column
  - $C_1 = 693$ lb (including two 30lb for both side bracings)
- Total weight of rafter 1
  - $R_1 = 974$ lb (including three 30lb for both side bracing)
- Total weight of rafter 2
  - $R_2 = 816.39$ lb (including two 30lb for both side bracings)

In Table 3.44, combined axial compression and flexural strength ratio is provided. In In Table 3.45 through 3.51, the elastic buckling loads under axial compression and flexure in each unbraced length are calculated.

Table 3.44 Unity of combined strength ratio of flexural strength and compression.

	Combined strength ratio
Column	0.979
Rafter1	0.9962
Rafter2	0.971

Table 3.45 The critical buckling load in each unbraced length of column subjected to positive flexure

	Segment1	Segment2	Segment3
γ_e	4.79	3.92	2.96

Table 3.46 The critical buckling load in each unbraced length of column subjected to axial compression

	Segment1	Segment2	Segment3
γ_e	0.16	0.17	0.178

Table 3.47 The critical buckling load in each unbraced length of rafter 1 subjected to positive flexure

	Segment1	Segment2	Segment3	Segment4
γ_e	8.36	8.91	11.14	15.85

Table 3.48 The critical buckling load in each unbraced length of rafter 1 subjected to negative flexure

	Segment1	Segment2	Segment3	Segment4
γ_e	1291	539	14.08	14.59

Table 3.49 The critical buckling load in each unbraced length of rafter 1 subjected to axial compression

	Segment1	Segment2	Segment3	Segment4
γ_e	0.11	0.109	0.108	0.107

Table 3.50 The critical buckling load in each unbraced length of rafter 2 subjected to negative flexure

	Segment1	Segment2	Segment3
γ_e	5.879	5.871	5.655

Table 3.51 The critical buckling load in each unbraced length of rafter 2 subjected to axial compression

	Segment1	Segment2	Segment3
γ_e	0.179	0.197	0.205

Critical location

Critical location in each member is shown in Figure 3.28. In each member, flexural strengths control the member strength.

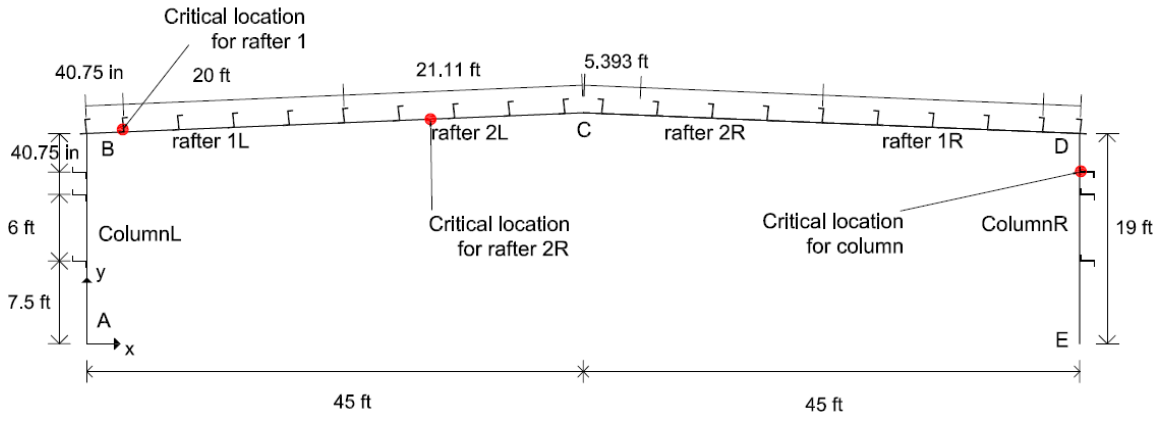

Figure 3.28 Critical locations for the clear-span frame design

Bracing

Bracing conditions in each member are shown in Figure 3.29. In each member, blue spot means that both inside and outside flange is lateral braced.

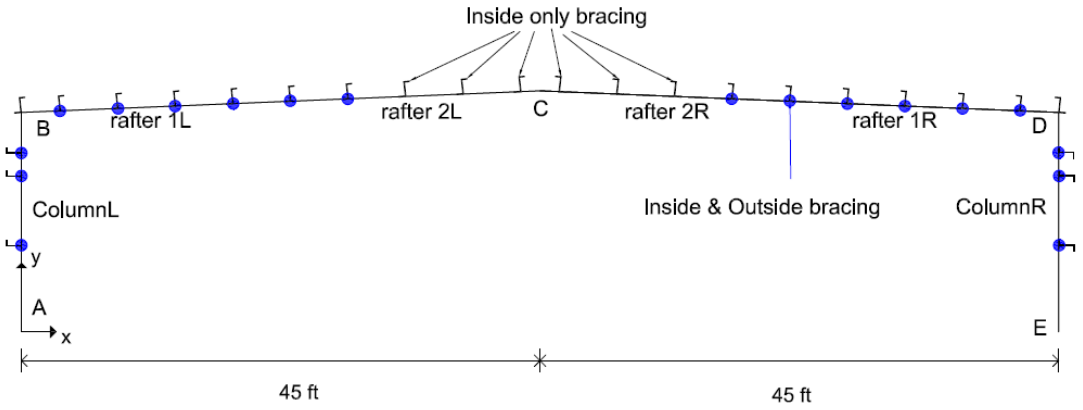

Figure 3.29 Bracing results for the clear-span frame design

CHAPTER 4

SUMMARY AND CONCLUSIONS

4.1 Summary

This research is composed of two major contributions. The first contribution is in the area of finite element procedures to calculate the buckling strength multipliers γ_e and γ_{eLTB} for general singly-symmetric, tapered and/or stepped cross-section members. The second addresses automatic optimized member and frame design tools for general nonprismatic members and frames.

Chapter 2 first reviews alternative methods such as the method of successive approximation, the Rayleigh Ritz method, the finite difference method, and finite element analysis using shell elements for lateral torsional buckling analysis. Then, the fundamental continuum mechanics are presented pertaining to the derivation of the finite element equations. The subject finite element formulation is based on open section thin-walled beam theory, assuming large displacement, large rotation, and small strain. The geometric nonlinear finite element equations are derived and formulated using a co-rotational approach. For the formulation, this research derives:

- A new projection matrix including the transformation between the global frame and element frame.
- A stiffness matrix that captures the load height effect, using the co-rotational formulation,

- A closed form stiffness matrix that addresses bracing and support height effects using rigid offsets.

The handling of steps in the flange thickness, flange width, and web thickness is addressed by using a short-length tapered element; this procedure is shown to be robust. The software system, SABRE2, which implements these finite element capabilities, is explained and various benchmark problems are presented for demonstration and validation.

In Chapter 3, the automatic optimized design of general nonprismatic members and frames is addressed. The current research seeks to take advantage of the continuity effects captured from an accurate eigenvalue buckling analysis without improperly penalizing non-adjacent unbraced lengths. This is achieved by focusing on a model involving a given unbraced length under consideration along with each of its adjacent unbraced lengths. The idealized assumption of torsionally and flexurally simply-supported conditions is moved "one segment away" from the ends of a given unbraced length when it is under evaluation.

Chapter 3 also reviews the limits of applicability of the AISC/MBMA Design Guide 25 (DG25) (Kaehler et al., 2011), Updated DG25 provisions pertaining to the application of a new unified effective area approach for determining the resistances of members subjected concentric axial compression are recommended that tie more explicitly to the direct calculation of γ_e values from calculation tools and account more accurately for slender element cross-section effects based on 2016 updates to the AISC Specification. Finally, corresponding examples are presented that compare the solutions

from the updated DG25 provisions, including the use of SABER2, to current DG25 results.

Pertaining to optimized design, Chapter 3 reviews the basic theory of Genetic Algorithms and the procedure to use SABRE2Design is presented. Then, the search ranges for the genes such as top flange width, top flange thickness, bottom flange width, bottom flange thickness, web thickness, web depth, web tapering angle, and web tapering location are defined. This is followed by a study of the algorithmic means for the design optimization using Genetic Algorithms. Lastly, several benchmark problems using SABRE2Design are evaluated to validate the optimized member and frame design capabilities.

4.2 Conclusions

Nonprismatic members have been employed widely for an optimized member design and DG25 provides guidance in the application of the provisions of the ANSI/AISC 360 Specification to the design of frames composed of web-tapered members as well as general nonprismatic members. For member design using DG25, the calculations of the elastic buckling multipliers γ_e and γ_{eLTB} are required. However, manual procedures for calculating the γ_e and γ_{eLTB} for general nonprismatic geometries subjected to general loadings and general bracing conditions (typically involving multiple brace points along a given member) do not exist. Furthermore, the automatic optimized member design for a general nonprismatic geometry by selecting an appropriate web-taper angle or angles, member section sizes, the location of braces, and the number of unbraced lengths has been largely unexplored in academics. In this research, SABRE2 is developed to calculate the γ_e and γ_{eLTB} for general nonprismatic geometries subjected to general loadings and general bracing conditions. Furthermore, SABRE2Design is developed to design automatically optimized members or frames for general nonprismatic geometries subjected to general loadings and general bracing conditions.

The accomplishments of this research are as follows:

1. The development of capabilities to calculate the buckling strength multipliers γ_e and γ_{eLTB} for the buckling load of general singly-symmetric, tapered and/or stepped cross-section members (steps in the flange thickness, web thickness, or flange width). This research focuses on:

a) Handling of general loadings within the plane of the structure including load height effects

b) Handling of multiple brace locations along web depth (lateral torsional bracing) which is derived and formulated using rigid offsets.

c) Proper 3D FEA modeling to address steps in flange thickness, flange width or web thickness.

d) Performing rigorous calculations and rendering nodal displacements, member force diagrams and 3D elastic buckling modes via an efficient graphical user-interface.

These capabilities are implemented in the software system SABRE2, and are verified using various benchmark problems. For prismatic, singly- or doubly- symmetric members and frames, SABRE2 agrees closely with exact solutions and the other finite element solutions. In addition, SABRE2 provides solutions that match closely with 3D shell FEA for linearly tapered and stepped cross-section members. The research shows clearly that the stepped prismatic representations of web-tapered members are not capable in general of providing accurate solutions for lateral torsional buckling of beams.

2. The derivation of a new projection matrix including the transformation between the global frame and element frame. That the element 3D rotations and moments are handled properly in the formulation and implementation of the element is verified using L-frame and is closely agreement with MASTAN2 and Yang (1984). The new projection matrix enables the elastic buckling analysis of frame.

3. Load height effect by transverse load. Without adding more elements to model the load height effects, SABRE2 solutions having load height effect of the derived and formulated stiffness matrix agree closely with finite element results using additional transverse stub elements to the load locations. Handling the load height effects in the formulation reduce modeling and computing time by reducing the required total number of degrees of freedom.

4. Rigid offset for bracing and support height effects. Without adding more elements to model the bracing and support effects, SABRE2 solutions having bracing and support effects of the derived and formulated stiffness matrix are in close agreement with finite element results using additional transverse stub elements to model the offset of the bracing or support positions. This again reduces the modeling and computing time by reducing total number of degrees of freedom.

5. Handling of 3D FEA capabilities to address steps in flange thickness. Steps in flange thickness result in a discontinuity in shear center of singly-symmetric members, which causes computational errors. SABRE2 handles these steps in flange thickness by using a short tapered element at the step in the cross-section geometry. The results are verified against 3D shell finite element solutions.

6. Setting up an easy-to-use graphical user-interface for the calculation of the elastic buckling load and the analysis of load-deflection. Being able to clearly see the buckling mode is essential. This is handled by a 3D surface rendering of the deformed flange and web including warping.

7. The development of algorithmic means to enable automatic optimized member design for the above types of members based on Genetic Algorithms (GA). This focus of the research includes:

a) Development and recommendation of updates to DG25.

b) Investigation of approaches to address the lateral torsional buckling design of members having multiple bracing locations, accounting for the continuity effects between adjacent unbraced lengths.

c) Recommendation of design procedures using the updated DG25 provisions, including the calculation of γ_e and γ_{eLTB} from a rigorous structural analysis.

d) Performing automatic optimized member or frame design and rendering 3D model based on a graphical user-interface.

SABRE2Design, the design computational tool implementing this research, is verified using several DG25 examples and a clear-span frame example from White and Kim (2006).

8. Updates to DG25. The development and recommendation of the updates to DG25 for the axial compression member design is very simple and results in reducing design time.

9. Handling of the axial compression and lateral torsional buckling design of members having multiple bracing locations along the entire member. When it comes to handling multiple unbraced lengths, SABRE2Design selects a better

solution between a single gamma and multiple gammas of a whole member for the optimized design based on cost.

4.2 Future Work

Based on the current study, the following future work is recommended:

1. SABRE2Design is a program which involves significant computational expense. Parallel computing can be employed to reduce the computational time.

2. The member ends are assumed torsionally simply-supported conditions at joints and supports in this research. This approach neglects the effects of continuity between members. The end restraint effects should be considered for the efficient member design.

3. SABRE2 currently addresses only the elastic analysis. It should be expanded to the inelastic analysis.

REFERENCES

Andrade, A. and Camotim, D. (2005). “Lateral-Torsional Buckling of Singly Symmetric Tapered Beams: Theory and Applications.” Journal of Engineering Mechanics, ASCE, 131:6, 586-597.

Andrade, A. and Camotim, D. (2007). “Lateral-Torsional Buckling of Singly Symmetric Web-Tapered Thin-Walled I-Beams: 1D model vs. Shell FEA.” Journal of Computers and Structures, 85, 1434-1359.

AISC (1989). “Specification (Ninth Edition) Allowable Bending Stress”, American Institute of Steel Construction, Inc. Chicago, IL.

AISC (2002). “Example Problems Illustrating the Use of the New Bracing Provisions – Section C3, Spec and Commentary”, Ad hoc Committee on Stability Bracing, November (revised from original version of August 1998).

AISC (2010). “Specification for Structural Steel Buildings”, ANSI/AISC 360-10, American Institute of Steel Construction, Inc. Chicago, IL.

AISC (2014). “Specification for Structural Steel Buildings”, ANSI/AISC 360-16, Ballot 2 Draft, American Institute of Steel Construction, Inc. Chicago, IL.

Bleich, F. (1952). Buckling Strength of Metal Structures, New York: McGraw-Hill.

Chen, W. F. and Lui, E. M. (1987). Structural Stability: Theory and Implementation, Prentice Hall

Crisfield, M. A. (1990). “A Consistent Co-Rotational Formulation for Non-Linear, Three-Dimensional, Beam-Elements.” Computer Methods in Applied Mechanics and Engineering, 81, pp. 131-150.

Crisfield, M. A. (1991). “Nonlinear Finite Element Analysis of Solids and Structures, Vol.1.”John Wiley & Sons.

Crisfield, M. A. (1997). “Nonlinear Finite Element Analysis of Solids and Structures, Vol.2: Advanced Topics.” John Wiley & Sons.

Chen, S.Y. (1997). “Using Genetic Algorithms for the Optimal Design of Structural Systems”, Doctoral Dissertation, Arizona State University, Tempe, AZ.

Chang, C. J. (2006). “Construction Simulation of Curved Steel I-Girder Bridges”, Doctoral Dissertation, Georgia Institute of Technology, Atlanta, GA.

Degertekin, S. O., Saka, M. P., and Hayalioglu, M. S. (2008). “Optimal Load and Resistance Factor Design of Geometrically Nonlinear Steel Space Frames via Tabu Search and Genetic Algorithm.” Journal of Structural Engineering 30,197-205.

Erbatur, F., Hasancebi, O., Tutuncu, I., and Kilic, H. (2000). “Optimal Design of Planar and Space Structures with Genetic Algorithms.”Journal of Computers and Structures 75,209-224.

Felippa, C. A. and Haugen, B. (2005). “Unified Formulation of Small-Strain Corotational Finite Elements: I. Theory”, Center for Aerospace Structures.

Goldberg, D. G. (1989). Genetic Algorithms in Search, Optimization, and Machine Learning, Adisson Wesley.

Gil, L. and Andreu, A. (2001). “Shape and Cross-Section Optimization of a Truss Structure.” Journal of Computers and Structures 79, 681-689.

Galambos, T. V. and Surovek, A. E. (2005). Structural Stability of Steel: Concepts and Applications for Structural Engineers, John Wiley and Sons, Inc.

Gero, M. B. P., Garcia, A. B., and Diaz, J. J. del C. (2005). “A Modified Elitist Genetic Algorithm Applied to the Design Optimization of Complex Steel Structures.”Journal of Constructional Steel Research 61,265-280.

Gero, M. B. P., Garcia, A. B., and Diaz, J. J. del C. (2006). “Design Optimization of 3D Steel Structures: Genetic Algorithms vs. Classical Techniques.” Journal of Constructional Steel Research 62,1303-1309.

Helwig, T. A., Frank K. H. and Yura, J. A. (1997). “Lateral-Torsional Buckling of Singly Symmetric I-Beams.” Journal of Structural Engineering, Vol.123, No. 9, 1172-1179.

Hayalioglu, M. S. (2000). “Optimum Design of Geometrically Non-linear Elastic-Plastic Steel Frames via Genetic Algorithm.”Journal of Computers and Structures 77,527-538.

Haupt, R. L. and Haupt, S. E. (2004). Practical Genetic Algorithms, John Wiley and Sons, Inc.

Jeong, W. Y., Earls, C. J., Philpot, W. D., and Zehnder, A. T. (2012). “Inverse thermographic characterization of optially unresolvable through cracks in thin metal plates” Journal of Mechanical Systems and Signal Processing, 27,634-650.

Kaehler, R.C., White, D.W., and Kim, Y.D. (2011). "Steel Design Guide 25; Frame Design Using Web-Tapered Members", American Institute of Steel Construction, Inc. Chicago, IL.

Kim, Y. D. (2010). "Behavior and Design of Metal Building Frames Using General Prismatic and Web-Tapered Steel I-Section Members", Doctoral Dissertation, Georgia Institute of Technology, Atlanta, GA.

Kitipornchai, S., Wang, C. M., and Trahair, N. S. (1986). "Buckling of Monosymmetric I-Bemas under Moment Gradient." Journal of Structural Engineering 112:781-799.

LTBeam (2013). <https://www.cticm.com/content/ltbeam-version-1011> (July 25,2014).

McGuire, W., Gallagher, R. H., and Ziemian, R. D. (2000). Matrix Structural Analysis, Second Edition, John Wiley and Sons, Inc.

MASTAN2 (2013). < http://www.mastan2.com/> (July 25,2014).

Newmark, N. M. (1942). "Numerical Procedure for Computing Deflections, Moments, and Buckling Loads", ASCE, 2202, 1161-1234

Ronagh, H. R., Bradford, M. A., and Attard, M. M. (2000a). "Nonlinear Analysis of Thin-Walled Members of Variable Cross-Section. Part 1: Theory." Journal of Computers and Structures 77, 285-299.

Ronagh, H. R., Bradford, M. A., and Attard, M. M. (2000b). "Nonlinear Analysis of Thin-Walled Members of Variable Cross-Section. Part 2: Application." Journal of Computers and Structures 77, 301-313.

Stűssi, F. (1935). “Stability of a Girder Subject to Bending”, IABSE publications, 401-420

Smith, M. D., Turner, K. A., and Uang, C. (2013). “Cyclic Lateral-Torsional Buckling Experiments on Web-Tapered I-Beams” Stability Session S2, Structural Stability Research Council Conference, St. Louis, MO, April.

StabLab (2013). ConSteel Solutions Ltd., Budapest, Hungary.< http://www.stablab.net/ > (July 25,2014).

Timoshenko, S. P. (1936). *Theory of Elastic Stability*, McGraw-Hill Book Company, New York, NY.

Timoshenko, S. P. and Gere. J. M. (1961). *Theory of Elastic Stability*, McGraw-Hill Book Company, New York, NY.

Yang, Y. B. (1984). “Linear and Nonlinear Analysis of Space Frames with Nonuniform Torsion Using Interactive Computer Graphics”, Doctoral Dissertation, Cornell University, Ithaca, NY.

Yang, Y. B. and Yau, J. D. (1987). “Stability of Beams with Tapered I-Sections” Journal of Engineering Mechanics, ASCE, 113:1337-1357.

White, D. W. and Kim, Y. D. (2006). “A Prototype Application of the AISC (2005) Stability Analysis and Design Provisions to Metal Building Structural Systems”, Report to Metal Building Manufacturers Assiciation.

VITA

Woo Yong Jeong was born in Jeongup, South Korea on 08 February 1977, the son of Tae Ki Jeong and Doo Rae Kim. He attended Chuang-Ang University where he studied architectural engineering in March 2002 and received his Bachelor of Science in August 2005 as the honor of Summa Cum Laude. He earned his Master of Engineering at the same University in August 2007. He moved to United States to attend the Graduate School of Civil and Environmental Engineering at Cornell University. He got his Master of Science in August 2010. He continued his graduate study pursuing his doctorate in Civil Engineering at Georgia Institute of Technonogy.